WYLE LABORATORIES
SCIENTIFIC SERVICES AND SYSTEMS GROUP

research REPORT

WYLE LABORATORIES - RESEARCH STAFF
RESEARCH REPORT WR 79-15

ANALYSIS OF
SRB REENTRY ACOUSTIC ENVIRONMENTS

by

T. Coffin
R. E. Dandridge
U. W. Haddock

for

NATIONAL AERONAUTICS AND SPACE ADMINISTRATION
GEORGE C. MARSHALL SPACE FLIGHT CENTER
Marshall Space Flight Center, Alabama 35812

June 1979

A Final Report of
Work Performed Under Contract Number NAS8-32112

WYLE LABORATORIES
SCIENTIFIC SERVICES AND SYSTEMS GROUP
P. O. BOX 1008 • HUNTSVILLE, ALABAMA 35807
TWX (810) 726-2225 • TELEPHONE (205) 837-4411

COPY NO. 12

FOREWORD

This report presents an empirical assessment of the reentry aeroacoustic environment for the Solid Rocket Booster (SRB) aft skirt/exit plane region. The results are based on an evaluation of the fluctuating pressure data obtained from SRB reentry aeroacoustic tests SS27F and SS28F, performed at the NASA Ames Research Center between March and November 1978.

The SRB aft section was first divided into environmental regions. Space average one-third octave-band aeroacoustic spectra representing full scale conditions were then derived for each region and test Mach number. The experimental approach, data acquisition, reduction, and evaluation procedures utilized to arrive at these results are summarized in subsequent sections. A cursory comparison between results for several SRB aft skirt configurations is also given.

The appended aeroacoustic spectra represent the most recent (May 1979) and comprehensive evaluation of the SS27F/SS28F test series performed under the present contract, NAS8-32112. Related studies performed under this contract have been reported previously, including references 1 through 4. It should be noted that the results presented herein are based on computer simulations performed after publication of reference 1, and therefore supersede that reference.

This report was prepared by Wyle Laboratories, Scientific Services and Systems Group, for the George C. Marshall Space Flight Center, National Aeronautics and Space Administration. The work was performed under contract NAS8-32112, entitled "Analysis of SRB Reentry Acoustic Environments." Mr. T. Coffin served as Principal Investigator. Administration of this study was provided under the technical direction of the Systems Dynamics Laboratory with Dr. Luke Schutzenhofer serving as T.C.O.R. Mr. W. Clever provided primary technical coordination of the effort.

ABSTRACT

Estimates of Space Shuttle Solid Rocket Booster reentry aeroacoustic environments have been made. Particular emphasis has been given to the aft skirt/exit plane region for the Mach number regime $0.6 \leqslant M_\infty \leqslant 3.5$. The analysis is based on the evaluation of wind tunnel model results in conjunction with Monte Carlo simulation of trajectory parameters. A brief description of the experimental approach is provided along with a discussion of the evaluation process utilized. Predicted environments are presented in terms of one-third octave band spectra representing space averaged values for critical regions on the Solid Rocket Booster.

TABLE OF CONTENTS

TABLE OF CONTENTS (CONCLUDED)

LIST OF FIGURES

1.0 INTRODUCTION

The Space Shuttle Vehicle (SSV) is a complex assemblage of components consisting of the orbiter spacecraft, external tank and two solid rocket boosters. The SSV will serve as the primary free world space transportation system for at least the next decade. A key to the efficiency of the SSV concept is the cost/effectiveness attained through the refurbishment and reuse of systems and components over multiple flights.

Sophisticated aerospace systems and components are inherently sensitive to the environments to which they are exposed. This sensitivity is significantly emphasized when considering the requirement of reusability. It is important that design efforts relating to structure and components consider, among other factors, the acoustic environments to which they are exposed. In addition, definition of these acoustic environments is equally important to allow accurate definition and assessment of test criteria for qualification and acceptance testing.

The acoustic and aeroacoustic environment anticipated for flight of the SSV has received considerable attention due to the fact that space flight components are likely to encounter unique environmental conditions and must function over a number of flight missions. The Solid Rocket Boosters (SRBs) will reenter the atmosphere after burnout and separation in a free-fall state followed by parachute deployment and splashdown. Subsequent to splashdown, the SRBs will be refurbished for reuse. During atmospheric reentry, the structure and components will experience severe aeroacoustic excitation. In order to establish aeroacoustic environmental estimates, which subsequently influence design and test criteria, NASA/MSFC and contractors have performed a number of analytical studies and wind tunnel experiments. Through these experiments, the aft skirt and exit plane region of the SRB has been singled out due to observed intense aeroacoustic excitation near the location of critical and sensitive equipment items.

A comprehensive wind tunnel test series was performed at the NASA Ames Research Center between March and November 1978. The series was performed in two major segments, based on tunnel facility utilized. The transonic Mach number regime was designated SS27F, and the supersonic regime SS28F. A 2.8% scale model of the SRB aft body was utilized with total internal motor volume simulated. Two heat

shield configurations were simulated: one representing the baseline flexible heat shield (Configuration II) and a second representing an inflated heat shield (Configuration XVIII). The model was instrumented with 35 dynamic pressure transducers in the model aft skirt/exit plane area. Testing was performed at eleven Mach numbers ranging from $M_\infty \sim 0.6$ to $M_\infty \sim 3.5$. At each Mach number the model was tested at four roll angles. For each Mach number and roll angle, angle of attack was varied from approximately 90 degrees to 180 degrees, depending on Mach number.

Complete results for the baseline configuration are included in the appendices. Comparisons are included between several other configurations. Aeroacoustic definition is provided in terms of one-third octave-band spectra for twelve geometric regions in the SRB aft skirt/exit plane area. These results, presented in the appendices, are shown for each of the eleven Mach numbers tested. A description of the experimental approach, data reduction and evaluation procedures implemented is given in the following sections.

2.0 EXPERIMENTAL APPROACH

This section presents a brief summary of the experimental approach utilized to define aeroacoustic loads in the aft skirt region of the SRB. A detailed description of test program requirements may be found in Reference 5.

2.1 MODEL DESCRIPTION

The model tested was a 2.8 percent scaled representation of the 146-inch diameter left-hand SRB configuration. Since it was known, from previous test and evaluation, that the aft skirt region is critical with respect to aeroacoustic loads, only that part of the SRB, with protuberances, was geometrically scaled. It was also known, however, that the internal motor volume exhibits a significant influence on the flow about the SRB exit plane. Therefore the total motor volume representing the SRB at reentry was simulated. A photograph of the model, installed in the Ames 14'x14' transonic wind tunnel is shown in Figure 1. A close up view of the aft skirt and nozzle is shown in Figure 2.

The full scale SRB will utilize an insulating cloth curtain suspended between the rocket nozzle and aft skirt in the form of an annulus. The purpose of this thermal curtain is to prevent excessive heat buildup in the aft skirt cavity, where substantial reusable equipment is located. This heat shield is designed to be relatively limp to minimize transmission of loads associated with nozzle gimbaling. A dynamically scaled heat shield (designated Configuration II) was therefore included in the model to provide the same influence on the fluctuating pressure levels as the full scale heat shield. Derivation of the similarity parameters required to dynamically scale the flexible heat shield, based on the equations of motion for a thin flexible membrane, is summarized in Reference 6. The resulting material for the heat shield layers was a nylon warp knit. An alternative configuration, representing an inflatable heat shield (designated Configuration XVIII) was also tested. This configuration was constructed of stainless steel screen laminated with nylon cloth. The heat shield mounted in place on the model can be seen in Figure 2.

The model aft region was instrumented with 35 miniature microphones. (The protective covers for three of these transducers may be seen between the aft separation motors and near hold-down post in Figure 2.) Transducer locations and designations (identification numbers) are shown in Figures 5 and 6. Also shown are body

coordinates on the model. Six static pressure probes are also shown, although results from these measurements are not included in this report The transducer outputs were hard wired through appropriate signal conditioning equipment to the data reduction system in the wind tunnel control room.

2.2 REENTRY FLIGHT CONDITIONS SIMULATED

The wind tunnel testing was performed at eleven discrete Mach numbers ranging from $M_\infty \sim 0.6$ to $M_\infty \sim 3.5$. At each Mach number the model was tested at four roll angles (ϕ). For each Mach number and roll angle, angle of attack (α) was varied from roughly 90 degrees to 180 degrees, depending on the specific Mach number. The reentry conditions simulated are summarized as follows:

Mach Number	Angle of Attack	Roll Angle
0.6, 0.8, 0.9, 1.0, 1.2	$90° \leq \alpha \leq 158°$	150°, 180°, 210°, 270°
1.55, 2.0, 2.4	$120° \leq \alpha \leq 180°$	150°, 180°, 210°, 270°
2.75, 3.10, 3.50	$90° \leq \alpha \leq 180°$	150°, 180°, 210°, 270°

Model/flow coordinate relations are defined in Figure 3. The angle of attack ranges defined above were designed to include the 95 percentile range in angle of attack anticipated in flight; see References 5 and 7.

2.3 DATA ACQUISITION AND REDUCTION

As stated previously, the aft SRB model was instrumented with 35 miniature microphones, wired into the data acquisition system. A schematic of the data acquisition and reduction system is illustrated in Figure 7. Dynamic range of the total system was approximately 140 dB to 180 dB. Frequency response was flat from 20 Hz to 20 kHz.

A typical data acquisition cycle was accomplished as follows: Stable tunnel conditions were attained and transducer gains optimized and recorded by the computer or disc. For a fixed Mach number and roll angle, the model was slowly pitched through an angle of attack (α) range dictated by the sector setting. At this time, the overall fluctuating pressure level (OAFPL) measurements were acquired from the dynamic transducers and stored in two forms. Instantaneous fluctuating pressure time histories were recorded on analog tape, and true root-mean-square (rms) detected values were stored in digital format on disc, as a function of α. A

computer search was then automatically performed to ascertain the eight data channels exhibiting the greatest maximum OAFPL, and hard copy OAFPL vs α plots were generated for these transducers. (Additional plots were obtained, as required, by keyboard instruction on the computer terminal.) Engineering evaluation of these data was next performed on-line, to define specific angles of attack representing the greatest excitation levels. Fixed α testing followed, for each selected α, at which time one-third octave-band spectra were extracted, detected and stored on disc for all transducers. Simultaneously, analog time histories of approximately 30 seconds duration were recorded on tape. In general, two spectra were obtained for each 30 degree segment in α.

The data stored on disc represent values appropriate to the model geometry, subject to the flow conditions experienced in the wind tunnel. Data reduction was performed by recalling appropriate files from disc, at which time amplitude and frequency scaling were applied by computer software, generating and cataloging hard copy plots.

One-Third Octave-Band Spectrum Scaling

Amplitude scaling was performed by letting

$$FPL_t = 20 \log\left(\frac{\tilde{C}_p}{P_r} \cdot \bar{q}_t\right) \qquad (1)$$

and

$$FPL_f = 20 \log\left(\frac{\tilde{C}_p}{P_r} \cdot \bar{q}_f\right)$$

where FPL = fluctuating pressure level

$\tilde{C}_p$ = fluctuating pressure coefficient

P_r = reference pressure

$\bar{q}$ = free stream dynamic pressure

subscripts t and f denote test and flight conditions, respectively.

So $$FPL_f = FPL_t - 20 \log \bar{q}_t + 20 \log \bar{q}_f. \qquad (2)$$

In the above equation, test conditions are deterministic in the sense that they have been observed, whereas $\bar{q}_f$ is a random variable governed by trajectory

statistics. Statistical definition of in-flight dynamic pressure was provided in terms of equaprobability ($\bar{q}$, α) contours for each Mach number. For the present case, $\bar{q}_f$ was defined by polynominal curve fit to the upper bound (with respect to $\bar{q}$) of the 95 percent probability contours.

Full scale frequencies were obtained by Strouhal similitude scaling using the relation

$$\left.\frac{f\ell}{V_\infty}\right|_M = \left.\frac{f\ell}{V_\infty}\right|_P \qquad (3)$$

where f = frequency

ℓ = characteristic length (such as main body diameter)

V_∞ = free stream velocity

subscripts M and P represent model and prototype, respectively.

Scaling the Overall Fluctuating Pressure Level (OAFPL)

"Quick look" ampltiude scaling was performed as above. For subsequent analysis, amplitude scaling was performed by simply normalizing the OAFPL by q, yielding an "aeroacoustic sensitivity indicator" (I), from which OAFPL statistics may be derived based on trajectory simulation, of the form

$$I(\alpha) = OAFPL_t - 20 \log q_t \ . \qquad (4)$$

As stated above, the transformations were performed automatically by the computer as the data was recalled from disc storage. For each test Mach number, roll angle and transducer, reduced data were obtained as

a) A plot of I vs α

b) A plot of OAFPL vs α

c) One-third octave-band spectra at selected angles of attack (usually four)

The above two types of information then form the basis for estimating the SRB reentry aeroacoustic environment. The evaluation procedure followed in deriving the appended results is summarized in the following section.

3.0 ANALYSIS

3.1 DEFINITION OF SRB ENVIRONMENTAL ZONES

The first step in the evaluation process was to divide the aft skirt/exit plane area into environmental regions for which to develop specific aeroacoustic environment definition. To this end, a review of sensitive equipment locations was made. This was done to associate critical equipment and structural locations with "nearby" measurements, which should represent the primary local excitation. A summary of environmental regions selected, local equipment and/or structural description and associated test measurement numbers follow:

Designation	Description	Measurements
A	Motor Nozzle	107 - 112
B	Compliance Ring	113 - 118
C	Skirt/Nozzle Cavity	119, 120, 122, 123
D-I	TVC Upper and Lower Frame Assemblies	100, 101
D-II	Actuator Brackets	89 - 92
D-III	Aft Separation Motors	96 - 98, 106
D-IV	External Skirt	99
D-V	External Skirt	93, 102, 103
D-VI	External Skirt	94, 95, 104, 105
D-VII	Separation Motor Subregion	96 - 98
D-VIII	Separation Motor Subregion	106
E	Internal Motor Volume	121

The exact definition of region boundaries is somewhat arbitrary. The regions selected and associated measurement locations are illustrated in Figures 4 through 6. For completeness, external skirt regions were defined for some areas where no sensitive equipment was known to exist. This was done to account for possible equipment relocation or addition.

Based on the reduced data format, evaluation was directed along two parallel paths: amplitude analysis to establish regional OAFPL estimates, and spectrum evaluation, to define associated one-third OB spectral shapes. Results of the above were then combined to yield the desired environmental estimates.

3.2 DERIVATION OF REGION OAFPL'S

The measured OAFPL vs α data was used to define full scale OAFPL estimates for each region and Mach number. This data was used since the "sweep" results embrace the entire α range of interest, as opposed to the spectral data, which were taken at several fixed angles of attack within the range. The derivation of OAFPL estimates for each region and Mach number was accomplished in three phases: (1) generation of aeroacoustic indicators by region, (2) computer simulation with random trajectories to obtain OAFPL flight statistics, and (3) sorting and interpolation of results to obtain OAFPL percentiles by Mach number.

A "regional" indicator was defined, similar to Equation 4, as

$$\langle I(\alpha) \rangle = \langle \mathrm{OAFPL}_t \rangle - 20 \log q_t \tag{5}$$

where $\langle \cdot \rangle$ denotes a space average over the region.

Assume a region containing N measurements, each contributing equally (for example, acting independently over identical subregions). The space average mean-square pressure over the region is then

$$\langle \overline{p^2} \rangle = 1/N \sum_i \langle \overline{p_i^2} \rangle \tag{6}$$

where $\overline{p_i^2}$ represents the mean-square pressure at location i.

The regional indicator was thus defined simply as

$$\langle I(\alpha) \rangle = 10 \log \left[\frac{1}{N \left(p_r \bar{q}_t \right)^2} \sum \overline{p_i^2} \right] \tag{7}$$

Equation 7 was evaluated for each region, Mach number and roll angle on a HP 21MX computer located at NASA/MSFC/ED35. The results were then formatted and punched for input to the trajectory simulation scheme operational on the MSFC UNIVAC 1108 system. Programming and trajectory simulation were performed by MSFC/ED15.

The full scale OAFPL for a given region is obviously a function of reentry parameters, specifically

$$\langle \mathrm{OAFPL} \rangle_f = \langle I(M_\infty, \phi, \alpha) \rangle + 20 \log \bar{q}_f \tag{8}$$

The method of computing the above parameters was through Monte Carlo simulation of reentry flight trajectories. Initial conditions (position, rates, etc), atmospheric properties, mass and aerodynamic characteristics for example, are not known exactly, but exhibit differing degrees of variability. In the Monte Carlo analysis, a set of these input variables was assigned at random, based on known or assumed probability laws. The dynamic equations of motion for reentry flight were then solved. The resulting set of output parameters represents the state of the system at each time step, for example,

$$\left\{ \begin{array}{c} M_\infty \\ \phi \\ \alpha \\ \bar{q} \\ -- \\ -- \\ -- \end{array} \right\}_{t_i} \tag{9}$$

For each time step within the increment encompassing the Mach number range for which the indicators were defined, the region OAFPL was solved for, by, symbolically

$$\left\{ \begin{array}{c} M_\infty \\ \phi \\ \alpha \\ \bar{q}_f \end{array} \right\}_{t_i} \Rightarrow \left[\left\langle I(M_\infty, \phi, \alpha) \right\rangle + 20 \log \bar{q}_f \right]_{t_i} \Rightarrow \left\langle \text{OAFPL} \right\rangle_{f_{t_i}} \tag{10}$$

In solving the above, it should be noted that the indicators are defined only for

Four distinct values of ϕ
Eleven distinct values of M_∞
Even values of α (that is, every two degrees)

whereas the simulated flight variables may lie at arbitrary points within limits. To effect solution, the following logic was applied for selection of the appropriate indicator/condition:

The vehicle roll angle range (2π) was divided into four sectors, each including one of the test roll angles. Sector division lines were determined by one-half the angular distance from a given test angle to each of the two adjacent test angles. To clarify, indicators were generated for ϕ = 150°, 180°, 210° and 270°. The indicator obtained for ϕ = 180° was therefore assigned the sector $165° < \phi \leq 195°$.

Since α was defined every 2° in α, the closest value to the flight simulation was used.

To determine the indicator as a function of simulation M_∞, the appropriate α and ϕ were first determined as above, and linear interpolation then performed between the encompassing test Mach number indicator values.

Solving Equation 10, then, yields a time history for the regional OAFPL and associated response quantities, say

$$\left\{ \begin{array}{c} \langle \text{OAFPL} \rangle \\ M_\infty \\ \phi \\ \alpha \\ \bar{q} \\ -- \\ -- \end{array} \right\}_{t_i} , \; i = 1, 2, \cdots, N \qquad (11)$$

The trajectory represented by the matrix, Equation 11, may be interpreted as one sample function, that is, one of the many possible outcomes associated with possible combinations of the random inputs.

The above computations were repeated for 246 sets of input conditions. (For some time points, the sample function Mach number computed in Equation 9 fell outside the range of indicator definition, yielding no OAFPL data.) Next, the vectors in Equation 11 were ranked according to the $\langle \text{OAFPL} \rangle$ magnitude only. (That is, when ranking was assigned, no attention was given the values of M_∞, ϕ, etc.) Finally, the 95 percentile vector based on the $\langle \text{OAFPL} \rangle$ was determined for each time step by sorting, and a single "synthetic" trajectory constructed identical in form

to Equation 11. (Sorting for 90 and 100 percentiles was also performed for comparison purposes, but do not represent the results presented in this report.)

The regional OAFPL for each of the eleven test Mach numbers was determined from the 95 percentile trajectory as follows: The continuous Mach number range was divided into eleven increments centered at the eleven test points. Each increment extended half the range between adjacent test points. End point increments (for example, M_∞ = 0.6 and 3.5) were defined to be symmetric with respect to adjacent interior points. Next, the 95 percentile OAFPL trajectory values were sorted, by Mach number, into the eleven increments described above. (Mach numbers outside the defined range were discarded.) Finally, the region OAFPL values within each Mach number increment were simply averaged, to define a region estimate by Mach number. (In several cases it occurred that no OAFPL values fell within a given increment. In this event, linear interpolation was performed between the OAFPL values determined for adjacent Mach number points.)

3.3 DERIVATION OF REGIONAL SPECTRA

The derivation of one-third octave-band spectrum shapes for each region and Mach number was quite straightforward, if tedious. The spectral data were first segregated by Mach number and roll angle for each SRB region. The region data set for each M_∞, ϕ combination was then superimposed and an envelope spectrum extracted. (This intermediary step — for example, maintaining roll angle identity — was performed to facilitate "back tracking" from the final envelopes, as required, to identify specific measurements and test runs dominating the results.) The envelopes were then combined by Mach number and a second set of envelopes derived, being dependent only on vehicle region and test Mach number. These resulting spectra were then "integrated" to define each associated OAFPL.

The aeroacoustic spectra reported herein were finally arrived at by assigning the 95 percentile OAFPL estimates, determined independently, to the above envelopes, performing the proper ordinate shift and replotting. A discussion of results obtained from this study is presented in the next section.

4.0 RESULTS AND OBSERVATIONS

One-third octave-band spectra representing the SRB reentry aeroacoustic environment for each region and Mach number considered are presented in the appendices. These spectra define the environment for the baseline flexible heat shield configuration (Configuration II). To provide the user a quick-look summary of these results, Figures 8 through 19 are included. These figures represent spectral envelopes, over the eleven Mach numbers utilized in testing, for each of the 12 SRB regions. These "summary curves" may be compared with environmental criteria spectra. The OAFPL associated with these spectra is meaningless, since the results represent diverse and mutually exclusive Mach number regimes.

Review of the OAFPL and spectral data before space averaging indicated that the aft separation motor region excitation is strongly driven by measurement #106. This behavior was observed previously from results of wind tunnel test SS26F at AEDC. Measurement #106 is located directly aft of the aft separation motors (see Figures 2 and 4) and appears to represent a highly localized excitation. For this reason, regional spectra were computed neglecting measurement #106 (Region D-VII) and for transducer #106 only (Region D-VIII).

Neglecting the local influence of measurement #106, the appended results indicate no significant exceedance of present aeroacoustic design/test criteria. This is in contrast with results published in February 1979 (Reference 1). Comparing the appended spectra with the reference results will indicate a difference ranging from approximately 2 to 12 dB in OAFPL. This difference is significant and is due to the data analysis procedure utilized. The reference results were based on 95 percentile (q, α) contours and represent envelopes with respect to roll angle. The present results represent a significantly more detailed analysis and simulation yielding the actual OAFPL distributions, with consideration of roll angle aeroacoustic sensitivity. The present results are considered a refinement of those previously obtained, and therefore supersede them.

A cursory comparison between reduced data results (for example, before Monte Carlo simulation) for the baseline configuration (Configuration II) and the inflatable heat shield (Configuration XVIII) case was made. The inflatable heat shield resulted in a reduction of approximately 5 dB for some conditions within the aft skirt cavity, with negligible apparent difference elsewhere on the SRB.

Since a possibility of heat shield failure before reentry exists, a comparison between internal cavity results for the no heat shield case (from test SS26F) and the base line configuration was made. For this evaluation, the SS26F data were reduced and subject to the same trajectory simulation scheme as discussed in the previous section. Results of this comparison are illustrated in Figures 20 and 21. A significant reduction in spectrum levels for the no heat shield case was afforded by the OAFPL simulation due to high selectivity with respect to angle of attack and roll angle. A notable difference between configurations is seen to exist in the 50 to 70 Hz frequency range.

The trajectory simulation approach to establishing aeroacoustic environments has proven to be highly feasible. The simulation approach utilized in this analysis is based on a 95 percentile synthetic trajectory, followed by sorting in terms of associated Mach number. Differing sorting routines, which yield slightly different interpretations and results, bear investigation. Two approaches other than that followed in this report are (1) sorting by Mach number region initially (as opposed to time) and (2) sorting by "worst value" per flight within each Mach number region. The latter approach (extreme values) would tend towards the conservative, but would permit concise statistical statements concerning the number of expected exceedances per, say, 100 flights. The former approach would yield information on the anticipated amount, or percentage, of time a given level will be exceeded.

REFERENCES

1. Coffin, T., and K. E. Dandridge. "Reentry Aeroacoustic Spectra for Regions on the Solid Rocket Booster," Wyle Laboratories Research Staff Report TM 79-3, February 1979.

2. Becker, R. S., and G. R. Anderson. "An Investigation of the Discrete Frequency Pressure Fluctuations Associated with SRB Reentry Using the Hydraulic Analogy," Wyle Laboratories Research Staff Report TM 78-4, May 1978.

3. Dandridge, R. E. "The Solid Rocket Booster Sensitivity to Discrete Frequencies Produced by Several Proposed Reentry Configurations," Wyle Laboratories Research Staff Report TM 78-5, May 1978.

4. Haddock, U. W. "Influence of a Flexible Heat Shield and Standard Blast Shield on the SRB Skirt/Nozzle Cavity and Motor Volume Aeroacoustic Environment," Wyle Laboratories Research Staff Report TM 78-6, November 1978.

5. Schutzenhofer, L. A. "Pretest Report, Ames 2.8% SRB Reentry Acoustics Model Tests, SS27F and SS28F," Memorandum ED 23-78-40, Marshall Space Flight Center, February 1978.

6. Clever, W. W. "Pretest Report, AEDC 2.8% SRB Reentry Acoustics Model Test SS26F," Memorandum ED 23-77-210, Marshall Space Flight Center, September 1977.

7. -----. "Procedures for Establishing Reentry SRB q-α Contours," Memorandum ED 15-77-26, Marshall Space Flight Center, June 1977.

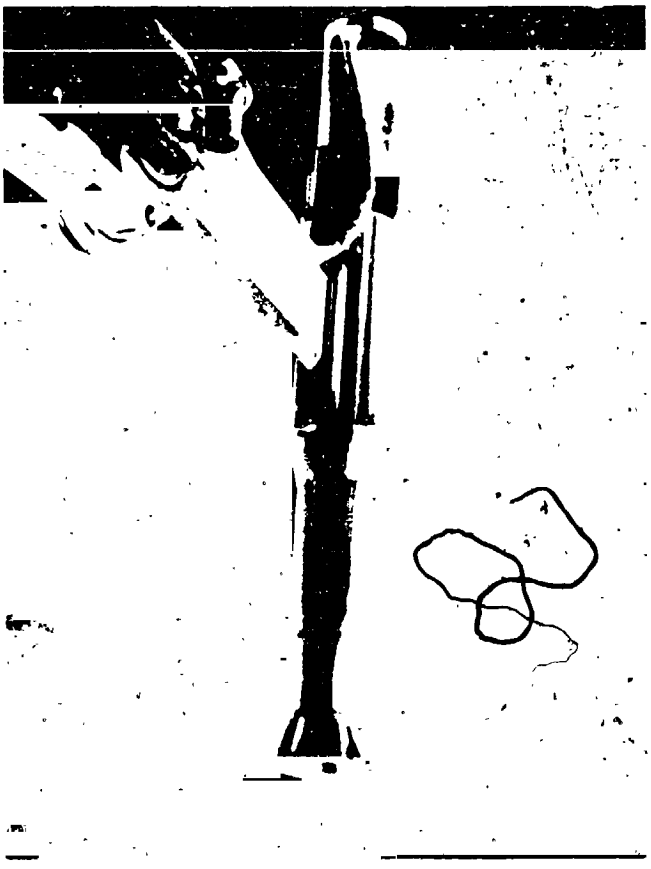

Figure 1. Illustration of the SRB Model Installed in the Ames Transonic Wind Tunnel

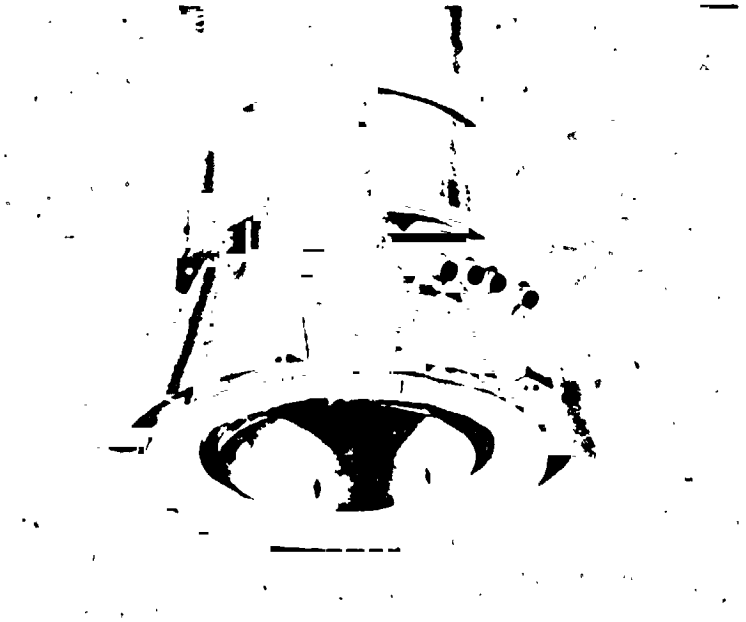

Figure 2. Illustration of the SRB Model Aft Section

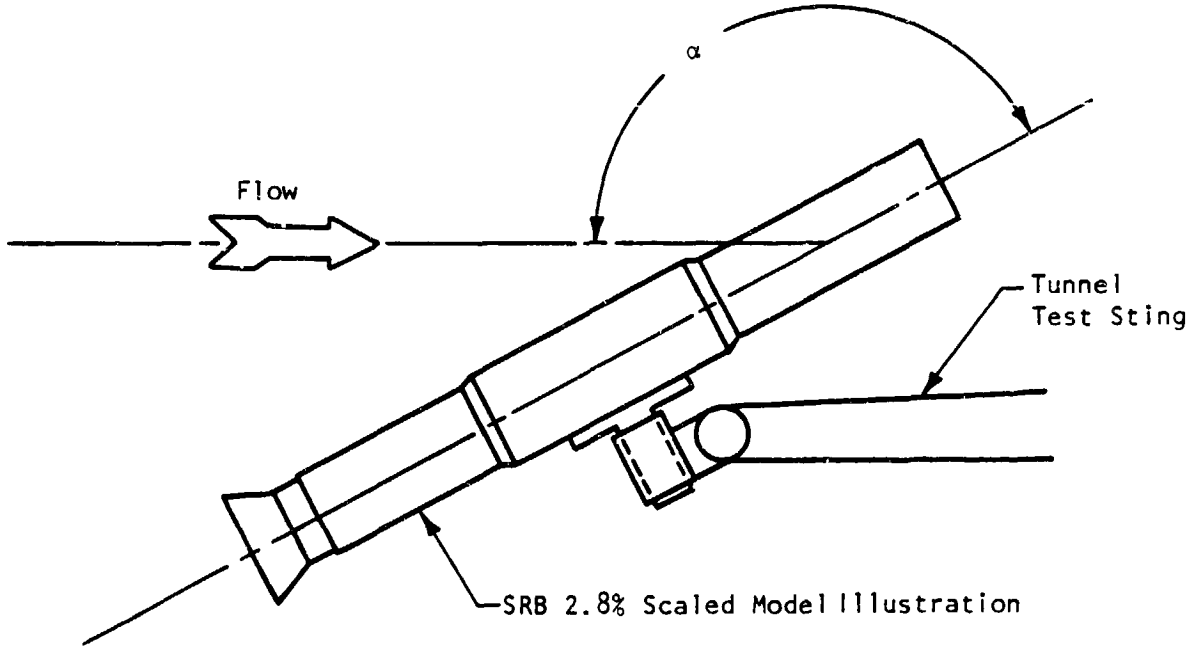

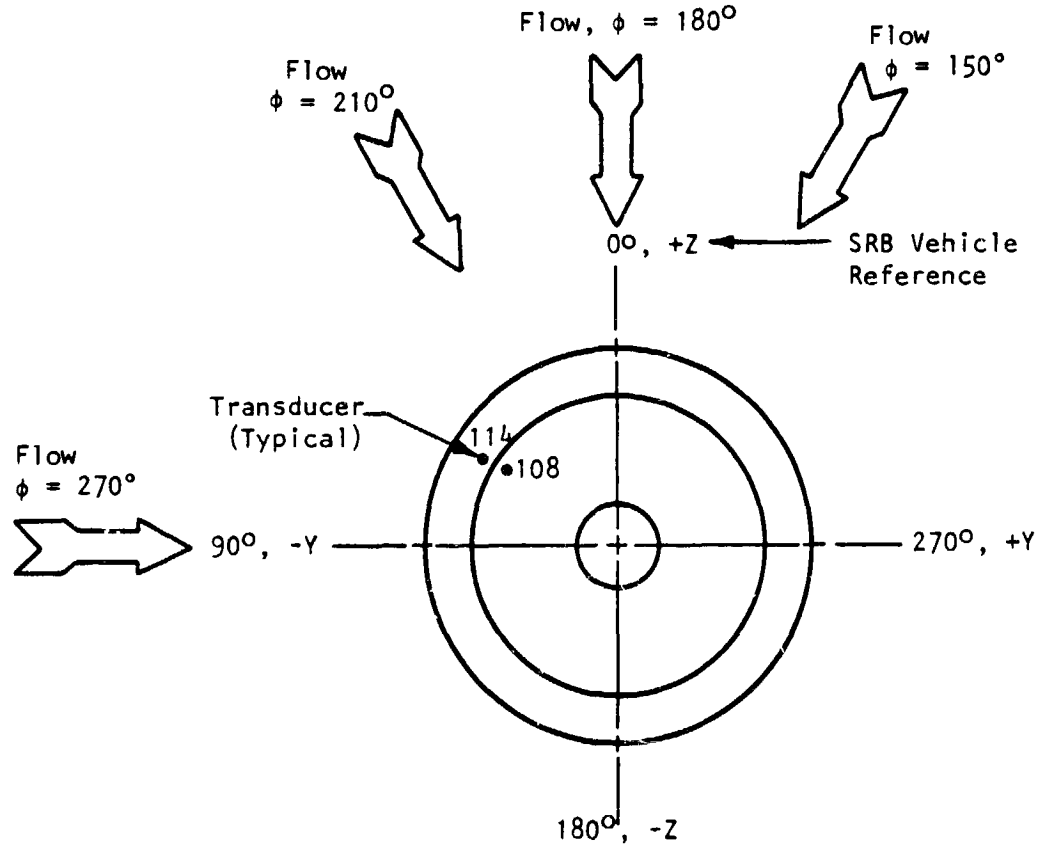

Figure 3. Sketch of SRB Model Indicating Coordinate Definition

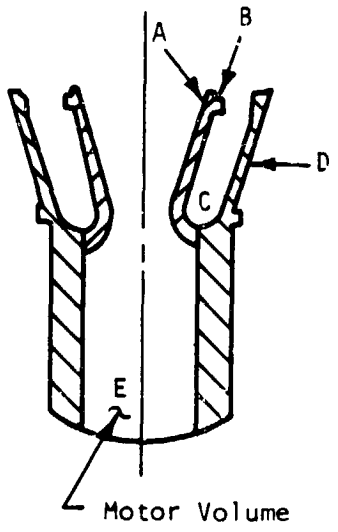

A - Nozzle Region

B - Compliance Ring

C - Skirt/Nozzle Cavity

D - External Aft Skirt

E - Motor Volume

Figure 4. Description of the Major SRB Aft Section Environmental Regions

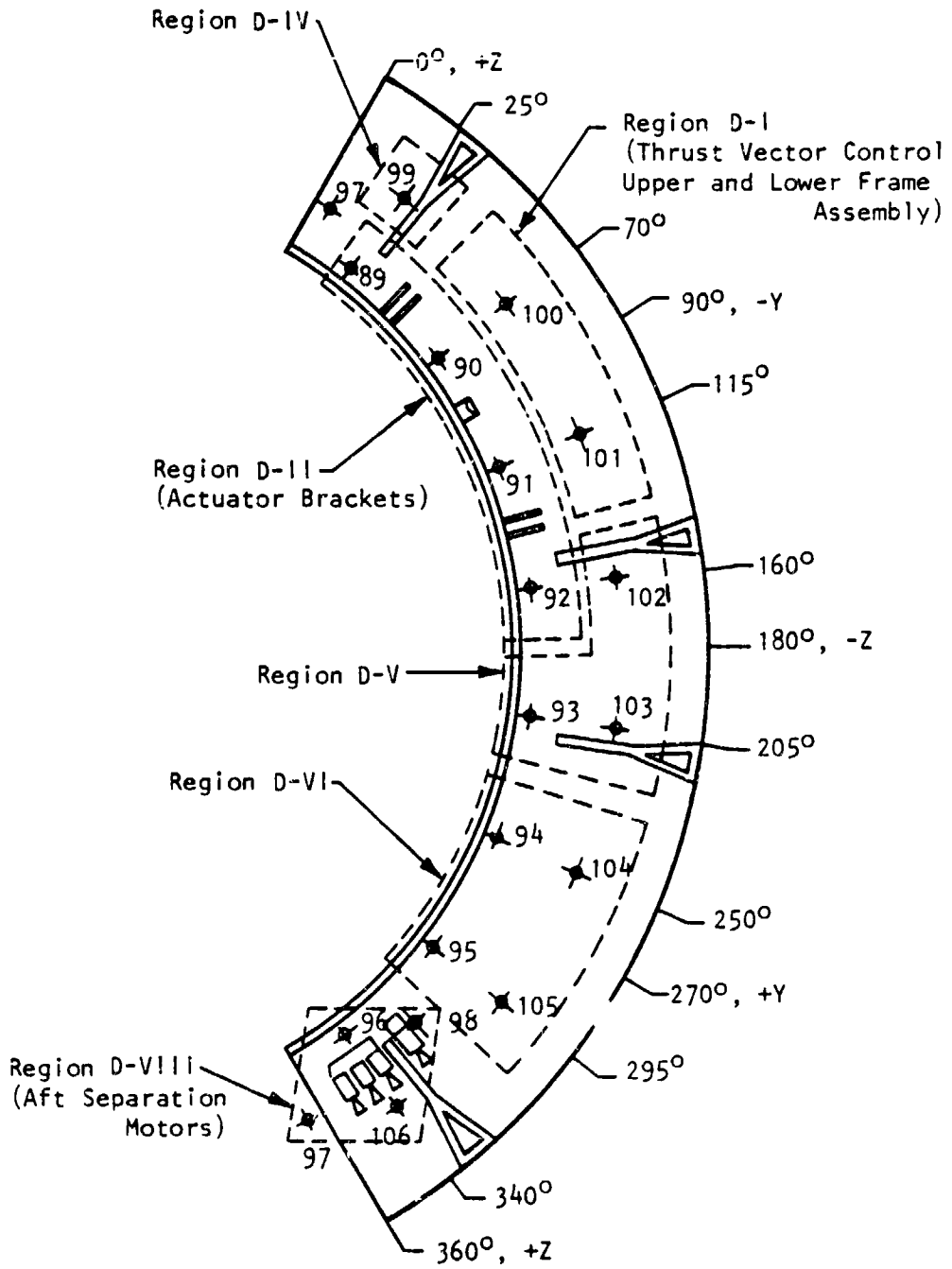

Figure 5. Definition of the SRB External Aft Skirt Transducer Locations

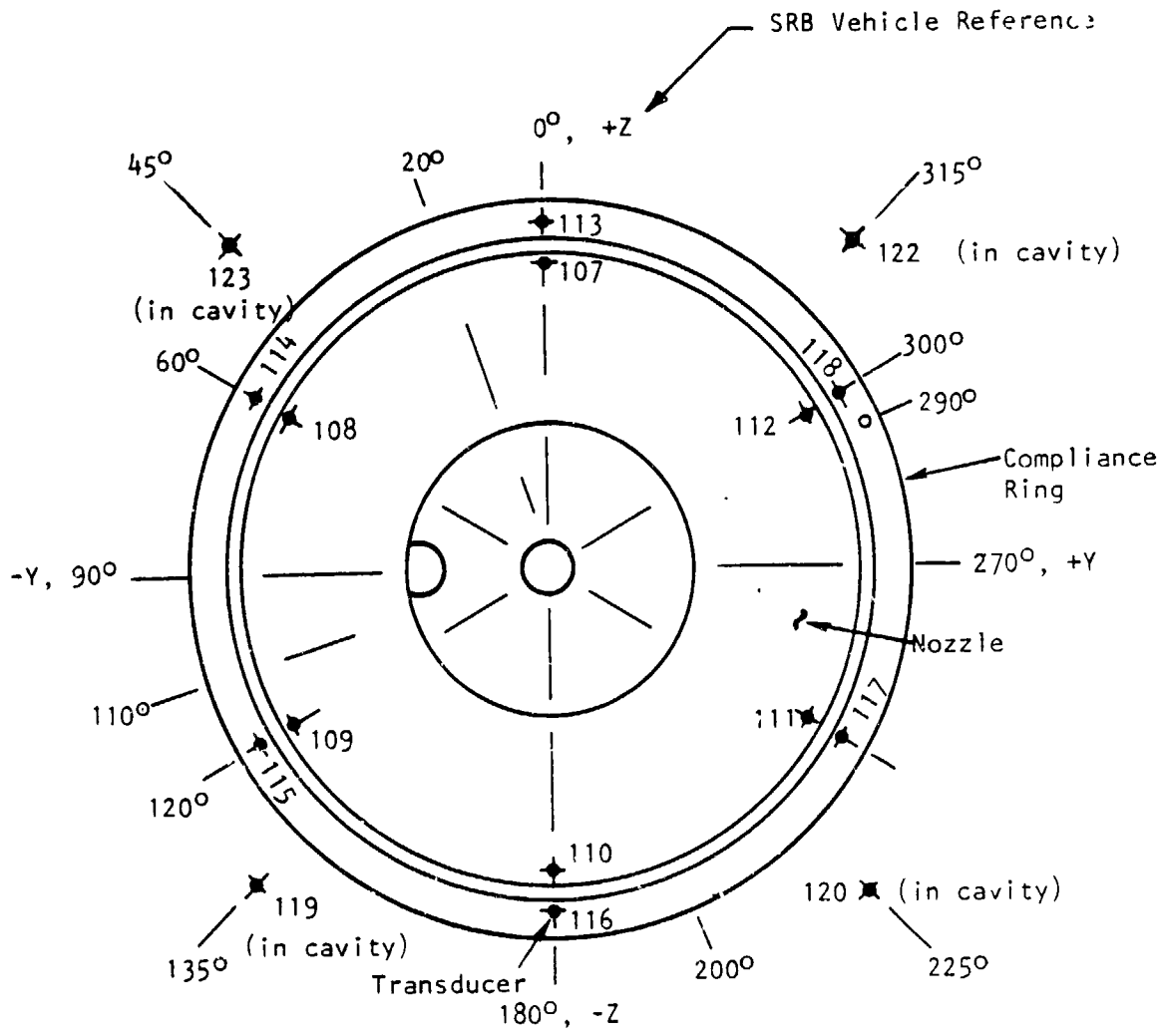

Nozzle End Looking Forward

NOTE: Transducer 121 is in Motor Volume Cavity

Figure 6. Description of SRB Transducer Locations for the Nozzle, Compliance Ring, Skirt Cavity and Motor Volume

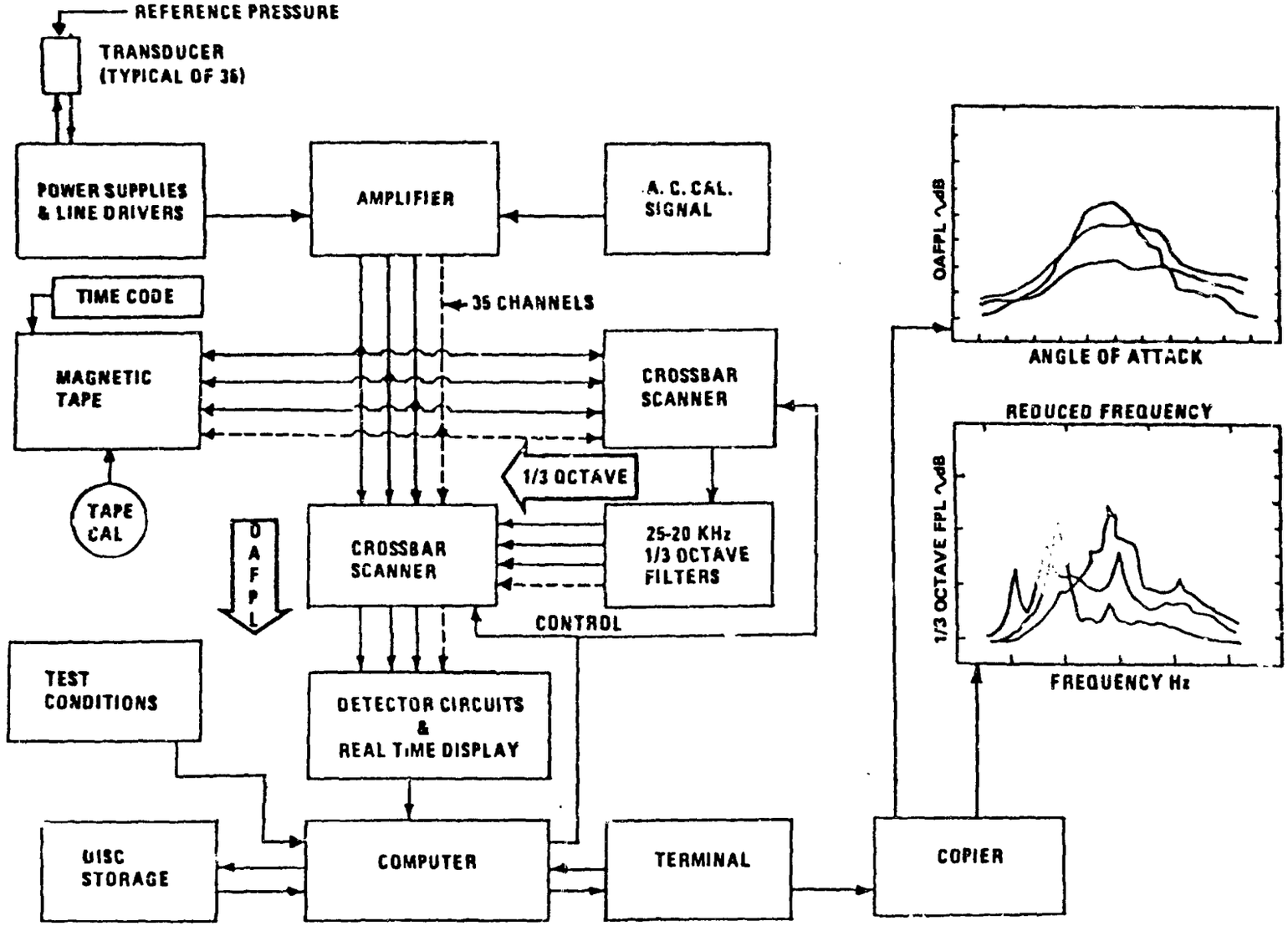

Figure 7. Schematic of Data Acquisition and Reduction System

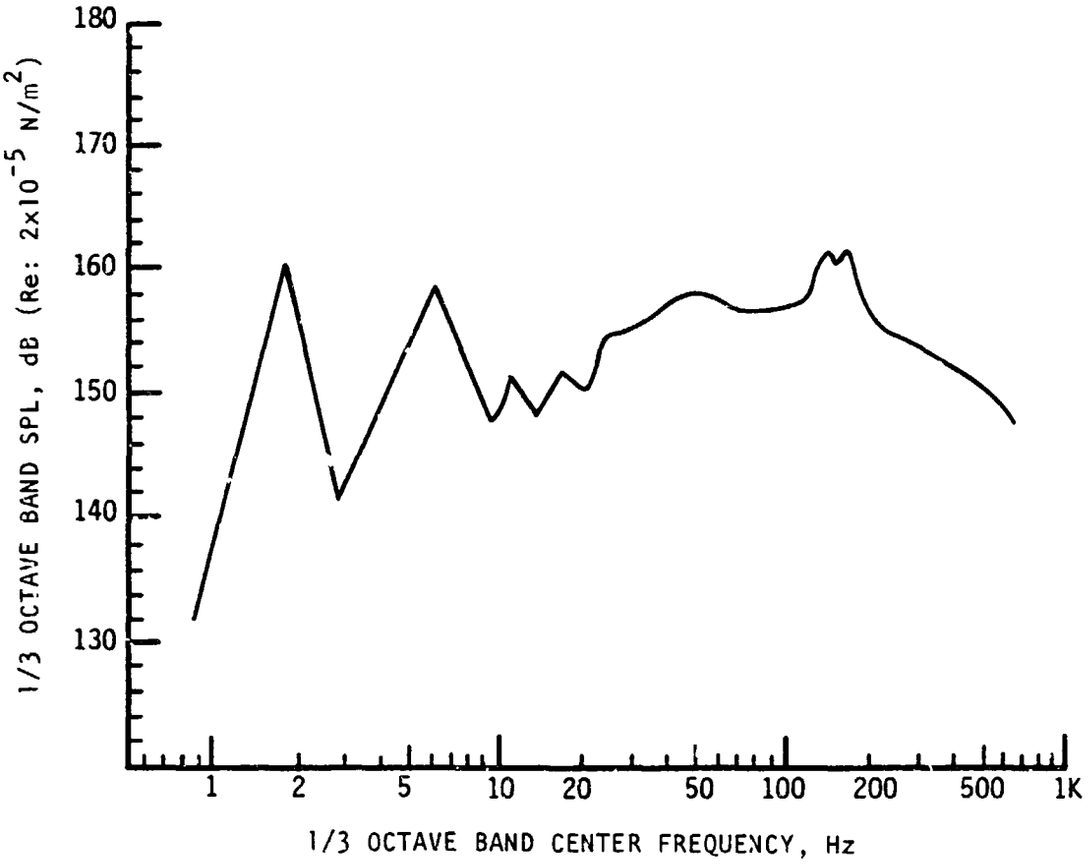

Figure 8. Envelope of SRB Aeroacoustic Spectra for Region A

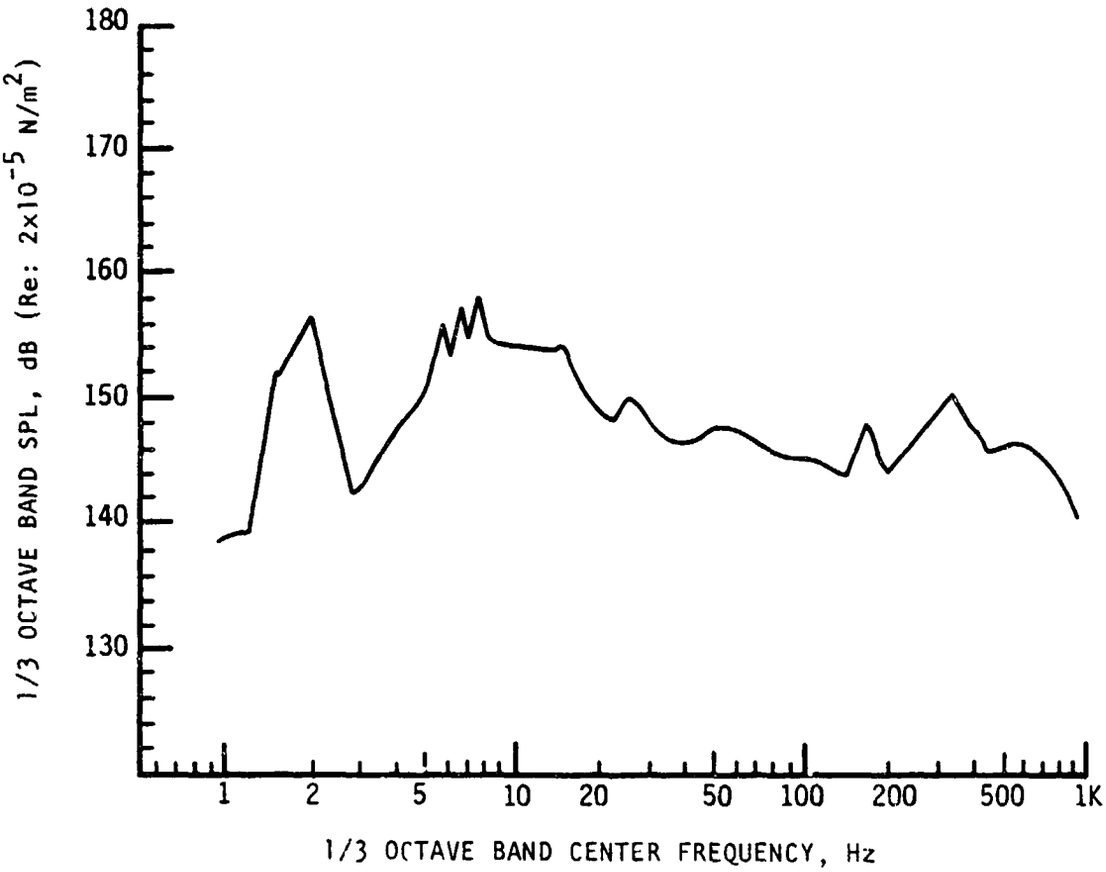

Figure 9. Envelope of SRB Aeroacoustic Spectra for Region B

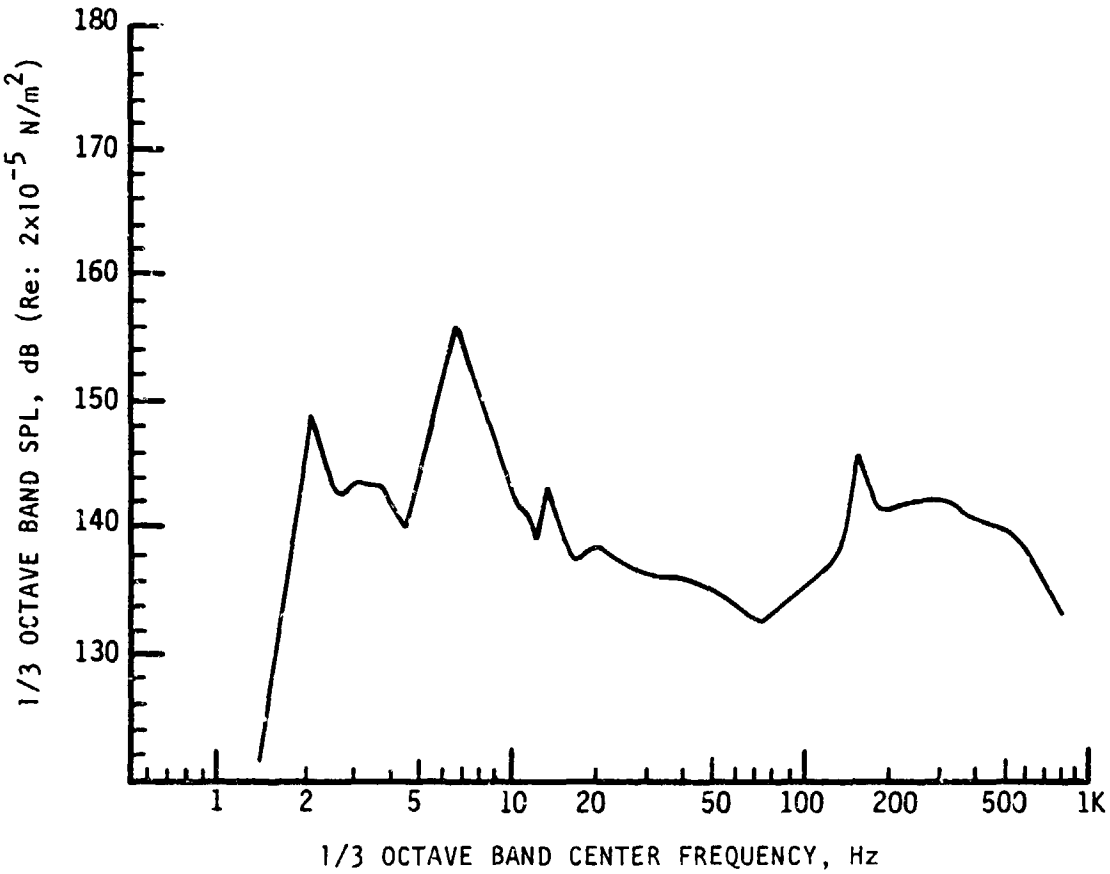

Figure 10. Envelope of SRB Aeroacoustic Spectra for Region C

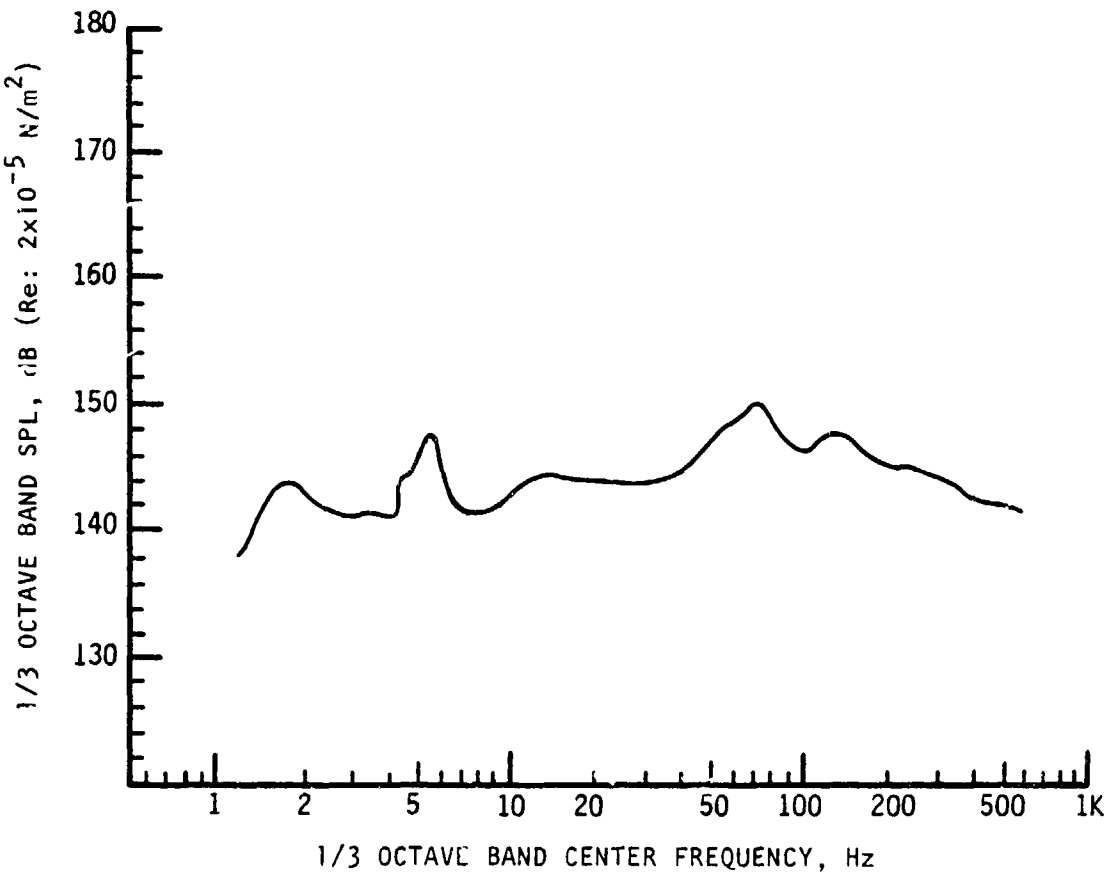

Figure 11. Envelope of SRB Aeroacoustic Spectra for Region D-1

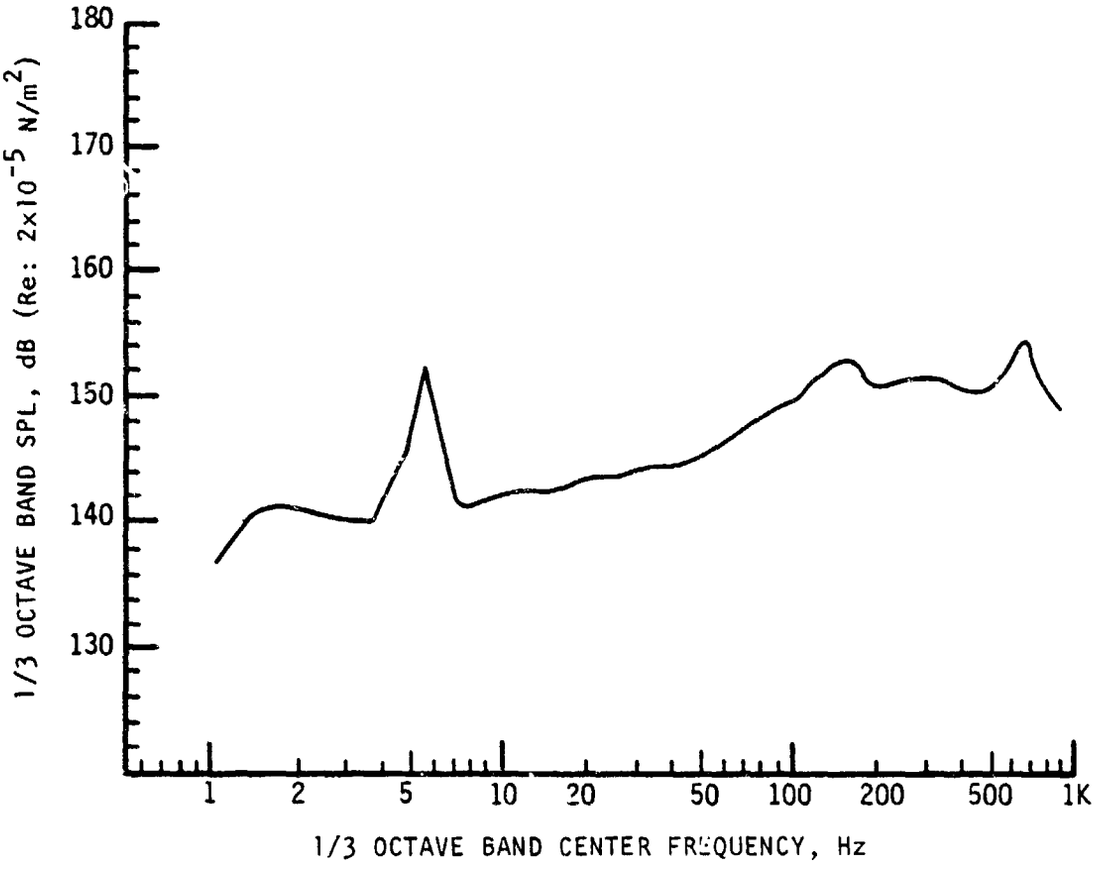

Figure 12. Envelope of SRB Aeroacoustic Spectra for Region D-II

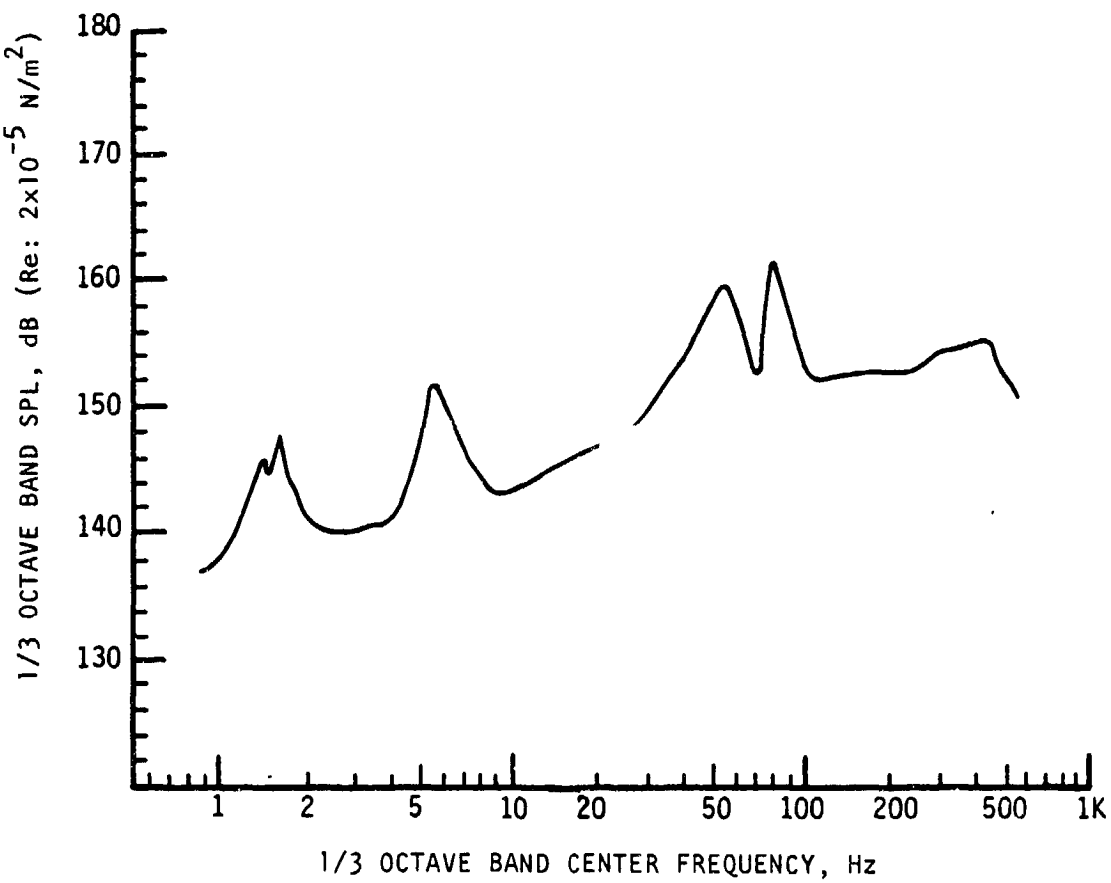

Figure 13. Envelope of SRB Aeroacoustic Spectra for Region D-III

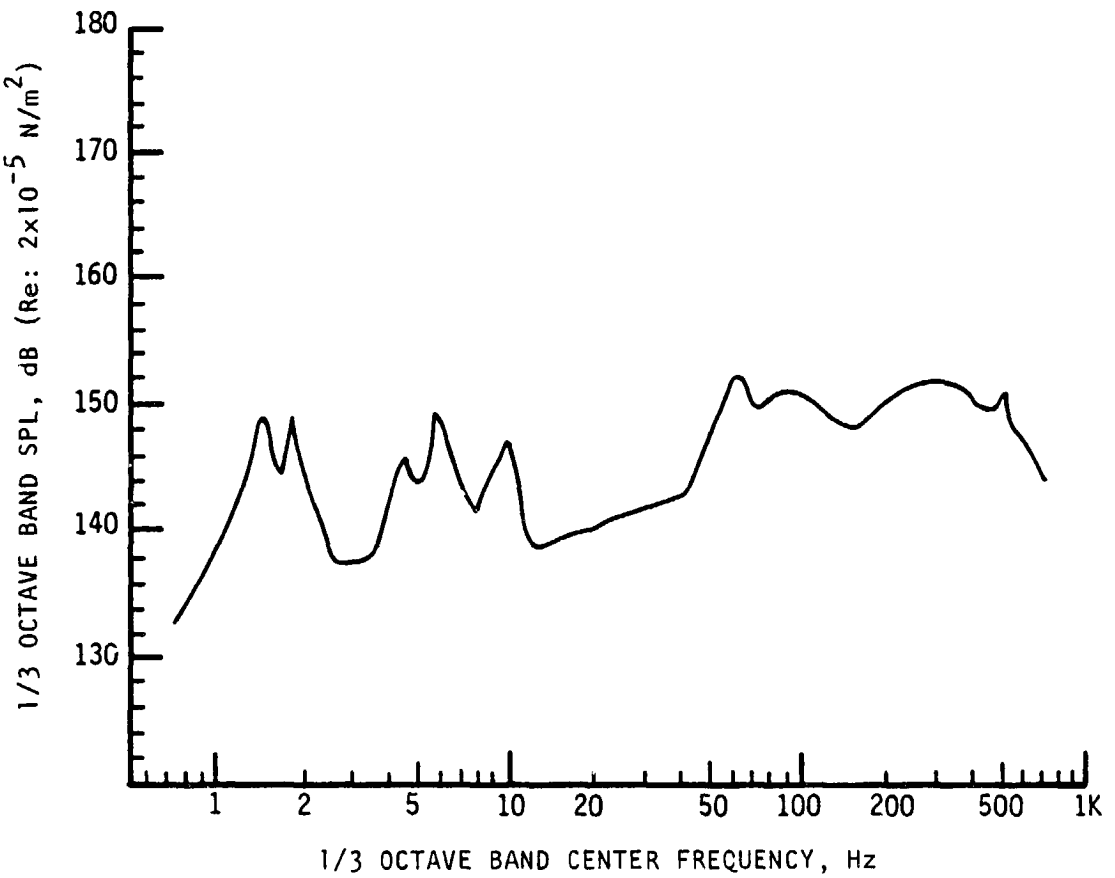

Figure 14. Envelope of SRB Aeroacoustic Spectra for Region D-IV

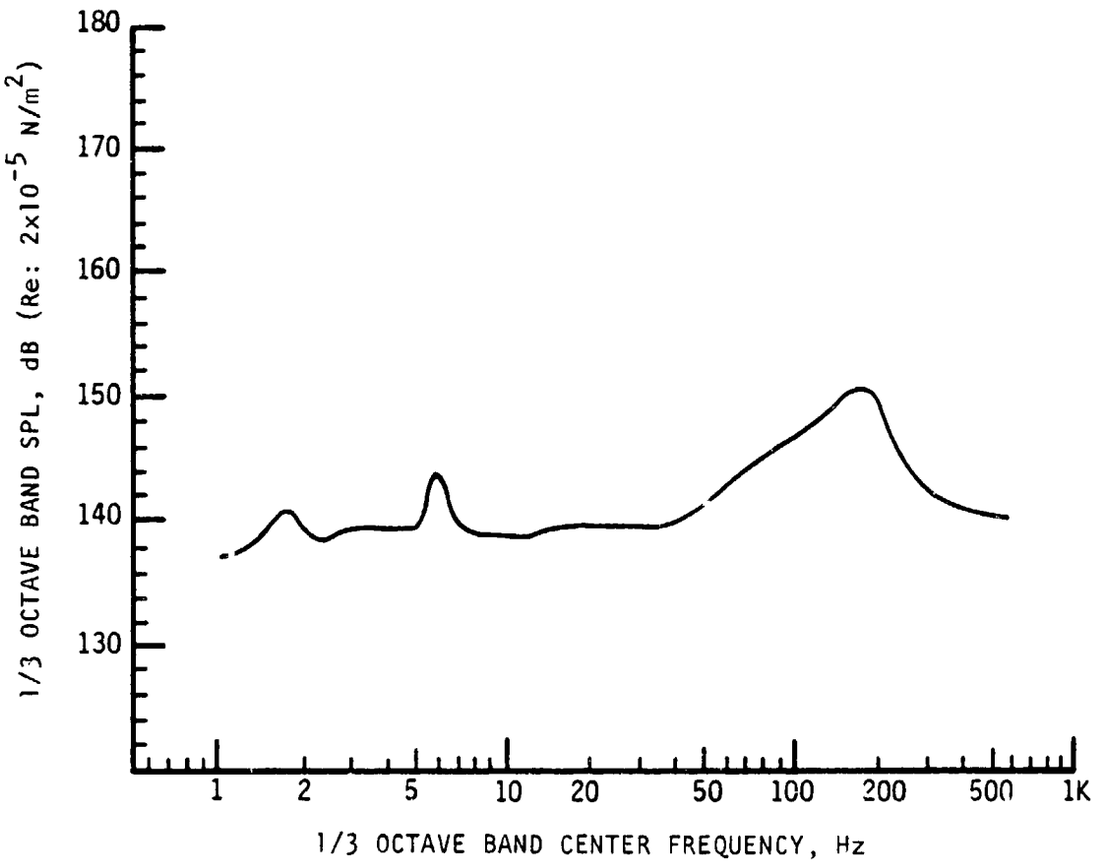

Figure 15. Envelope of SRB Aeroacoustic Spectra for Region D-V

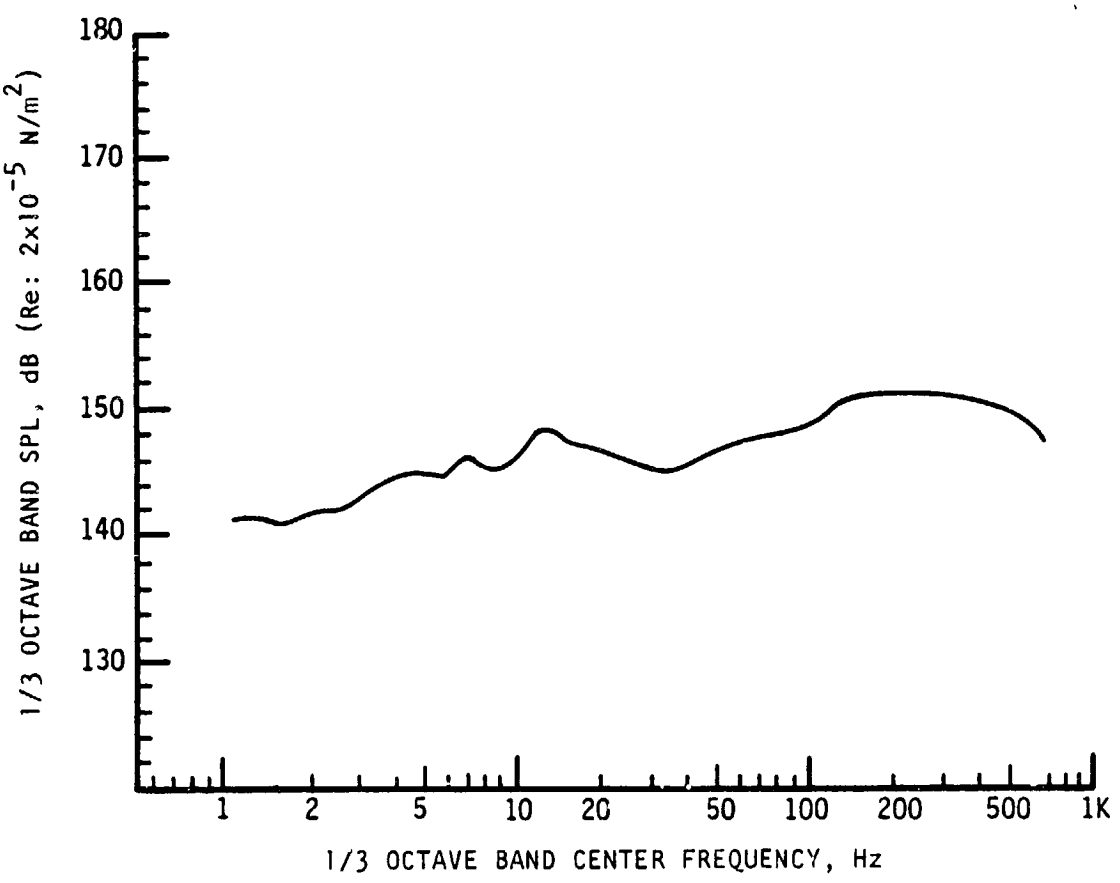

Figure 16. Envelope of SRB Aeroacoustic Spectra for Region D-VI

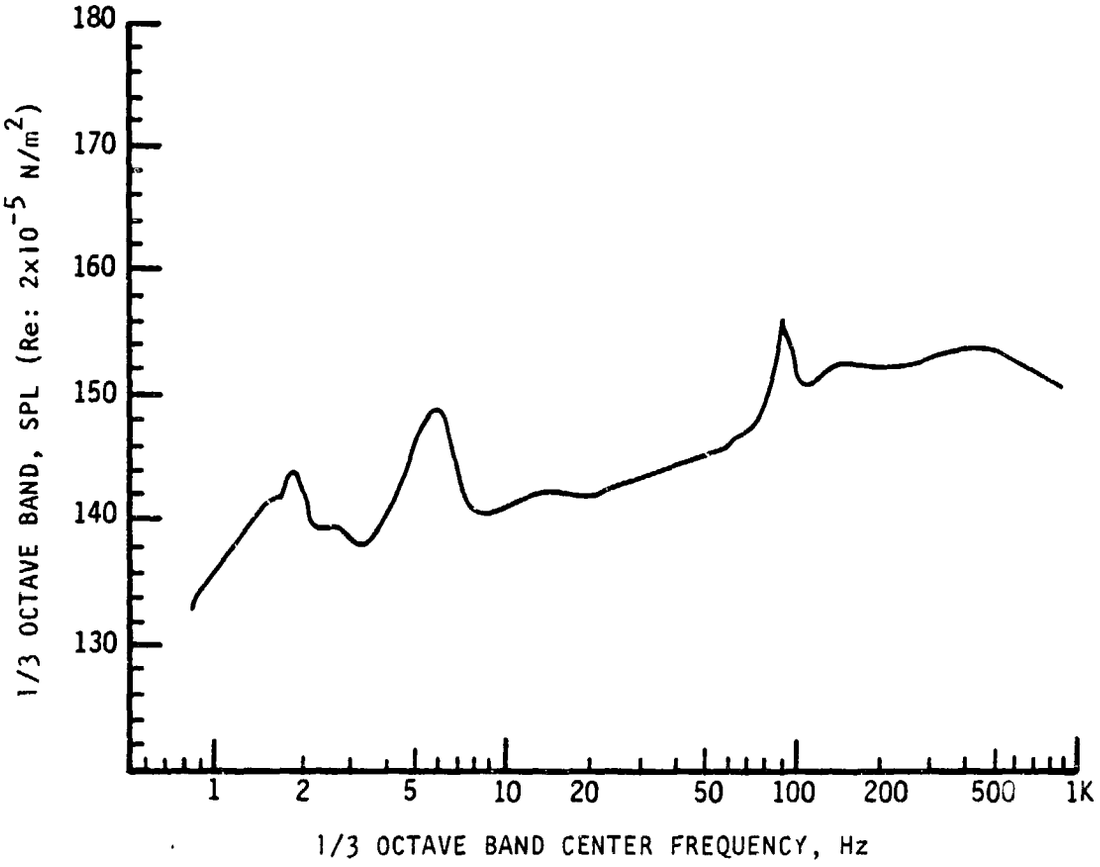

Figure 17. Envelope of SRB Aeroacoustic Spectra for Region D-VII

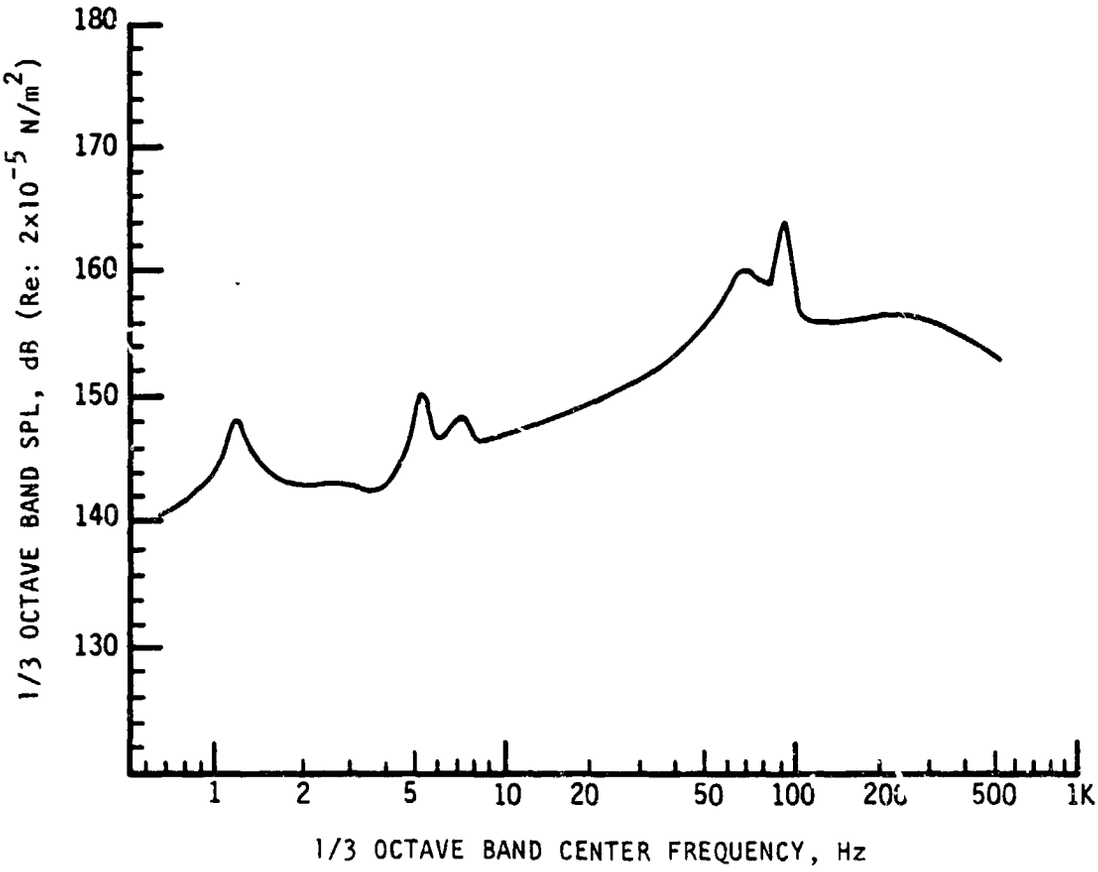

Figure 18. Envelope of SRB Aeroacoustic Spectra for Region D-VIII

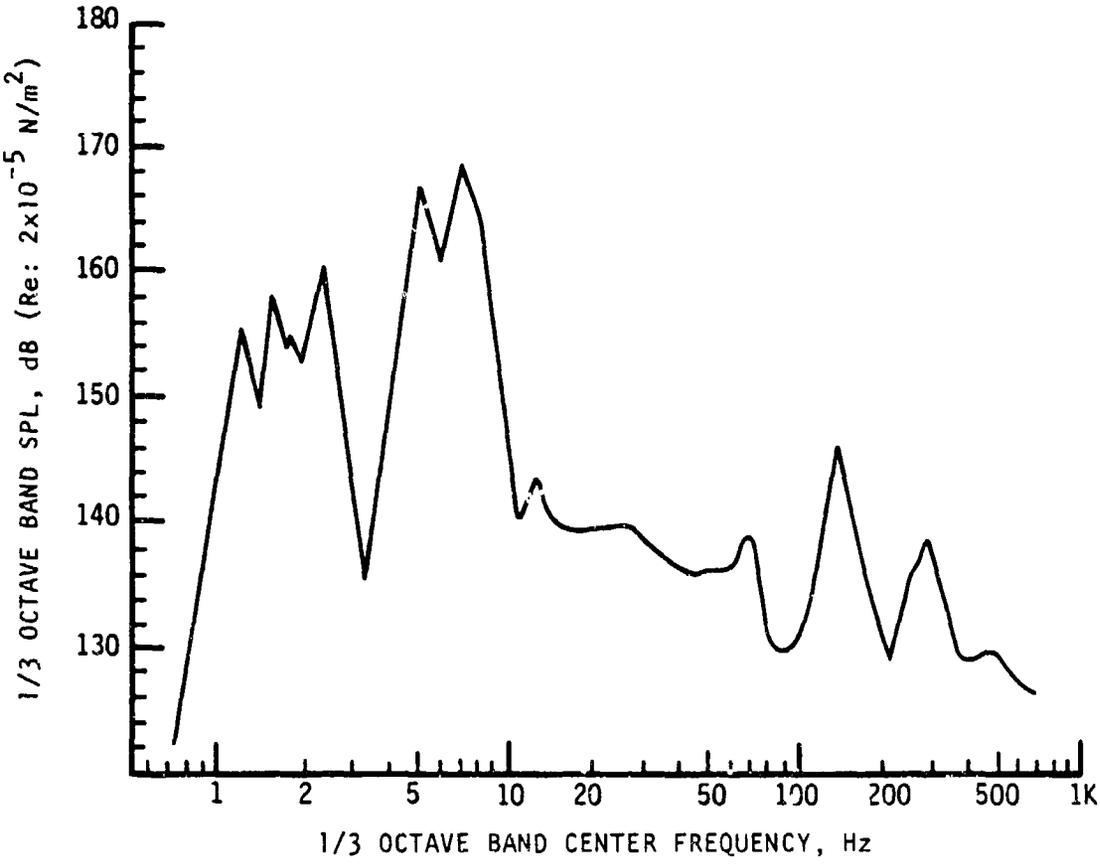

Figure 19. Envelope of SRB Aeroacoustic Spectra for Region E

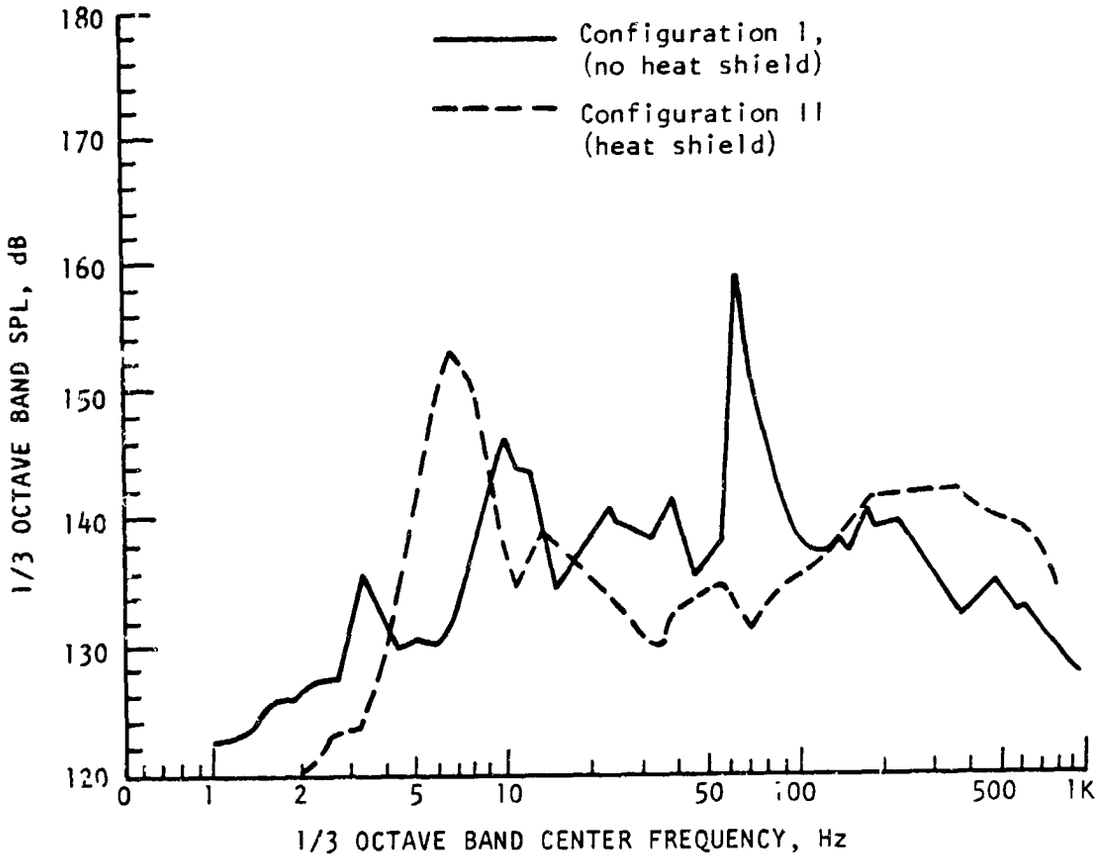

Figure 20. Spectrum Comparison for the Internal Skirt Cavity at $M_\infty = 2.75$

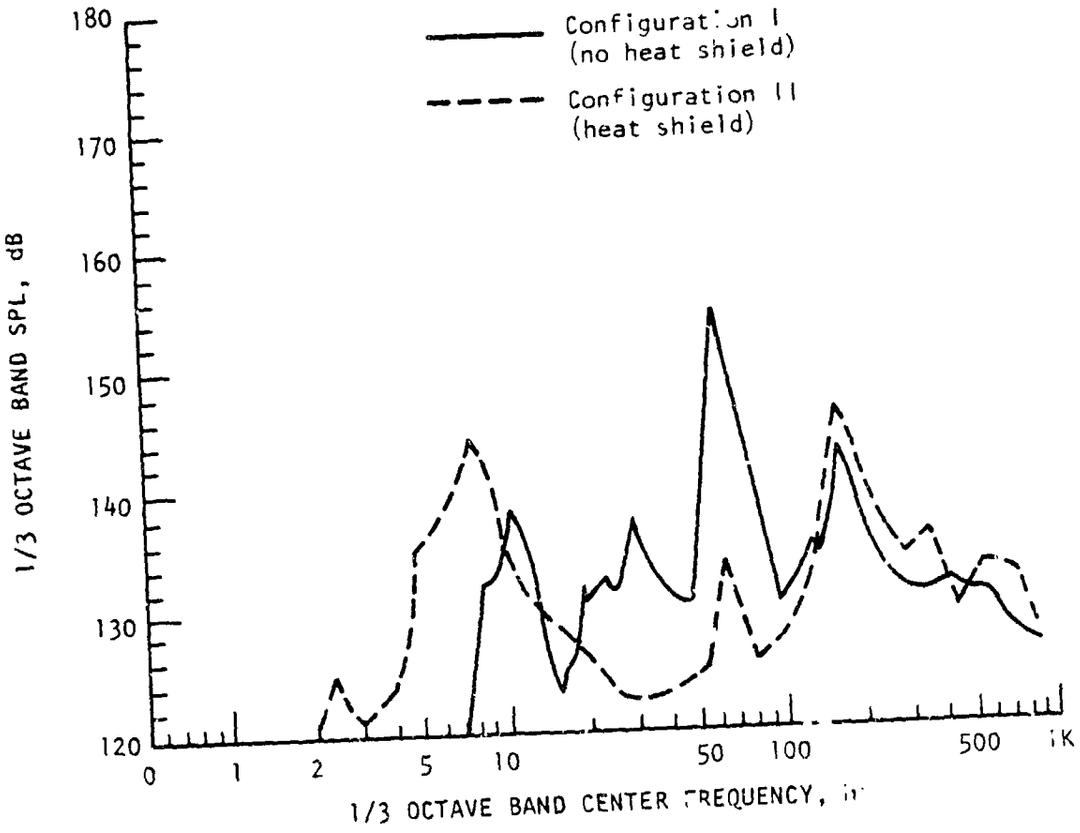

Figure 21. Spectrum Comparison for the Internal Skirt Cavity at $M_\infty = 3.5$

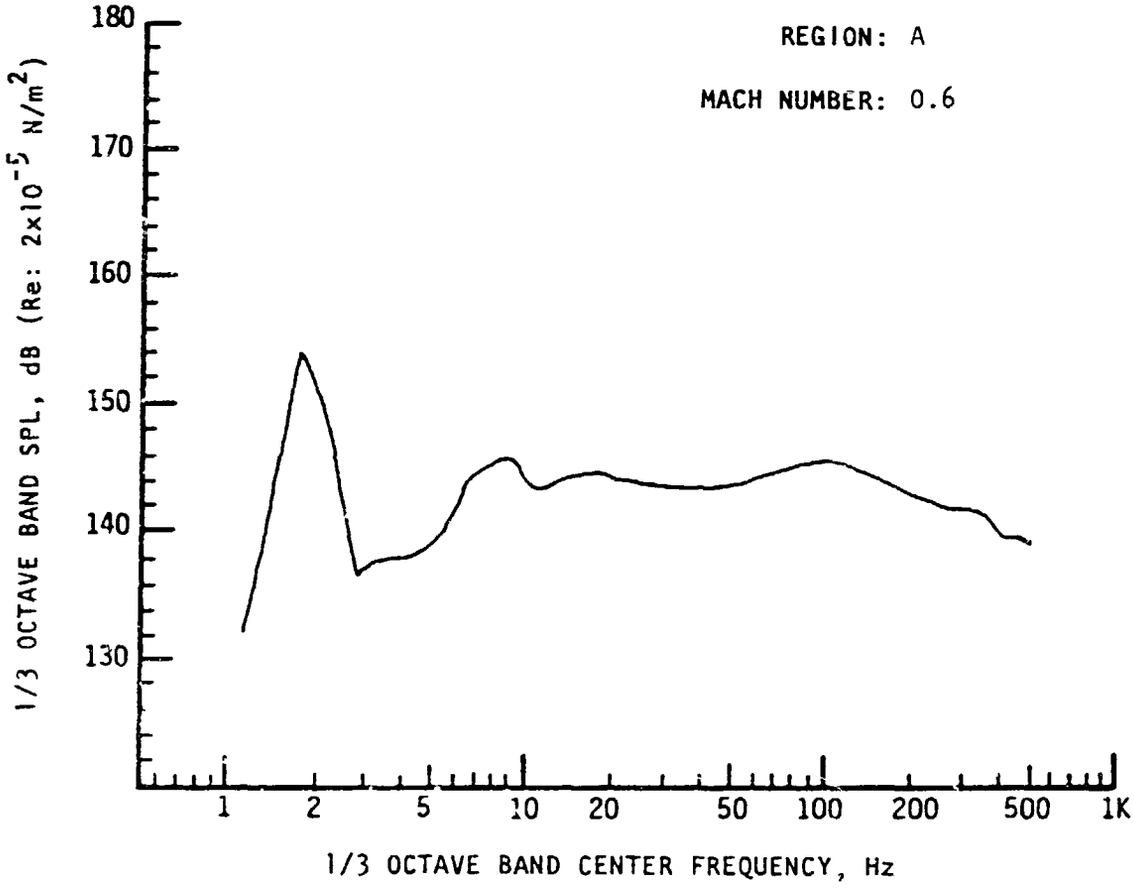

Note: Results based on 95 percentile OAFPL from Monte Carlo trajectory simulation.

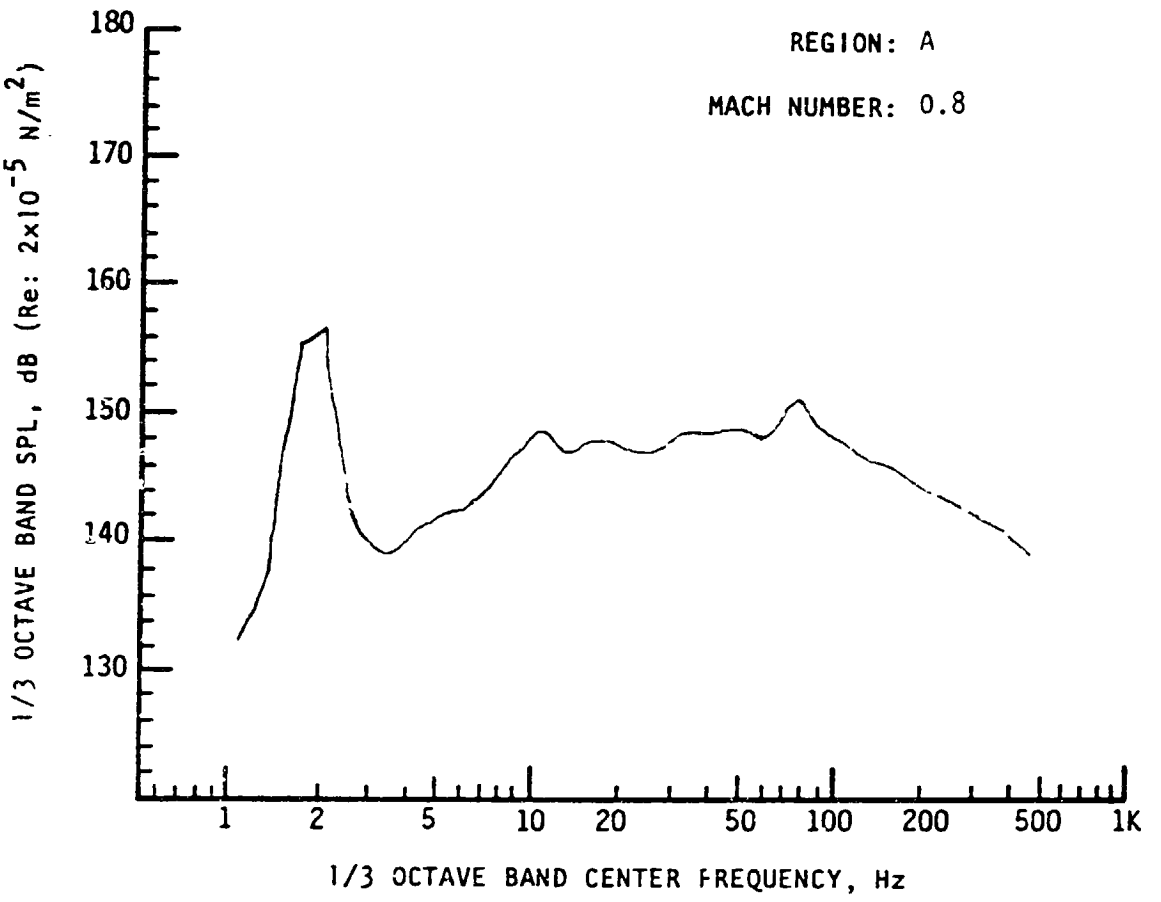

Note: Results based on 95 percentile OAFPL from Monte Carlo trajectory simulation.

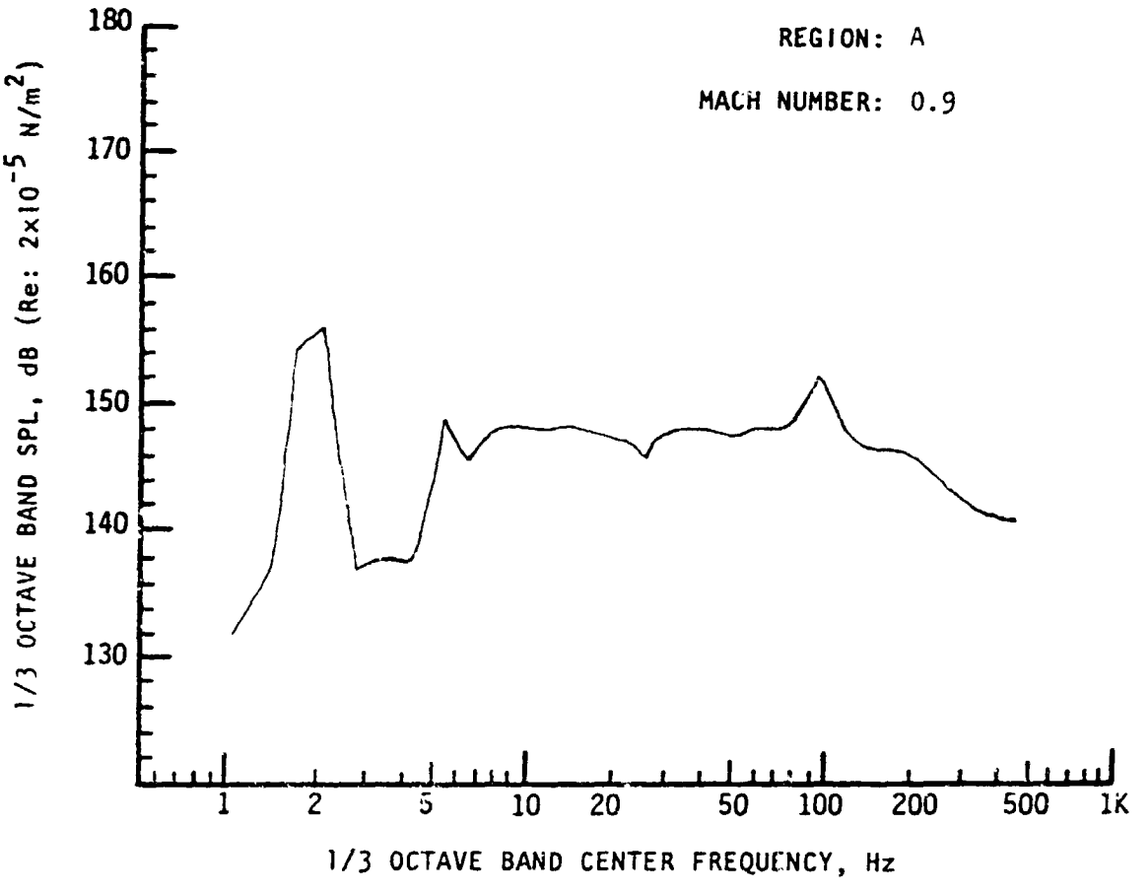

Note: Results based on 95 percentile OAFPL from Monte Carlo trajectory simulation.

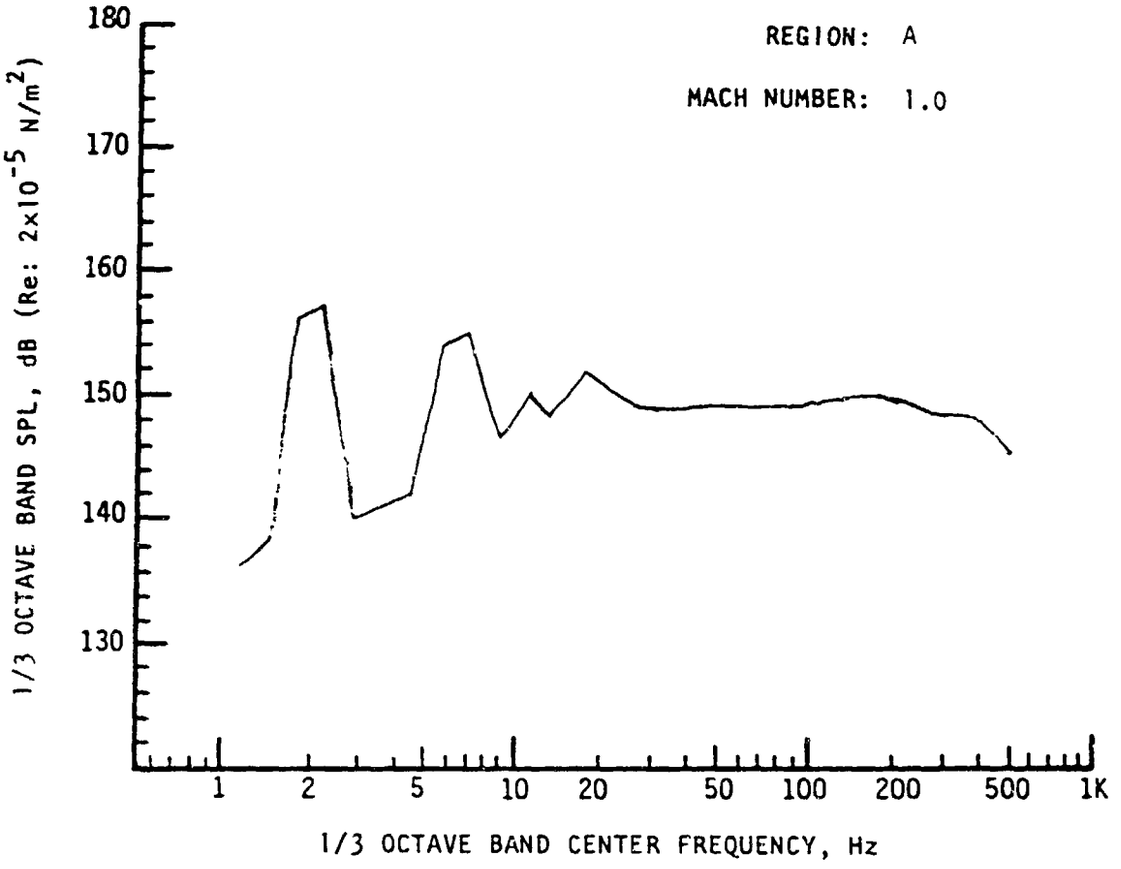

Note: Results based on 95 percentile OAFPL from Monte Carlo trajectory simulation.

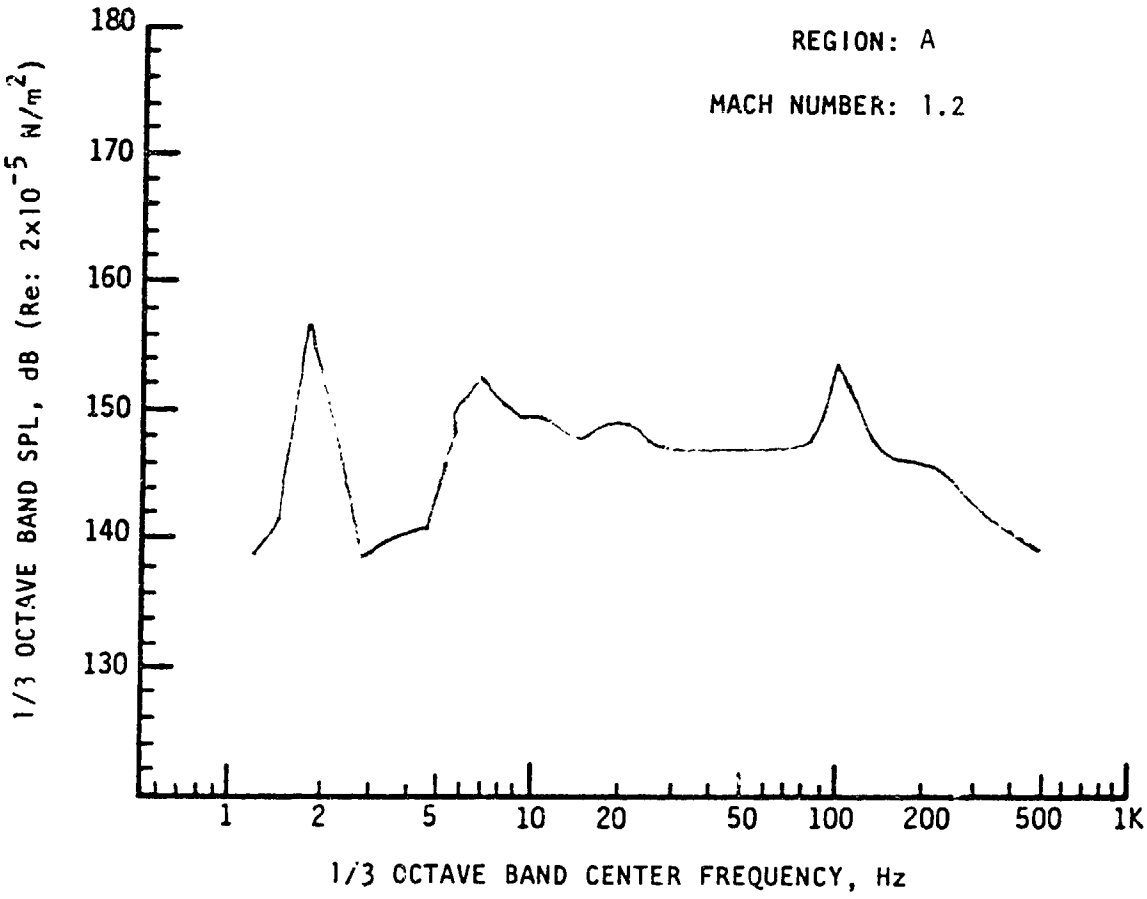

Note: Results based on 95 percentile OAFPL from Monte Carlo trajectory simulation.

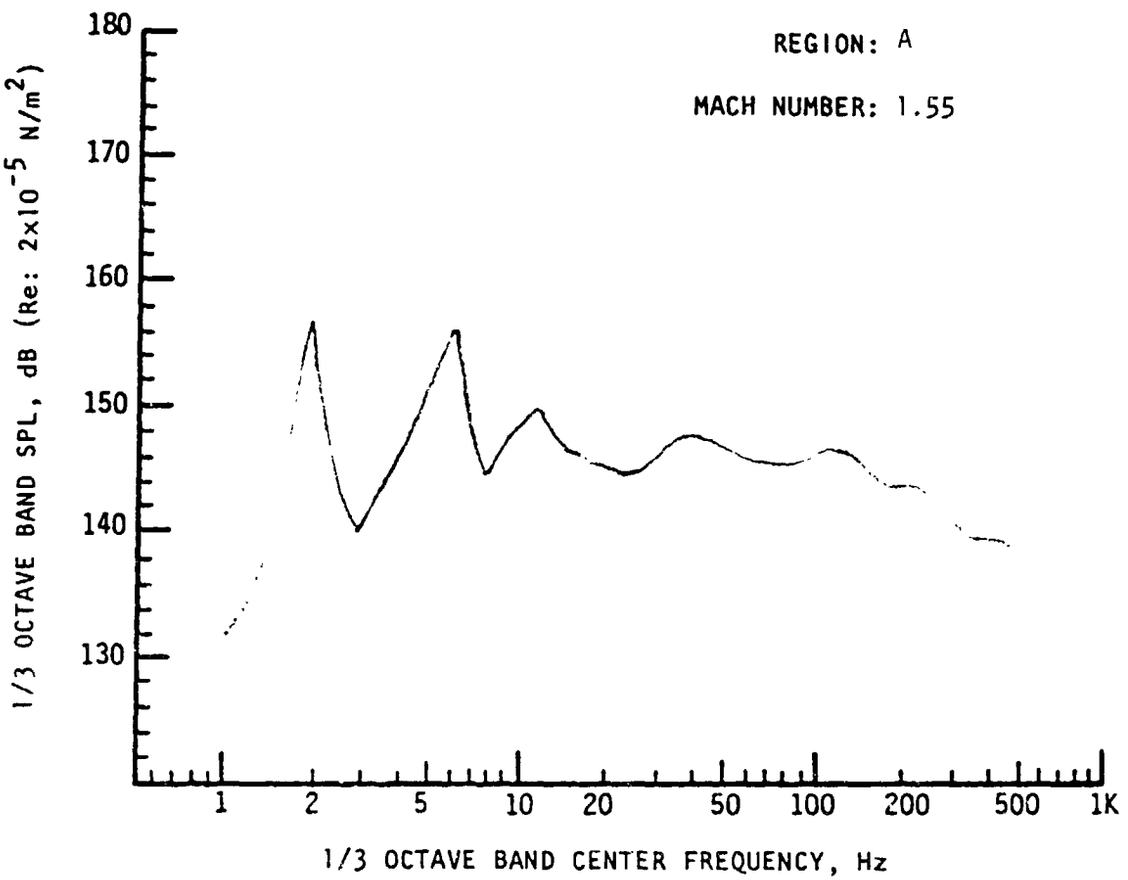

Note: Results based on 95 percentile OAFPL from Monte Carlo trajectory simulation.

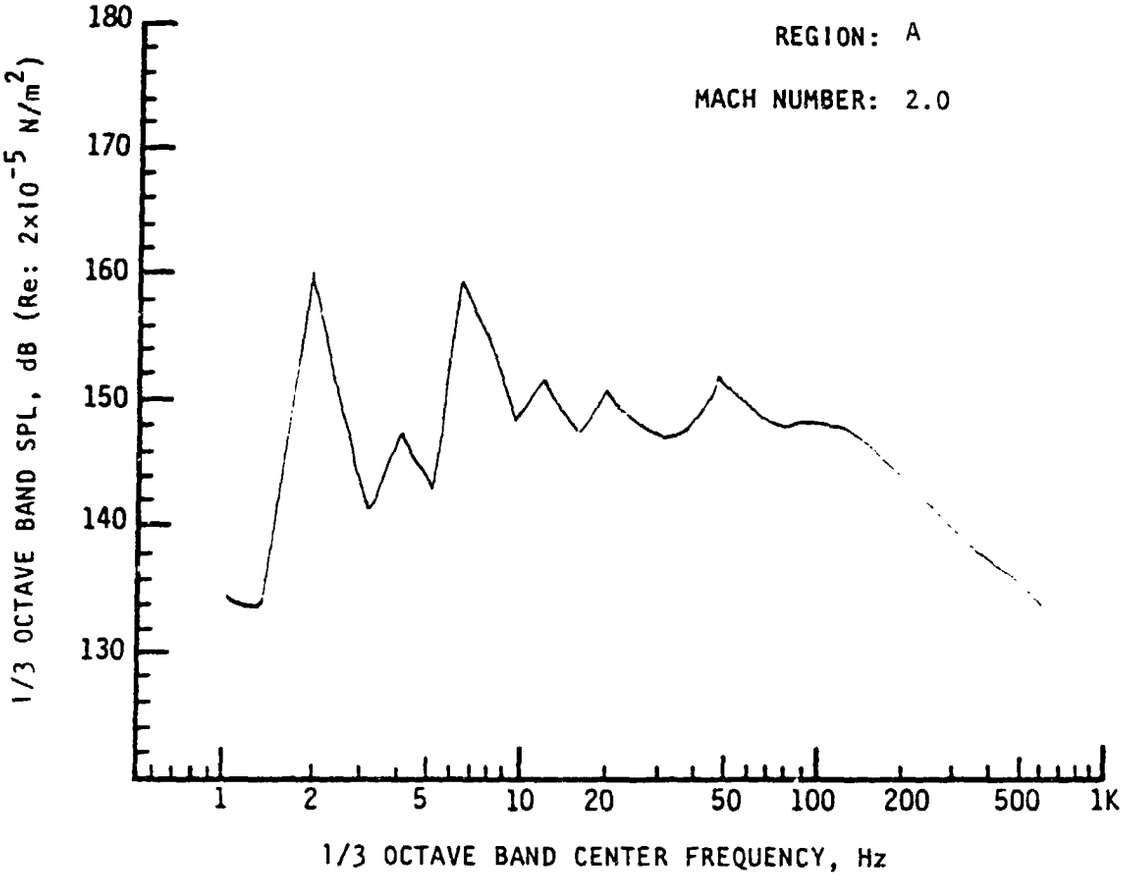

Note: Results based on 95 percentile OAFPL from Monte Carlo trajectory simulation.

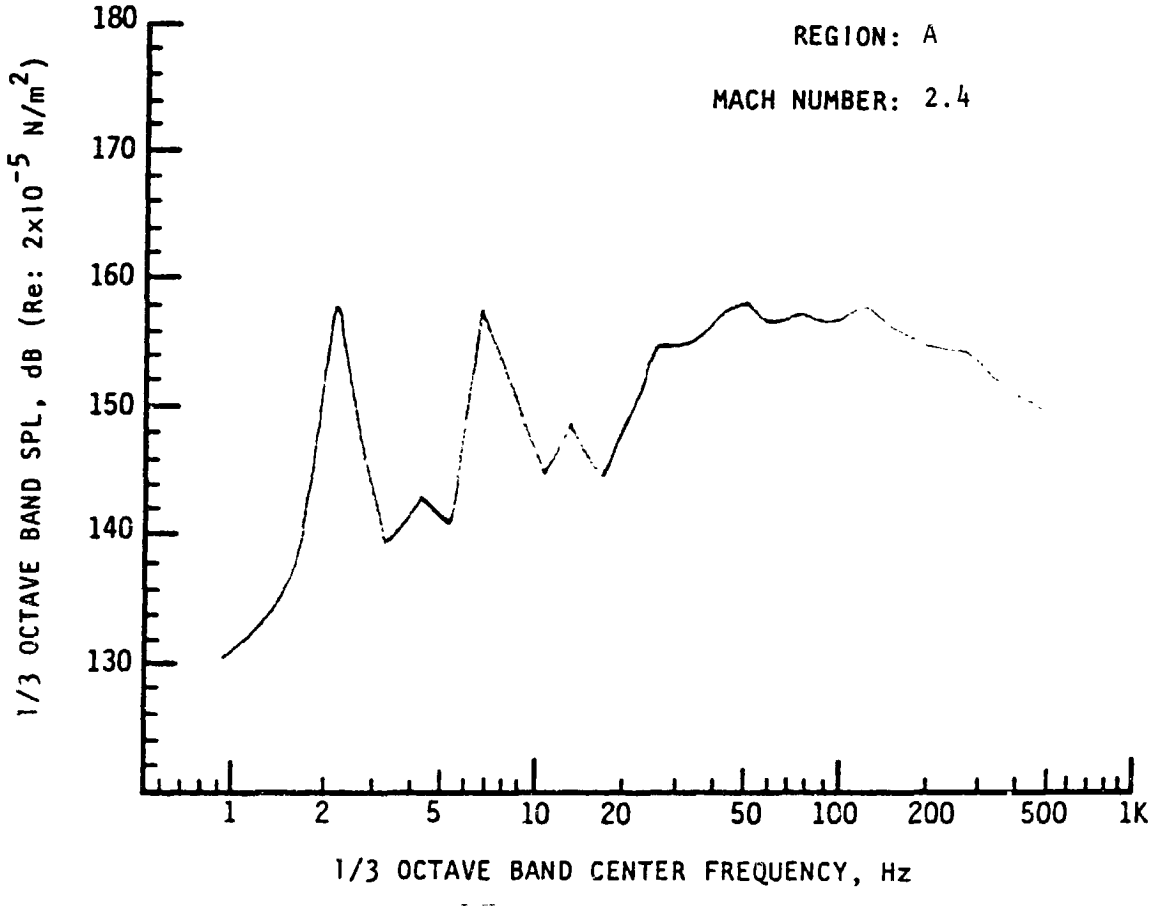

Note: Results based on 95 percentile OAFPL from Monte Carlo trajectory simulation.

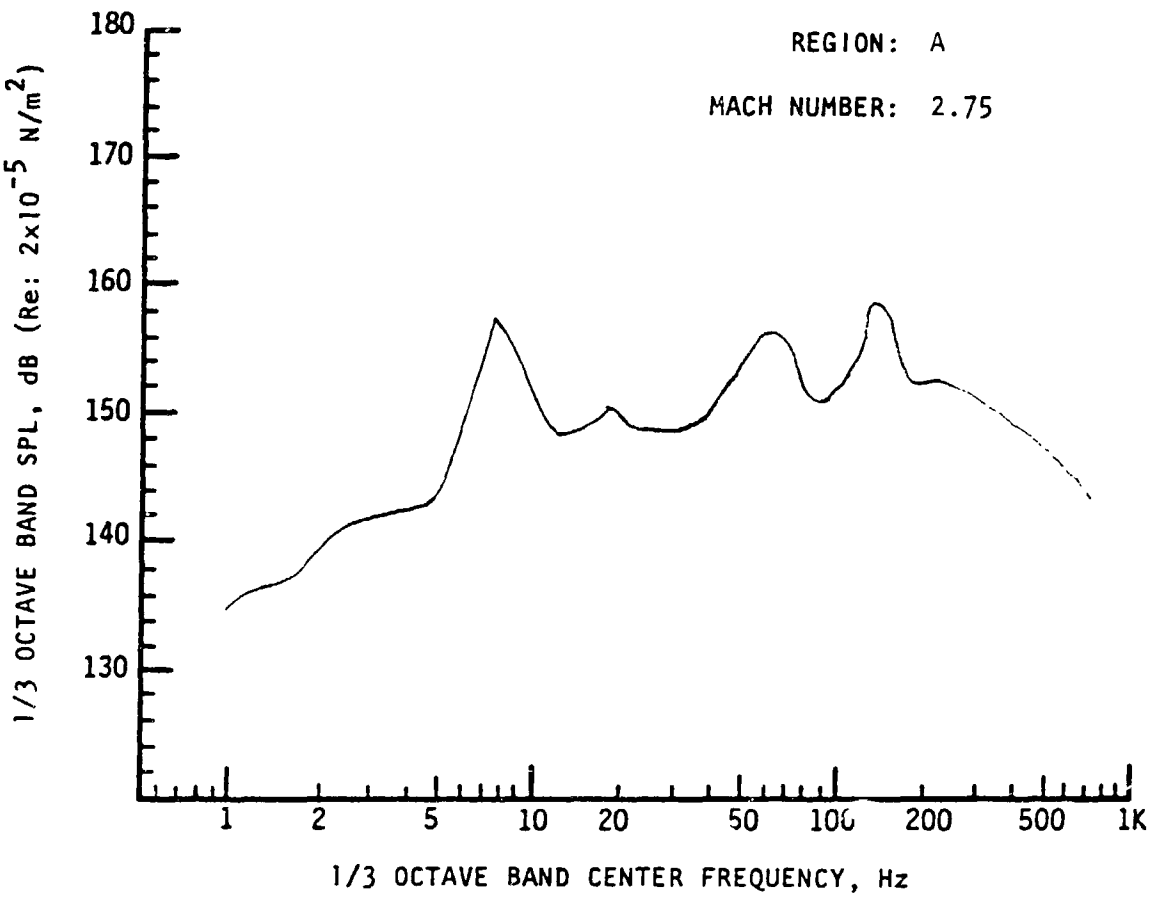

Note: Results based on 95 percentile OAFPL from Monte Carlo trajectory simulation.

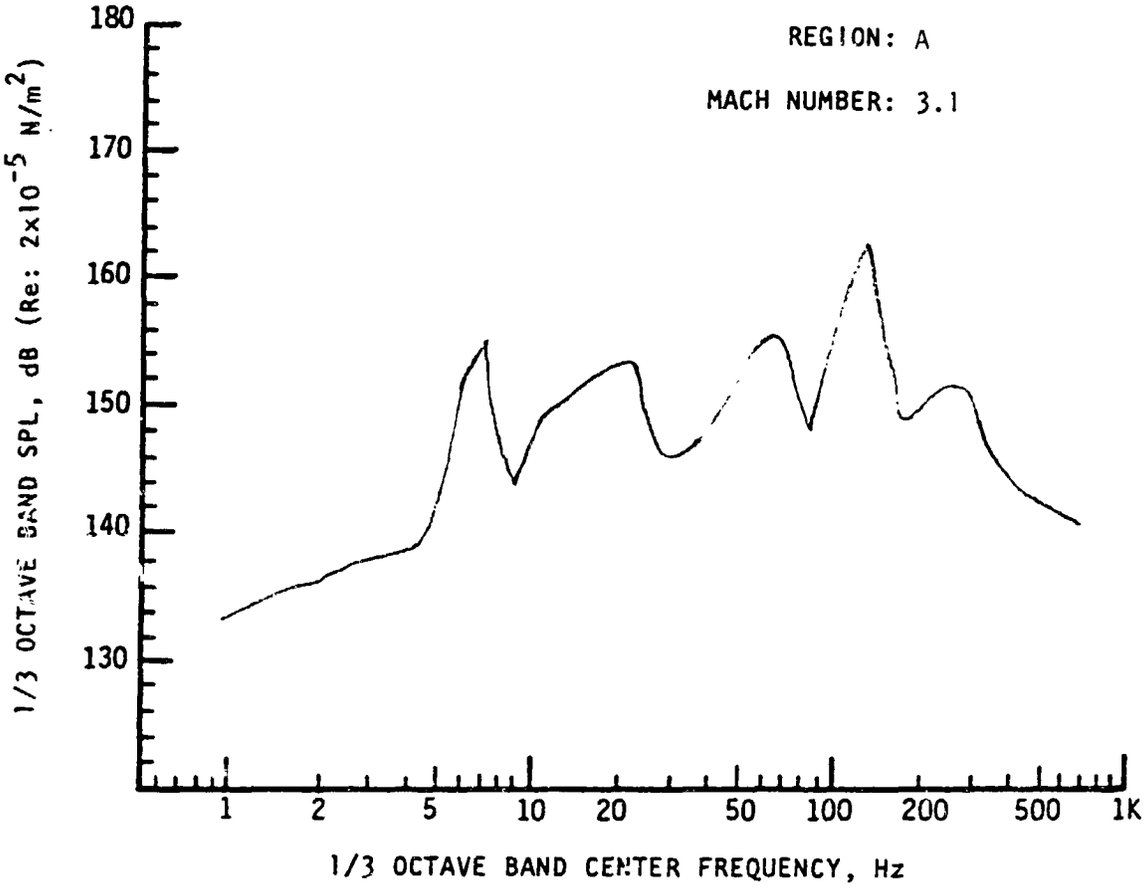

Note: Results based on 95 percentile OAFPL from Monte Carlo trajectory simulation.

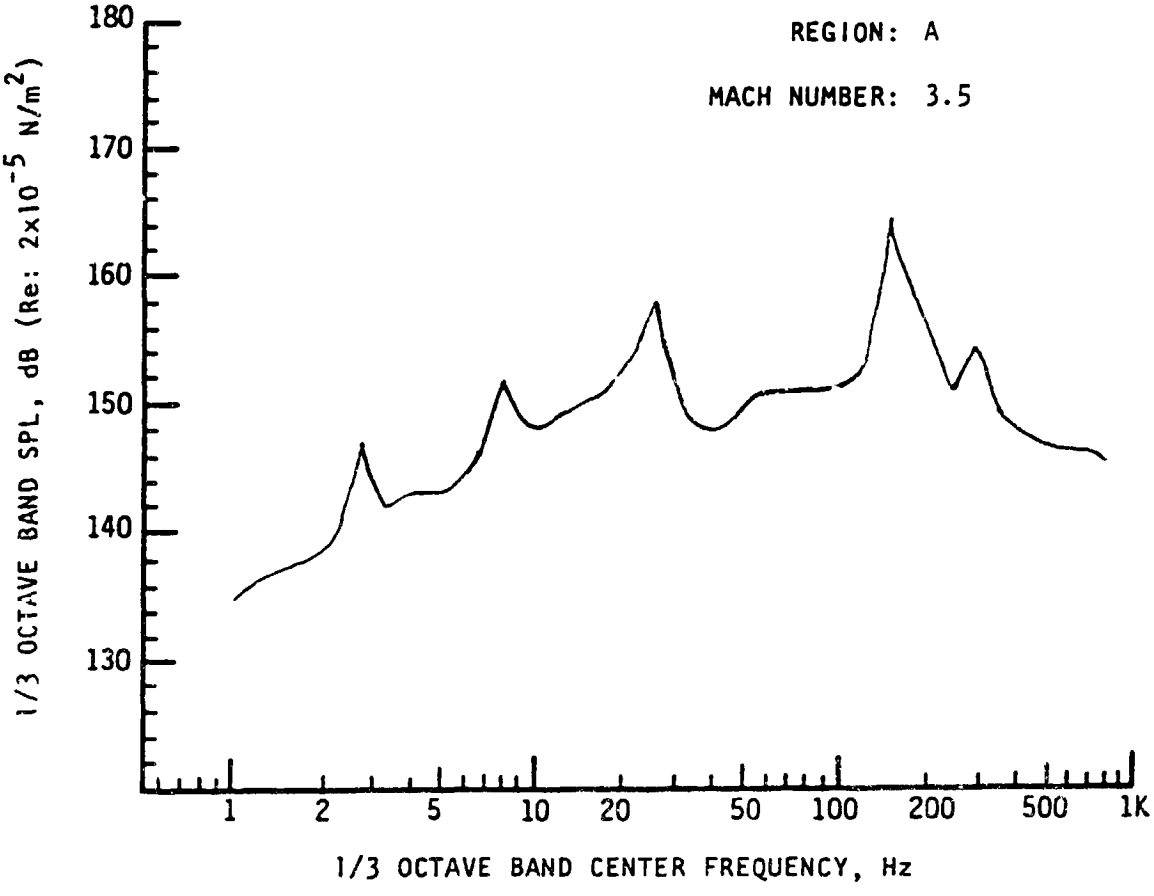

Note: Results based on 95 percentile OAFPL from Monte Carlo trajectory simulation.

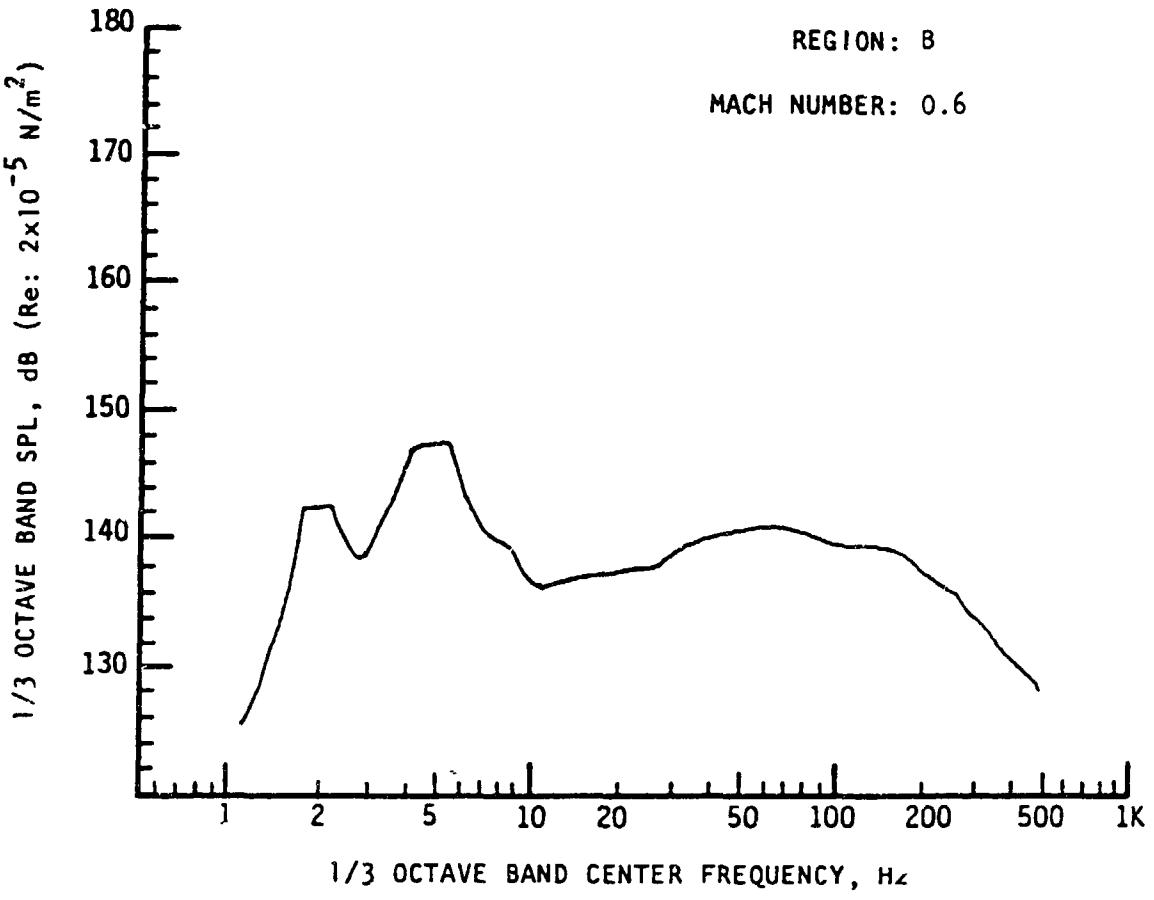

Note: Results based on 95 percentile OAFPL from Monte Carlo trajectory simulation.

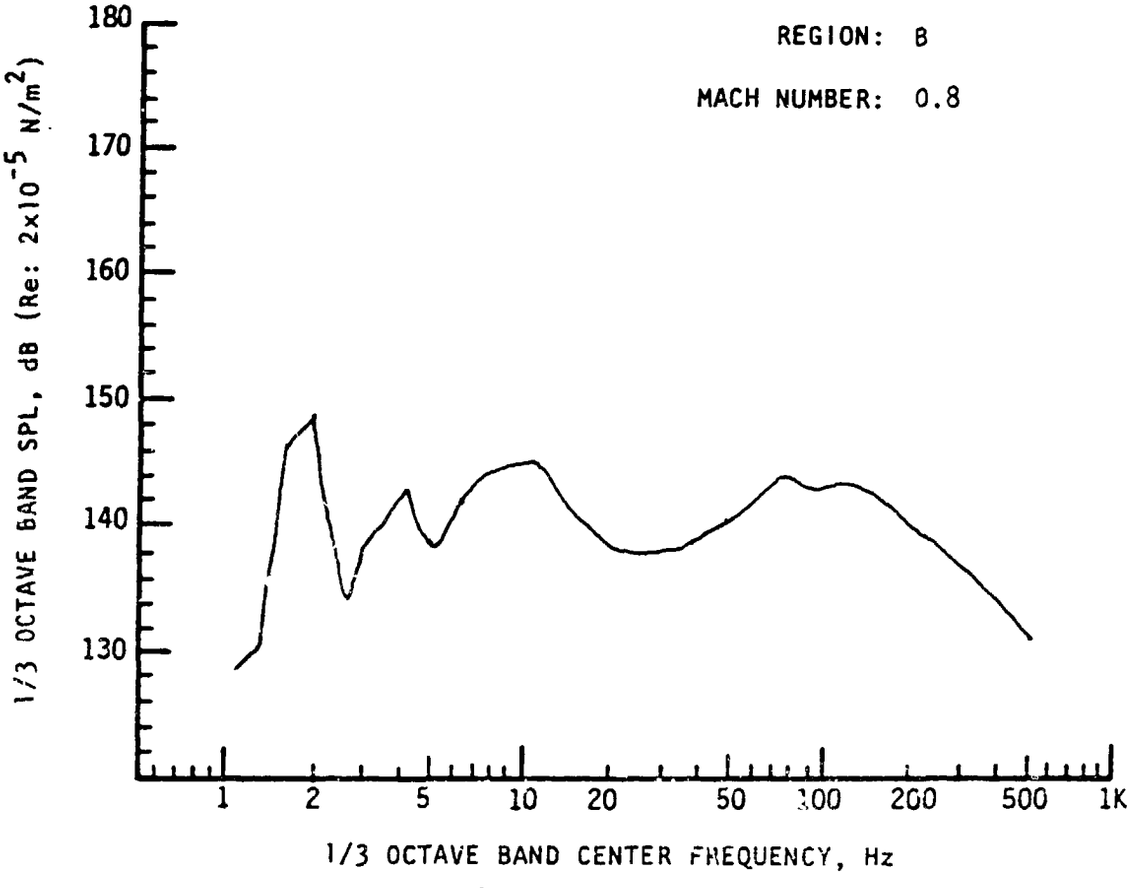

Note: Results based on 95 percentile OAFPL from Monte Carlo trajectory simulation.

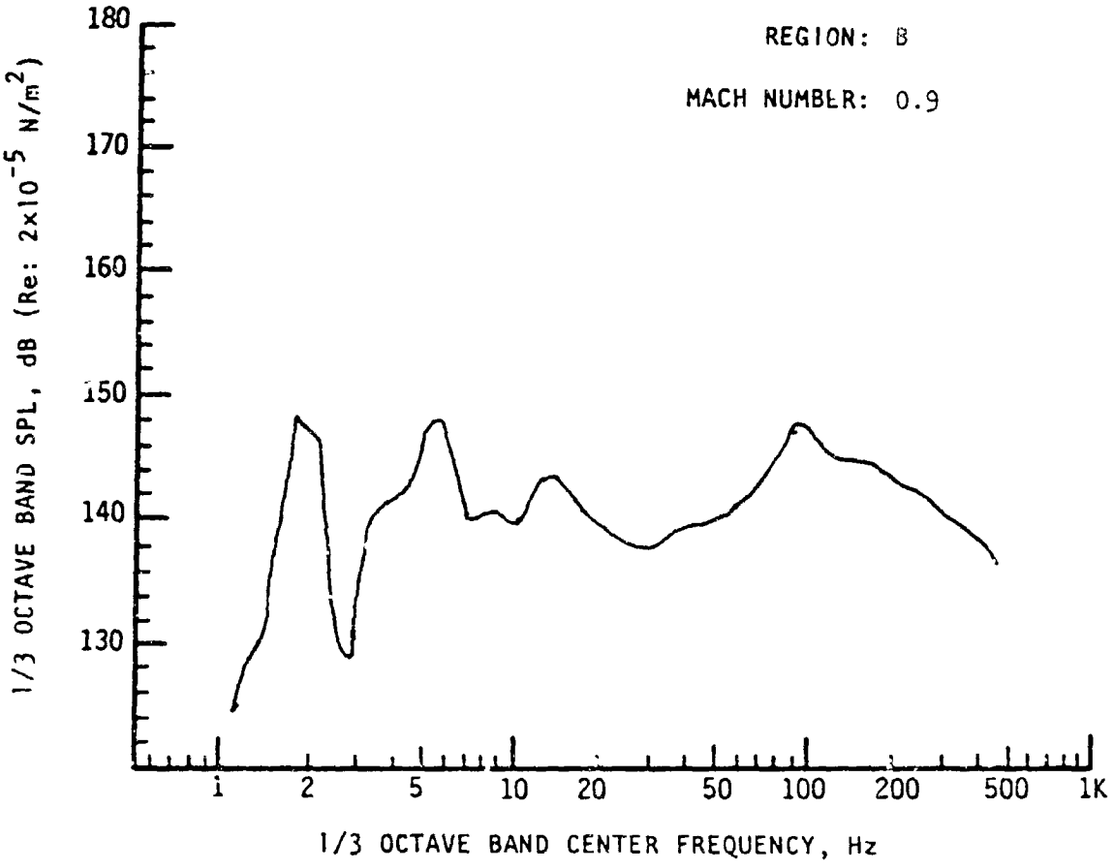

Note: Results based on 95 percentile OAFPL from Monte Carlo trajectory simulation.

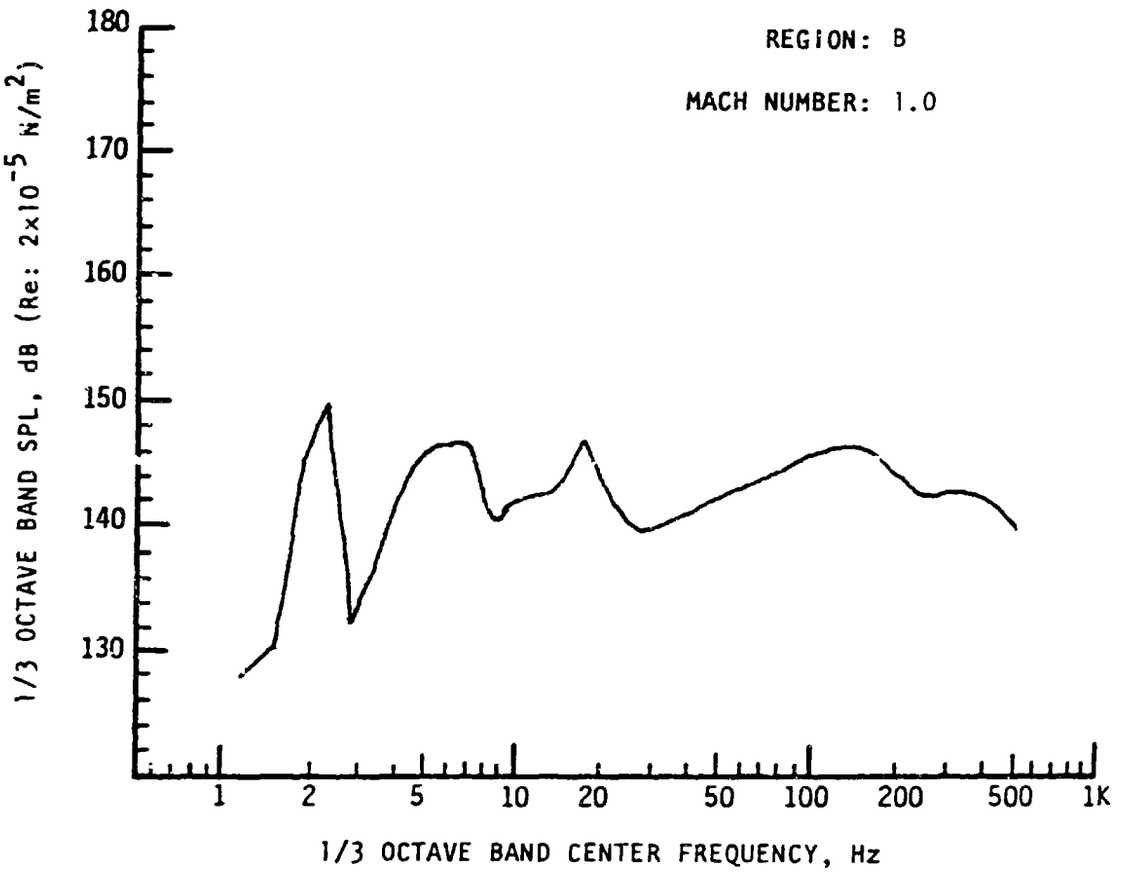

Note: Results based on 95 percentile OAFPL from Monte Carlo trajectory simulation.

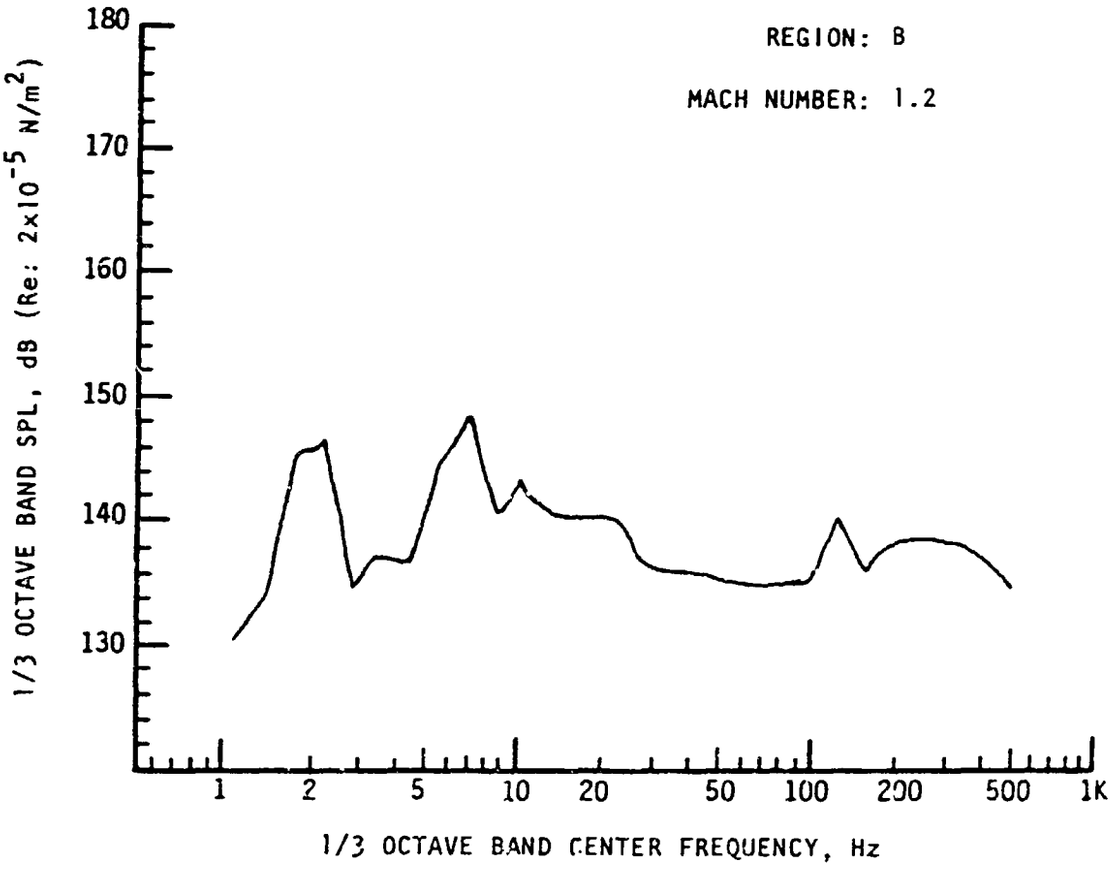

Note: Results based on 95 percentile OAFPL from Monte Carlo trajectory simulation.

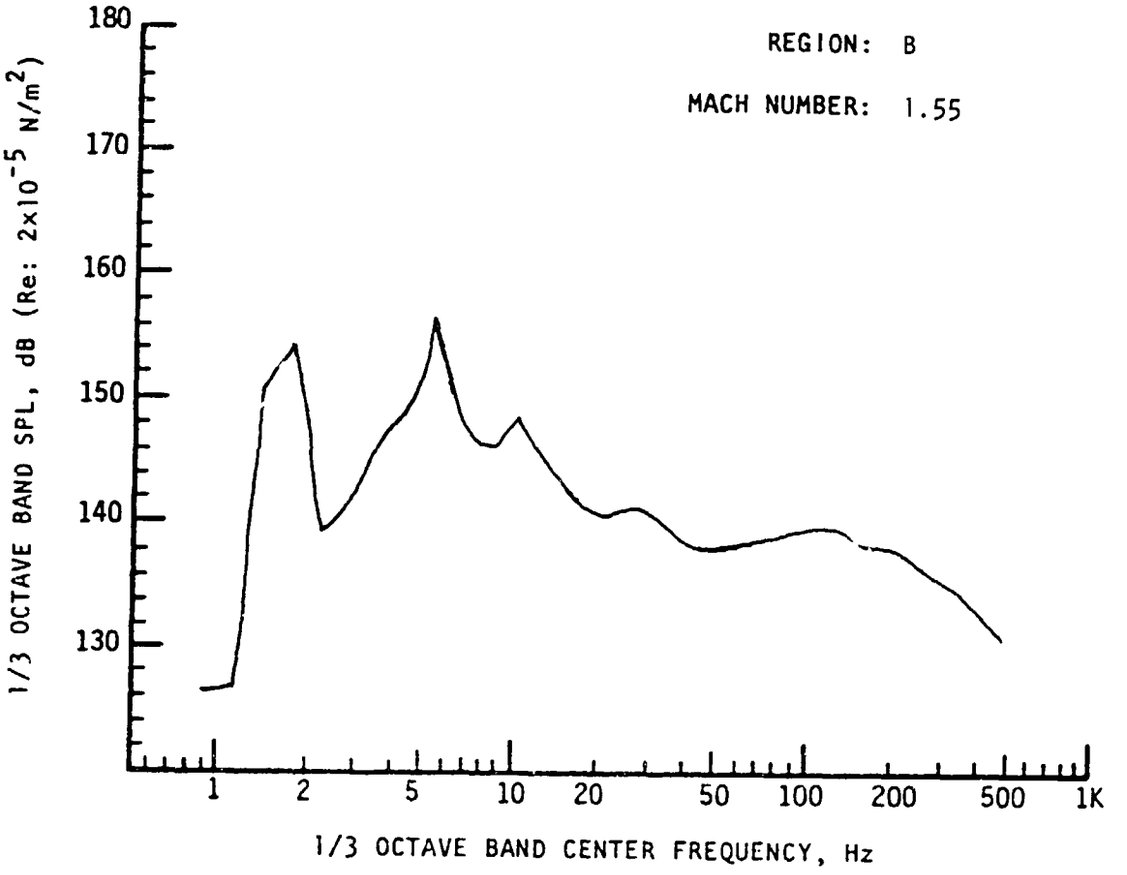

Note: Results based on 95 percentile OAFPL from Monte Carlo trajectory simulation.

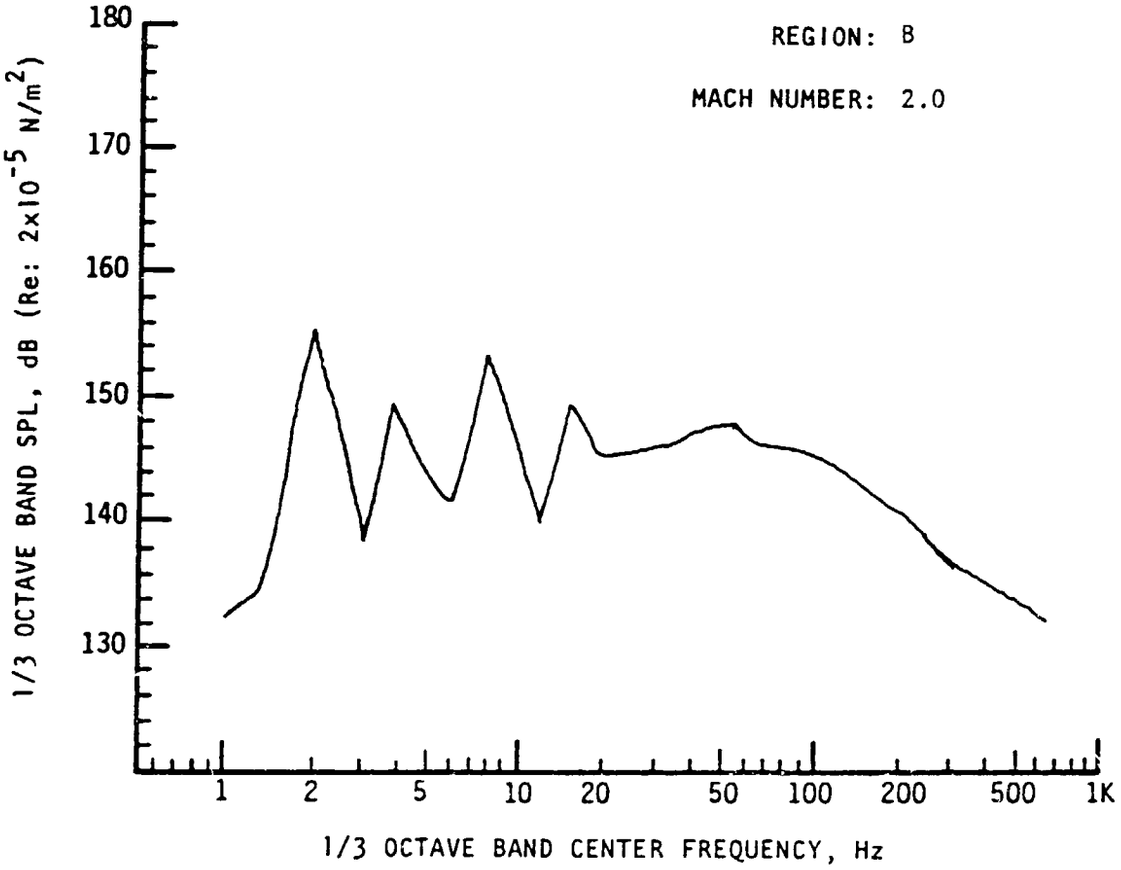

Note: Results based on 95 percentile OAFPL from Monte Carlo trajectory simulation.

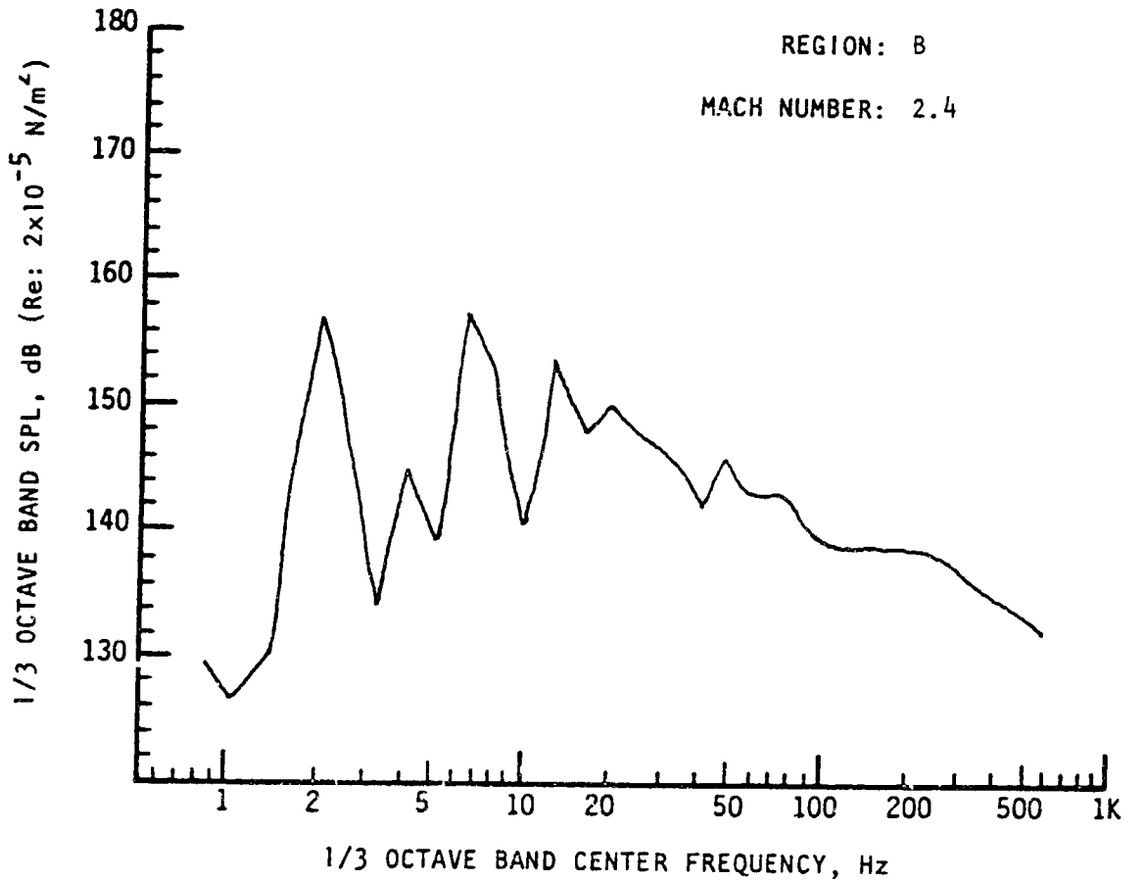

Note: Results based on 95 percentile OAFPL from Monte Carlo trajectory simulation.

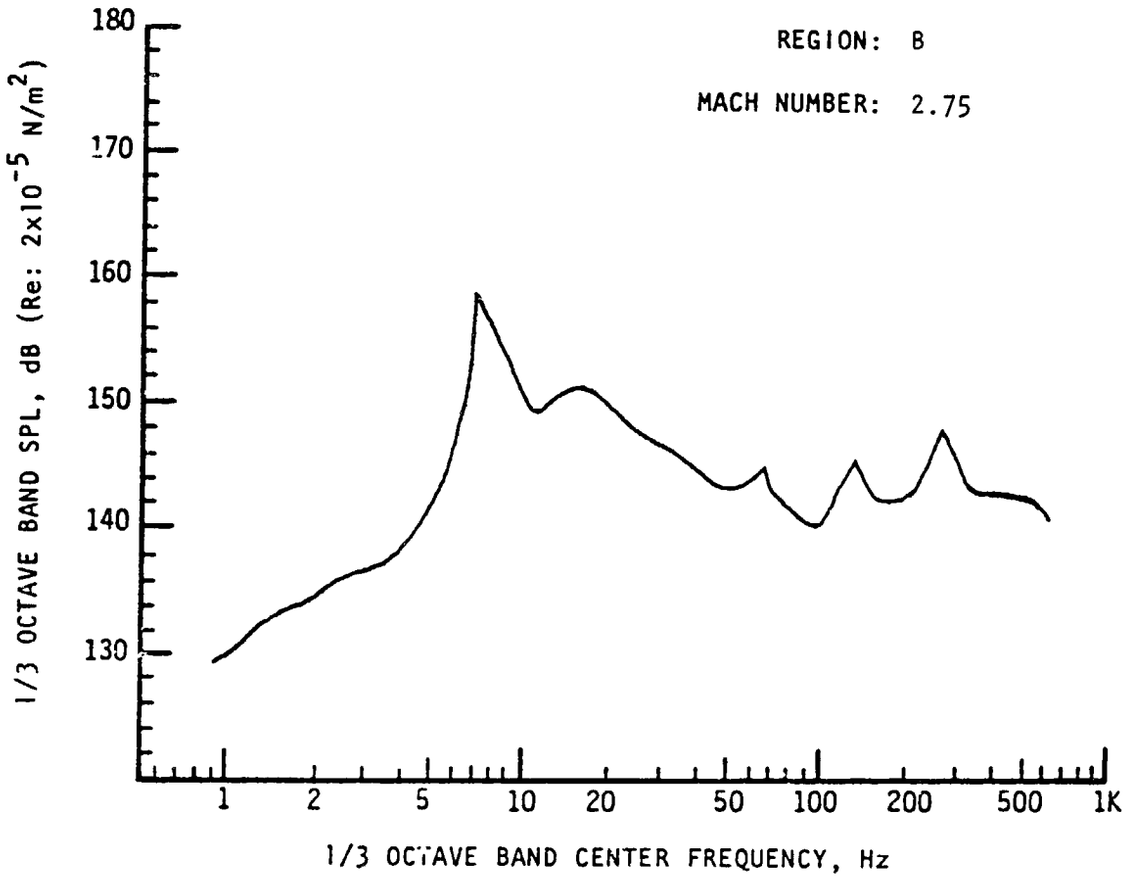

Note: Results based on 95 percentile OAFPL from Monte Carlo trajectory simulation.

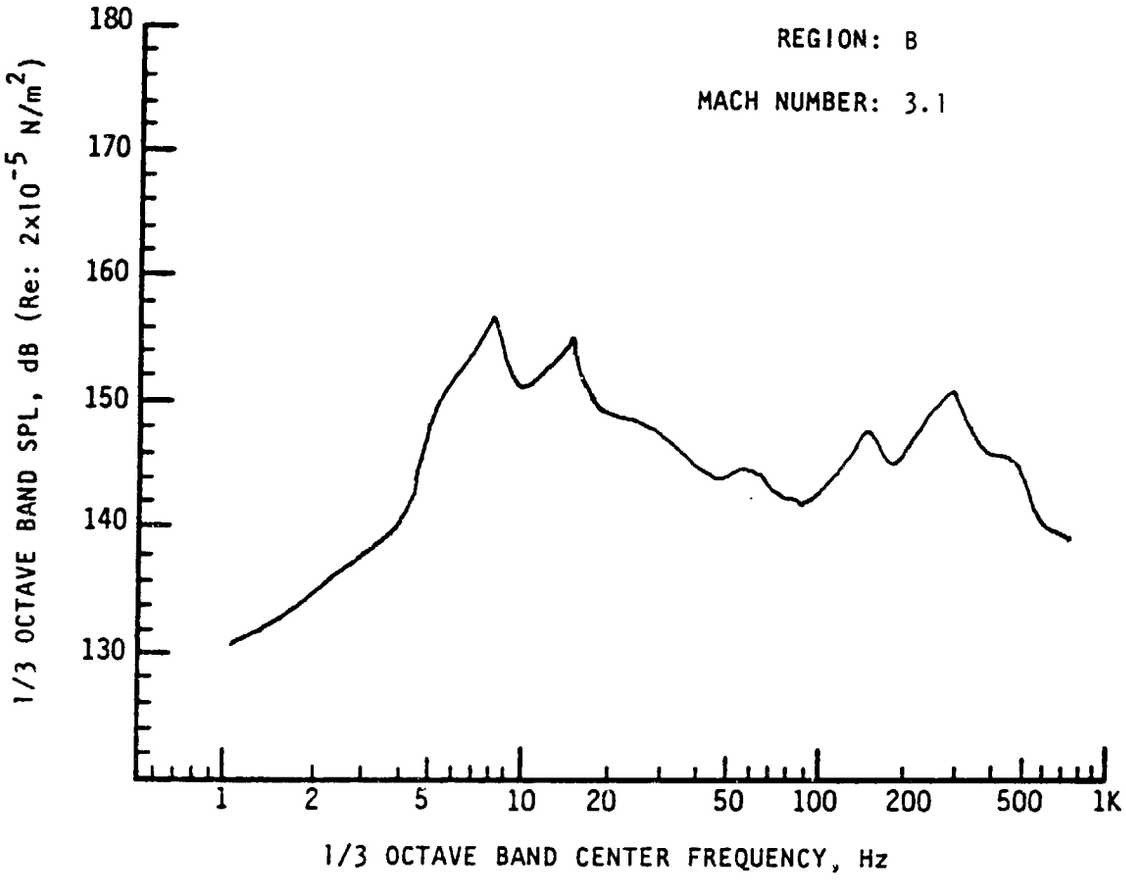

Note: Results based on 95 percentile OAFPL from Monte Carlo trajectory simulation.

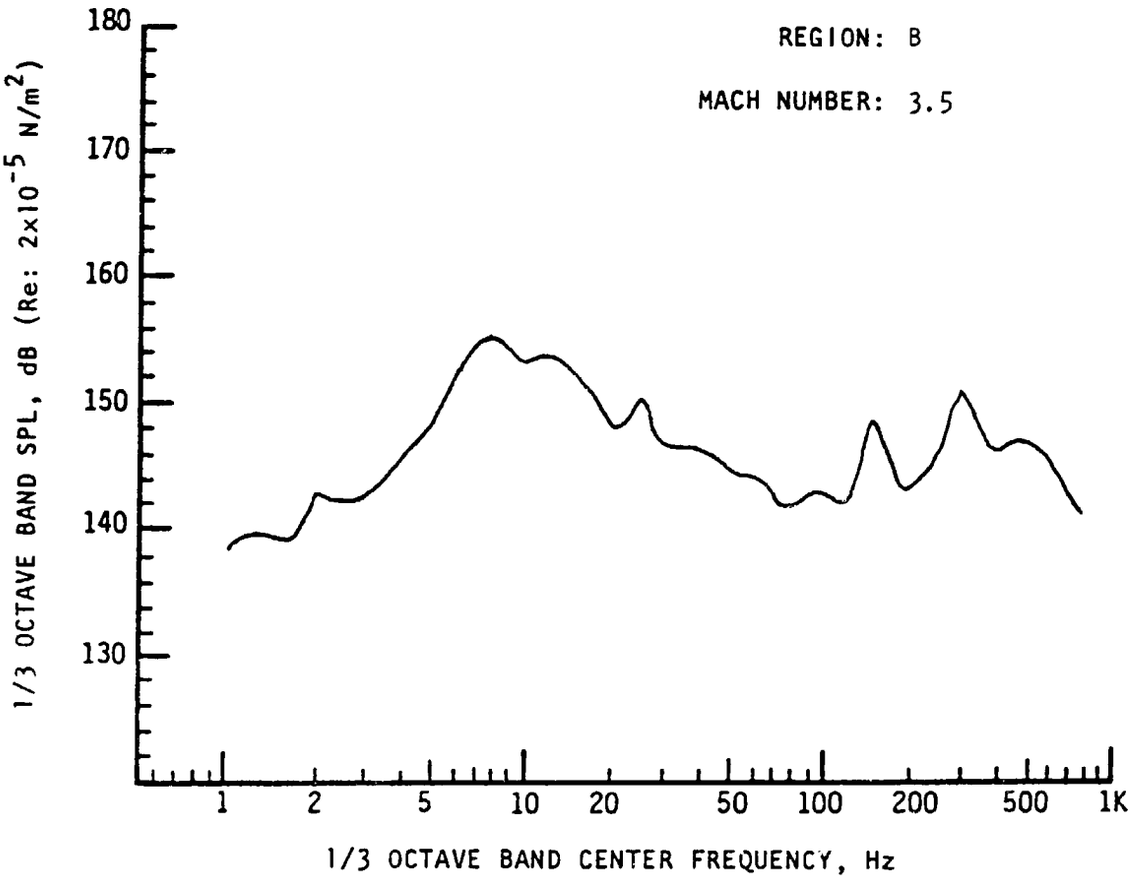

Note: Results based on 95 percentile OAFPL from Monte Carlo trajectory simulation.

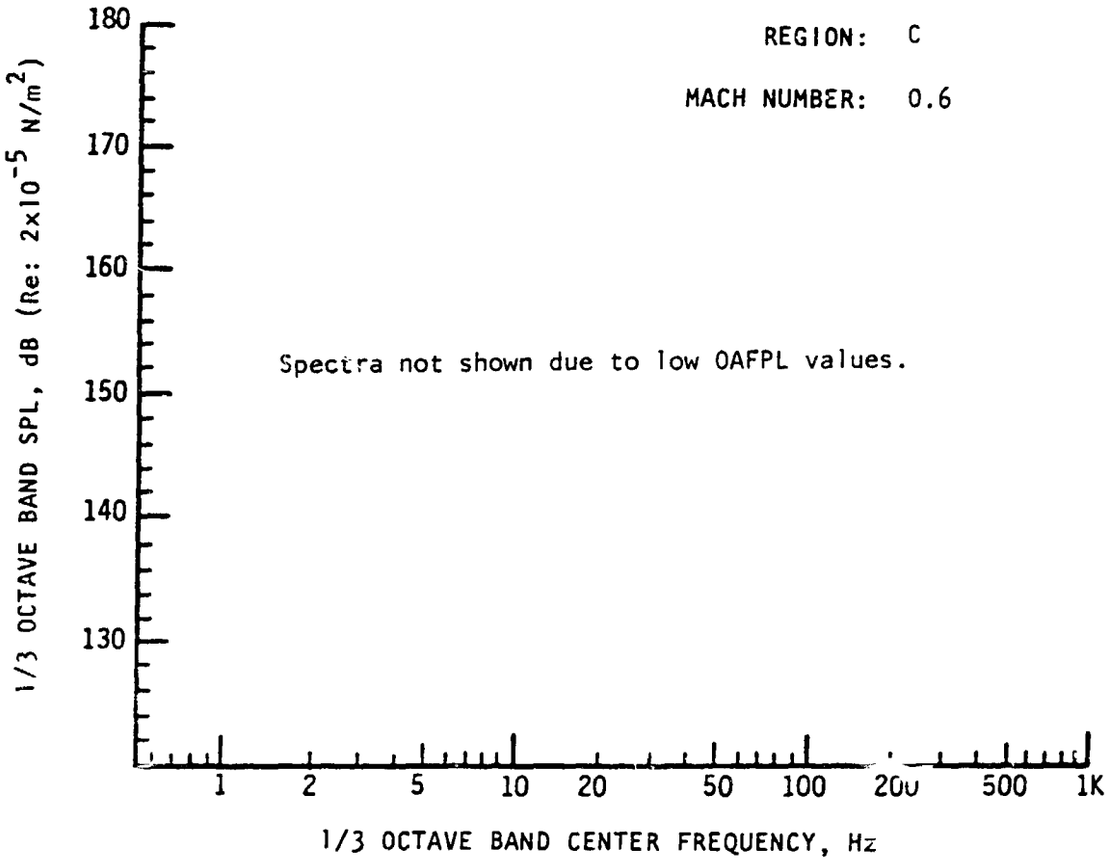

Note: Results based on 95 percentile OAFPL from Monte Carlo trajectory simulation.

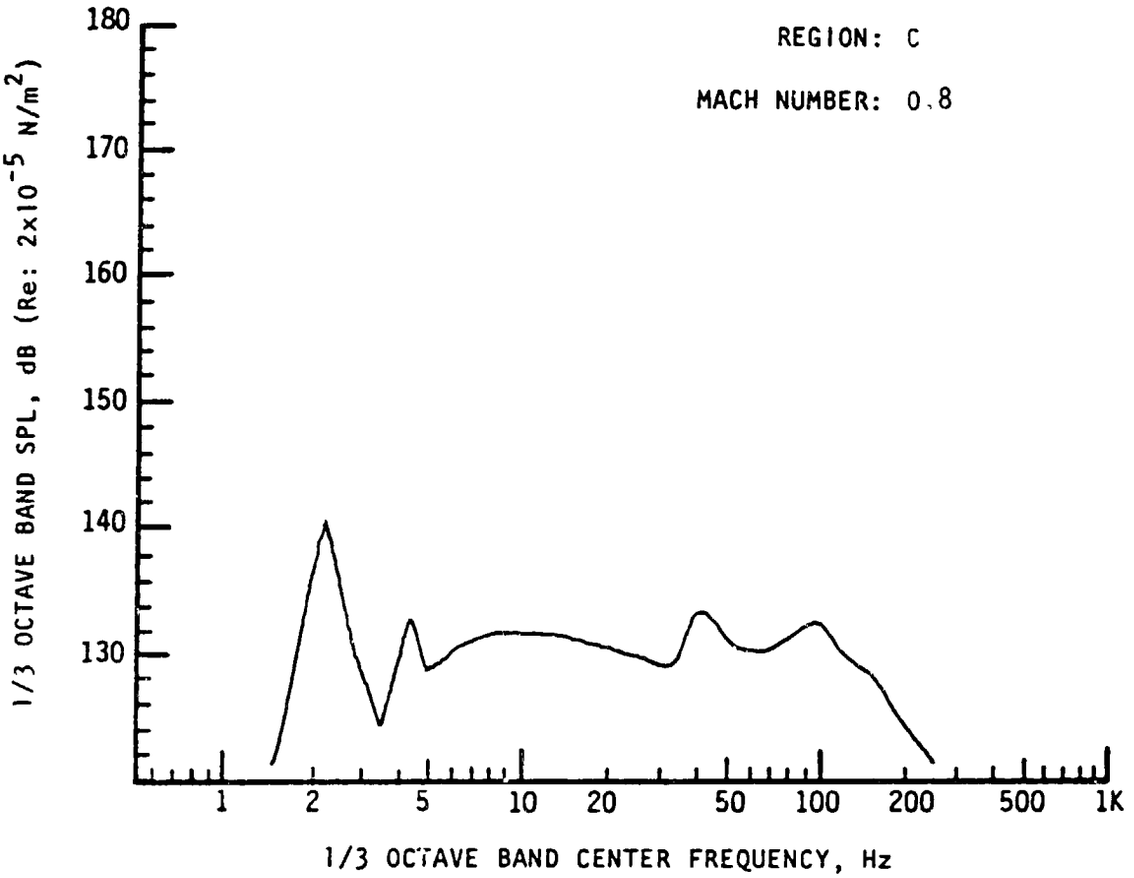

Note: Results based on 95 percentile OAFPL from Monte Carlo trajectory simulation.

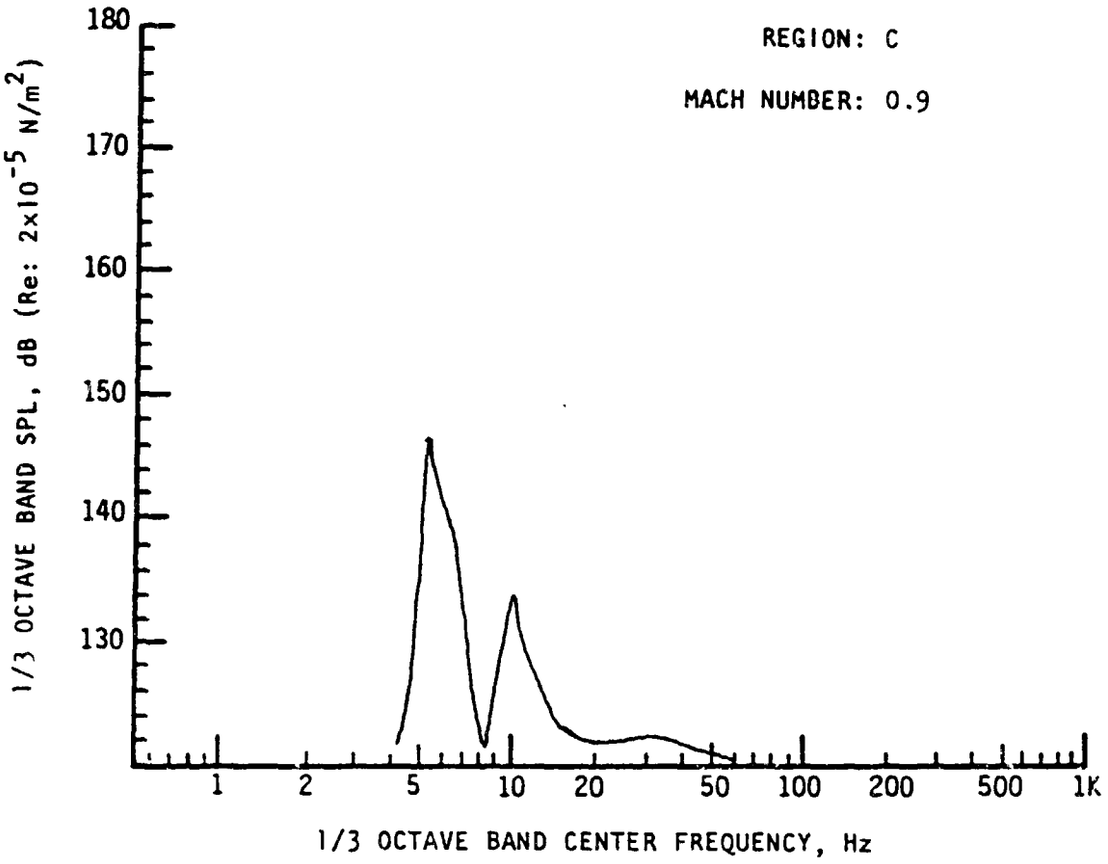

Note: Results based on 95 percentile OAFPL from Monte Carlo trajectory simulation.

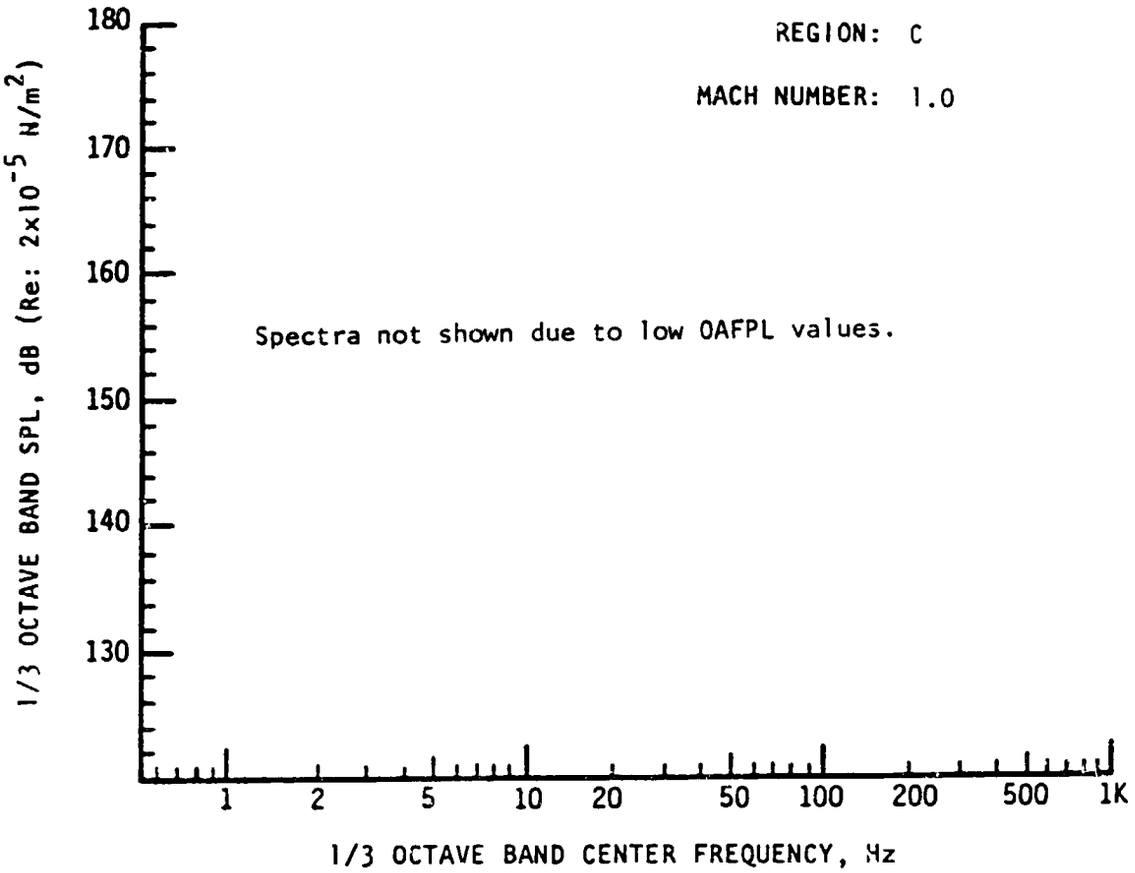

Note: Results based on 95 percentile OAFPL from Monte Carlo trajectory simulation.

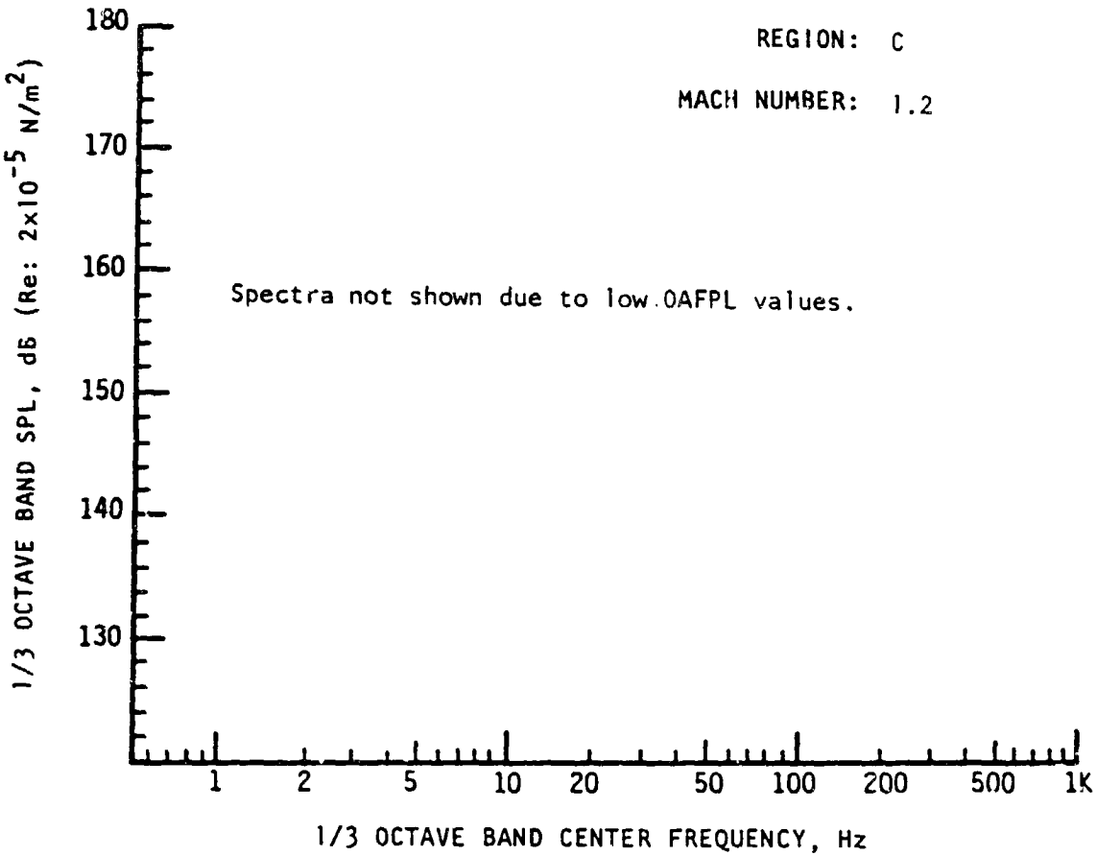

Note: Results based on 95 percentile OAFPL from Monte Carlo trajectory simulation.

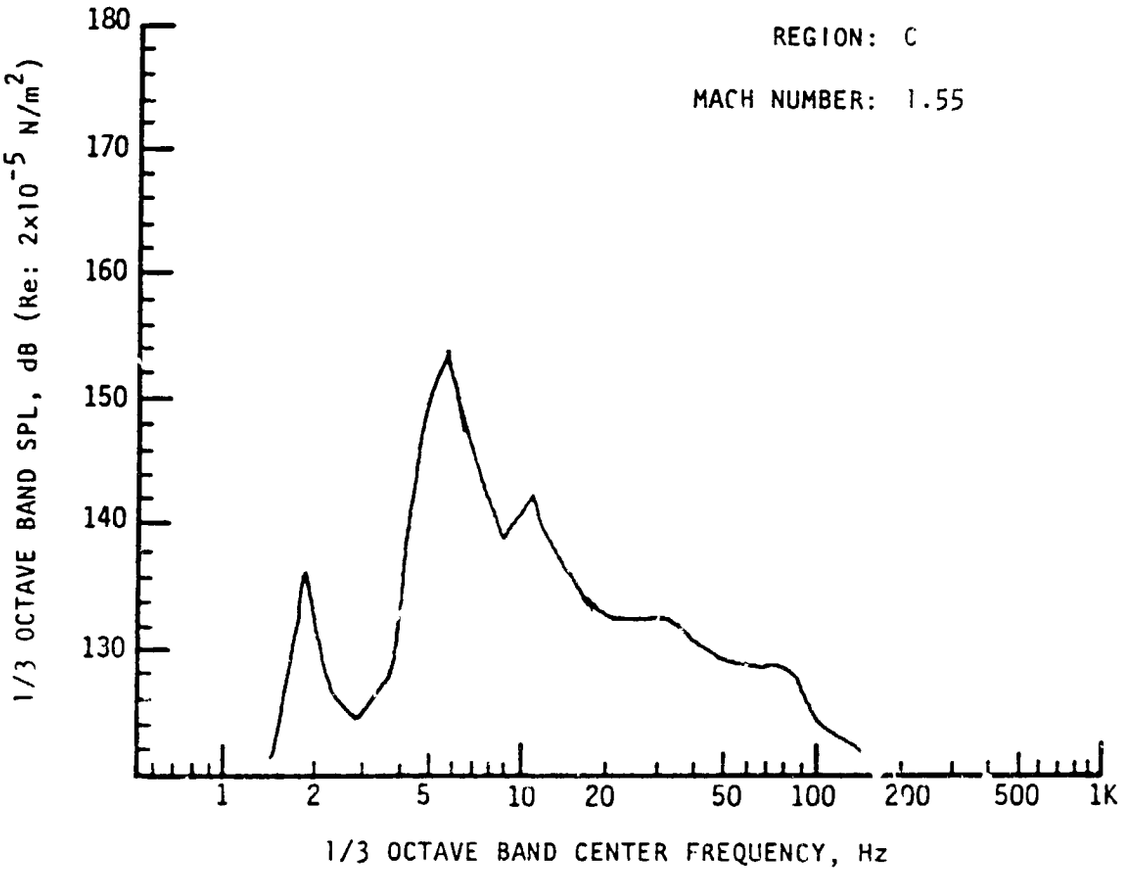

Note: Results based on 95 percentile OAFPL from Monte Carlo trajectory simulation.

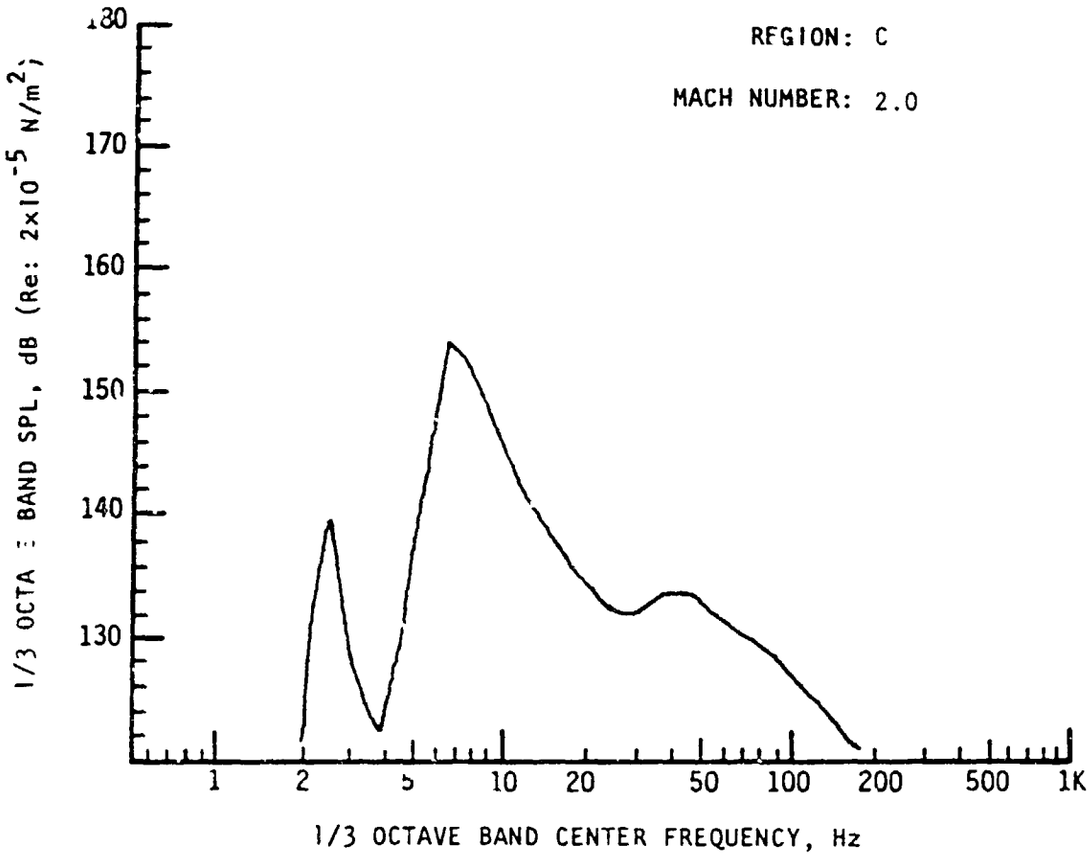

Note: Results based on 95 percentile OAFPL from Monte Carlo trajectory simulation.

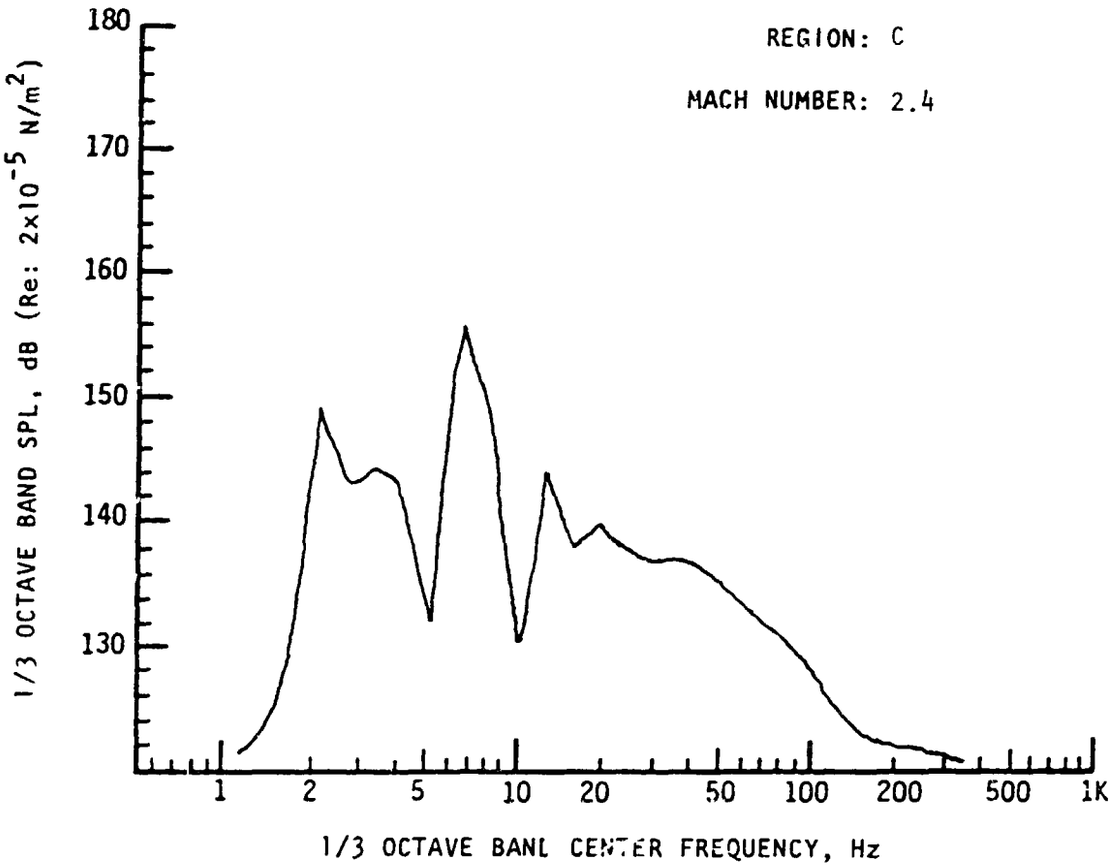

Note: Results based on 95 percentile OAFPL from Monte Carlo trajectory simulation.

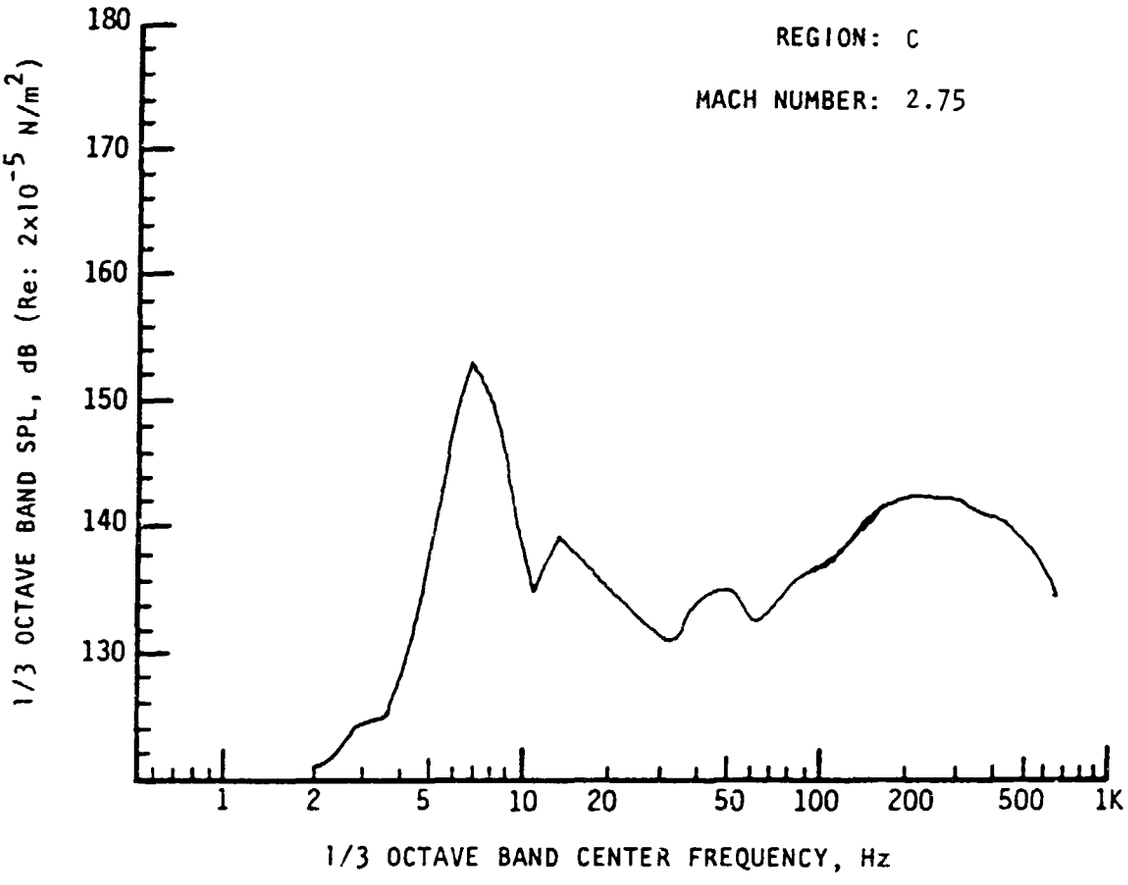

Note: Results based on 95 percentile OAFPL from Monte Carlo trajectory simulation.

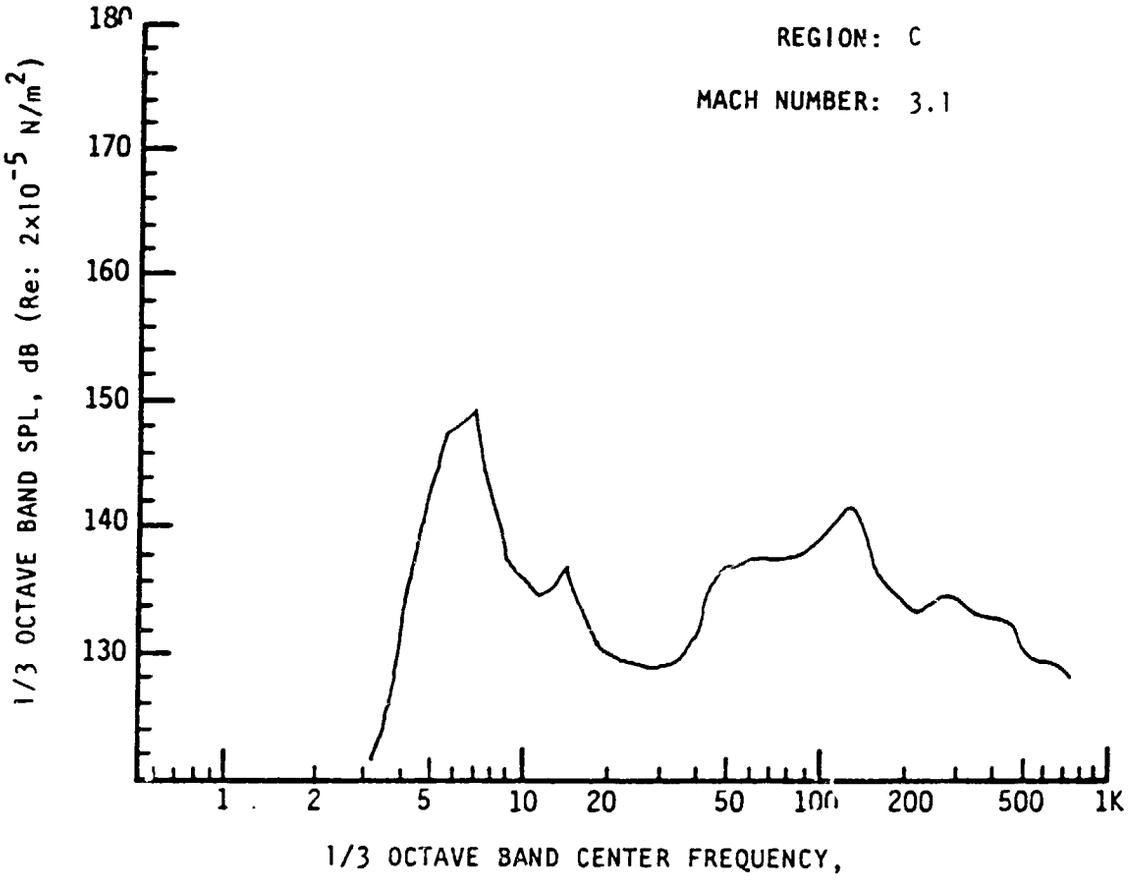

Note: Results based on 95 percentile OAFPL from Monte Carlo trajectory simulation.

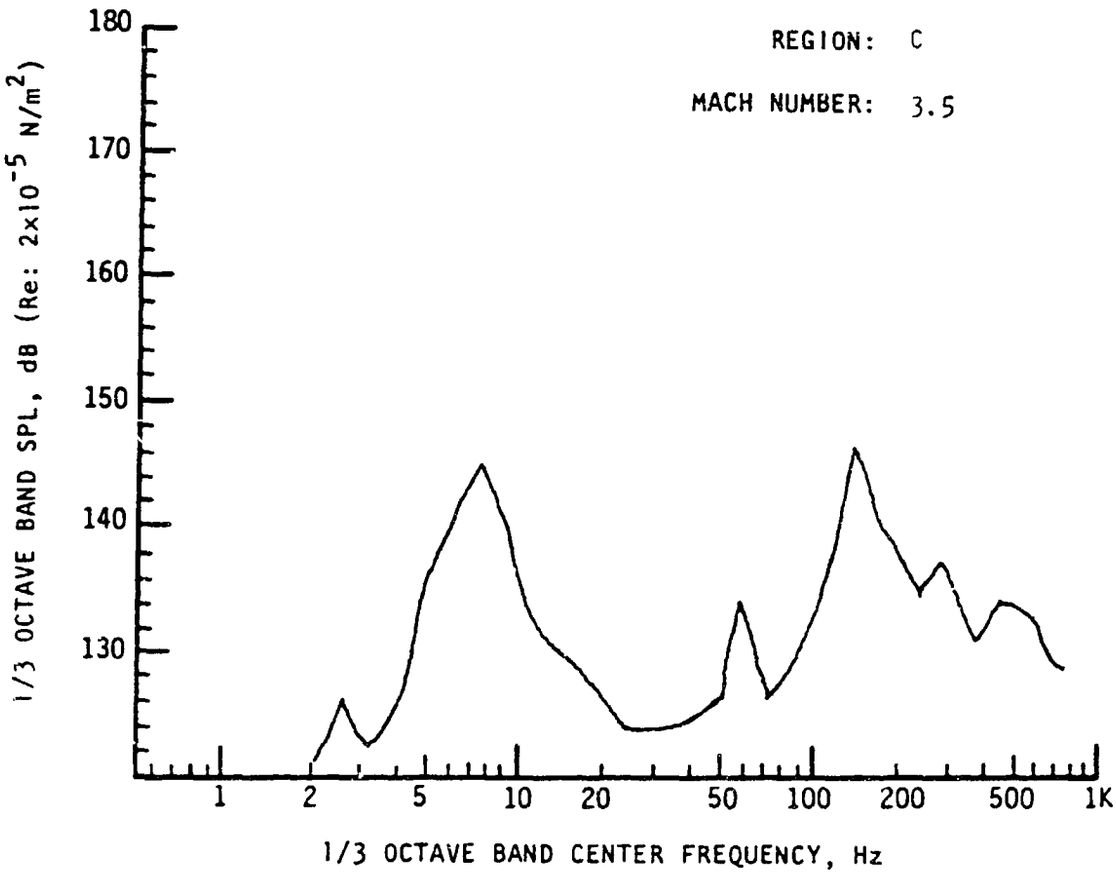

Note: Results based on 95 percentile OAFPL from Monte Carlo trajectory simulation.

APPENDIX D-I

SRB FLEXIBLE HEAT SHIELD CONFIGURATION
ONE-THIRD OCTAVE-BAND AEROACOUSTIC SPECTRA FOR REGION D-I
TVC UPPER AND LOWER FRAME ASSEMBLIES
(TRANSDUCERS 100, 101)

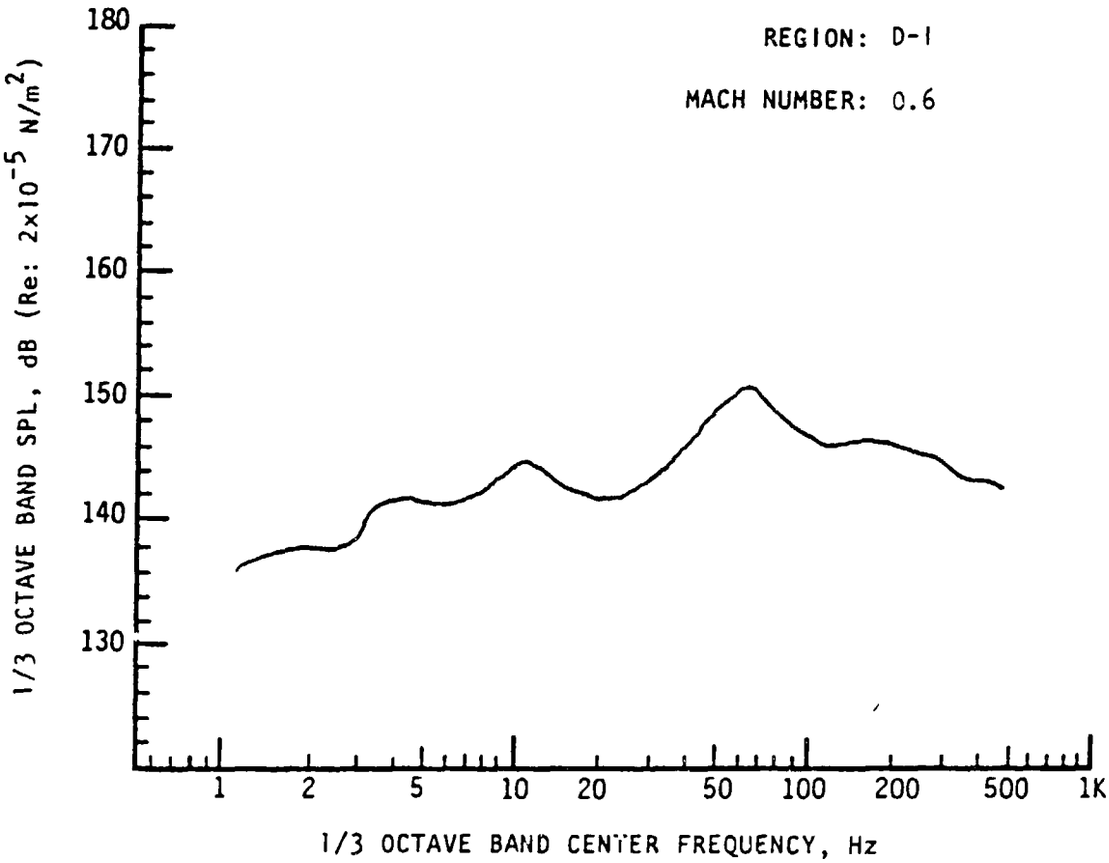

Note: Results based on 95 percentile OAFPL from Monte Carlo trajectory simulation.

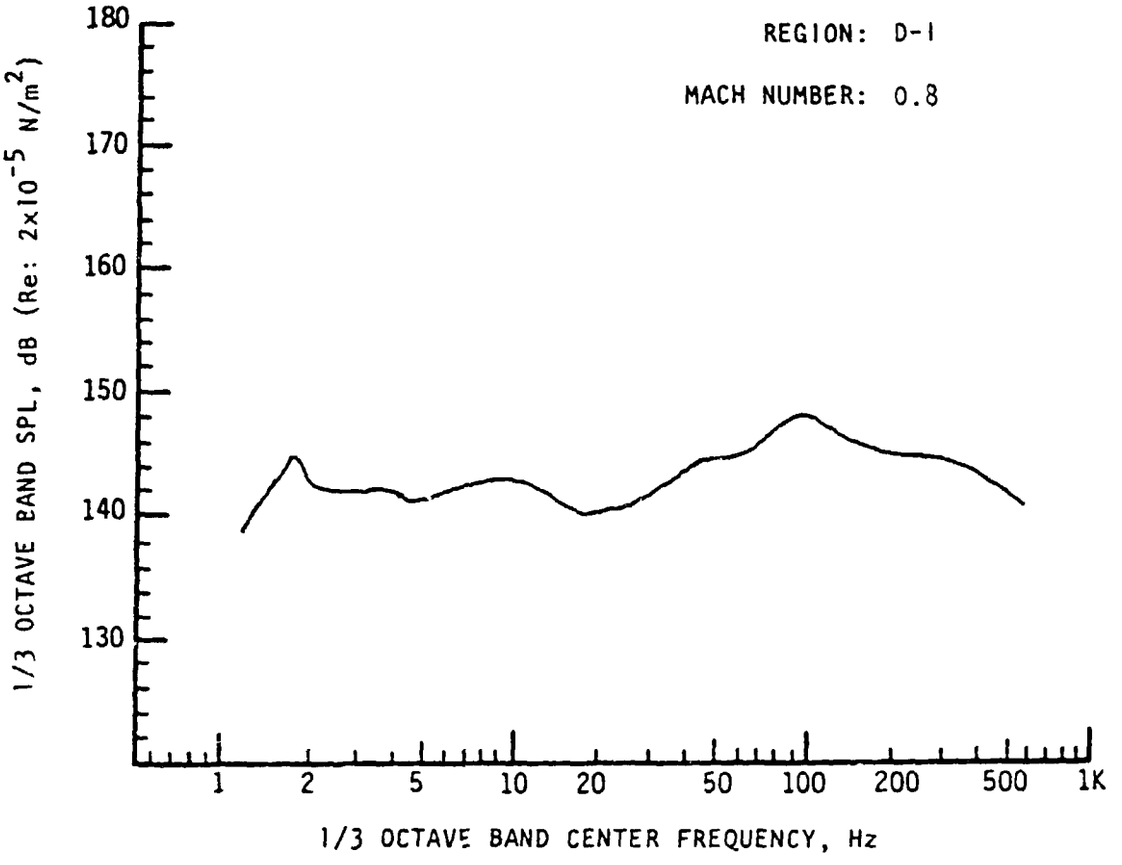

Note: Results based on 95 percentile OAFPL from Monte Carlo trajectory simulation.

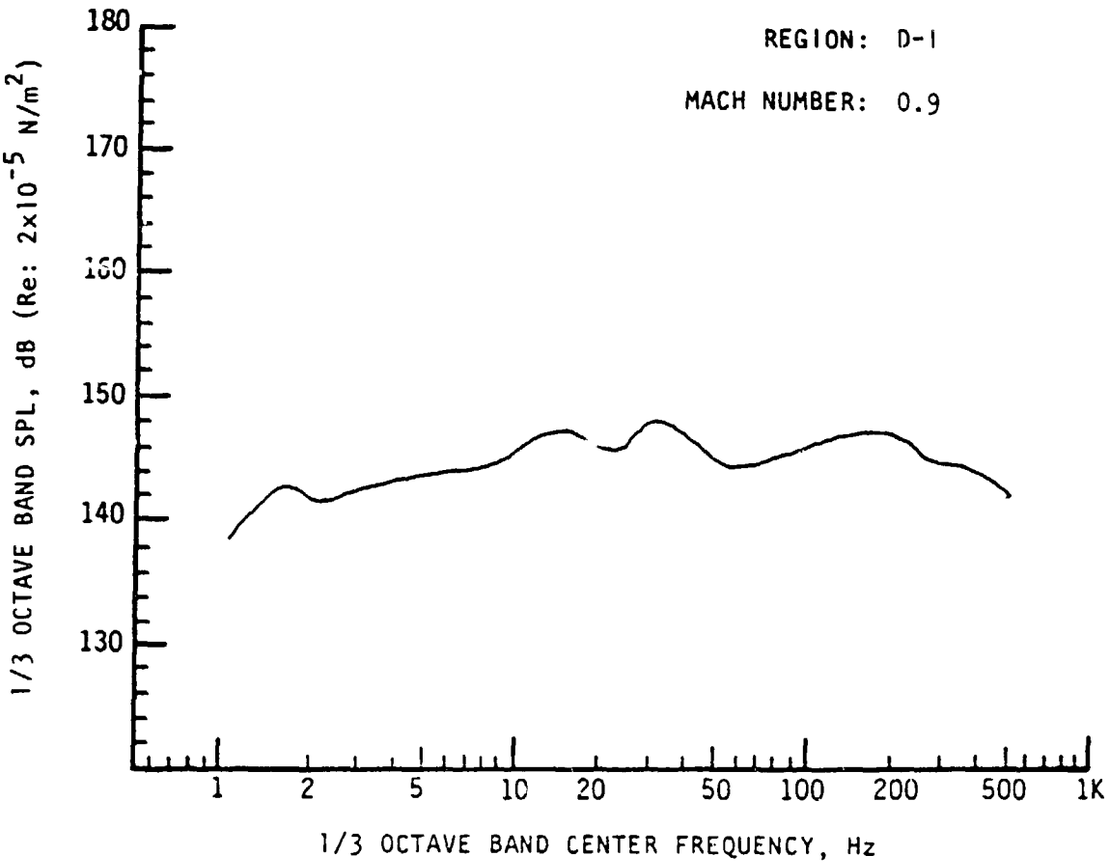

Note: Results based on 95 percentile OAFPL from Monte Carlo trajectory simulation.

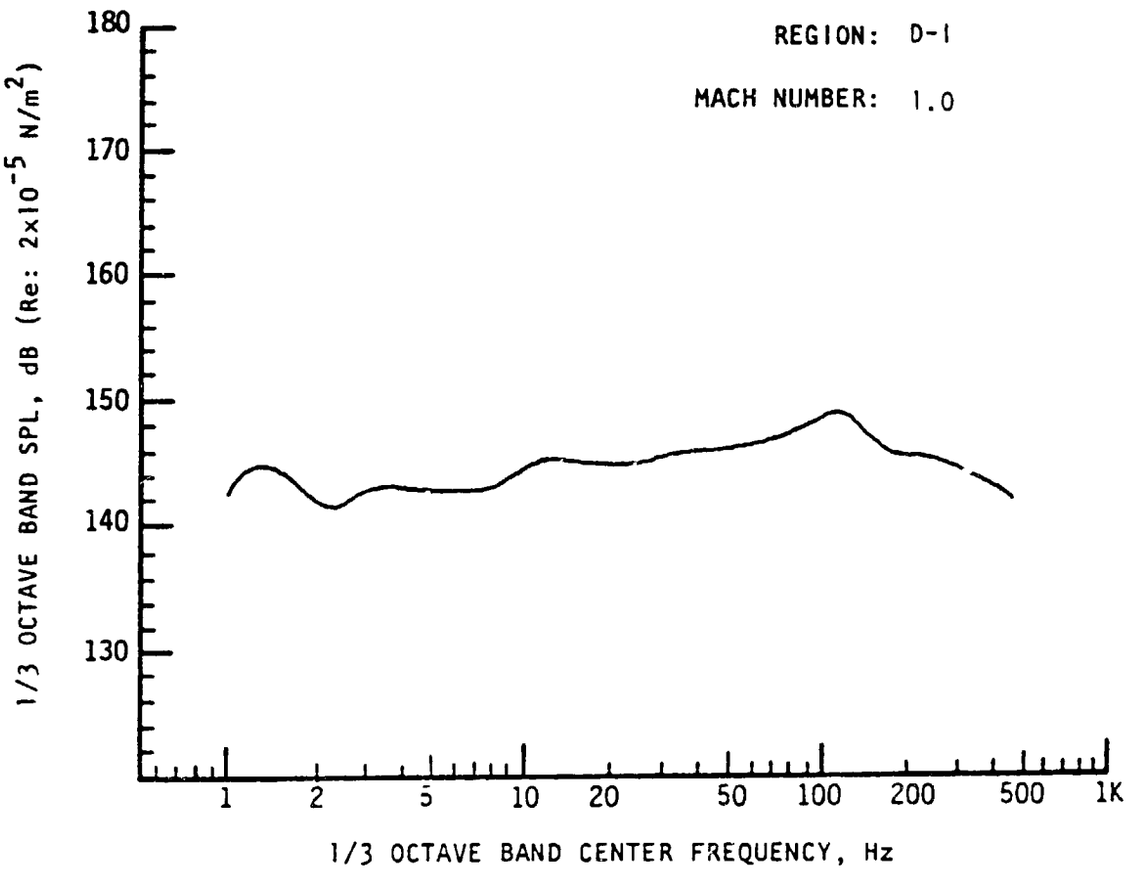

Note: Results based on 95 percentile OAFPL from Monte Carlo trajectory simulation.

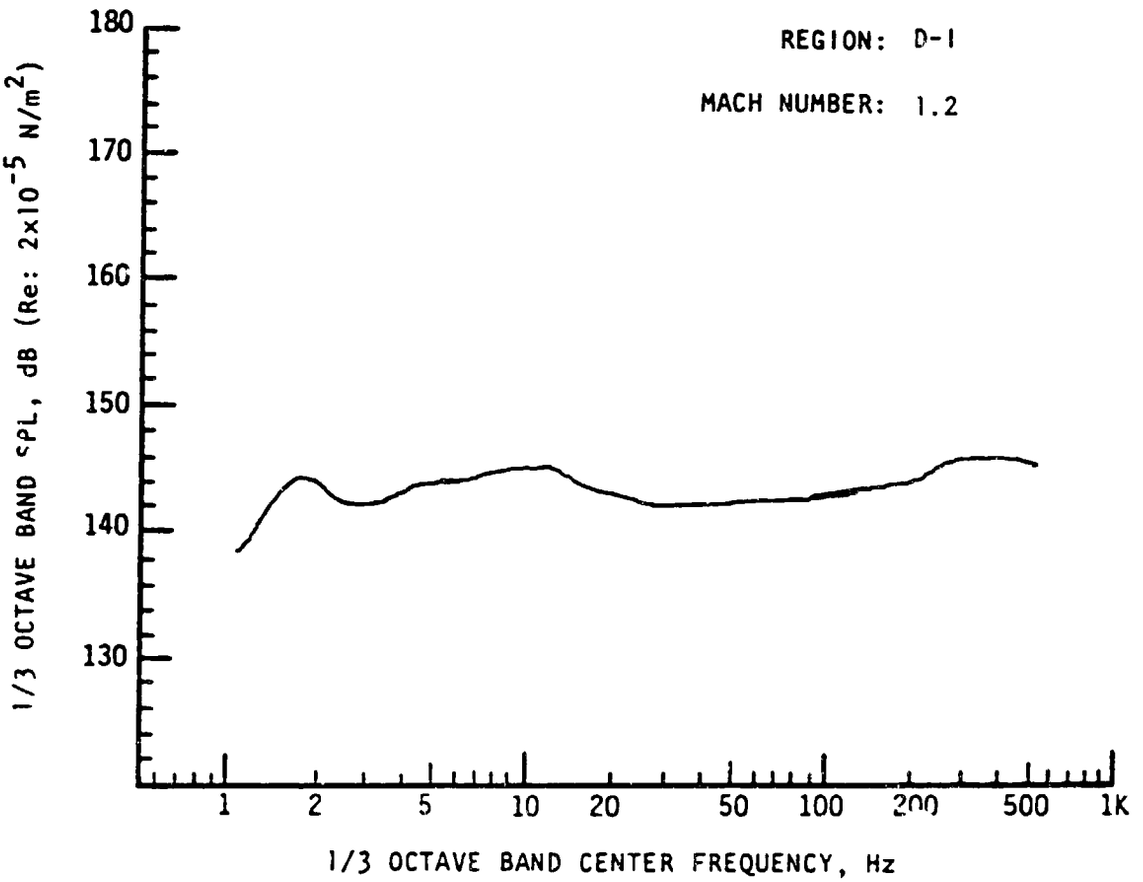

Note: Results based on 95 percentile OAFPL from Monte Carlo trajectory simulation.

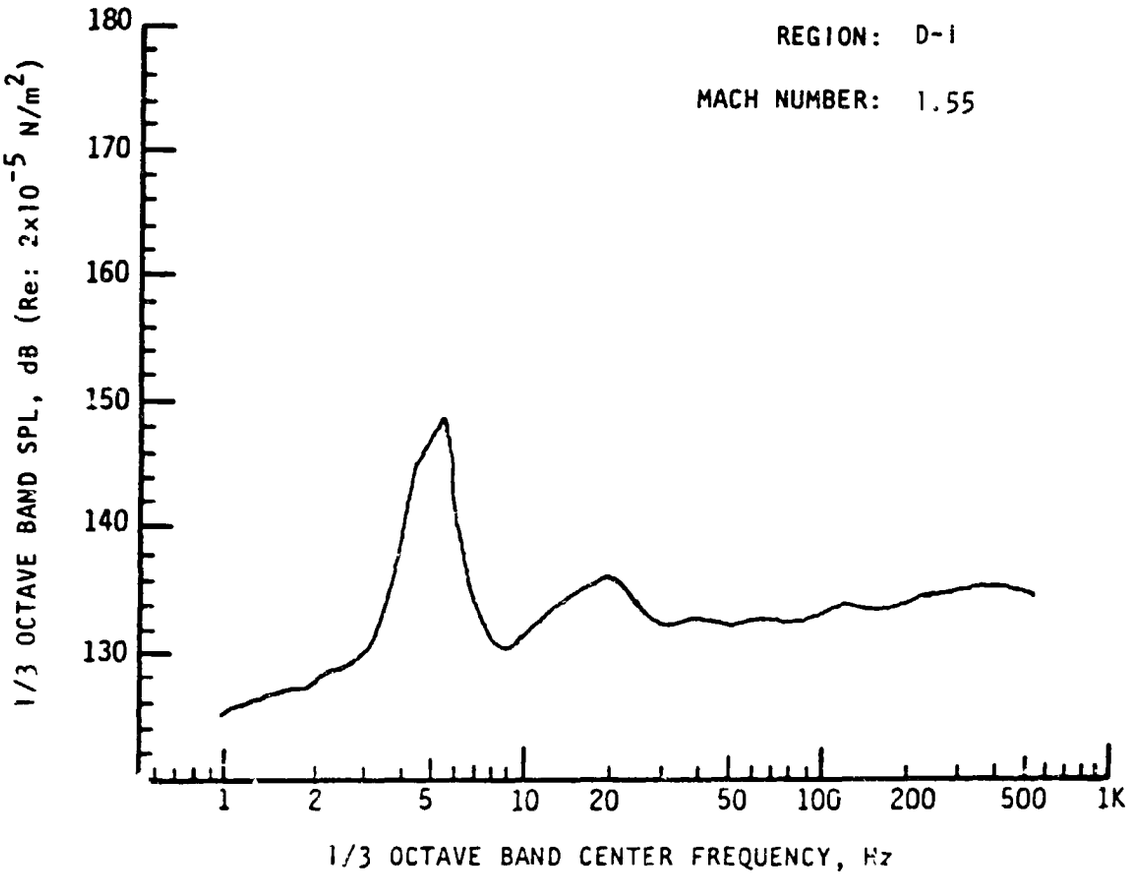

Note: Results based on 95 percentile OAFPL from Monte Carlo trajectory simulation.

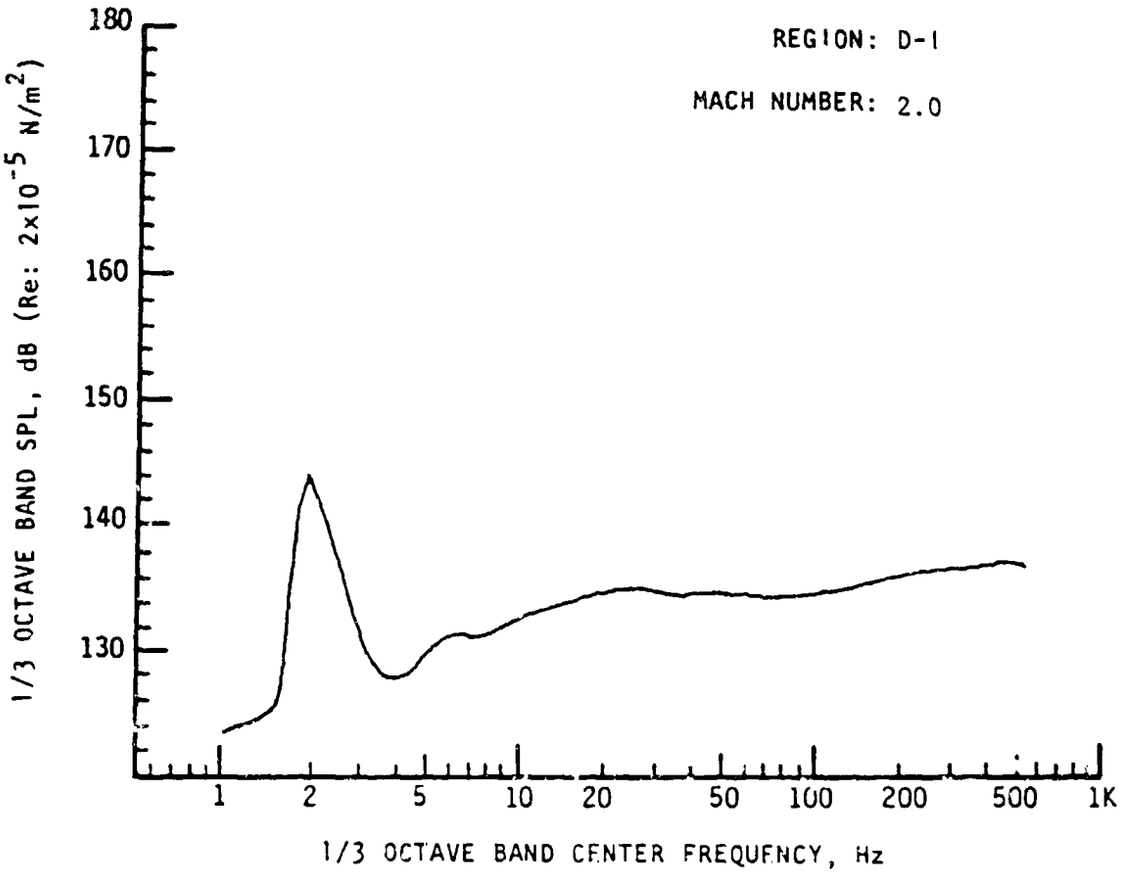

Note: Results based on 95 percentile OAFPL from Monte Carlo trajectory simulation.

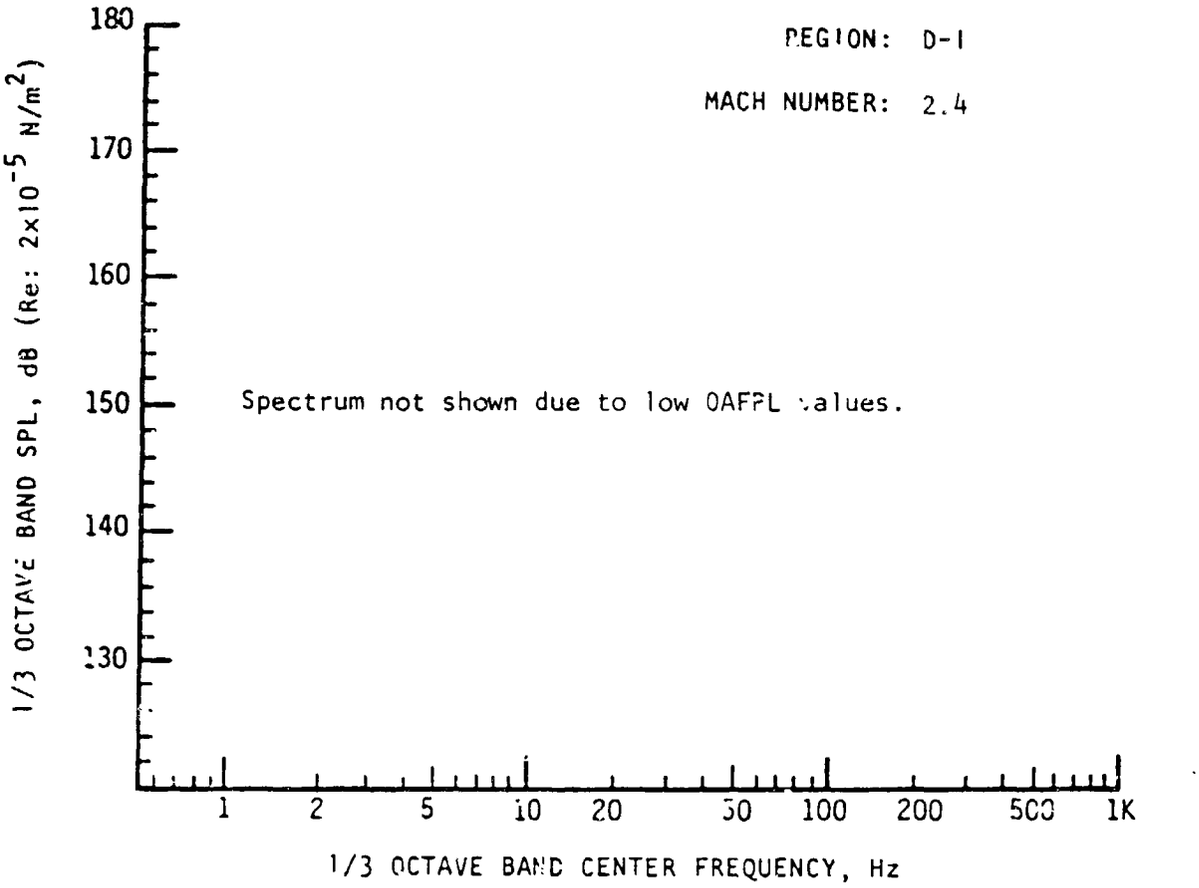

Note: Results based on 95 percentile OAFPL from Monte Carlo trajectory simulation.

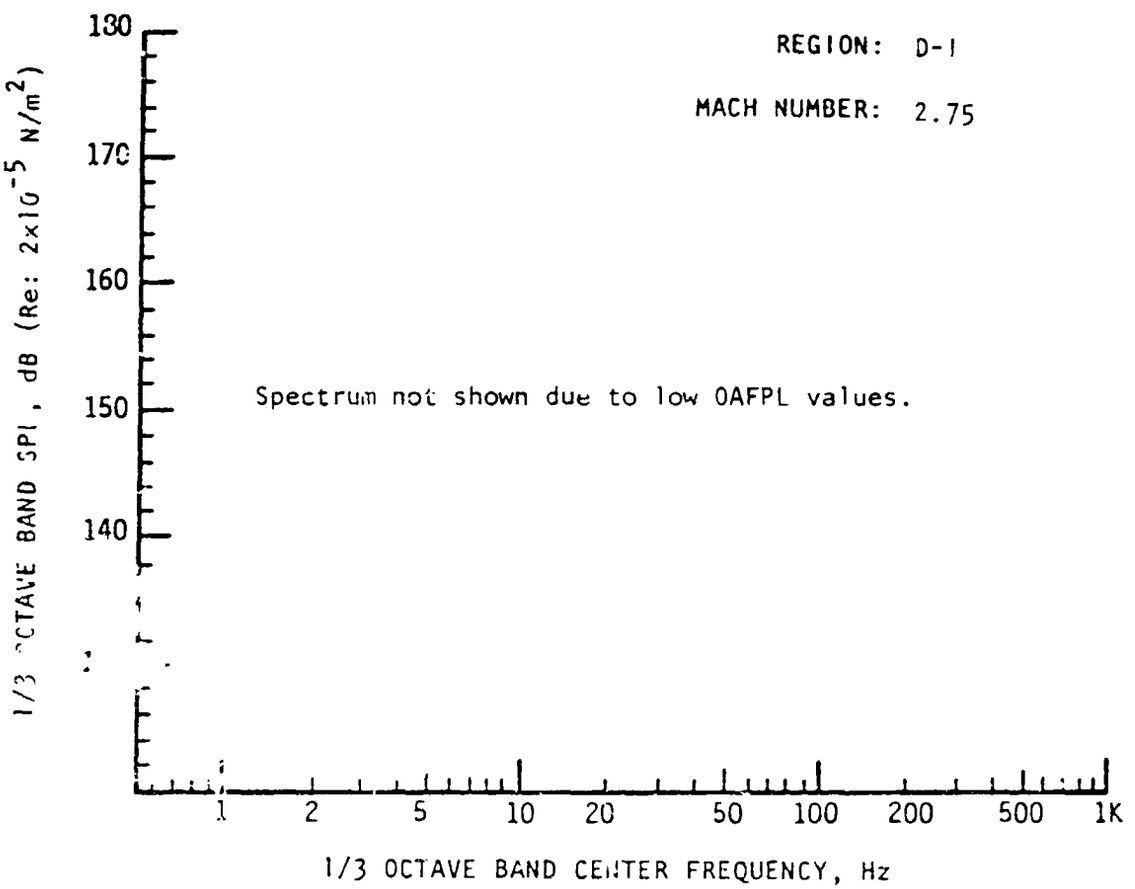

Note: Results based on 95 percentile OAFPL from Monte Carlo trajectory simulation.

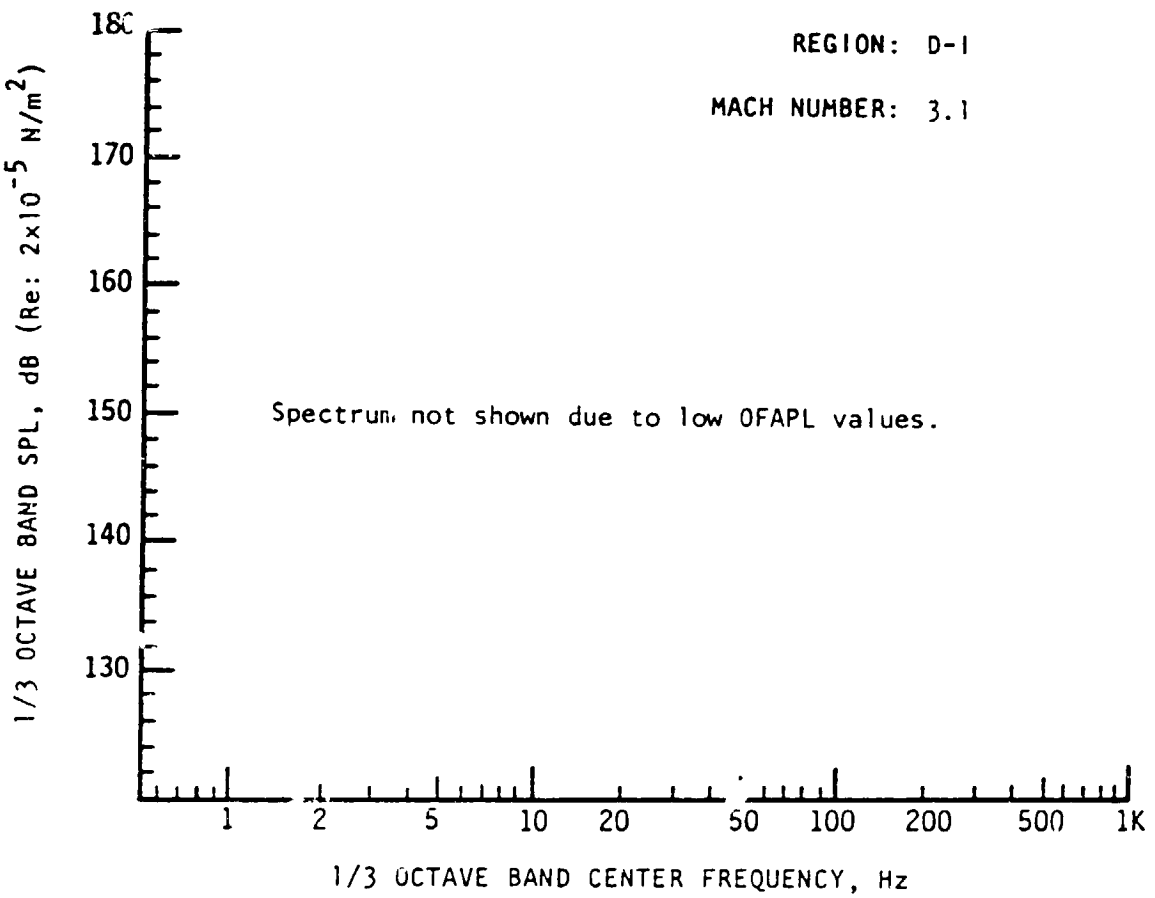

Note: Results based on 95 percentile OAFPL from Monte Carlo trajectory simulation.

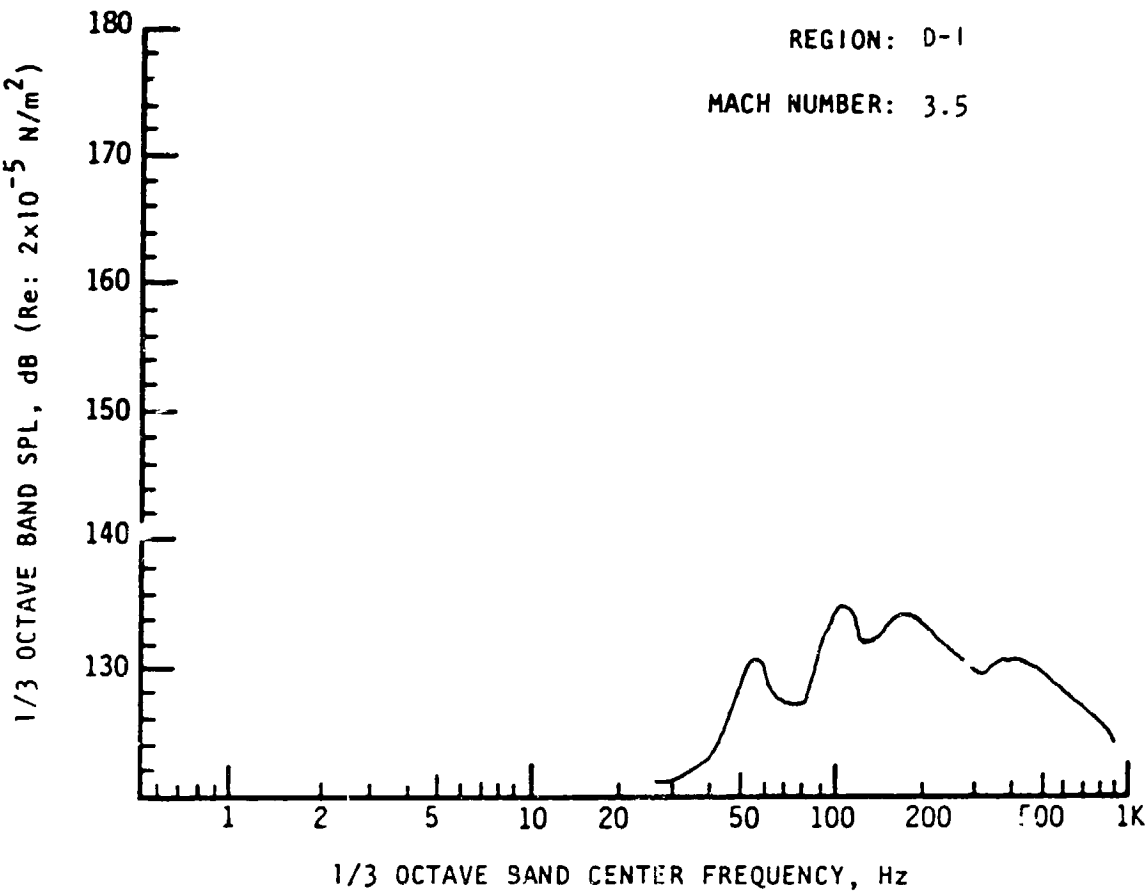

Note: Results based on 95 percentile OAFPL from Monte Carlo trajectory simulation.

APPENDIX D-II

SRB FLEXIBLE HEAT SHIELD CONFIGURATION

ONE-THIRD OCTAVE-BAND AEROACOUSTIC SPECTRA FOR REGION D-II

ACTUATOR BRACKETS

(TRANSDUCERS 89 - 92)

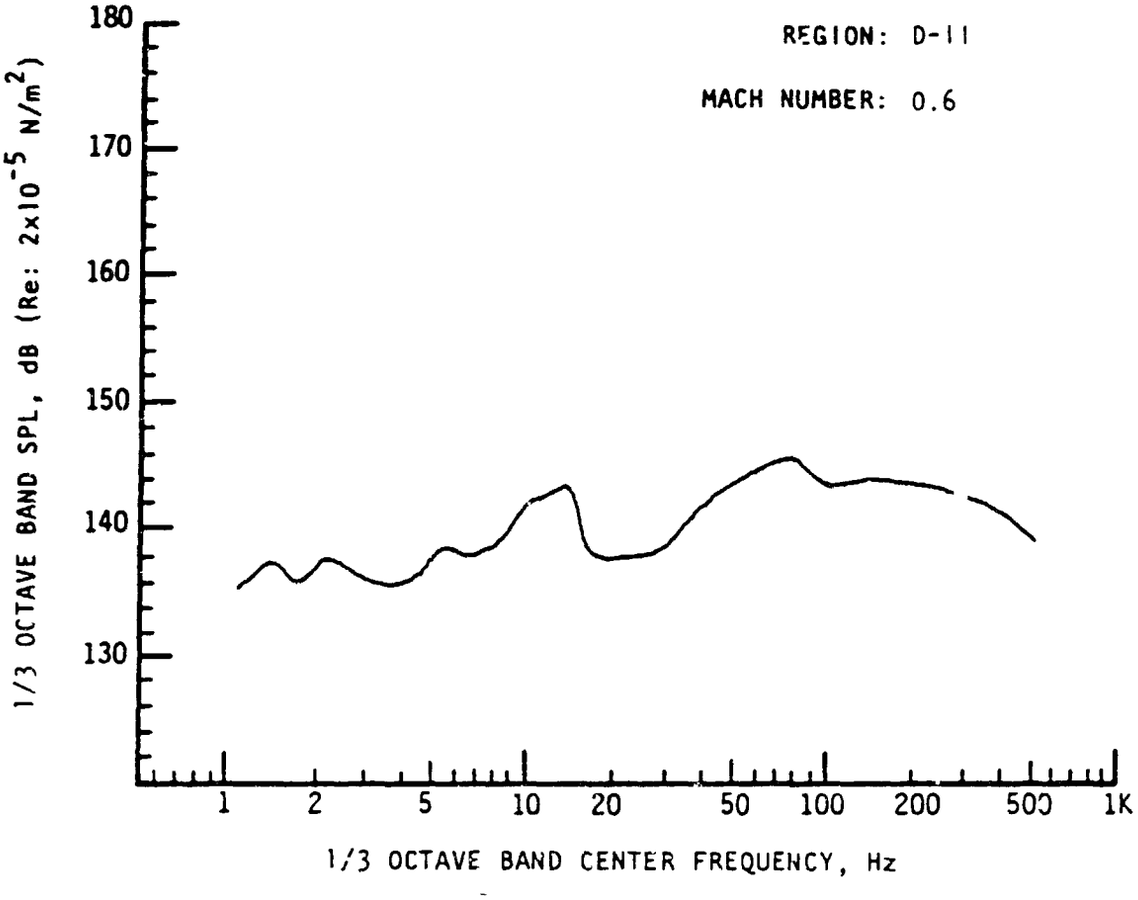

Note: Results based on 95 percentile OAFPL from Monte Carlo trajectory simulation.

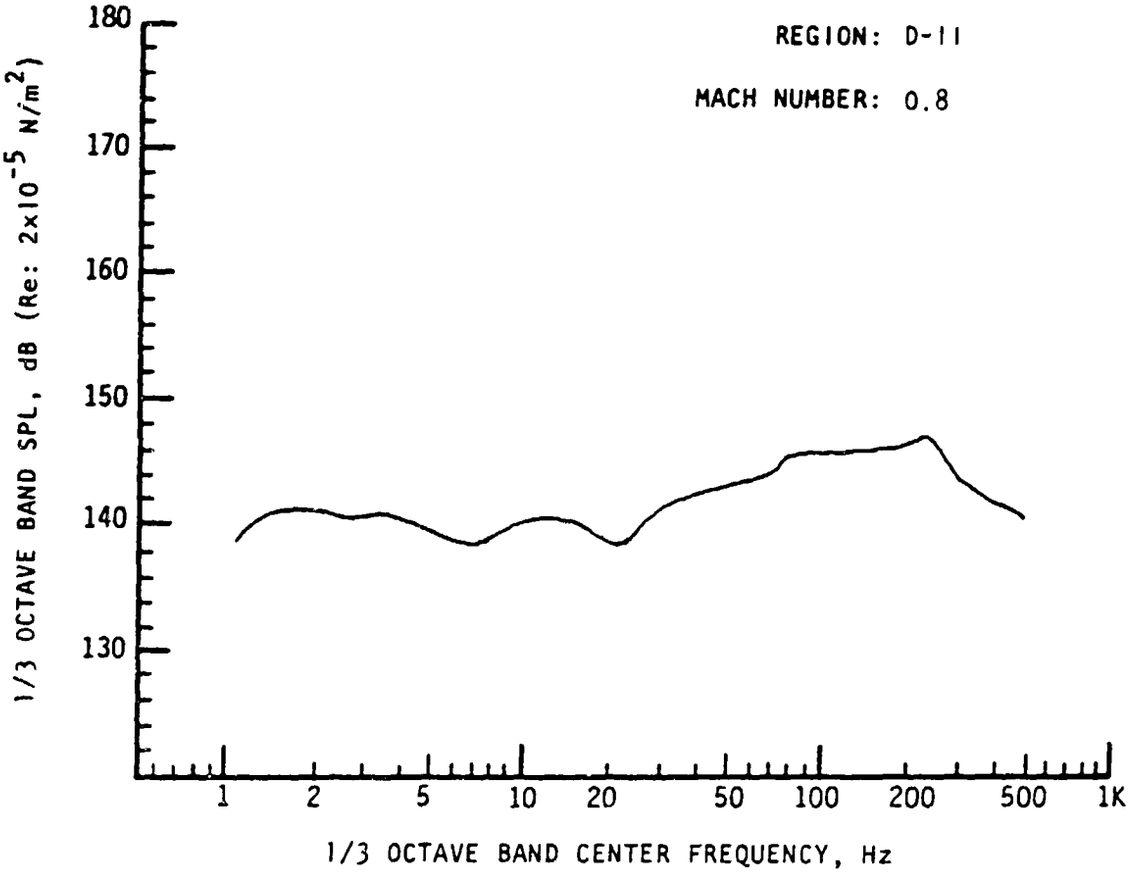

Note: Results based on 95 percentile OAFPL from Monte Carlo trajectory simulation.

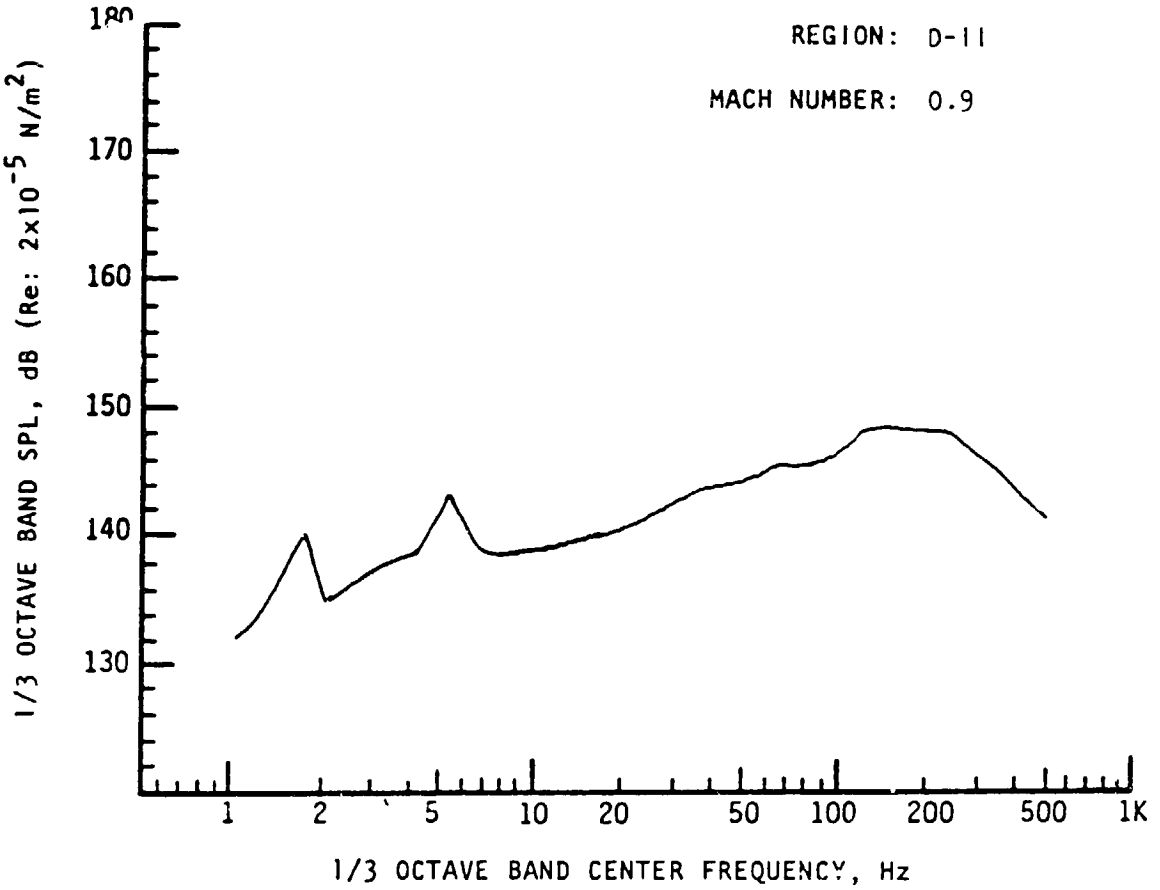

Note: Results based on 95 percentile OAFPL from Monte Carlo trajectory simulation.

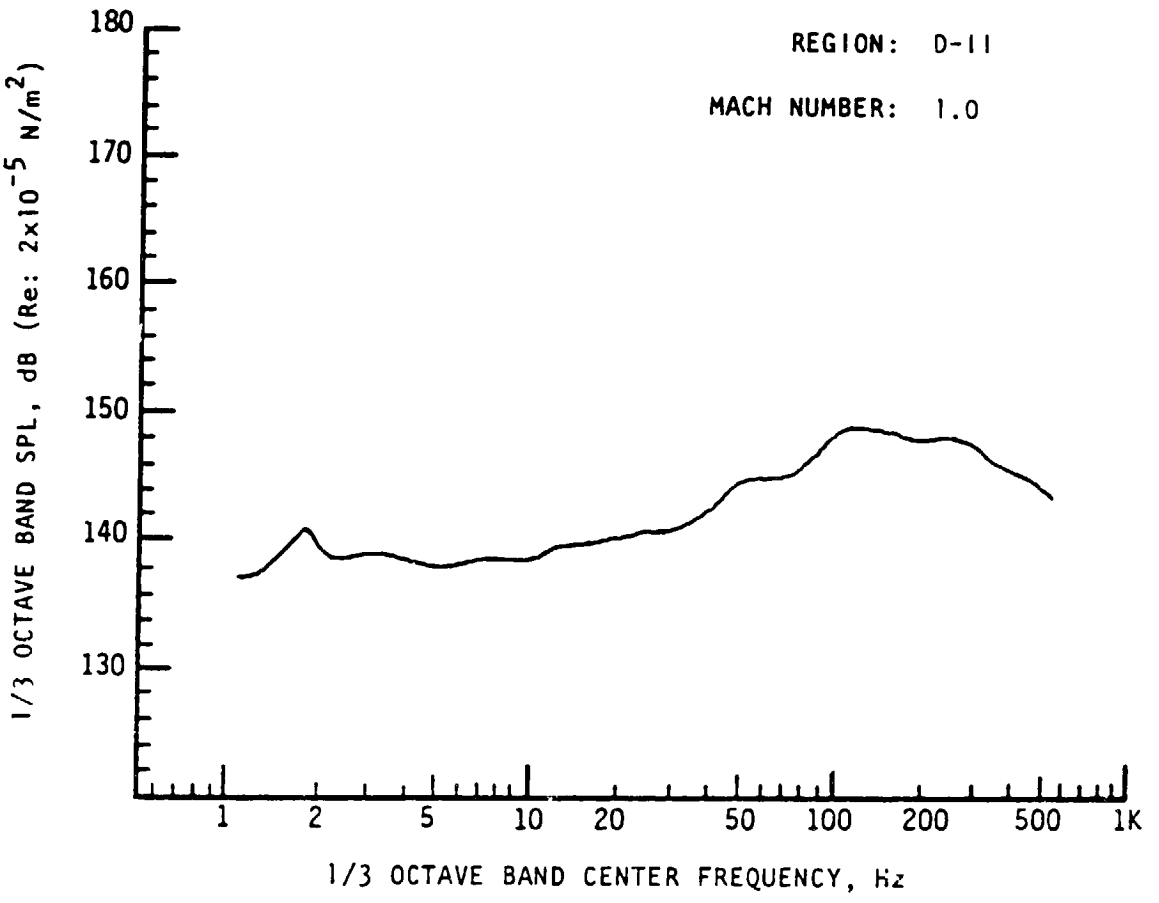

Note: Results based on 95 percentile OAFPL from Monte Carlo trajectory simulation.

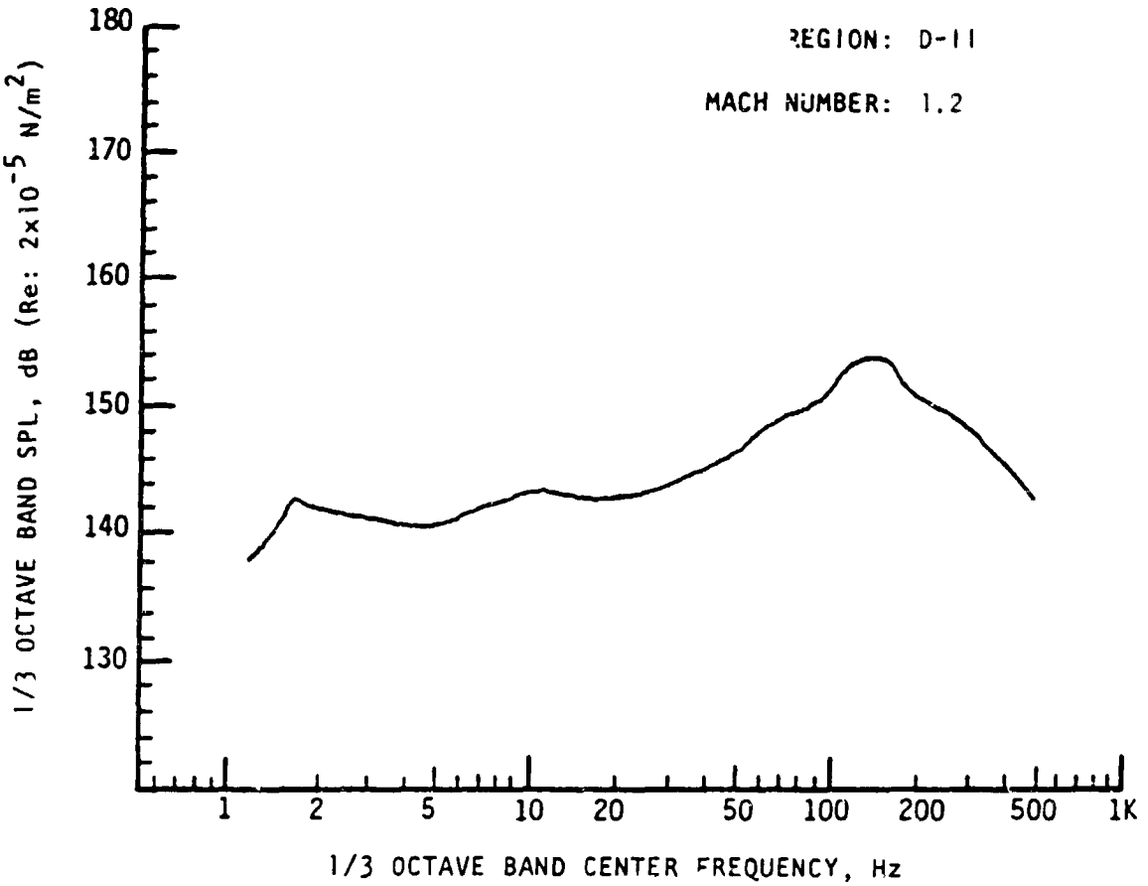

Note: Results based on 95 percentile OAFPL from Monte Carlo trajectory simulation.

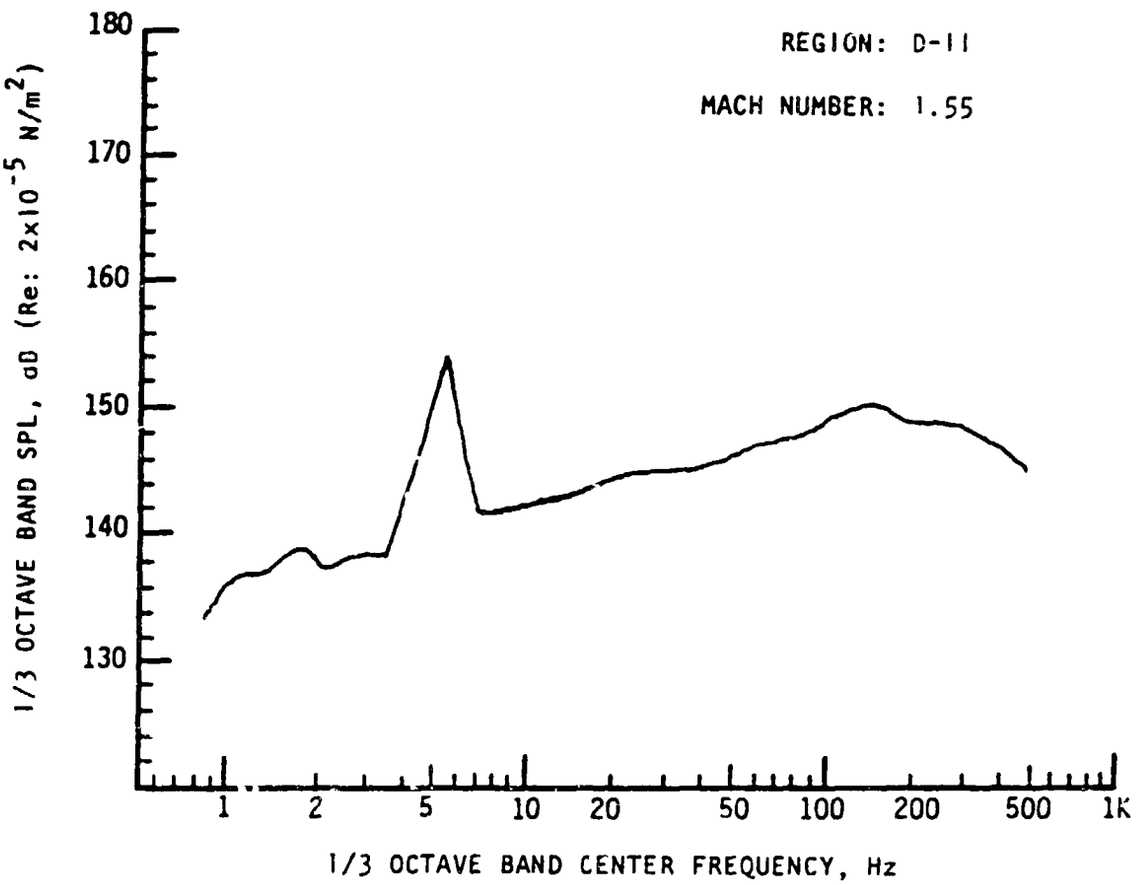

Note: Results based on 95 percentile OAFPL from Monte Carlo trajectory simulation.

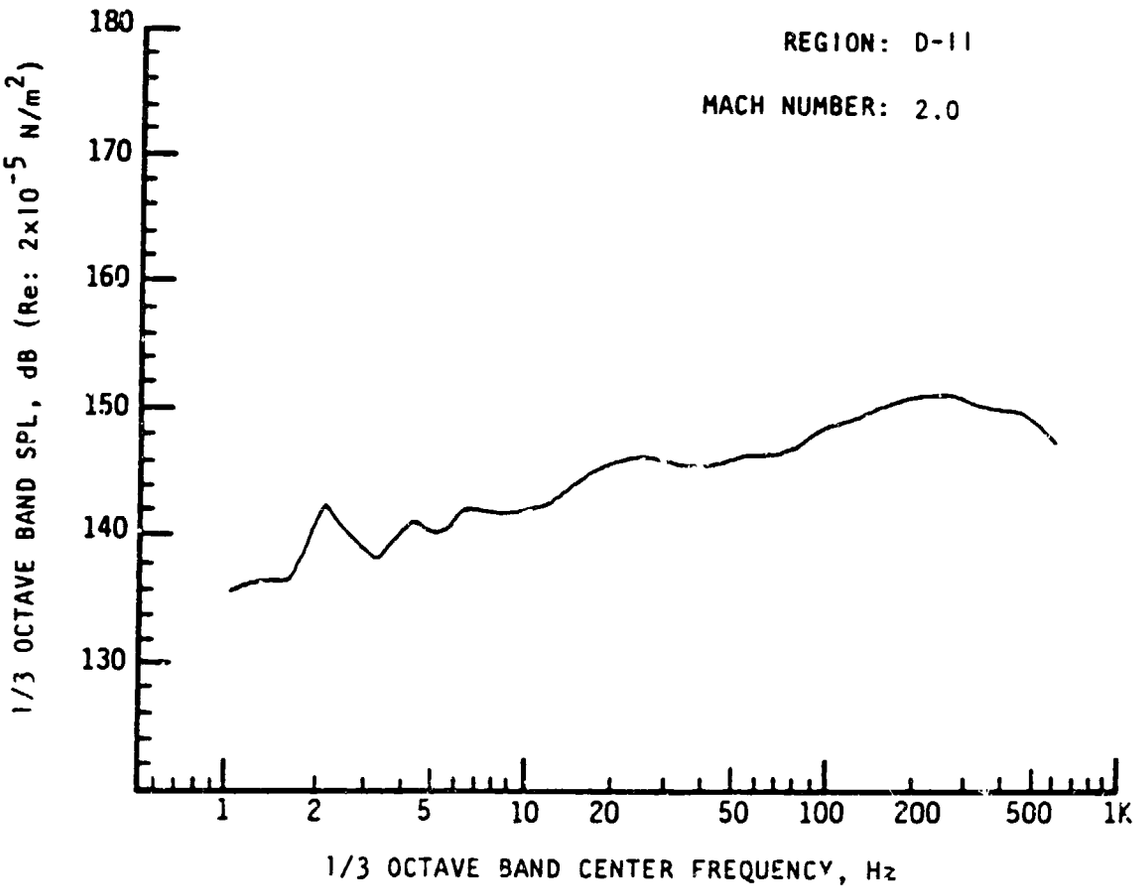

Note: Results based on 95 percentile OAFPL from Monte Carlo trajectory simulation.

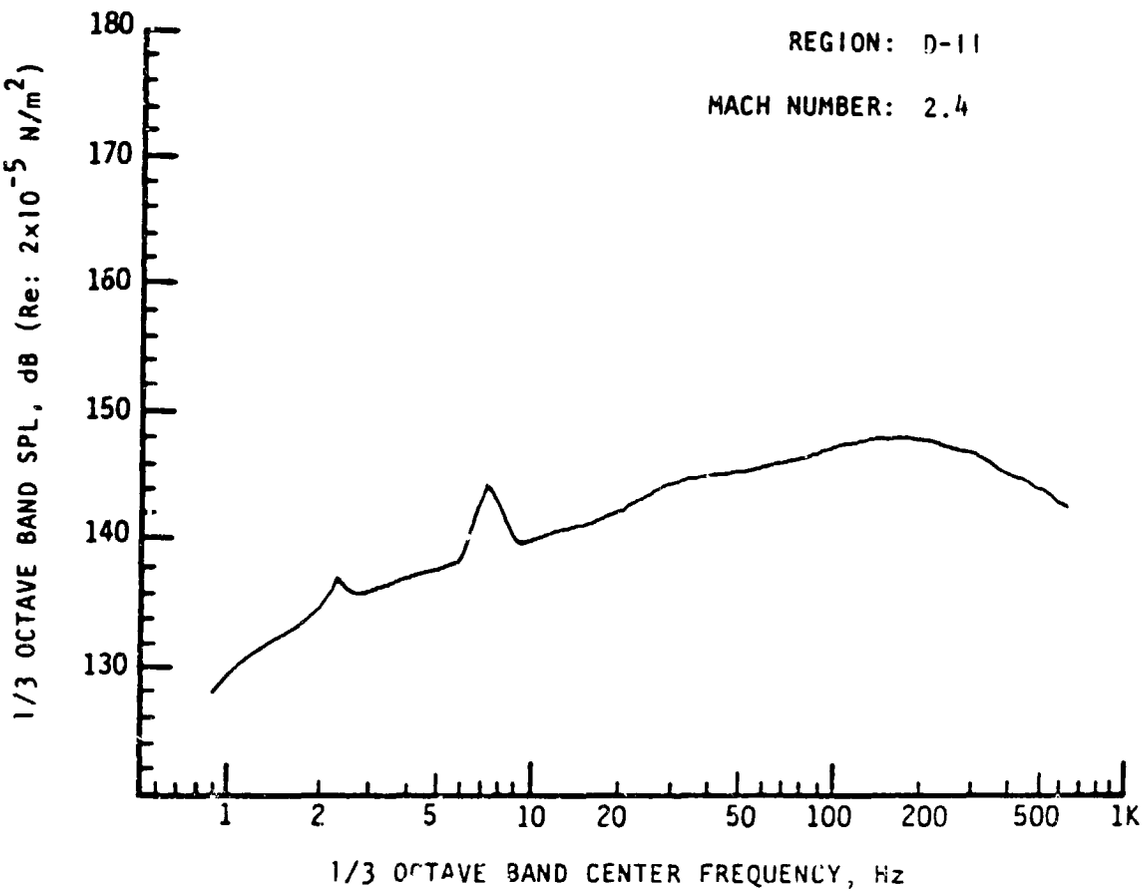

Note: Results based on 95 percentile OAFPL from Monte Carlo trajectory simulation.

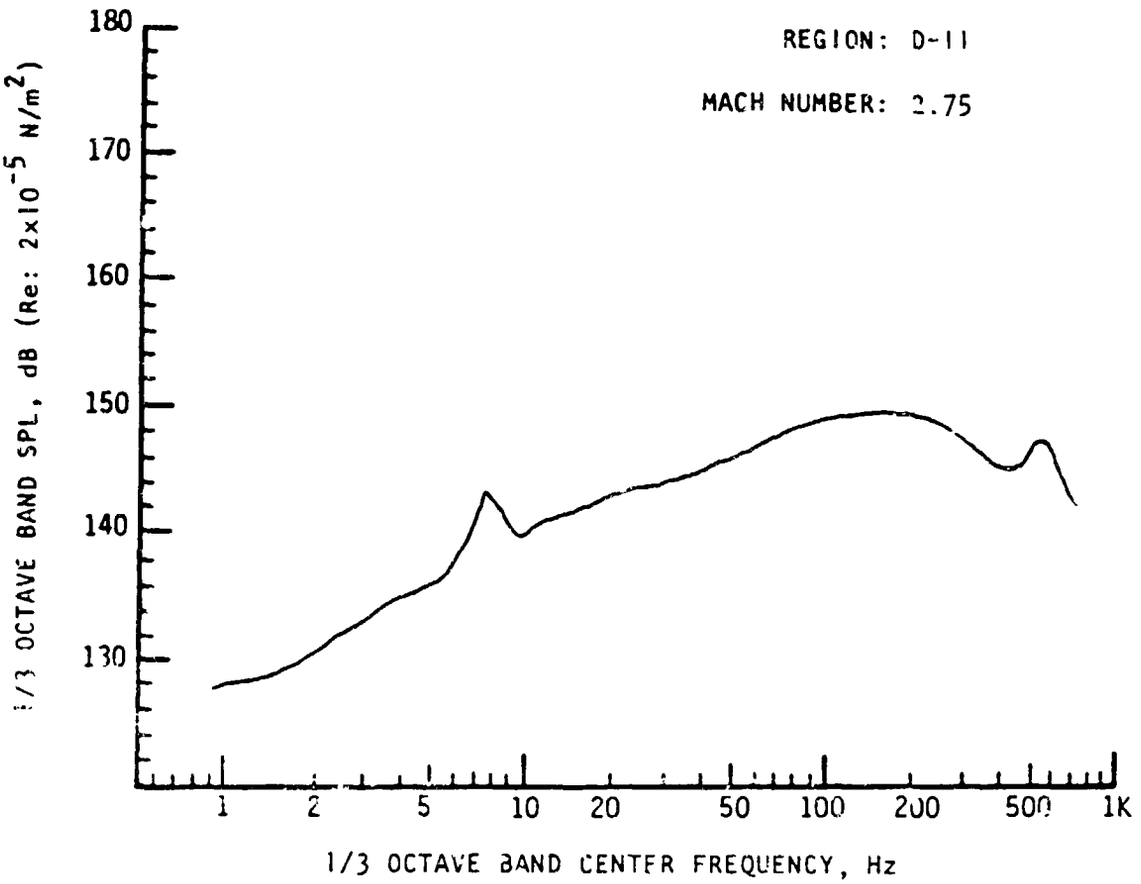

Note: Results based on 95 percentile OAFPL from Monte Carlo trajectory simulation.

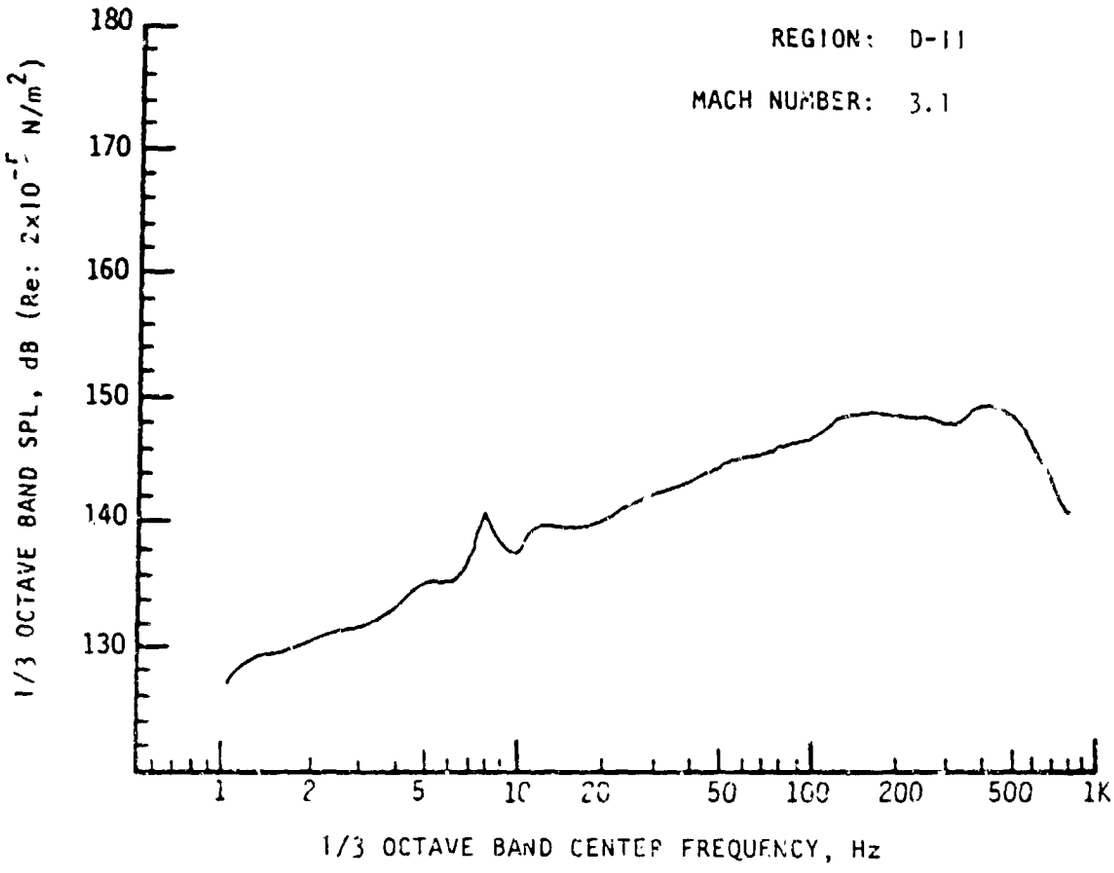

Note: Results based on 95 percentile OAFPL from Monte Carlo trajectory simulation.

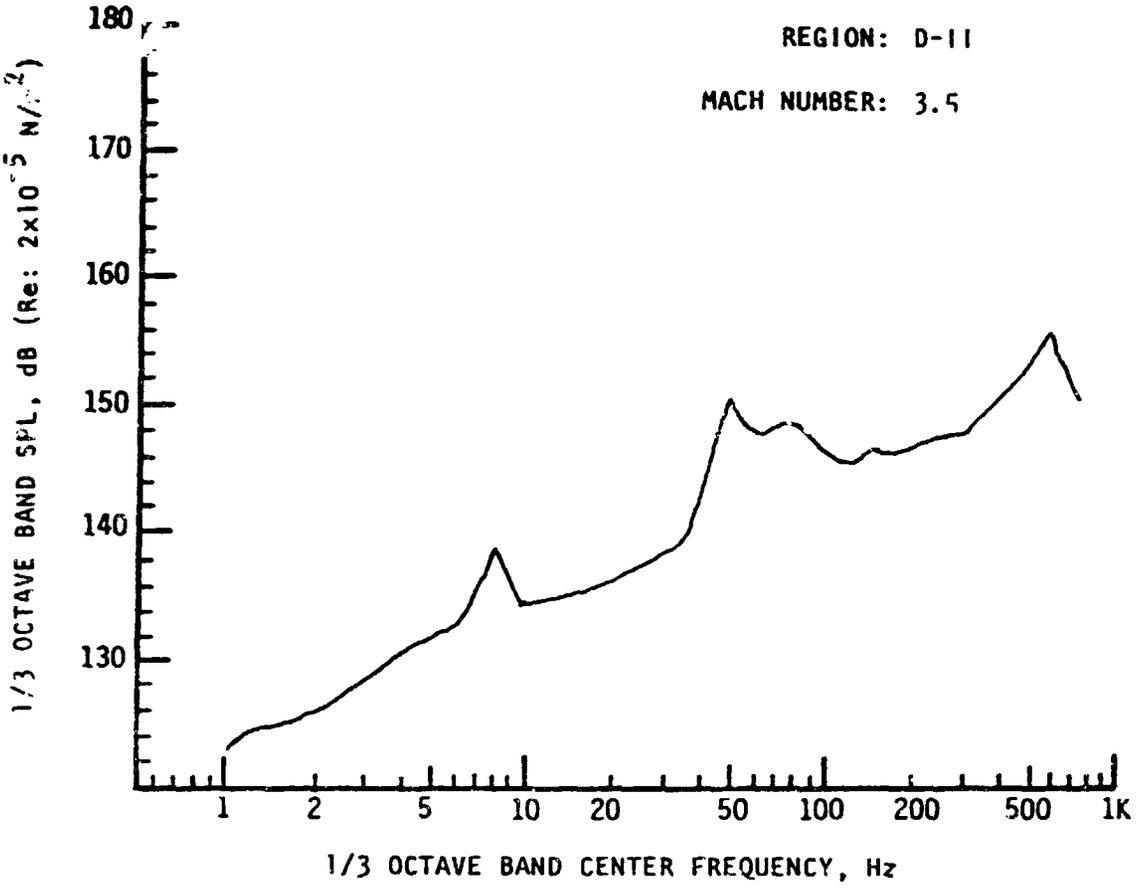

Note: Results based on 95 percentile OAFPL from Monte Carlo trajectory simulation.

APPENDIX D-III

SRB FLEXIBLE HEAT SHIELD CONFIGURATION
ONE-THIRD OCTAVE-BAND AEROACOUSTIC SPECTRA FOR REGION D-III
AFT SEPARATION MOTORS
(TRANSDUCERS 96 - 98, 106)

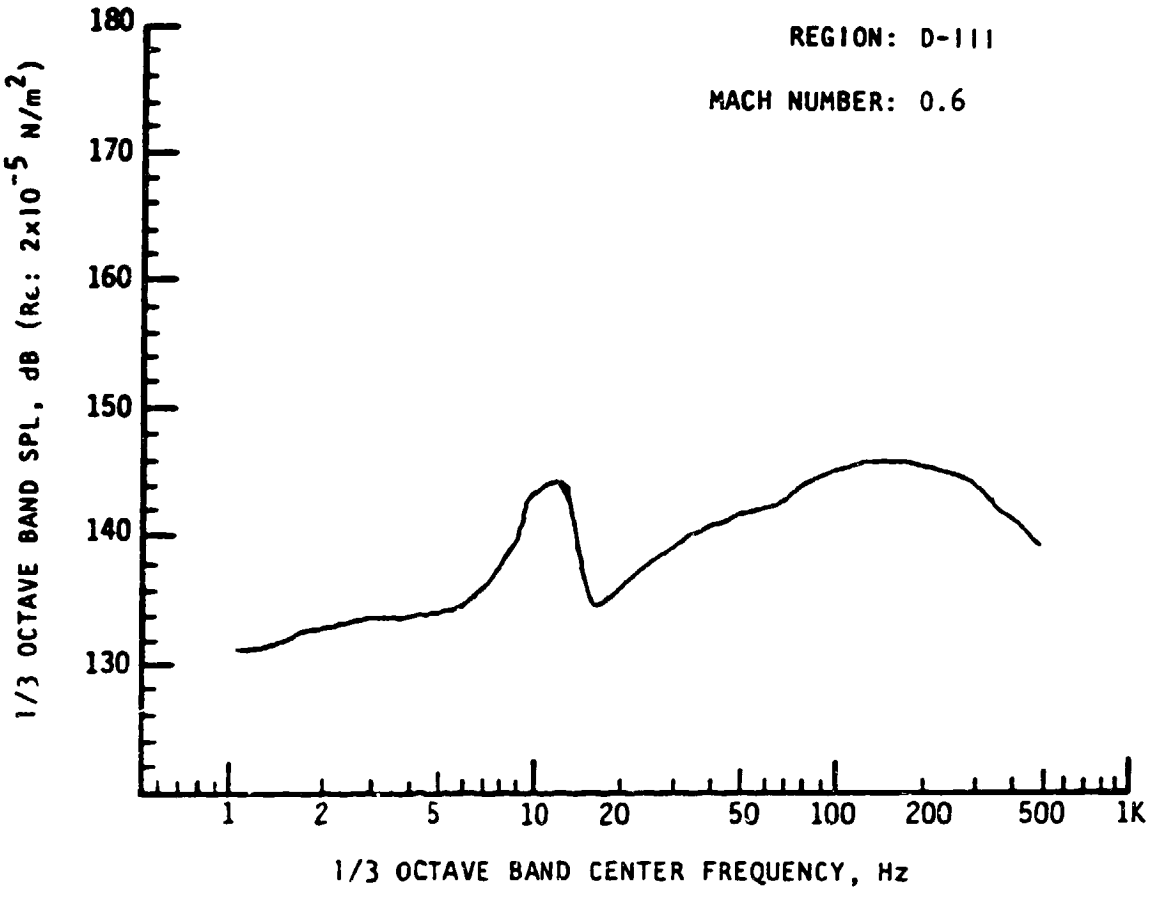

Note: Results based on 95 percentile OAFPL from Monte Carlo trajectory simulation.

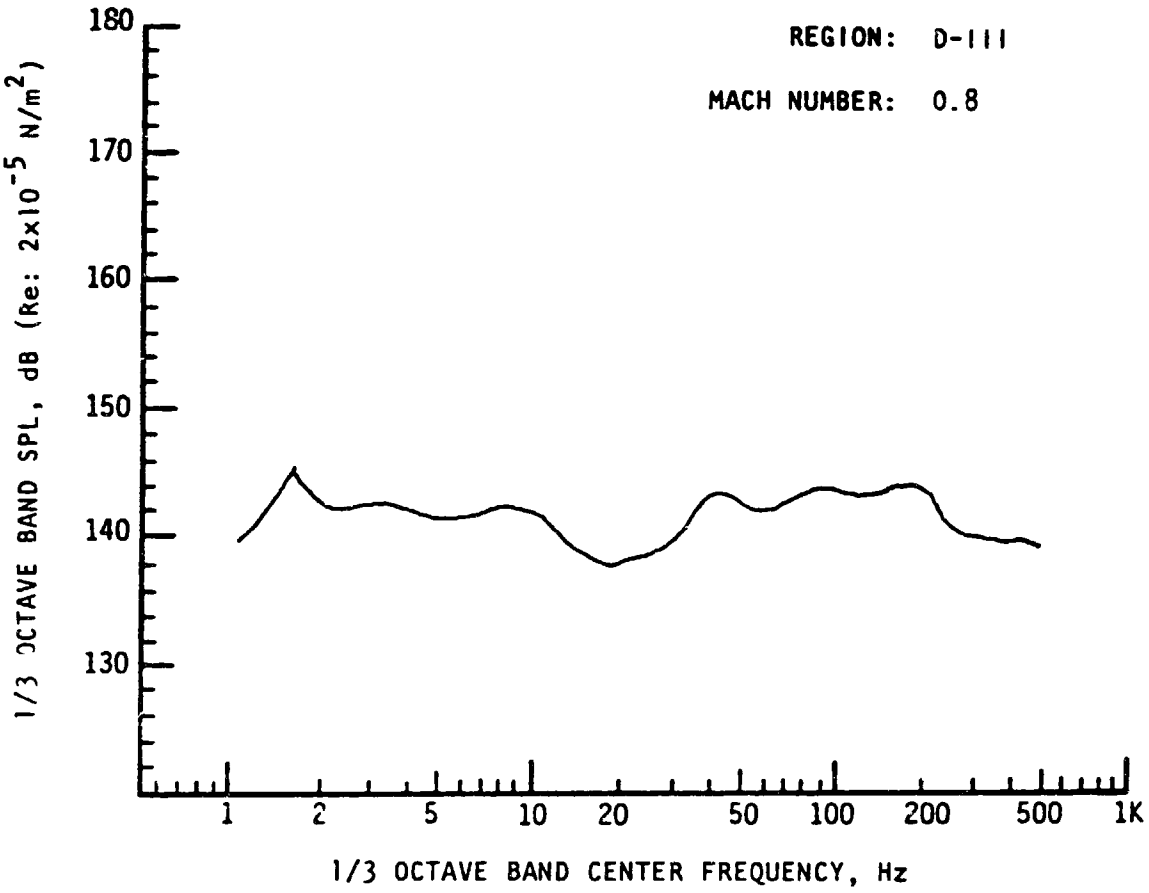

Note: Results based on 95 percentile OAFPL from Monte Carlo trajectory simulation.

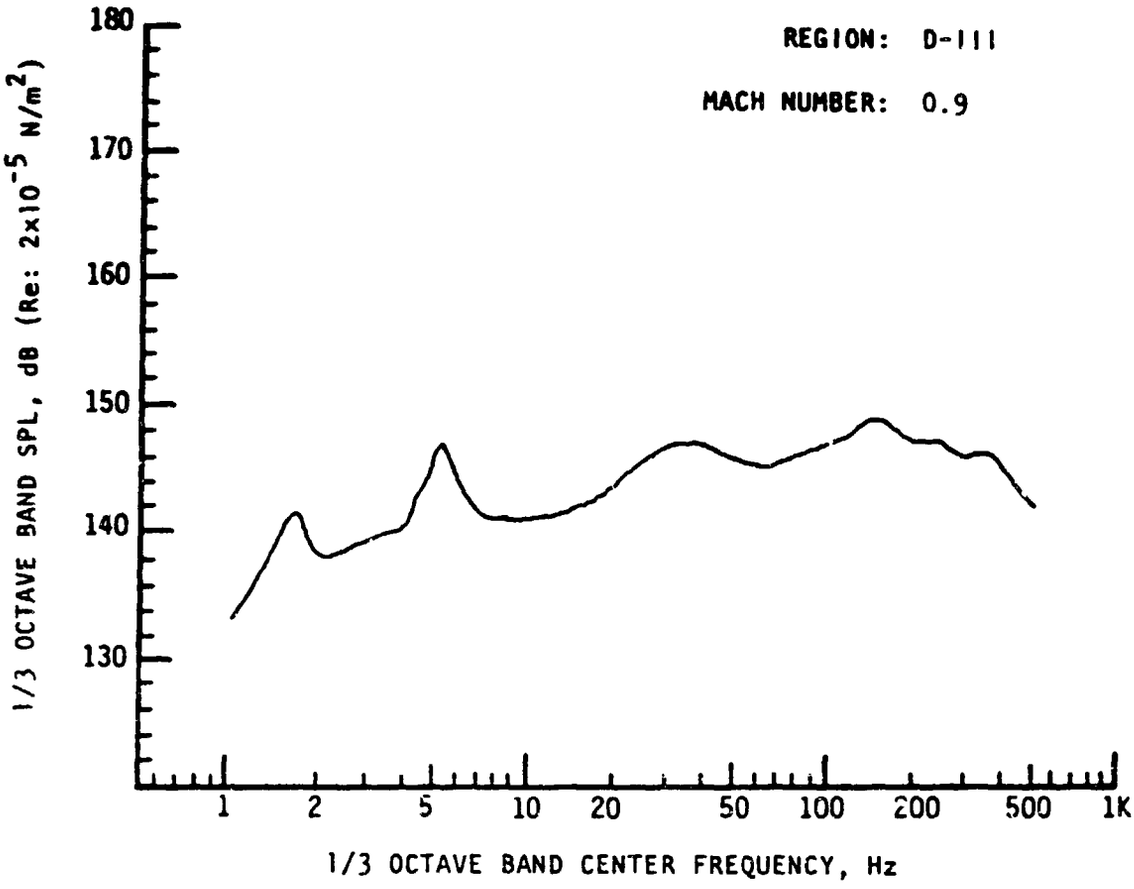

Note: Results based on 95 percentile OAFPL from Monte Carlo trajectory simulation.

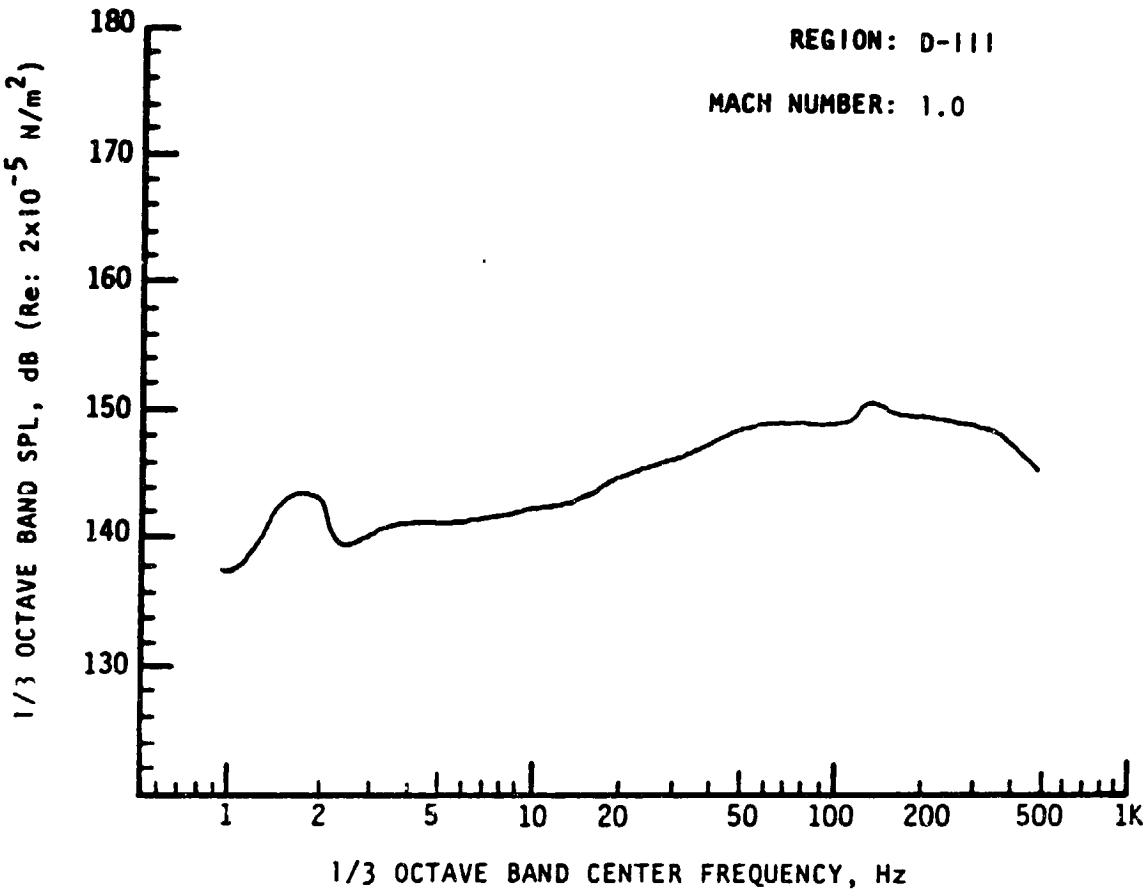

Note: Results based on 95 percentile OAFPL from Monte Carlo trajectory simulation.

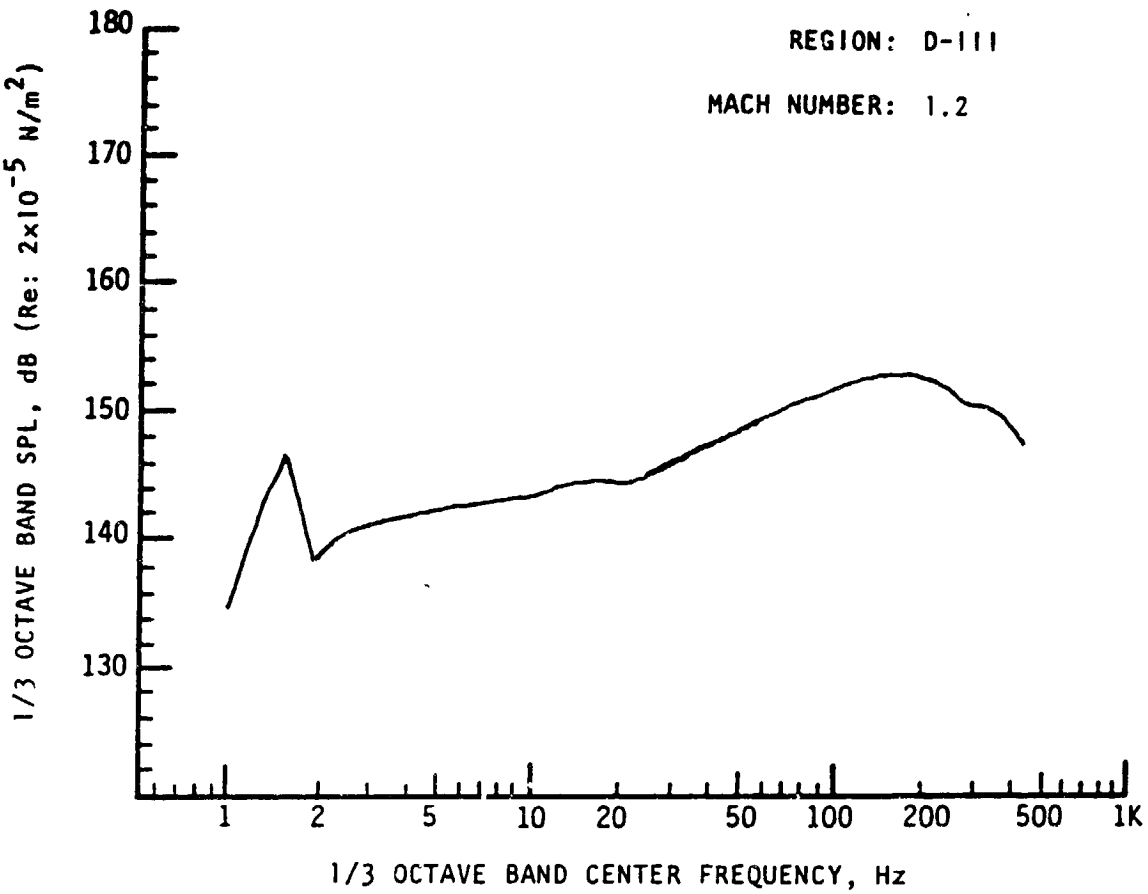

Note: Results based on 95 percentile OAFPL from Monte Carlo trajectory simulation.

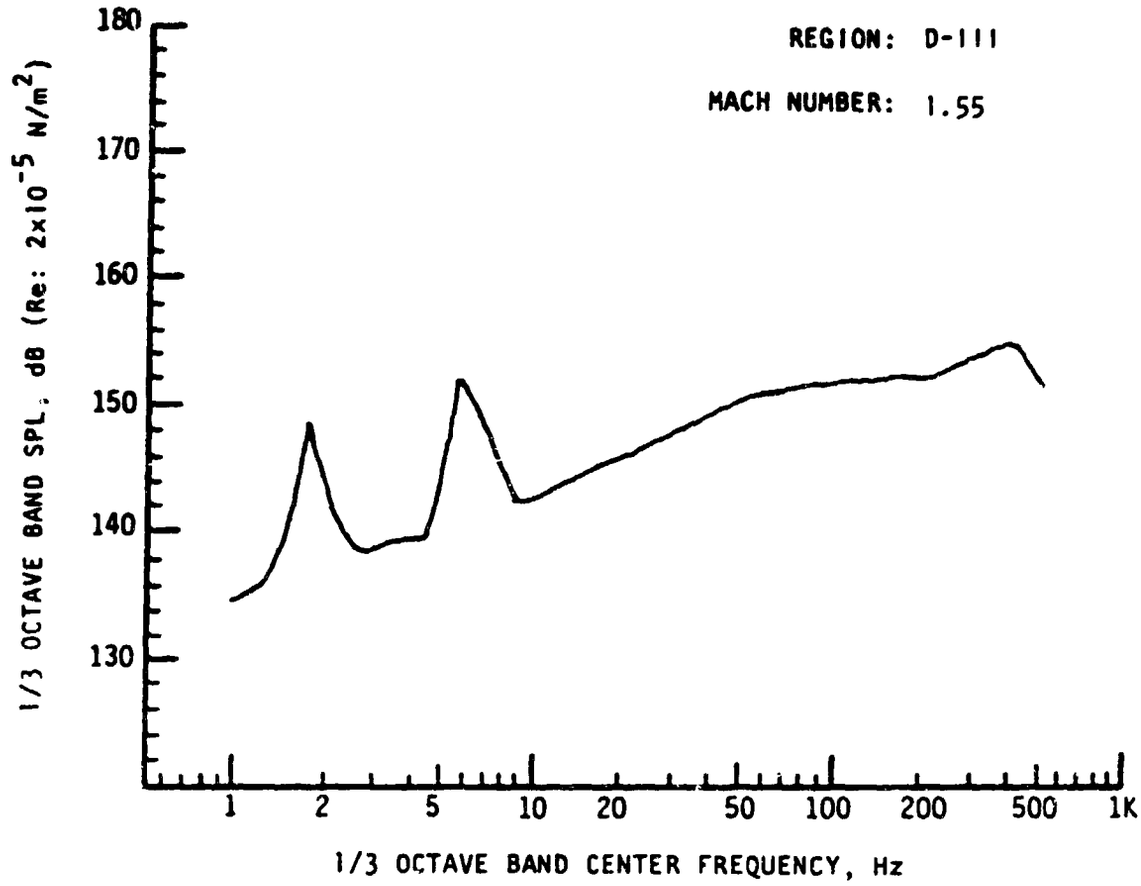

Note: Results based on 95 percentile OAFPL from Monte Carlo trajectory simulation.

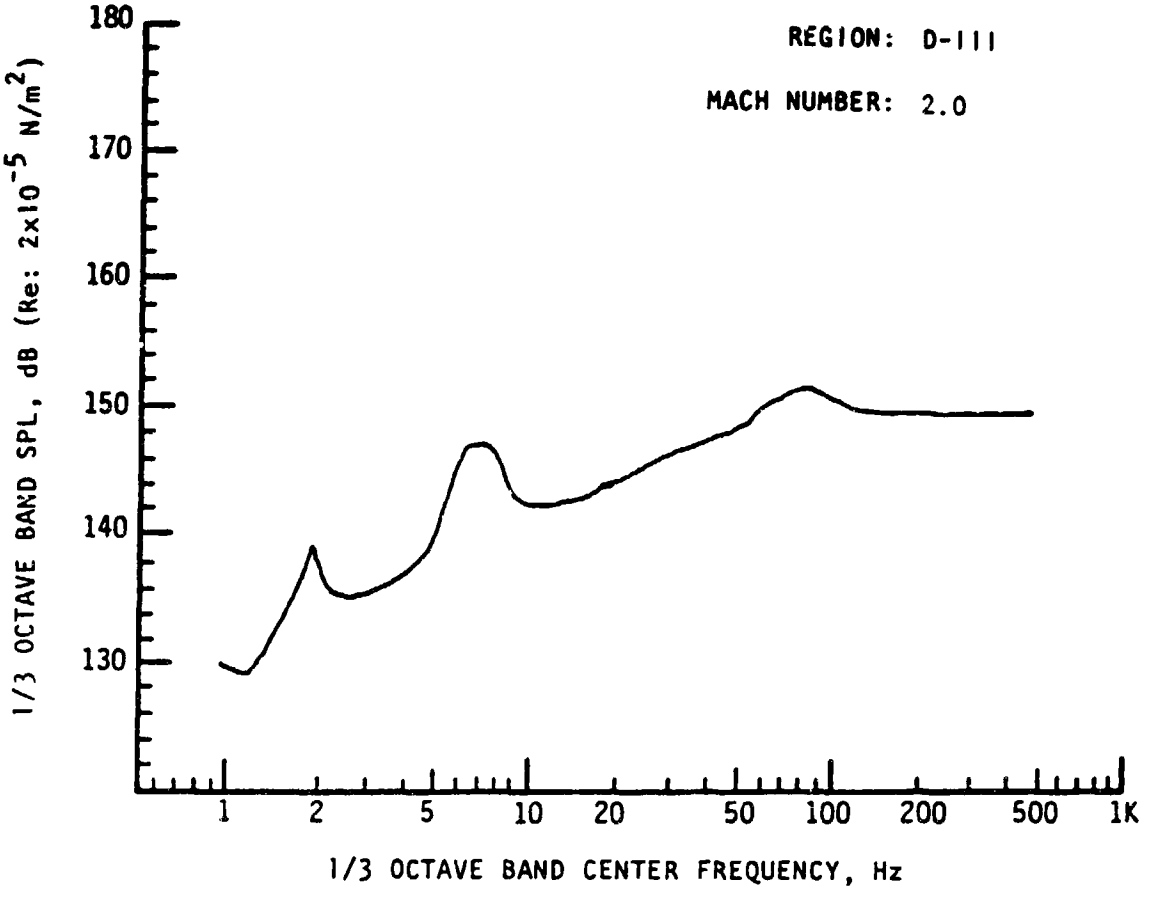

Note: Results based on 95 percentile OAFPL from Monte Carlo trajectory simulation.

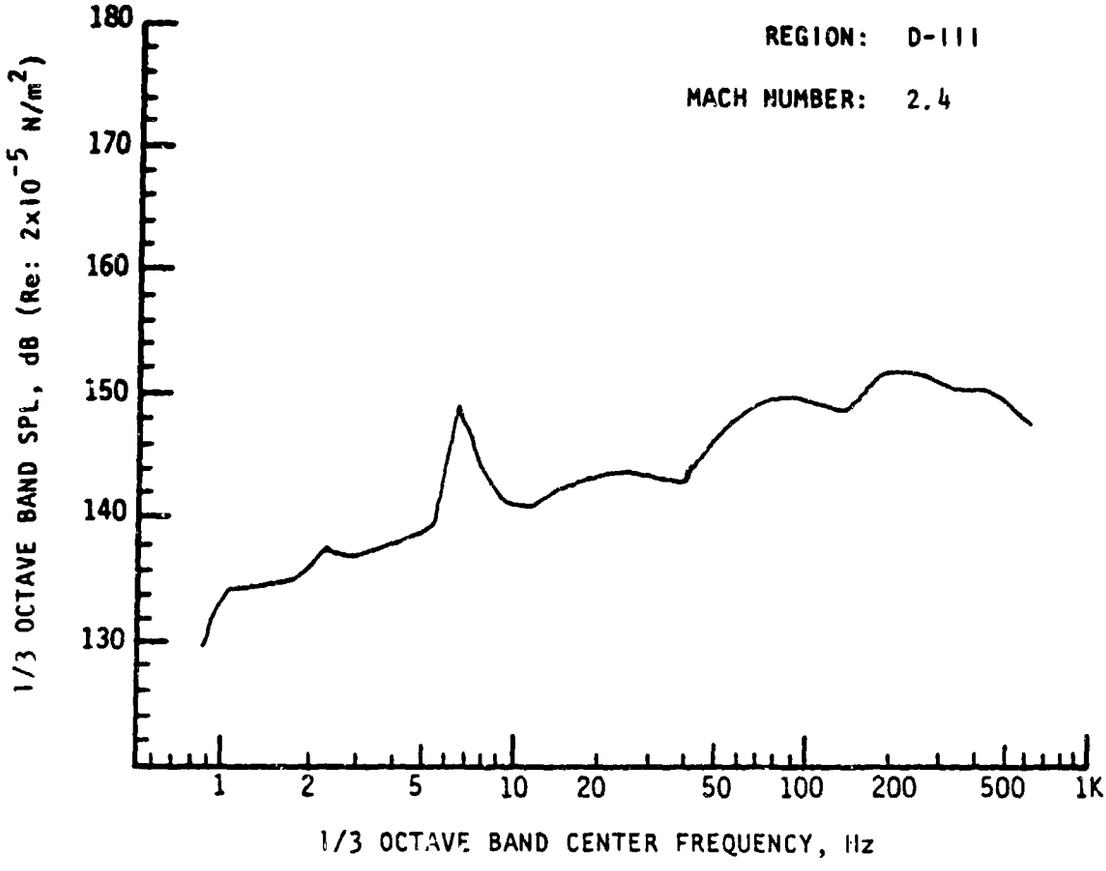

Note: Results based on 95 percentile OAFPL from Monte Carlo trajectory simulation.

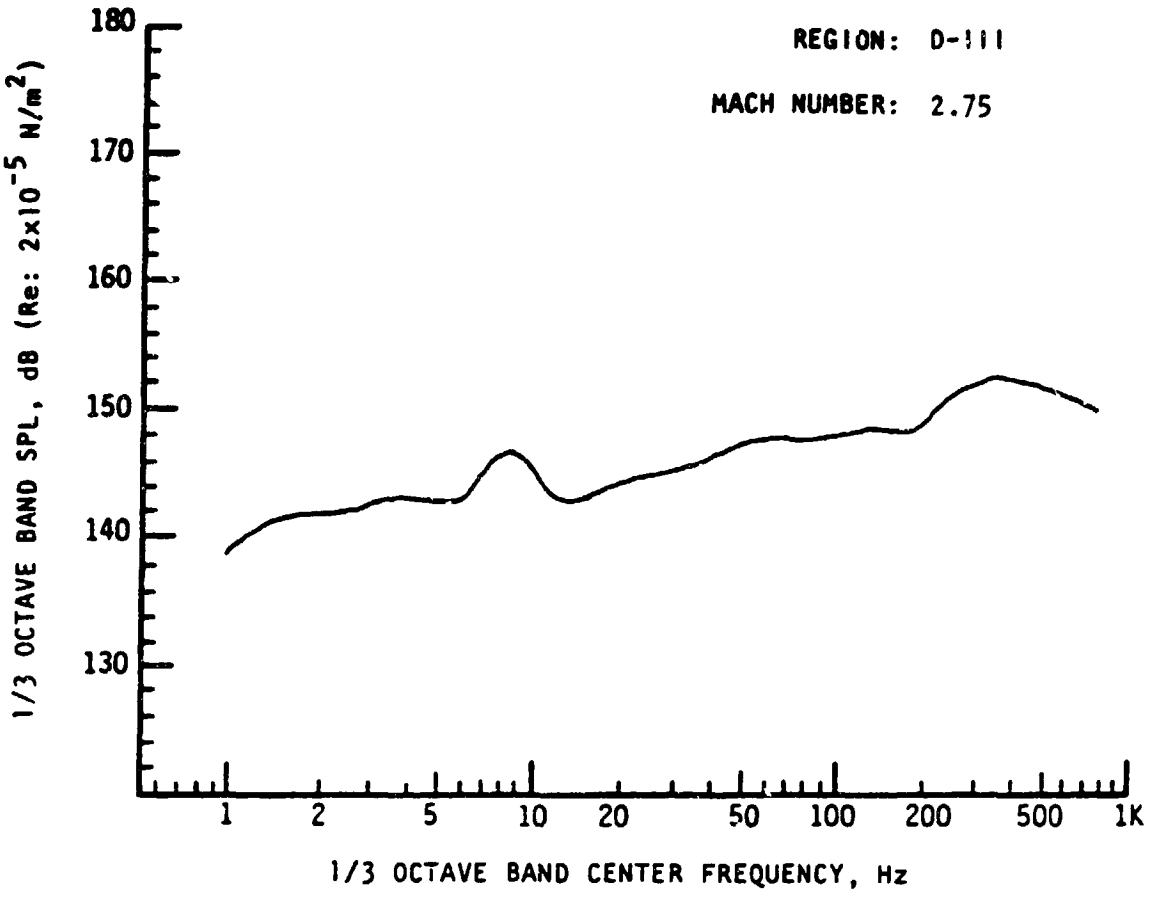

Note: Results based on 95 percentile OAFPL from Monte Carlo trajectory simulation.

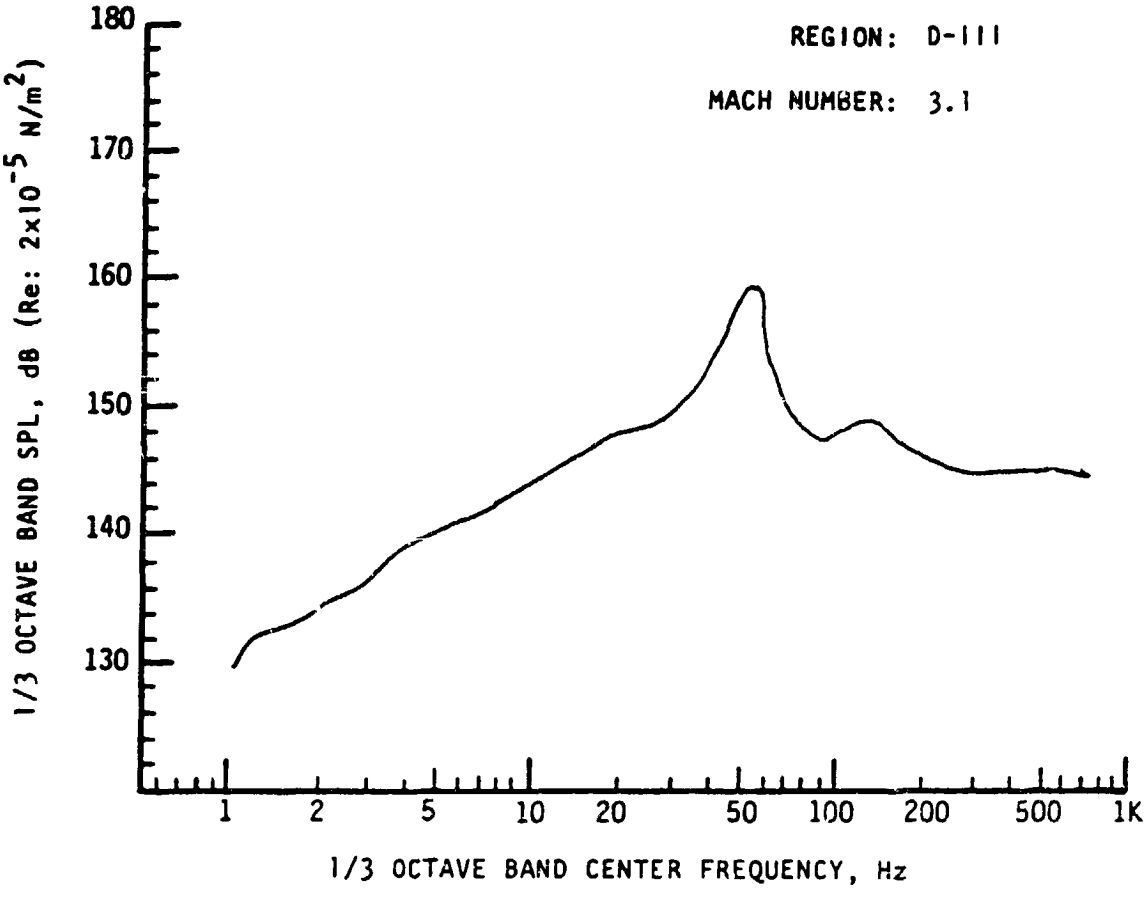

Note: Results based on 95 percentile OAFPL from Monte Carlo trajectory simulation.

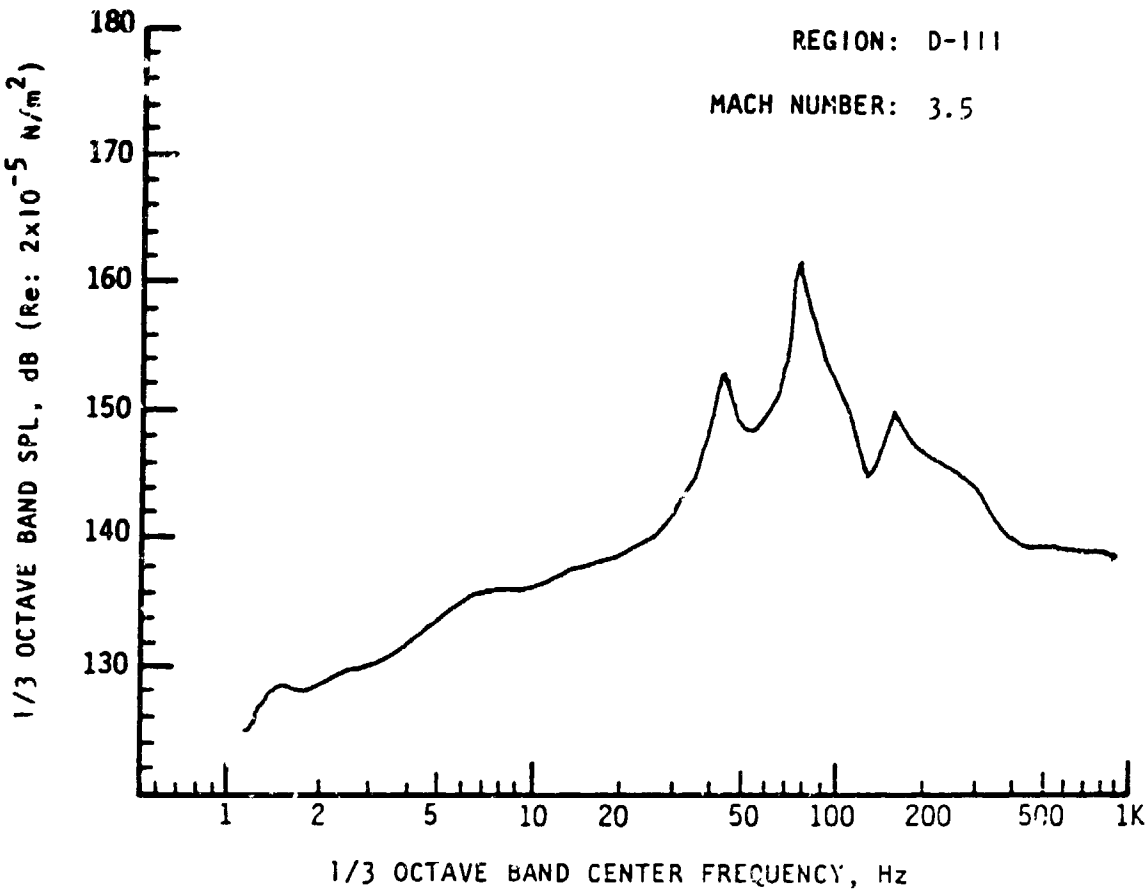

Note: Results based on 95 percentile OAFPL from Monte Carlo trajectory simulation.

APPENDIX D-IV

SRB FLEXIBLE HEAT SHIELD CONFIGURATION
ONE-THIRD OCTAVE-BAND AEROACOUSTIC SPECTRA FOR REGION V-IV
EXTERNAL SKIRT
(TRANSDUCER 99)

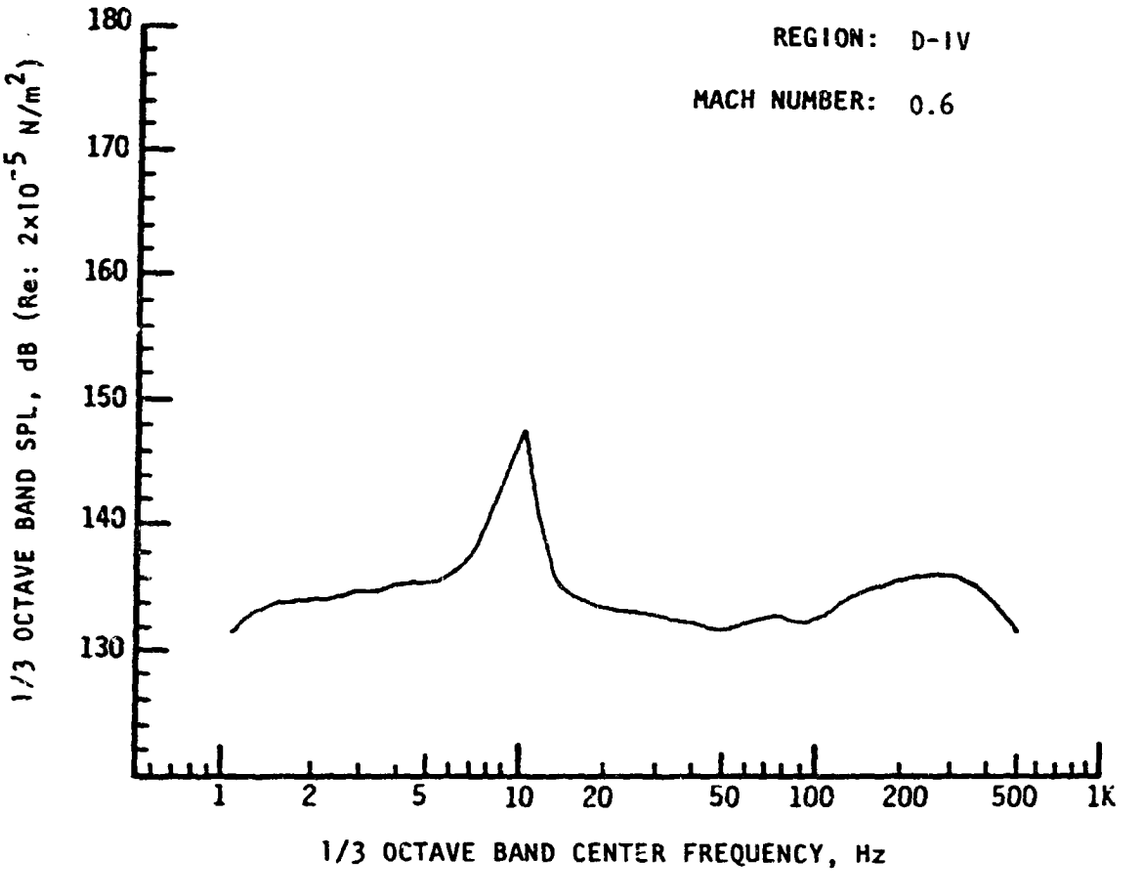

Note: Results based on 95 percentile OAFPL from Monte Carlo trajectory simulation.

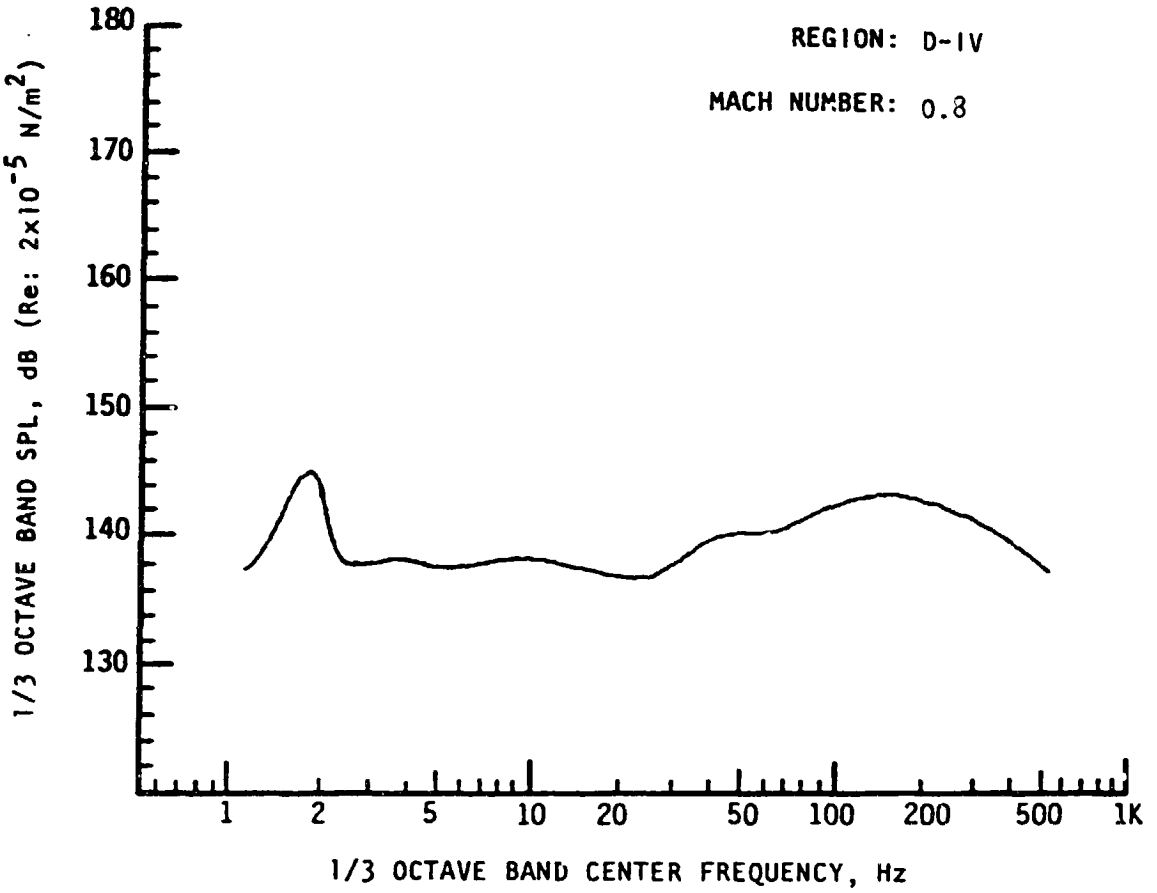

Note: Results based on 95 percentile OAFPL from Monte Carlo trajectory simulation.

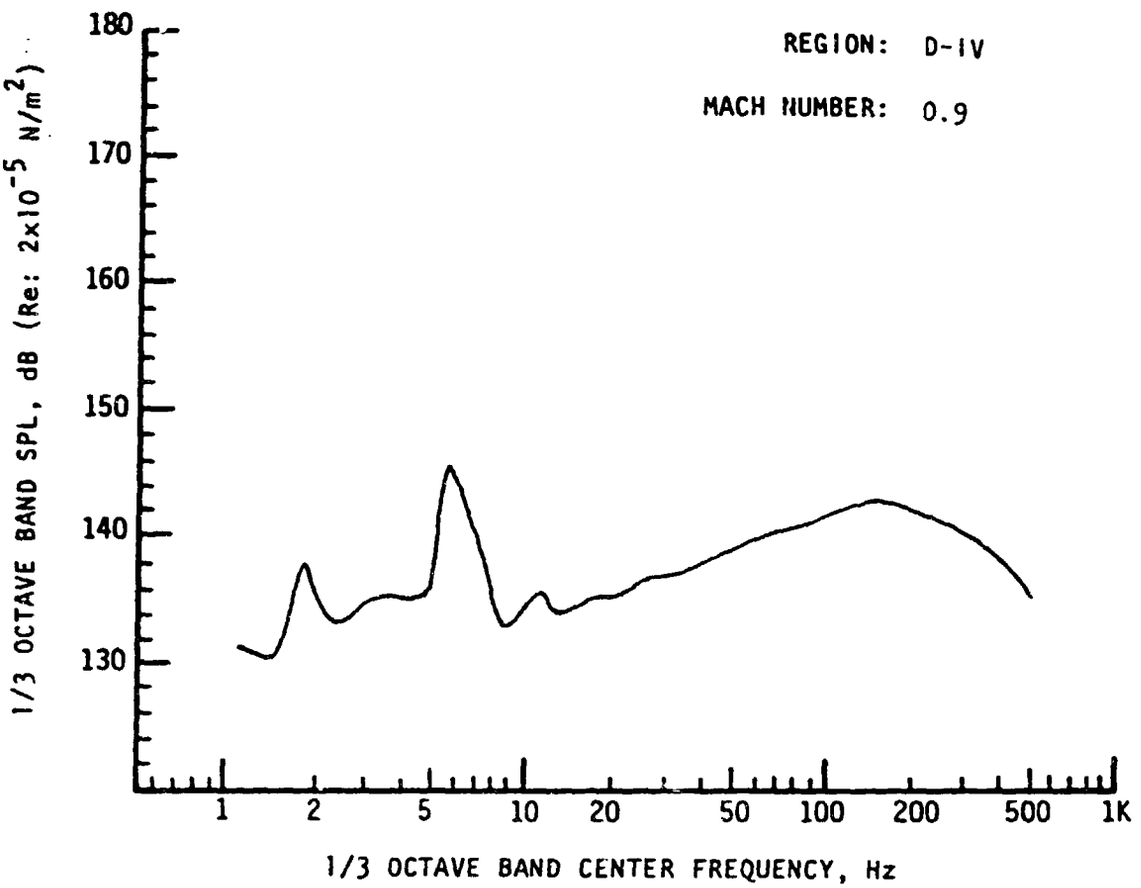

Note: Results based on 95 percentile OAFPL from Monte Carlo trajectory simulation.

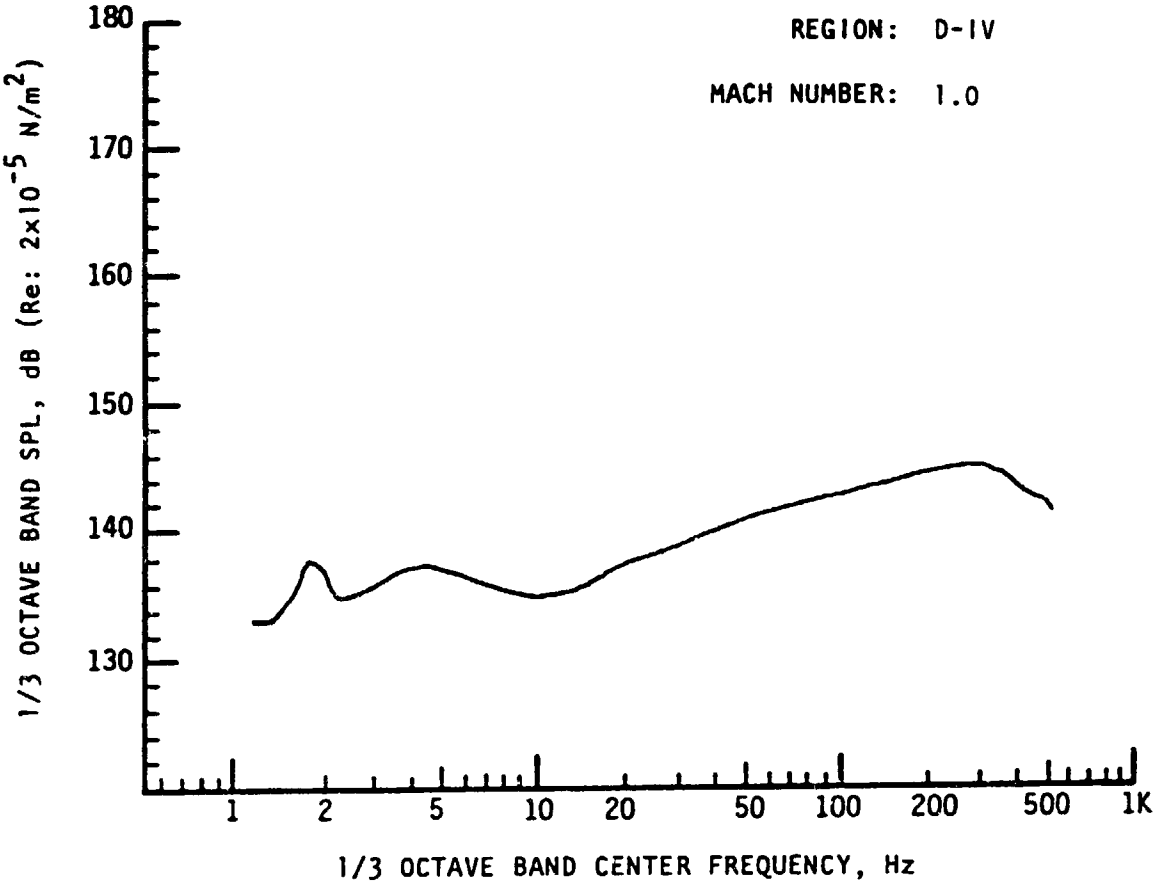

Note: Results based on 95 percentile OAFPL from Monte Carlo trajectory simulation.

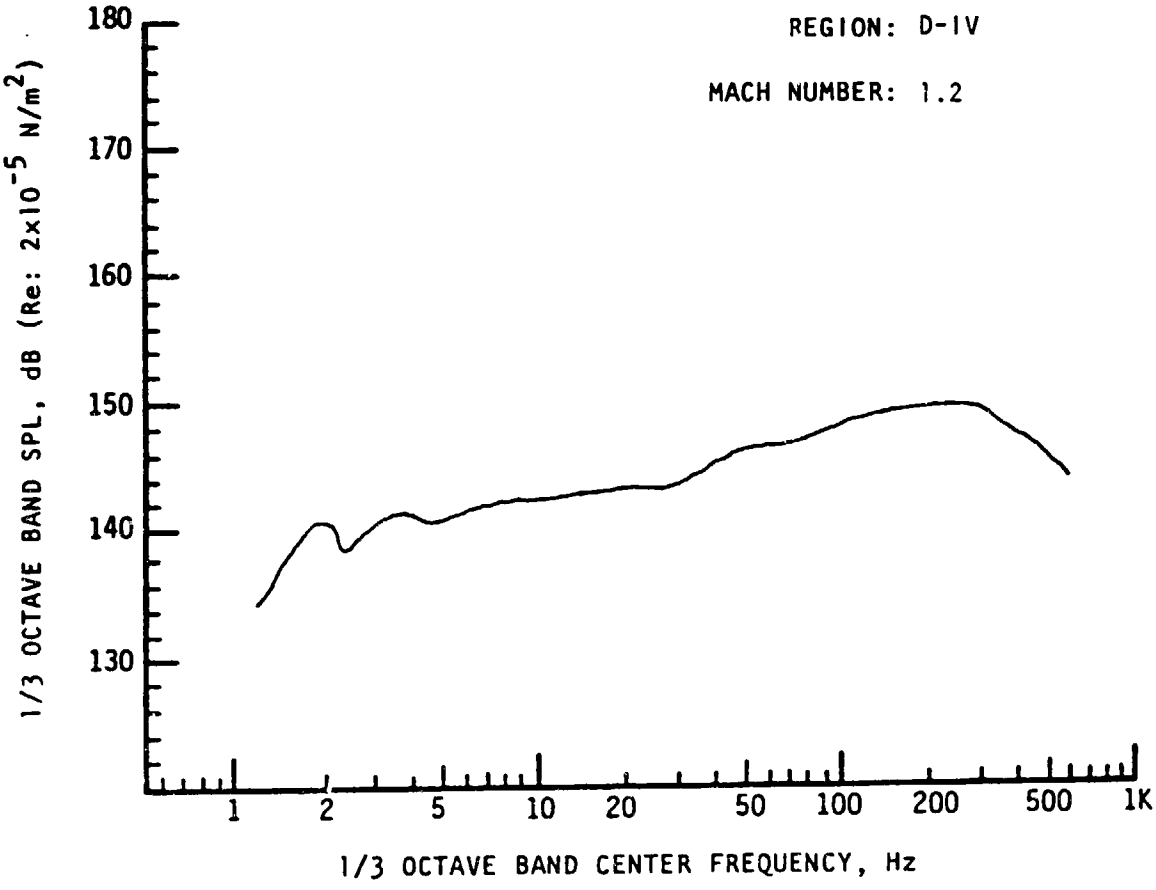

Note: Results based on 95 percentile OAFPL from Monte Carlo trajectory simulation.

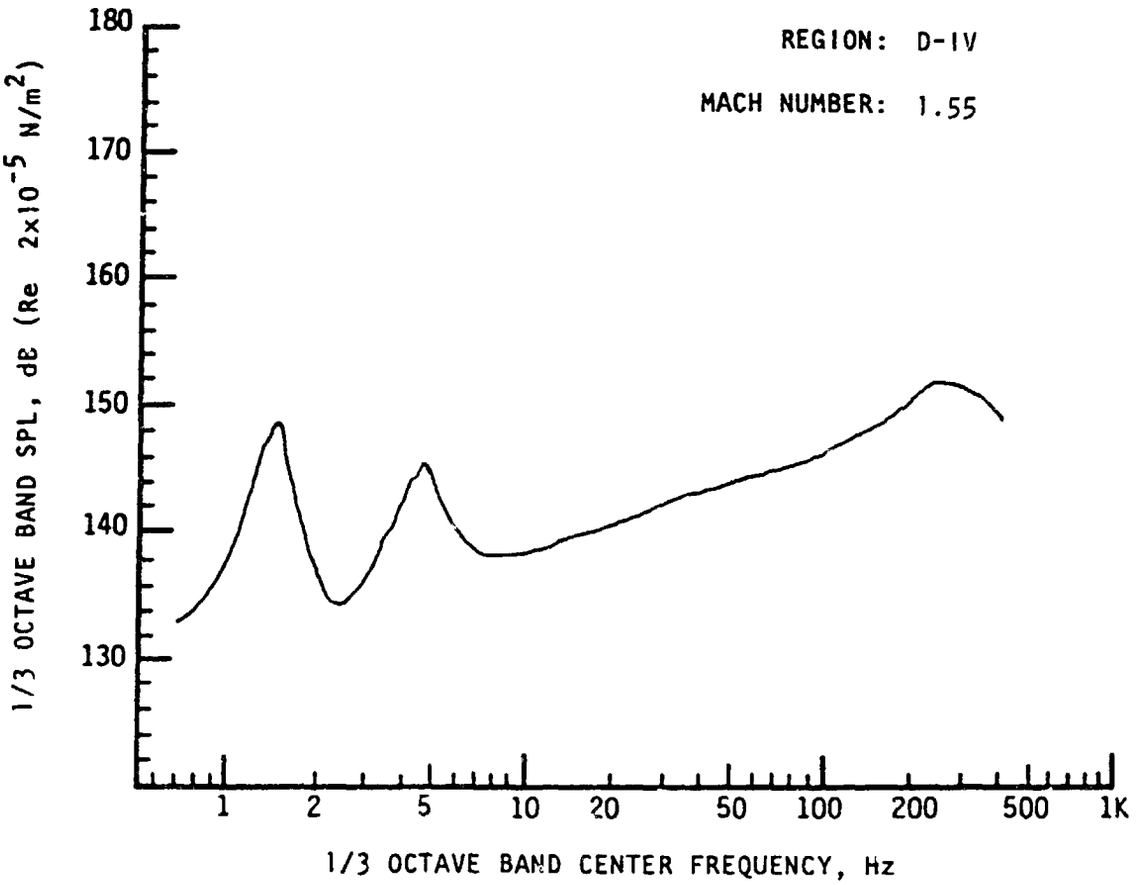

Note: Results based on 95 percentile OAFPL from Monte Carlo trajectory simulation.

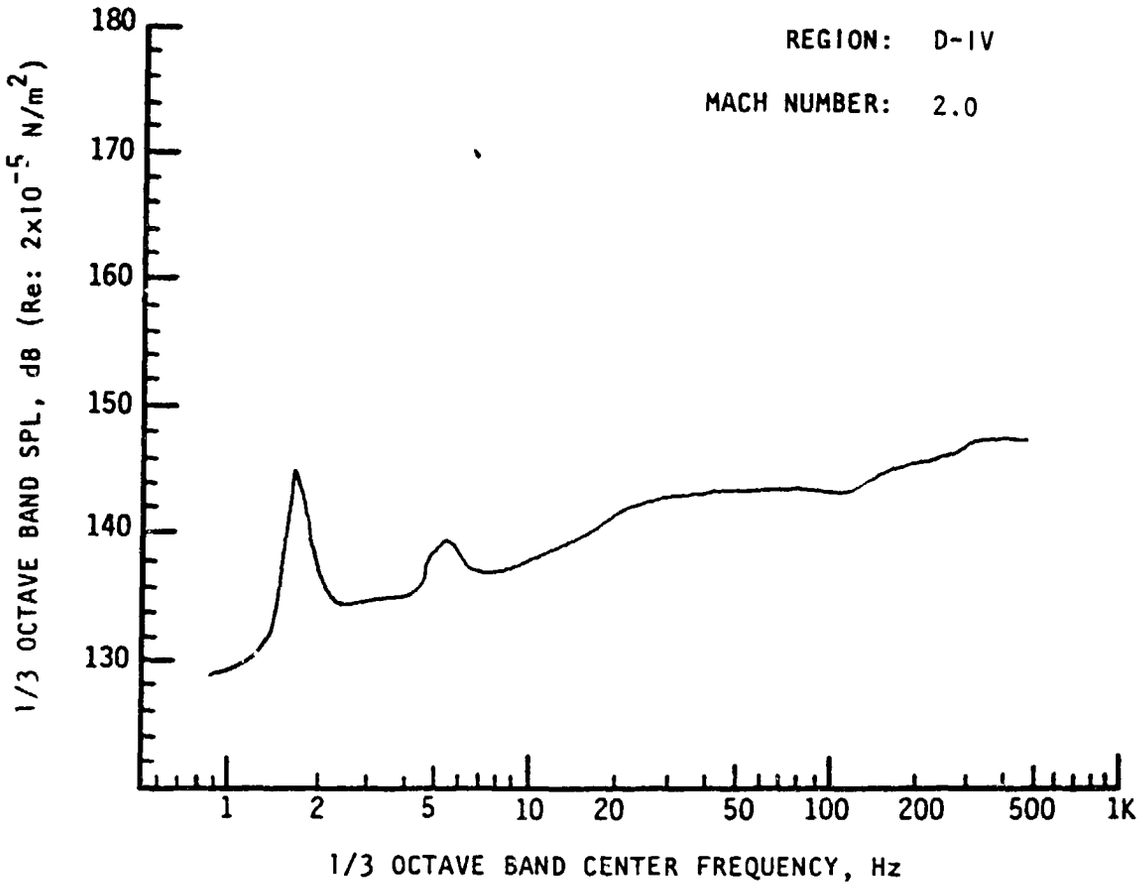

Note: Results based on 95 percentile OAFPL from Monte Carlo trajectory simulation.

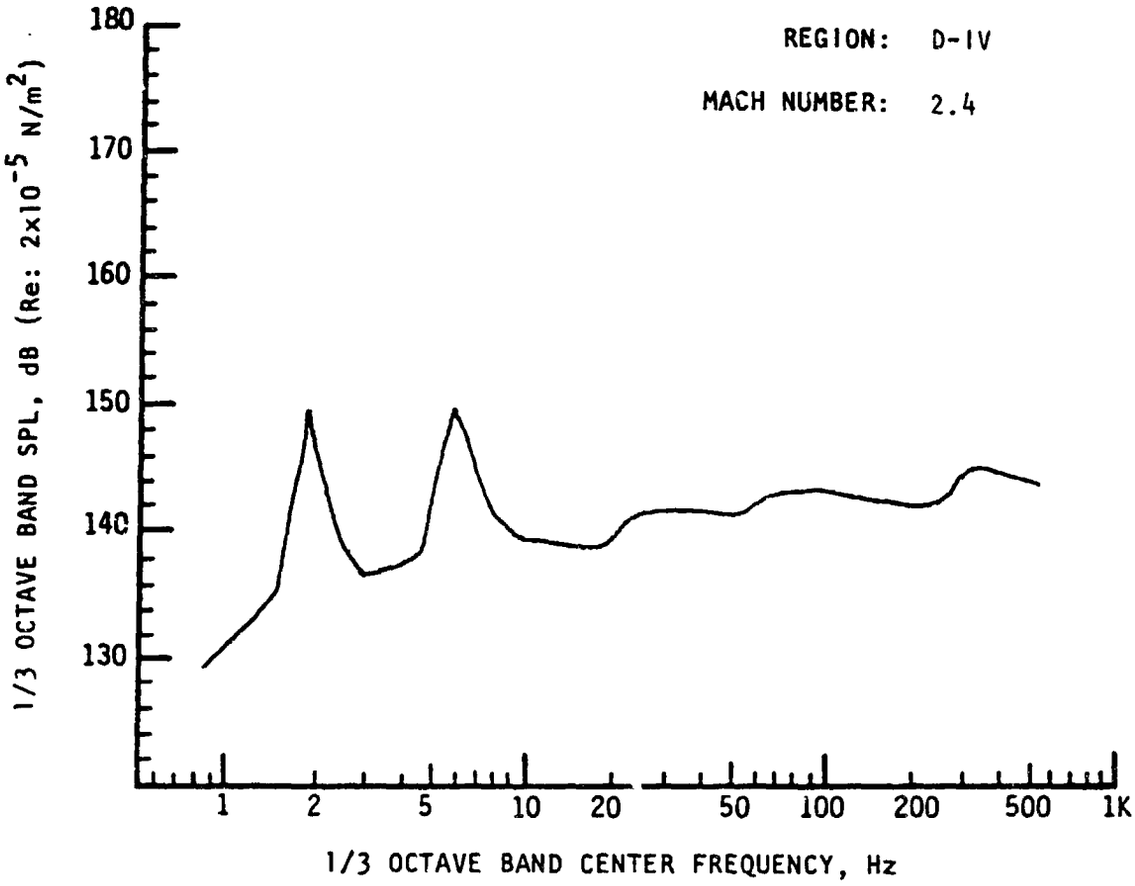

Note: Results based on 95 percentile OAFPL from Monte Carlo trajectory simulation.

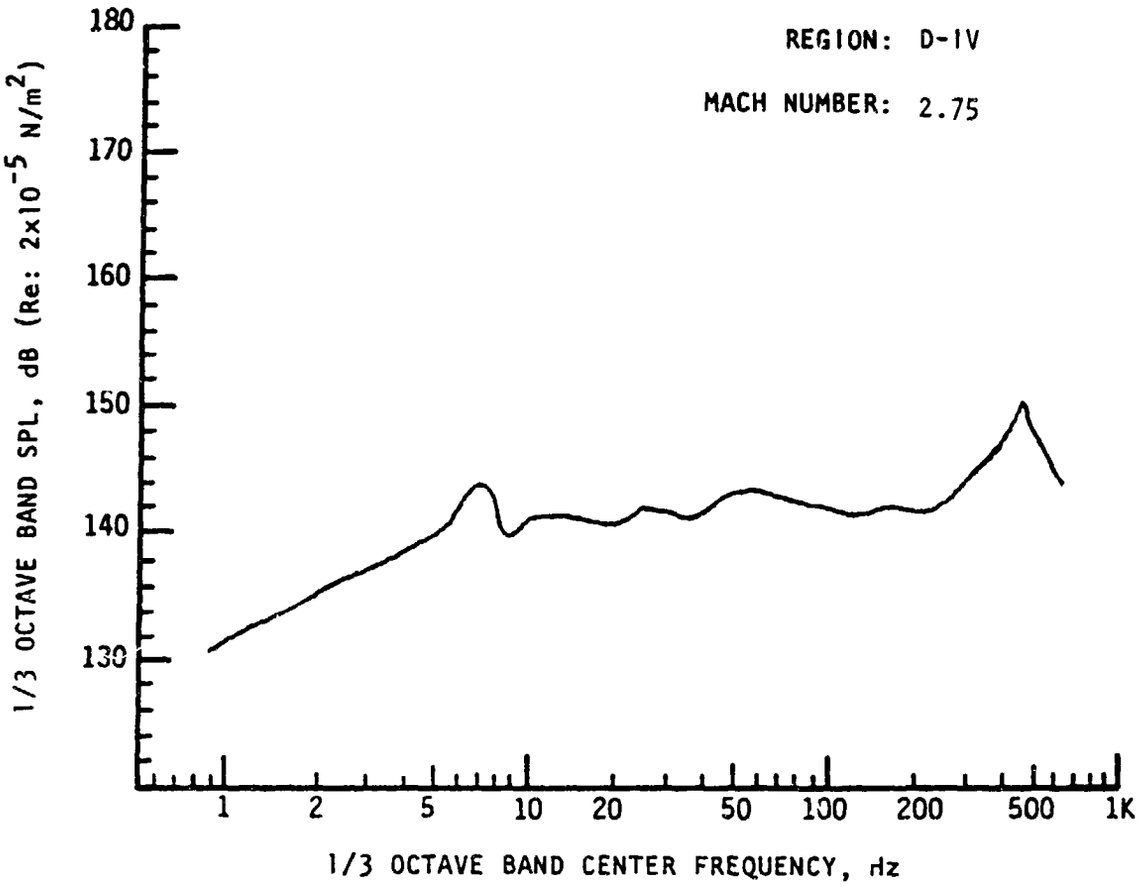

Note: Results based on 95 percentile OAFPL from Monte Carlo trajectory simulation.

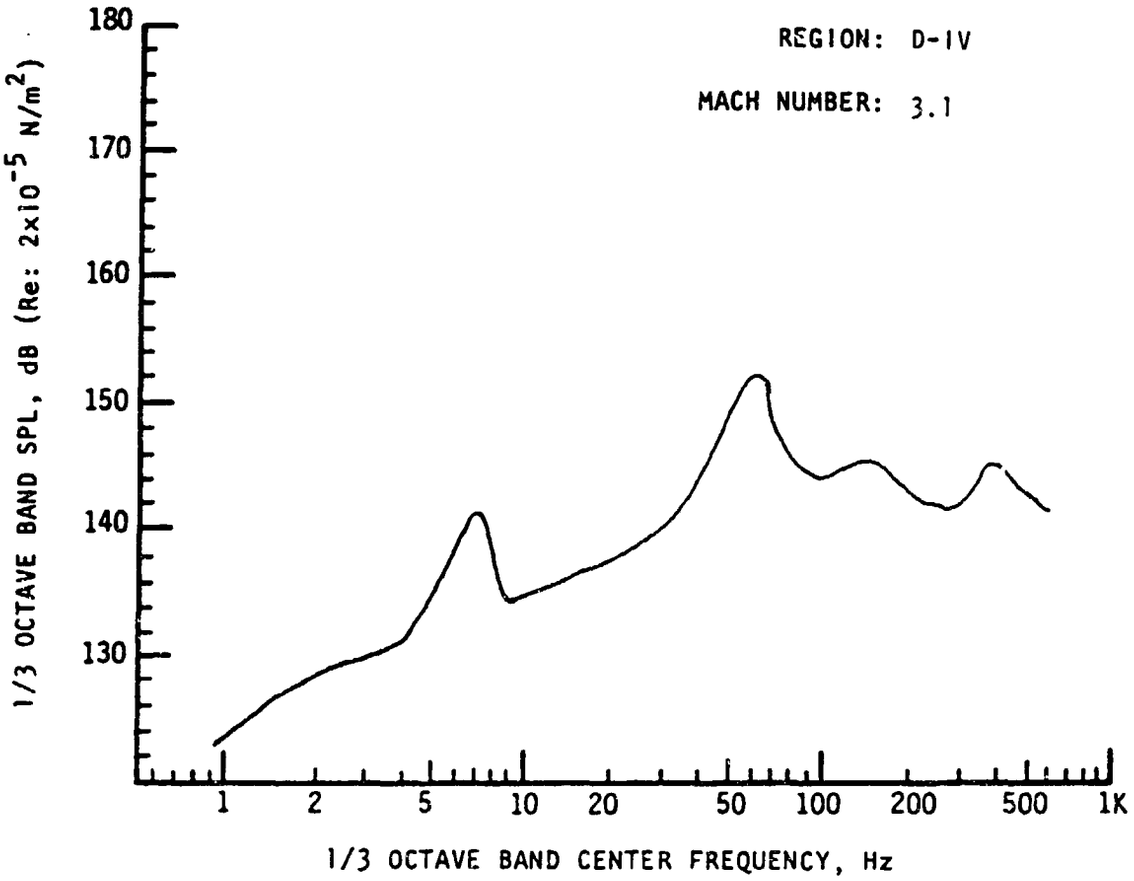

Note: Results based on 95 percentile OAFPL from Monte Carlo trajectory simulation.

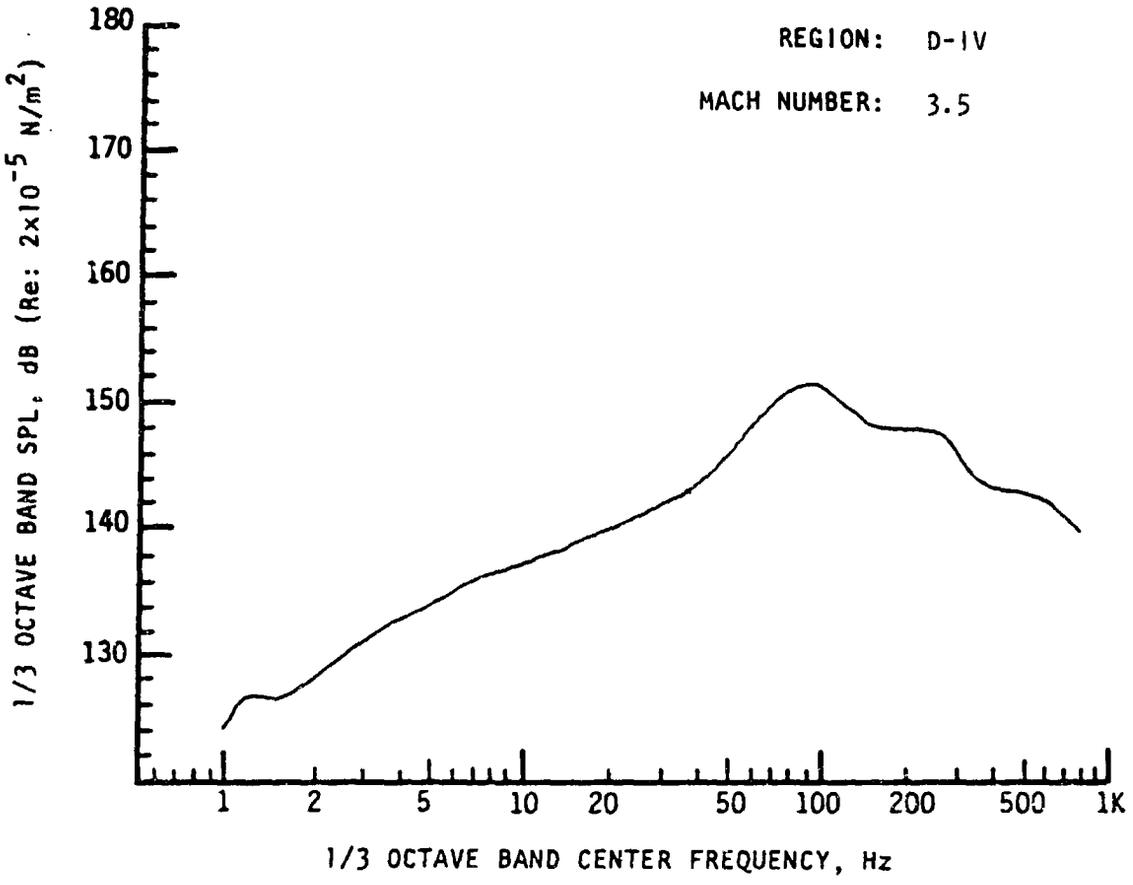

Note: Results based on 95 percentile OAFPL from Monte Carlo trajectory simulation.

APPENDIX D-V

SRB FLEXIBLE HEAT SHIELD CONFIGURATION
ONE-THIRD OCTAVE-BAND AEROACOUSTIC SPECTRA FOR REGION D-V
EXTERNAL SKIRT
(TRANSDUCERS 93, 102, 103)

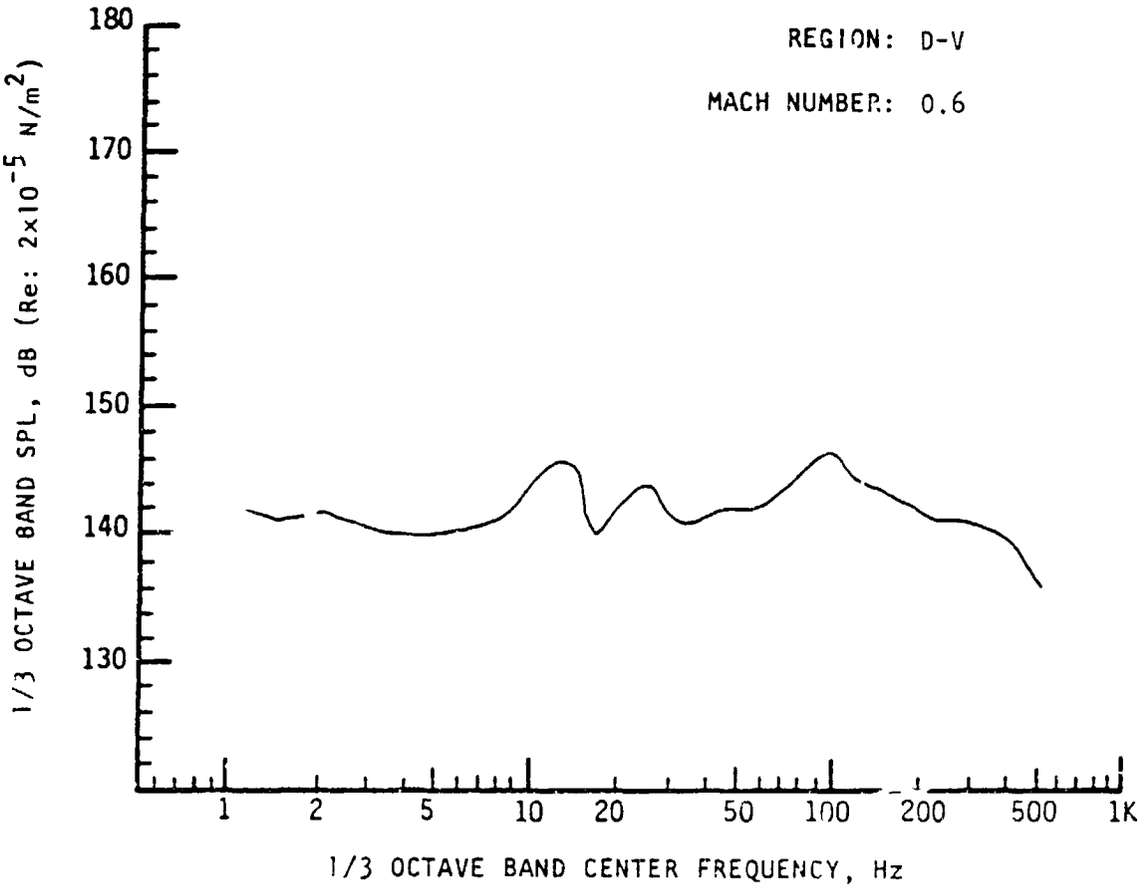

Note: Results based on 95 percentile OAFPL from Monte Carlo trajectory simulation.

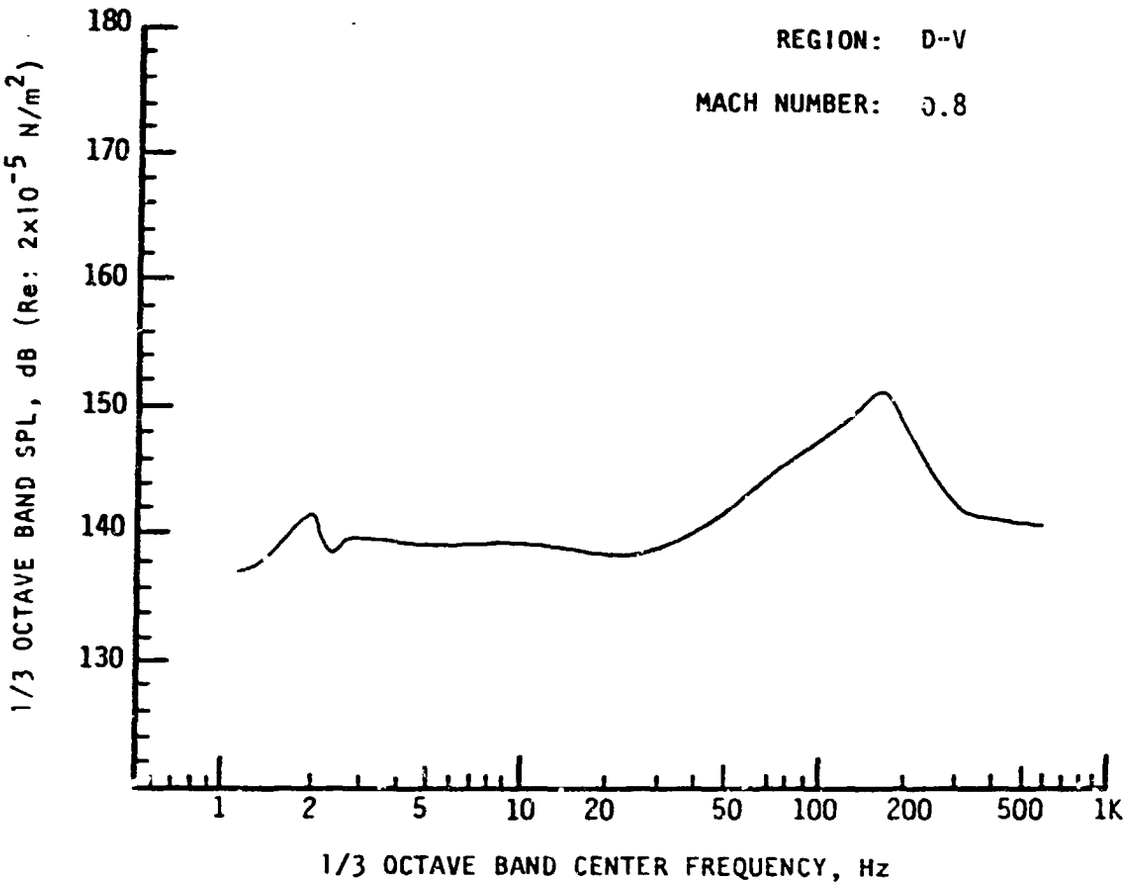

Note: Results based on 95 percentile OAFPL from Monte Carlo trajectory simulation.

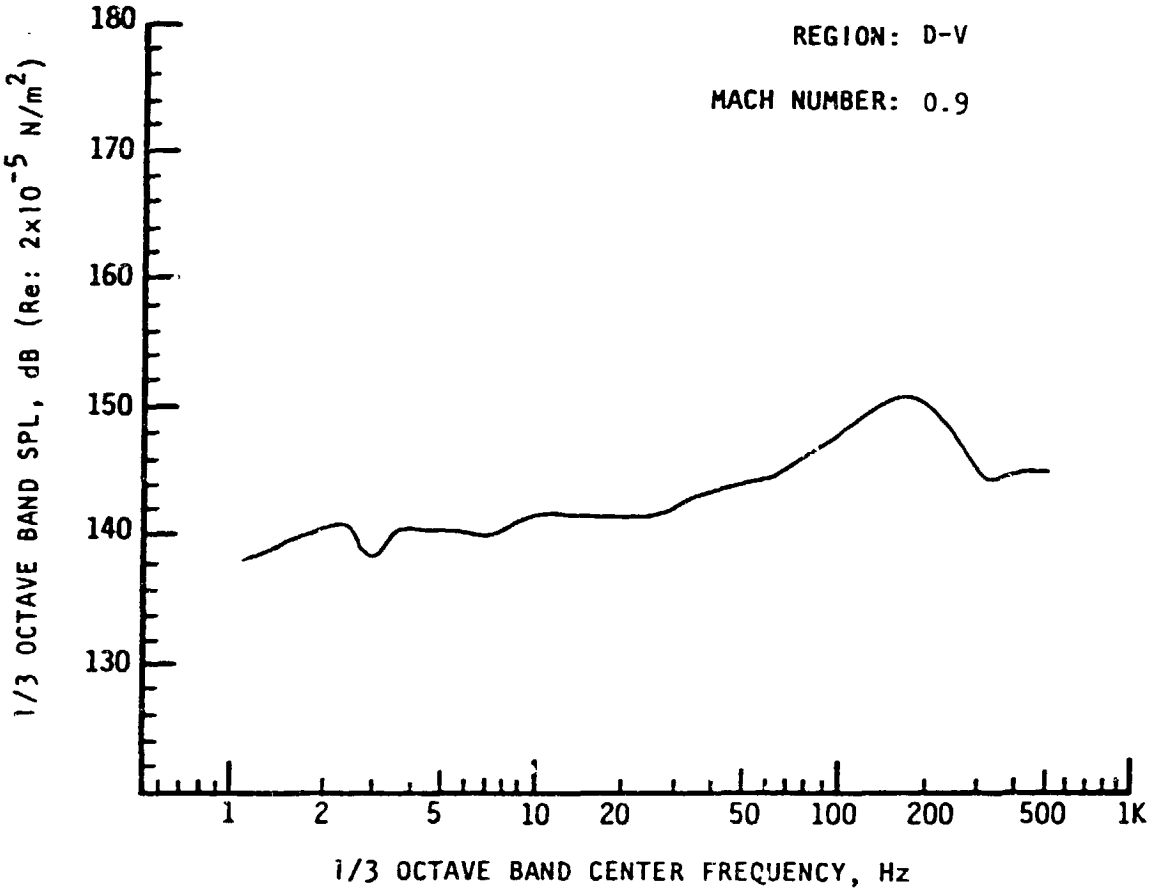

Note: Results based on 95 percentile OAFPL from Monte Carlo trajectory simulation.

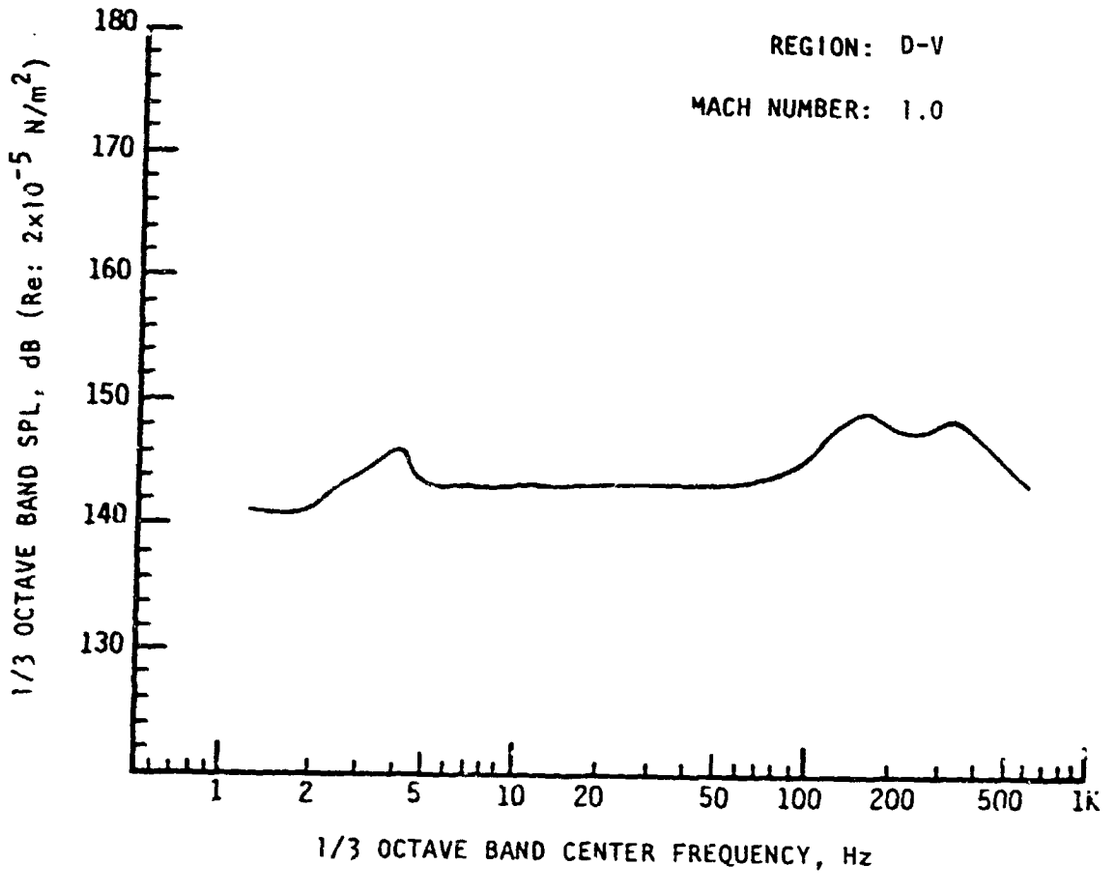

Note: Results based on 95 percentile OAFPL from Monte Carlo trajectory simulation.

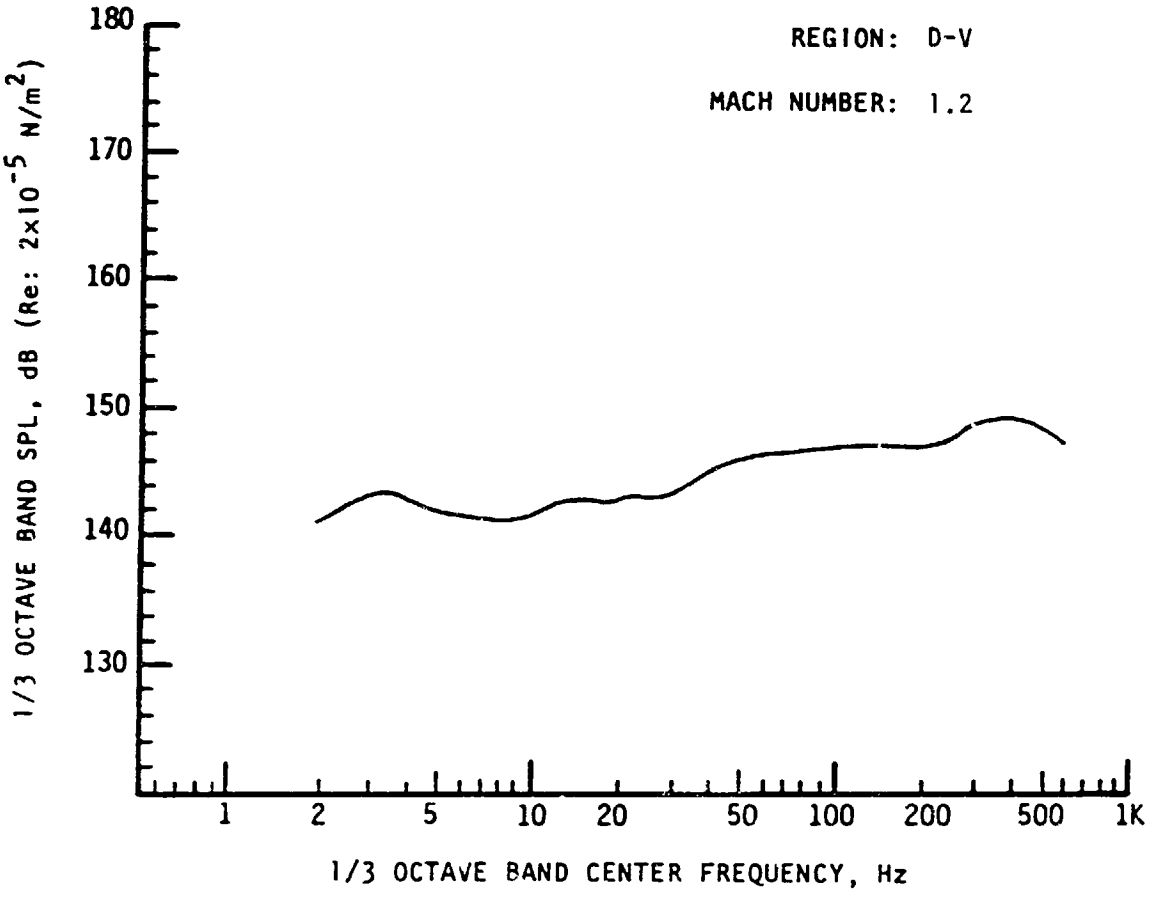

Note: Results based on 95 percentile OAFPL from Monte Carlo trajectory simulation.

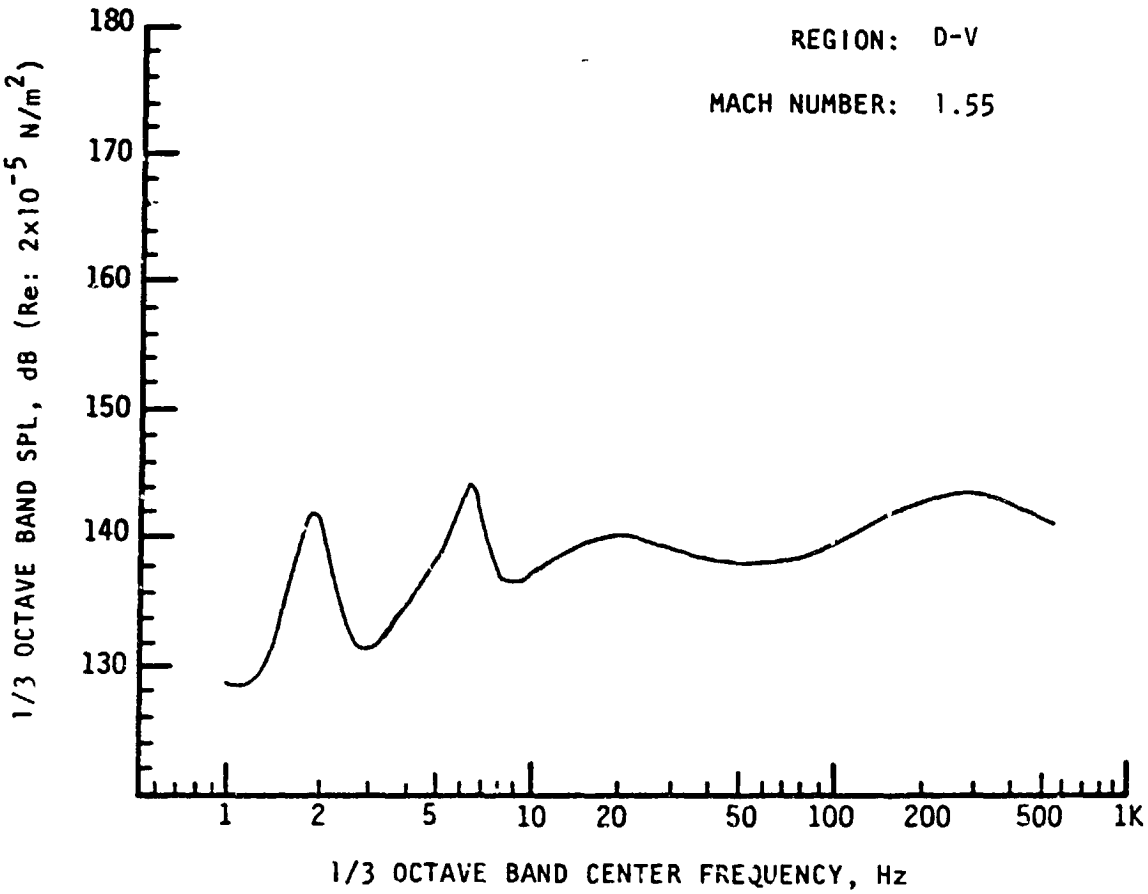

Note: Results based on 95 percentile OAFPL from Monte Carlo trajectory simulation.

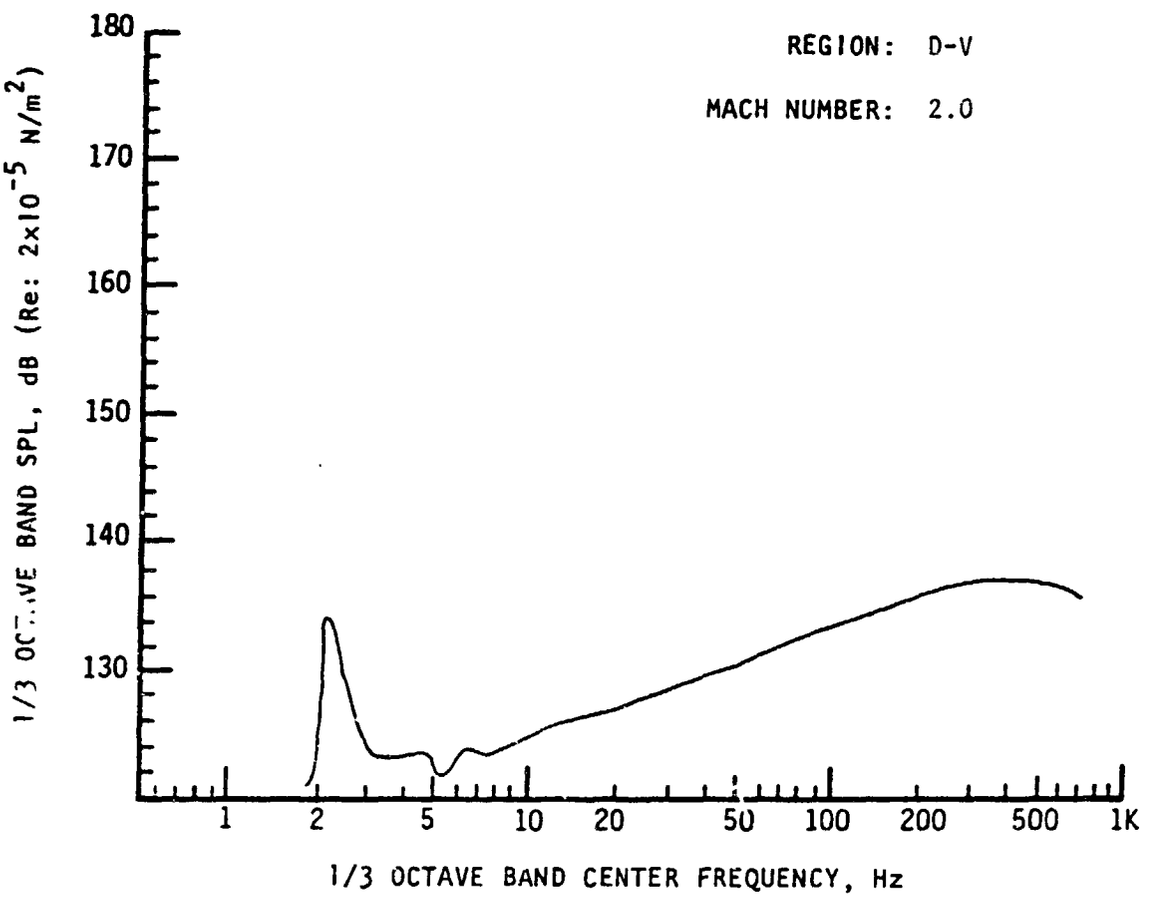

Note: Results based on 95 percentile OAFPL from Monte Carlo trajectory simulation.

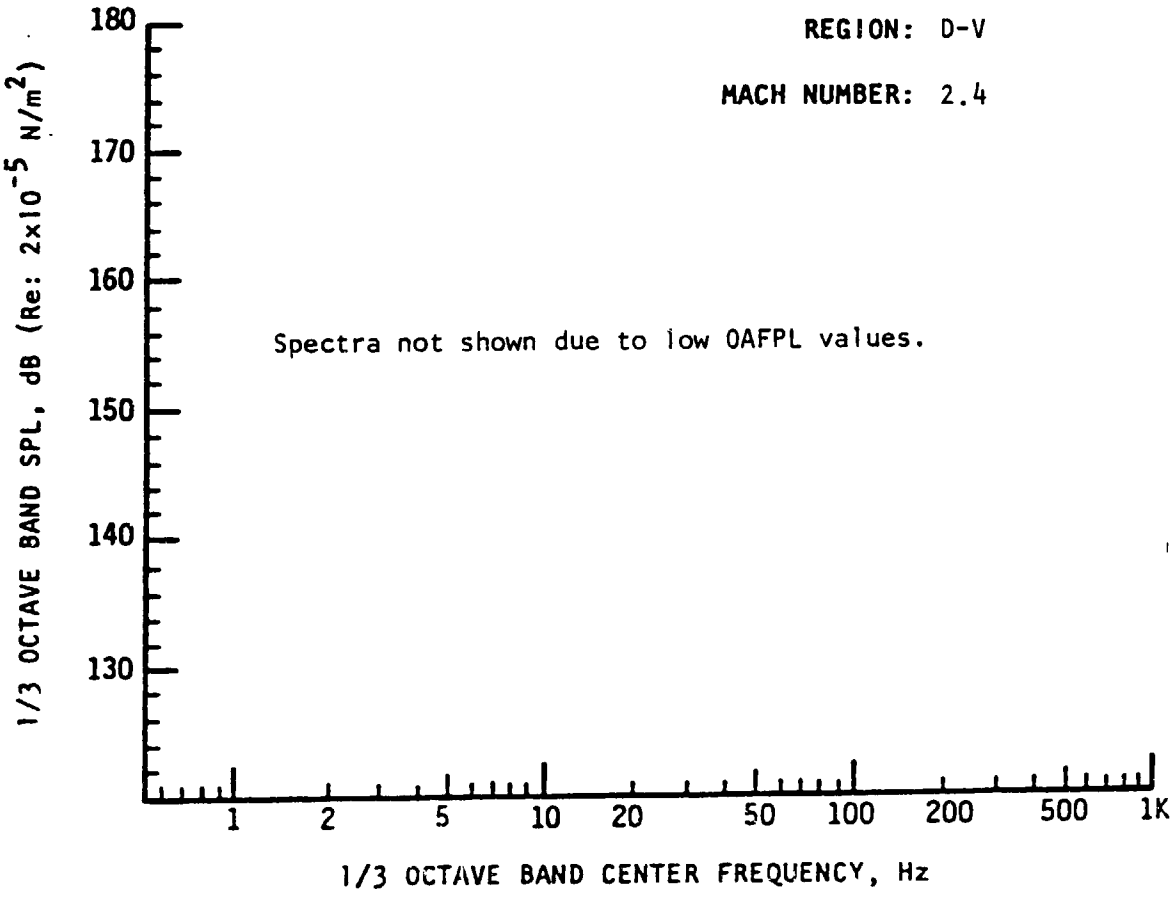

Note: Results based on 95 percentile OAFPL from Monte Carlo trajectory simulation.

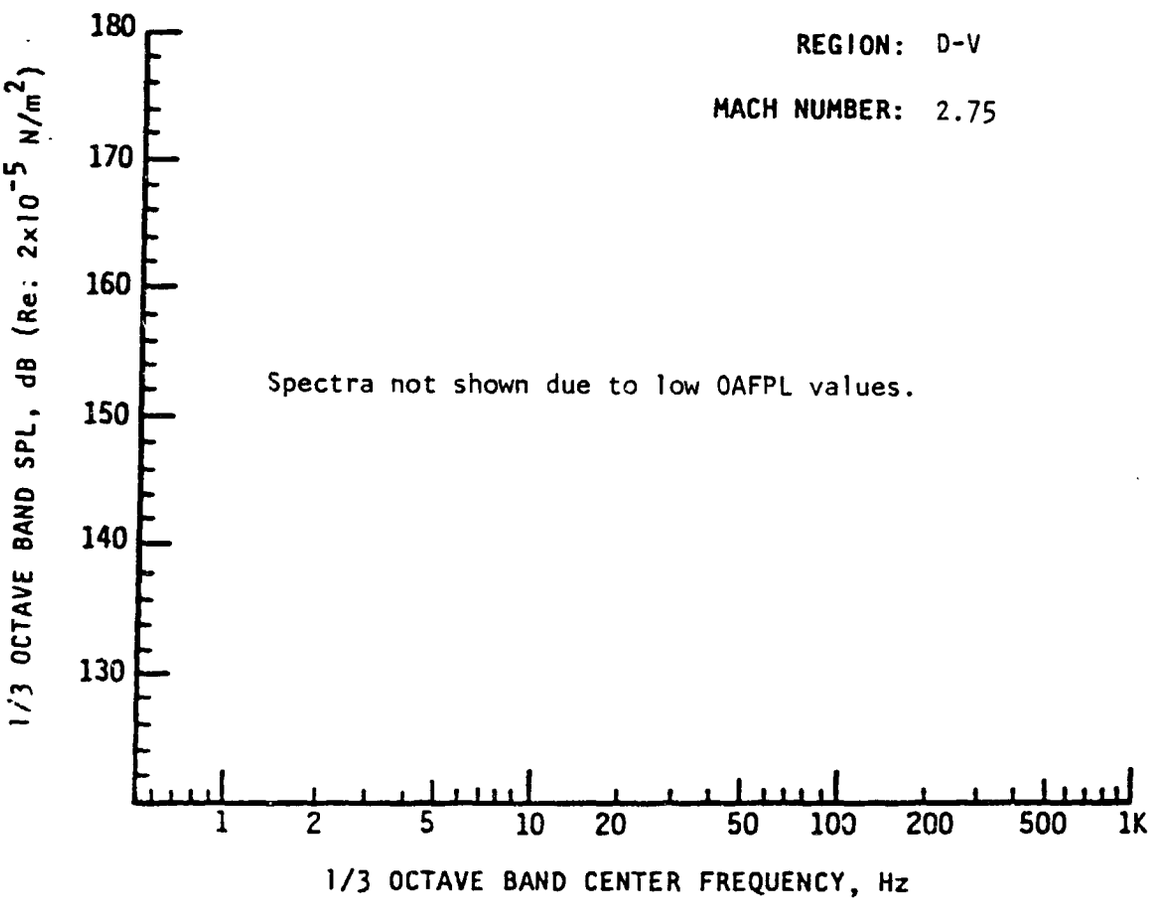

Note: Results based on 95 percentile OAFPL from Monte Carlo trajectory simulation.

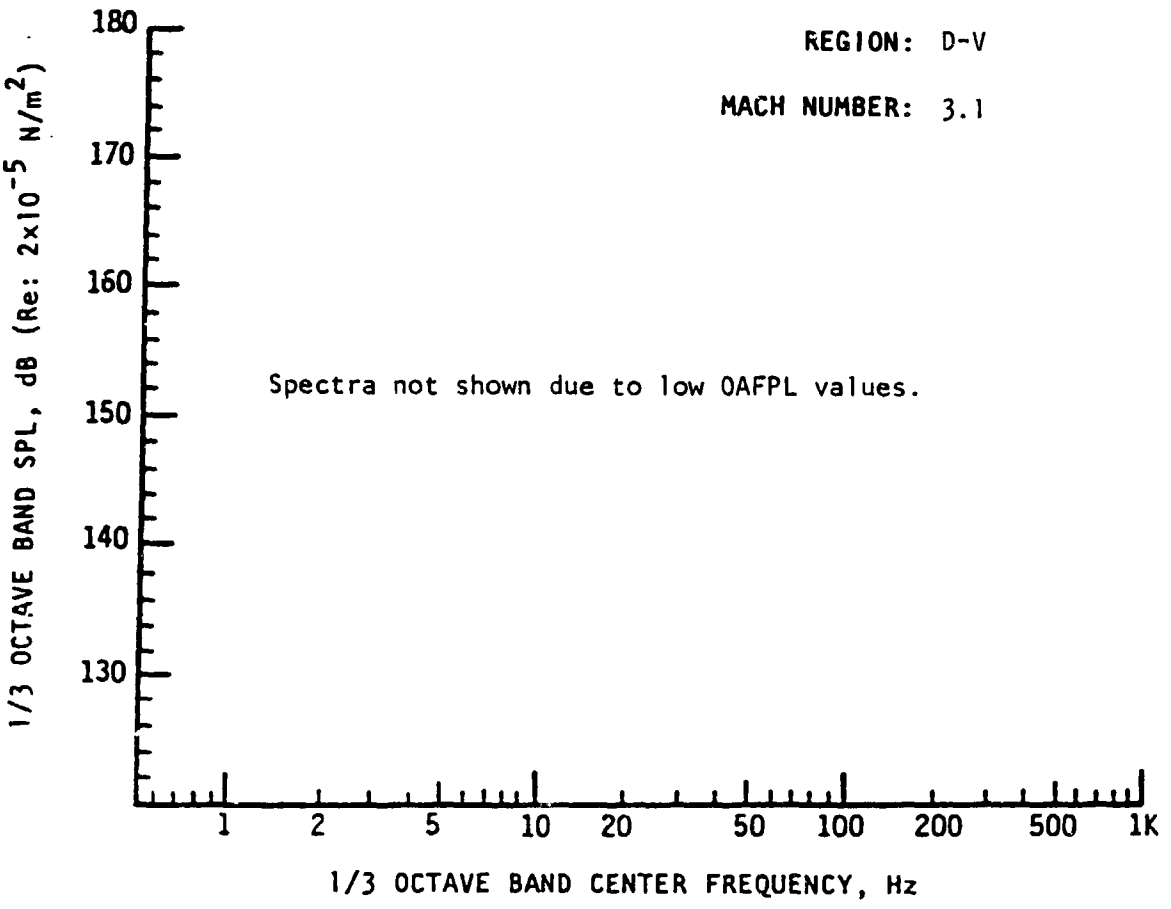

Note: Results based on 95 percentile OAFPL from Monte Carlo trajectory simulatcn.

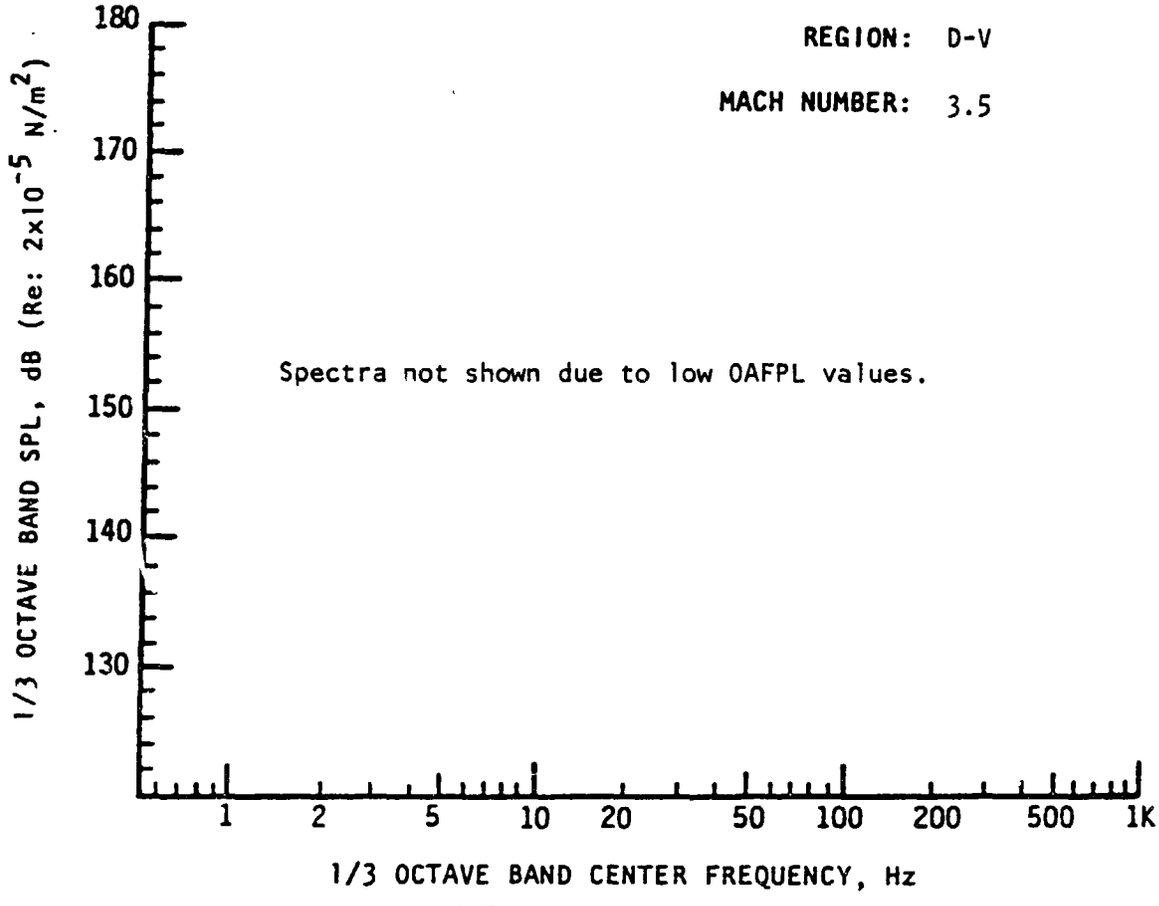

Note: Results based on 95 percentile OAFPL from Monte Carlo trajectory simulation.

APPENDIX D-VI

SRB FLEXIBLE HEAT SHIELD CONFIGURATION
ONE-THIRD OCTAVE-BAND AEROACOUSTIC SPECTRA FOR REGION D-VI
EXTERNAL SKIRT
(TRANSDUCERS 94, 95, 104, 105)

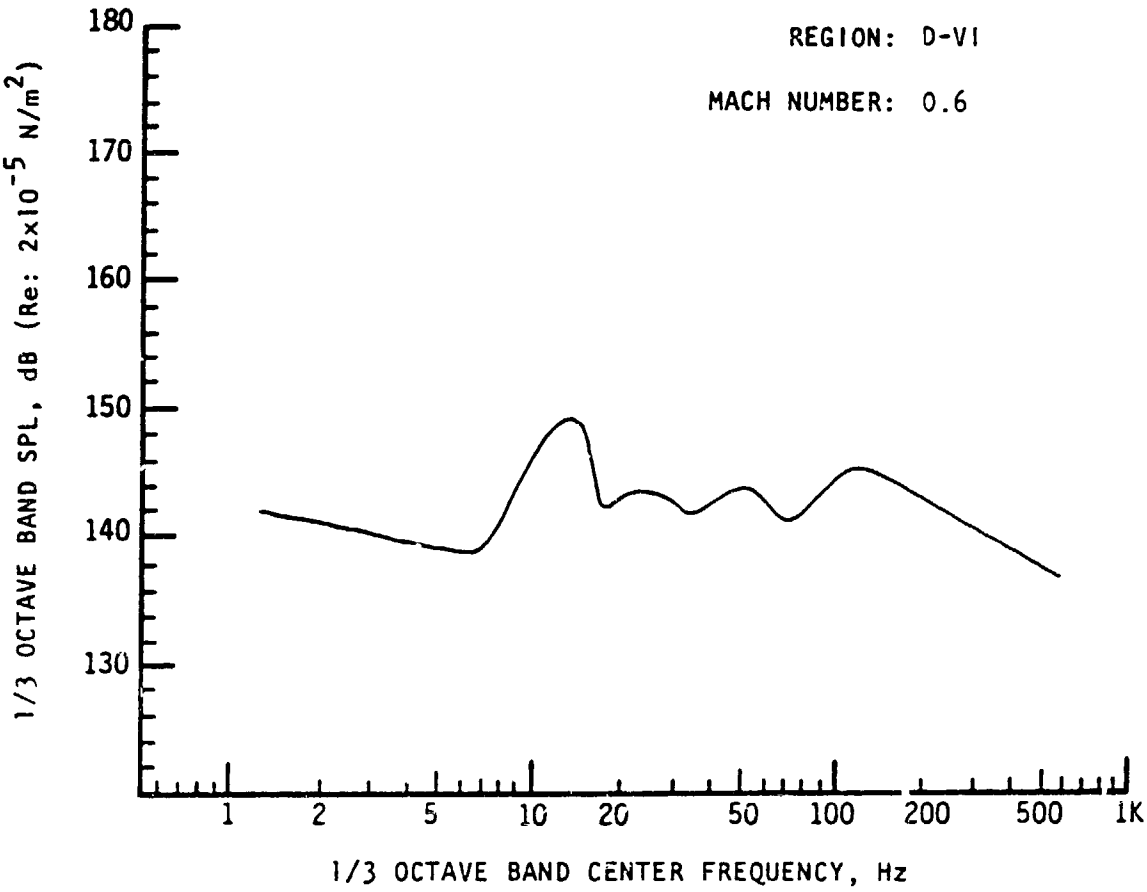

Note: Results based on 95 percentile OAFPL from Monte Carlo trajectory simulation.

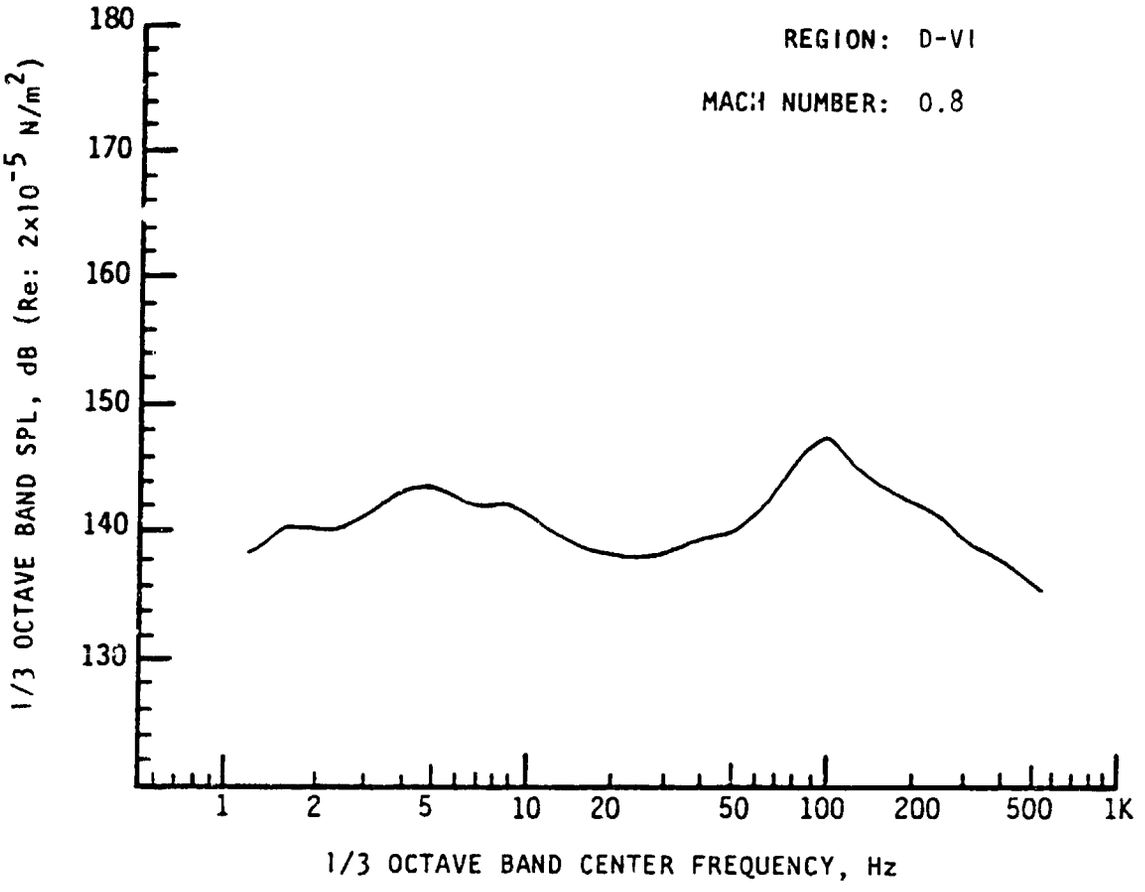

Note: Results based on 95 percentile OAFPL from Monte Carlo trajectory simulation.

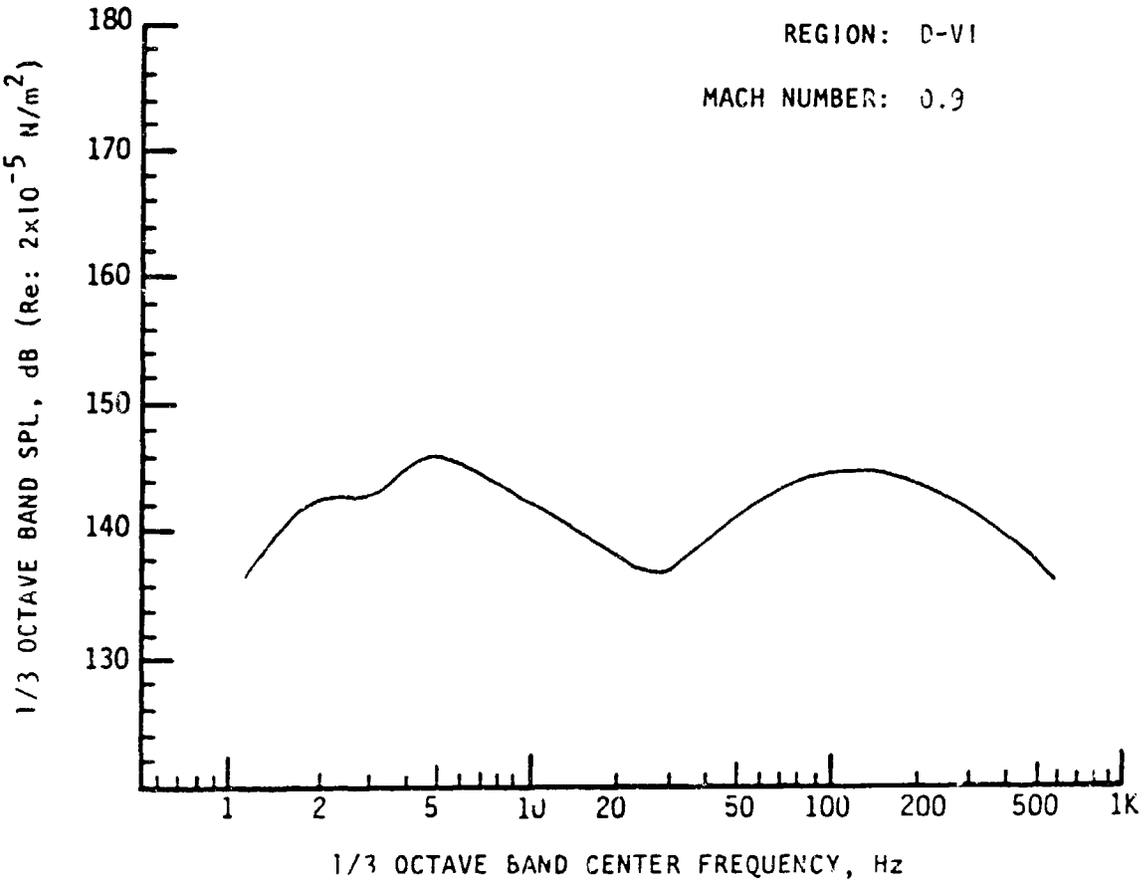

Note: Results based on 95 percentile OAFPL from Monte Carlo trajectory simulation.

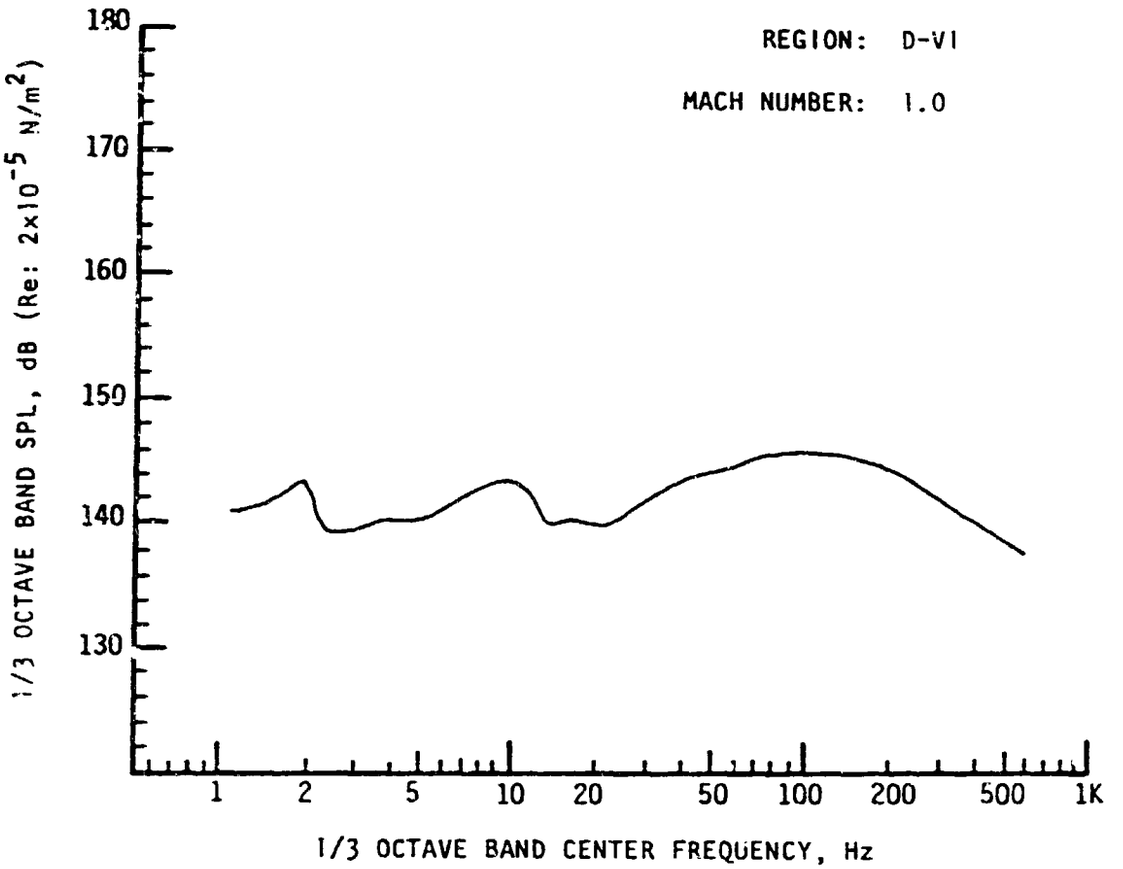

Note: Results based on 95 percentile OAFPL from Monte Carlo trajectory simulation.

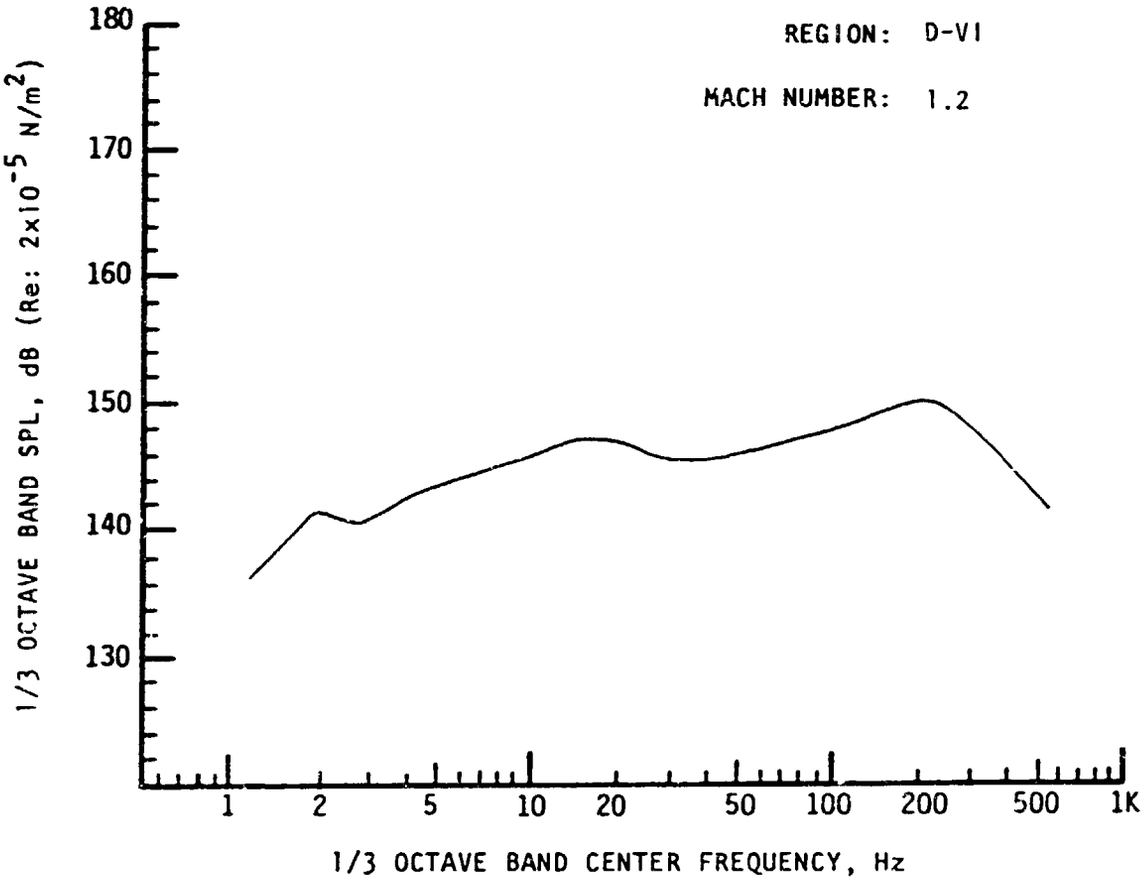

Note: Results based on 95 percentile OAFPL from Monte Carlo trajectory simulation.

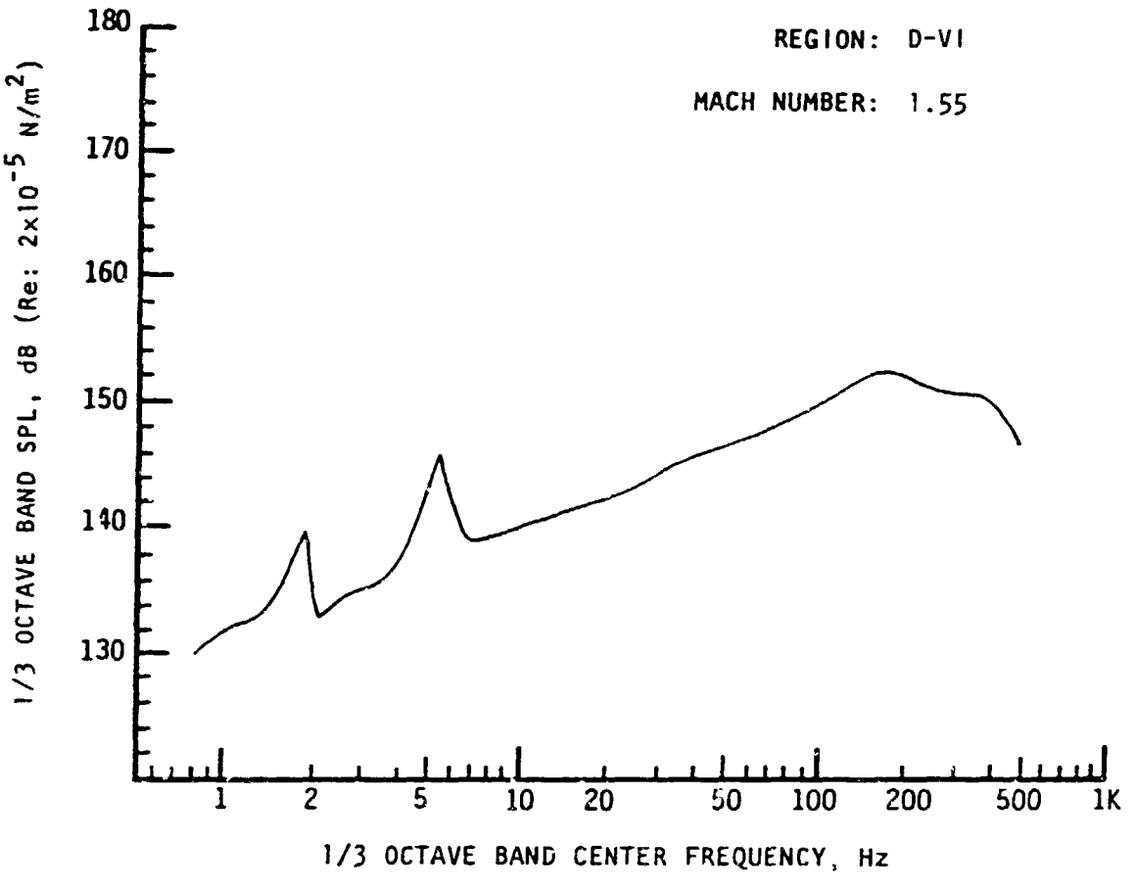

Note: Results based on 95 percentile OAFPL from Monte Carlo trajectory simulation.

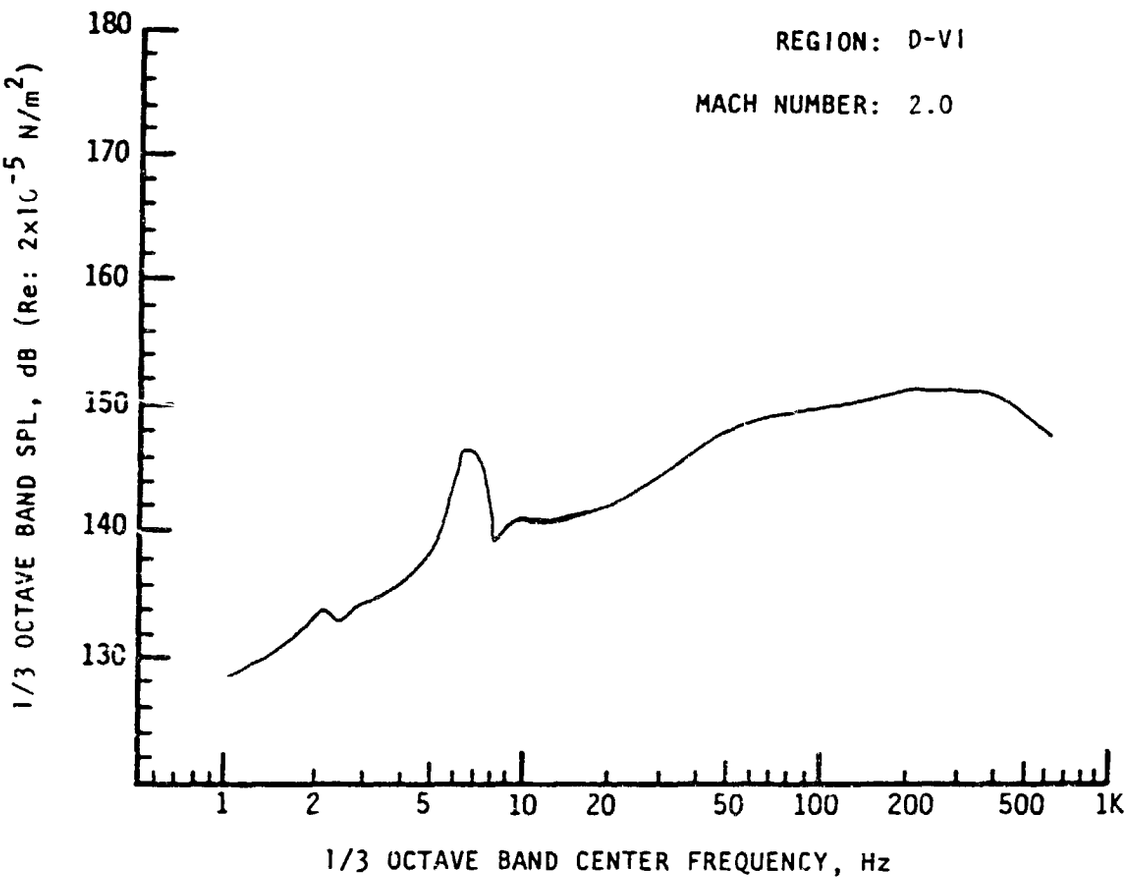

Note: Results based on 95 percentile OAFPL from Monte Carlo trajectory simulation.

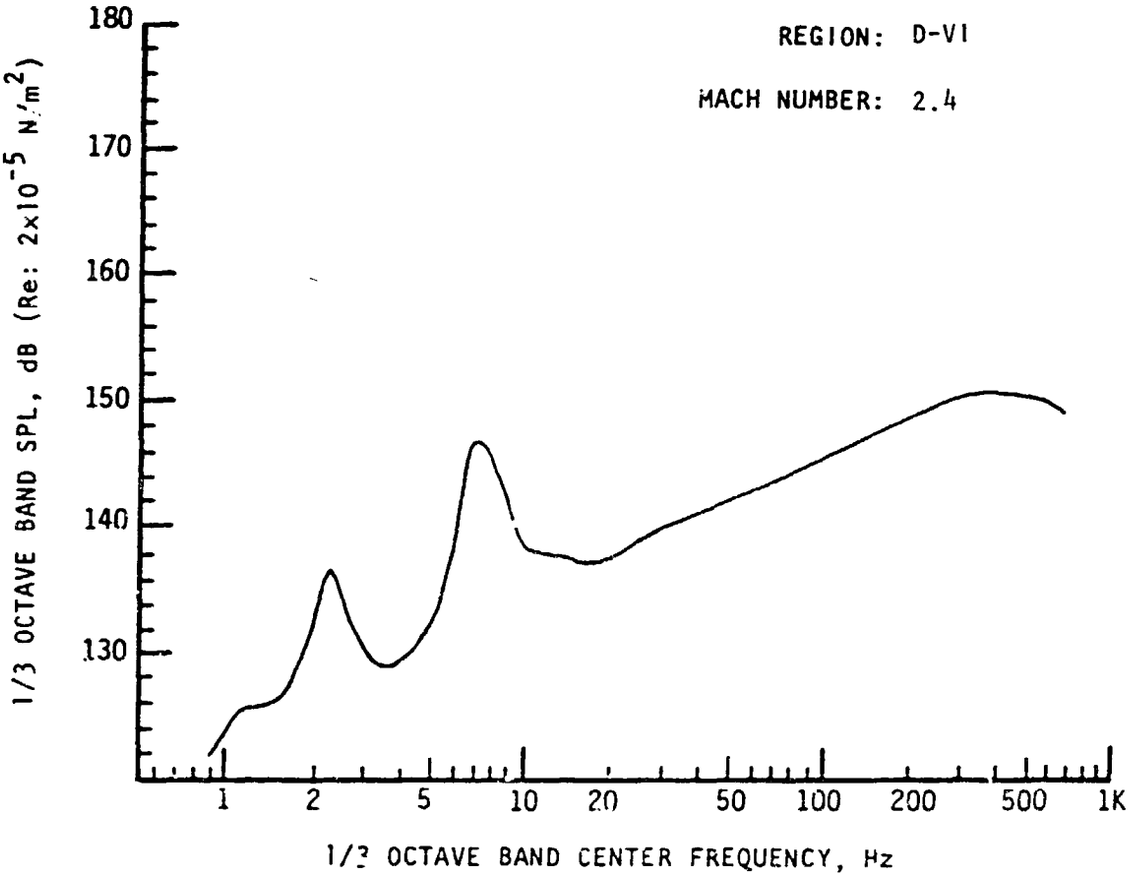

Note: Results based on 95 percentile OAFPL from Monte Carlo trajectory simulation.

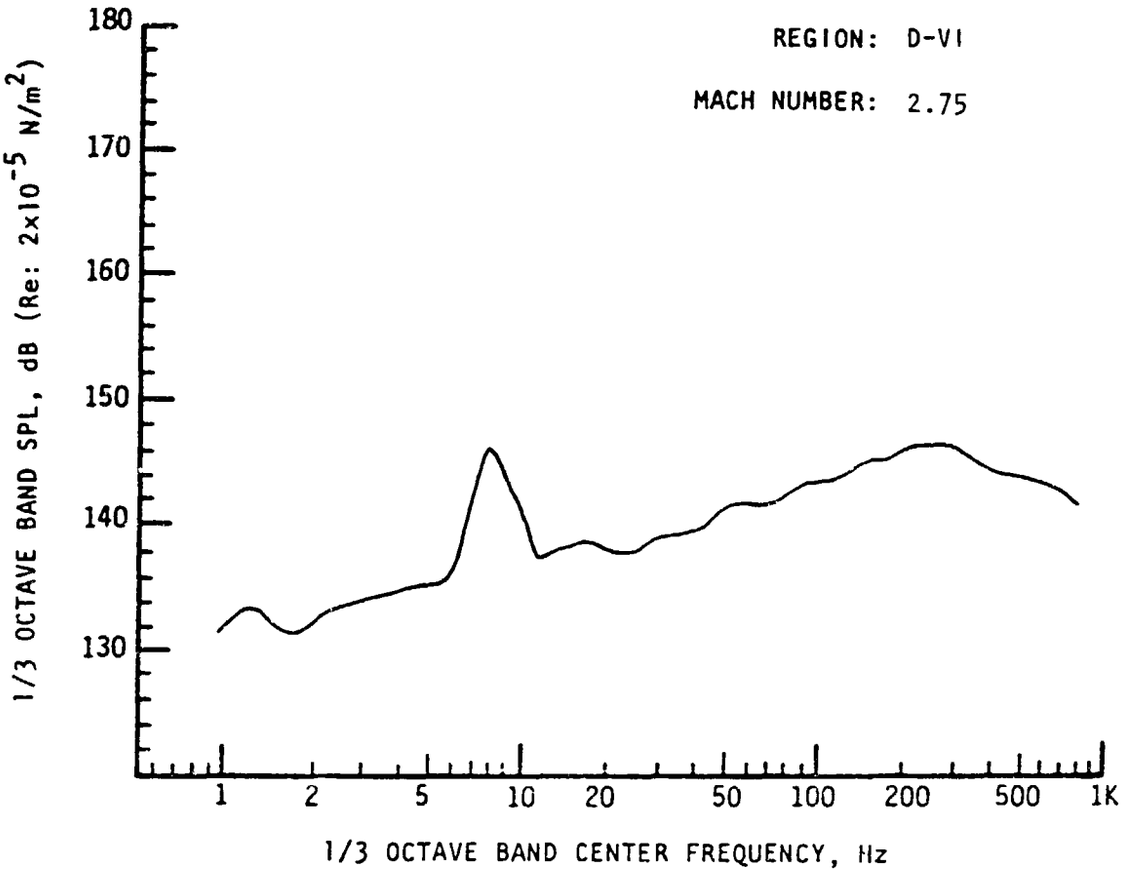

Note: Results based on 95 percentile OAFPL from Monte Carlo trajectory simulation.

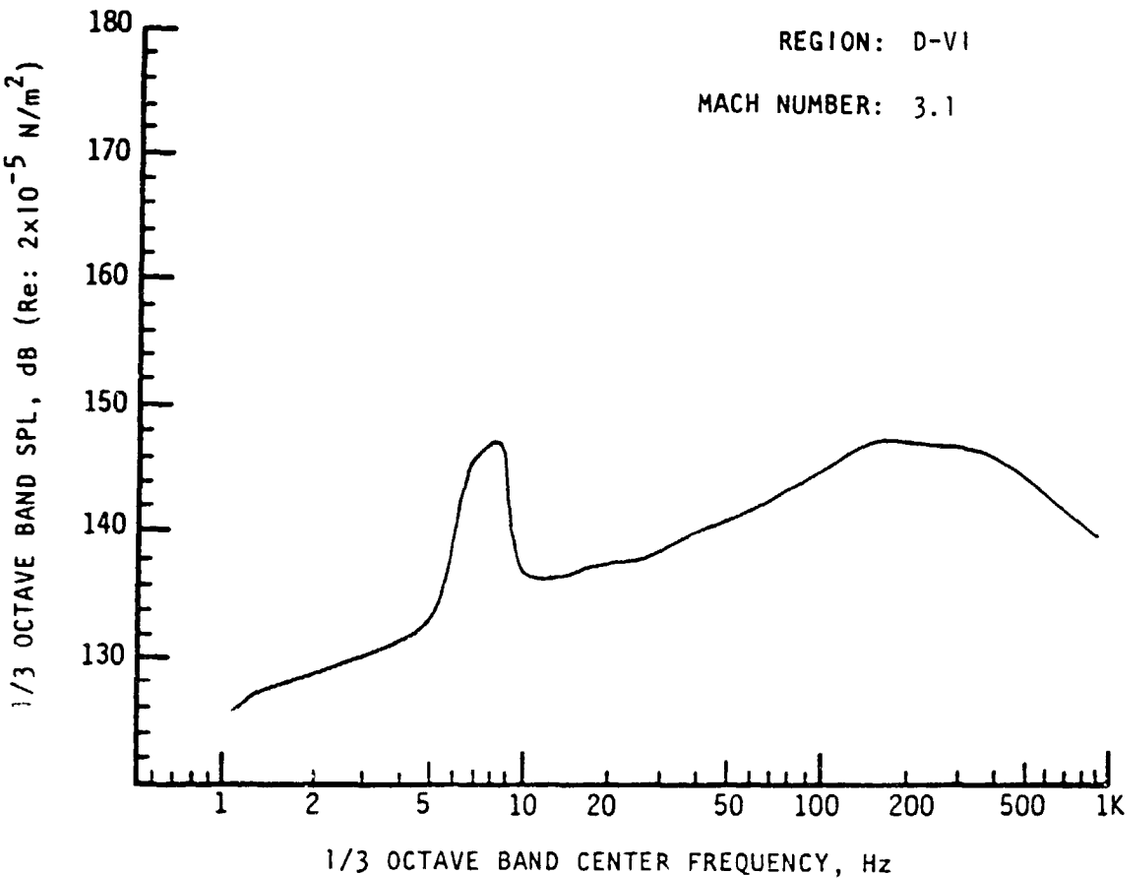

Note: Results based on 95 percentile OAFPL from Monte Carlo trajectory simulation

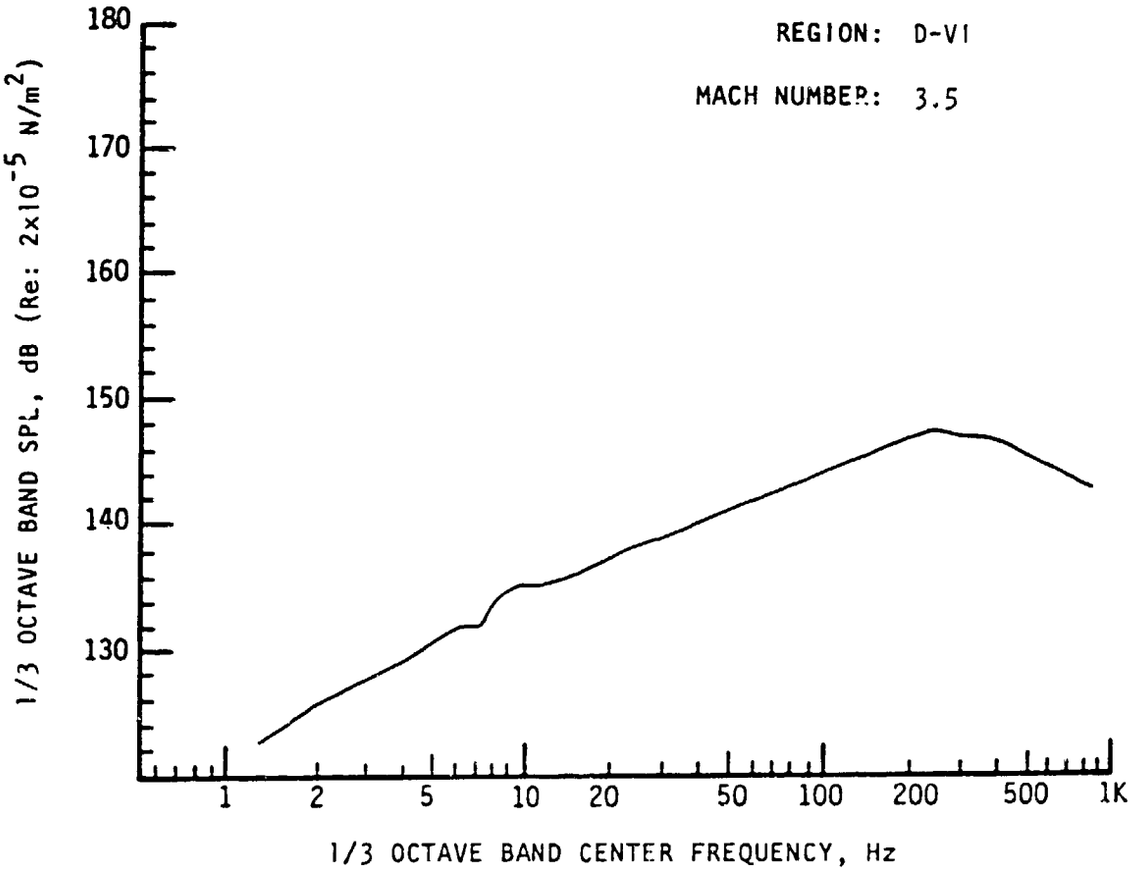

Note: Results based on 95 percentile OAFPL from Monte Carlo trajectory simulation.

APPENDIX D-VII

SRB FLEXIBLE HEAT SHIELD CONFIGURATION
ONE-THIRD OCTAVE-BAND AEROACOUSTIC SPECTRA FOR REGION D-VII
SEPARATION MOTOR SUBREGION
(TRANSDUCERS 96 - 98)

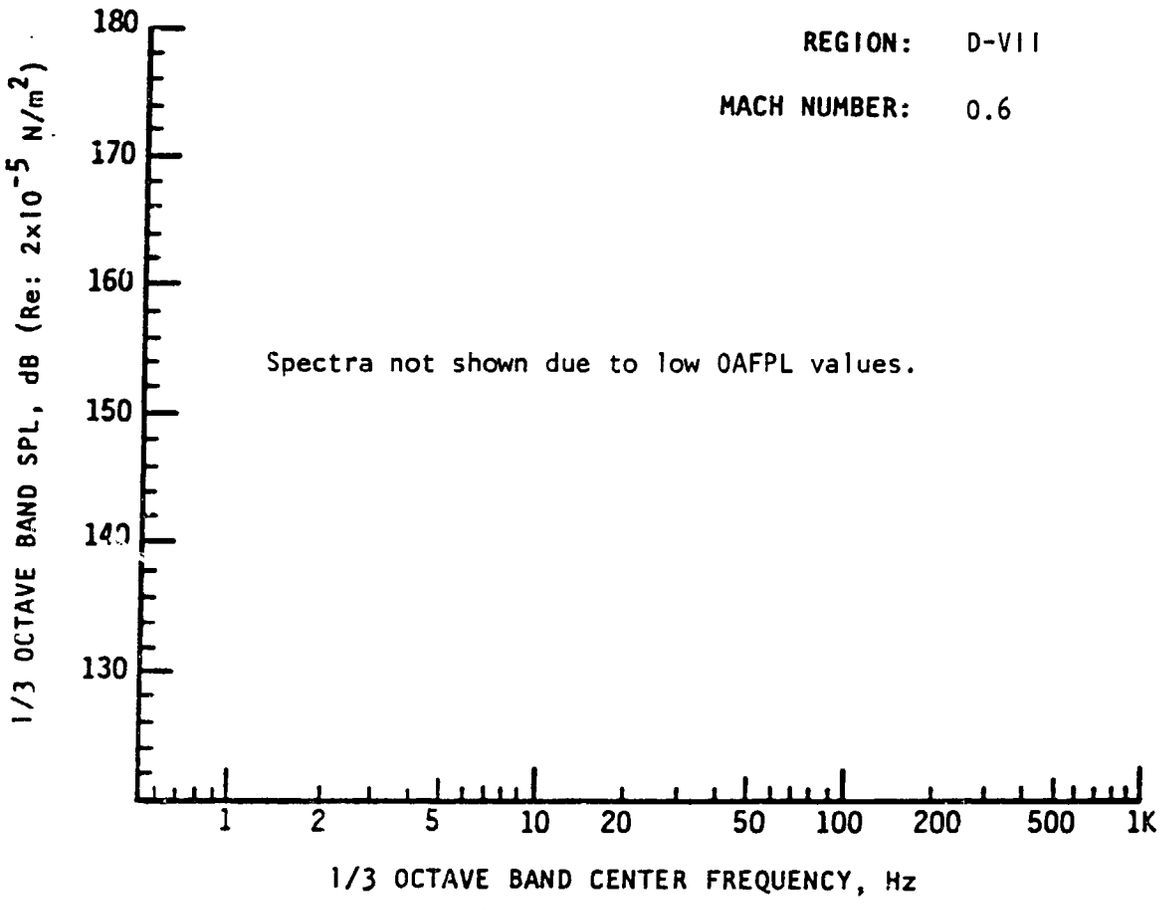

Note: Results based on 95 percentile OAFPL from Monte Carlo trajectory simulation.

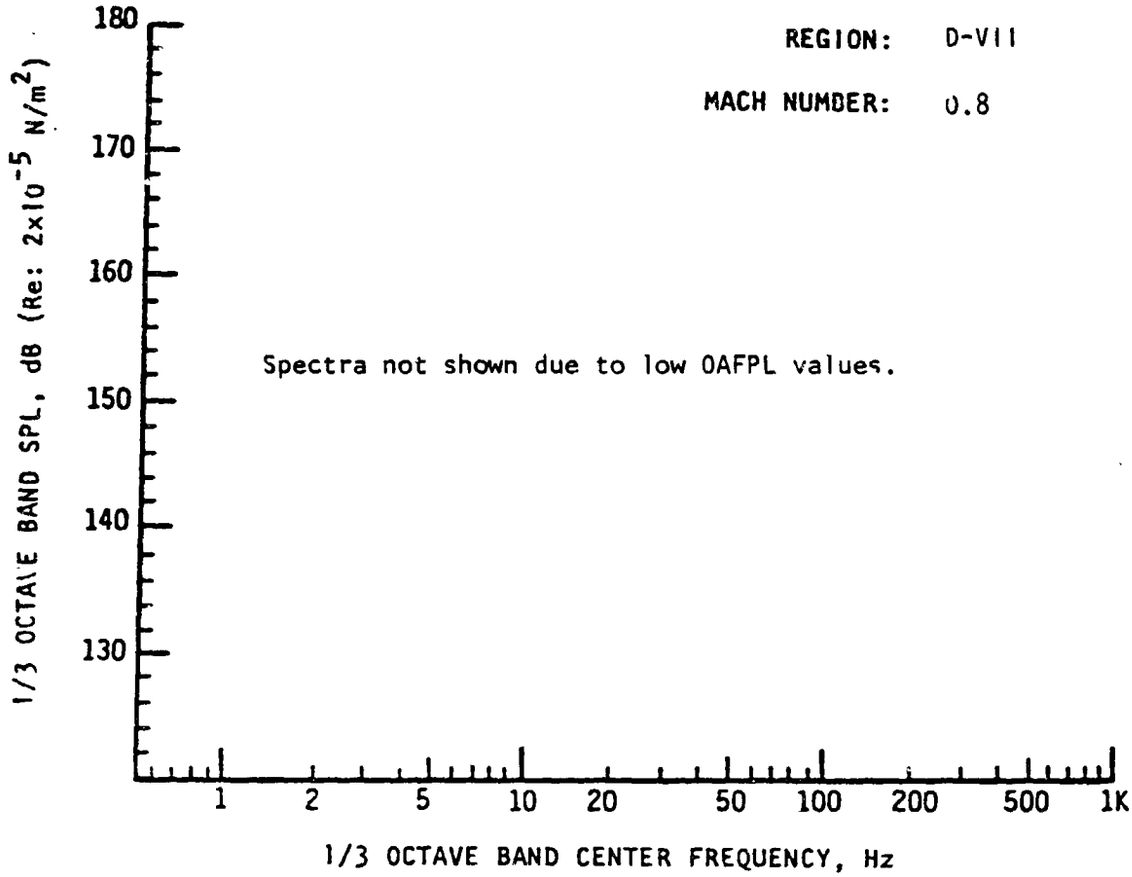

Note: Results based on 95 percentile OAFPL from Monte Carlo trajectory simulation.

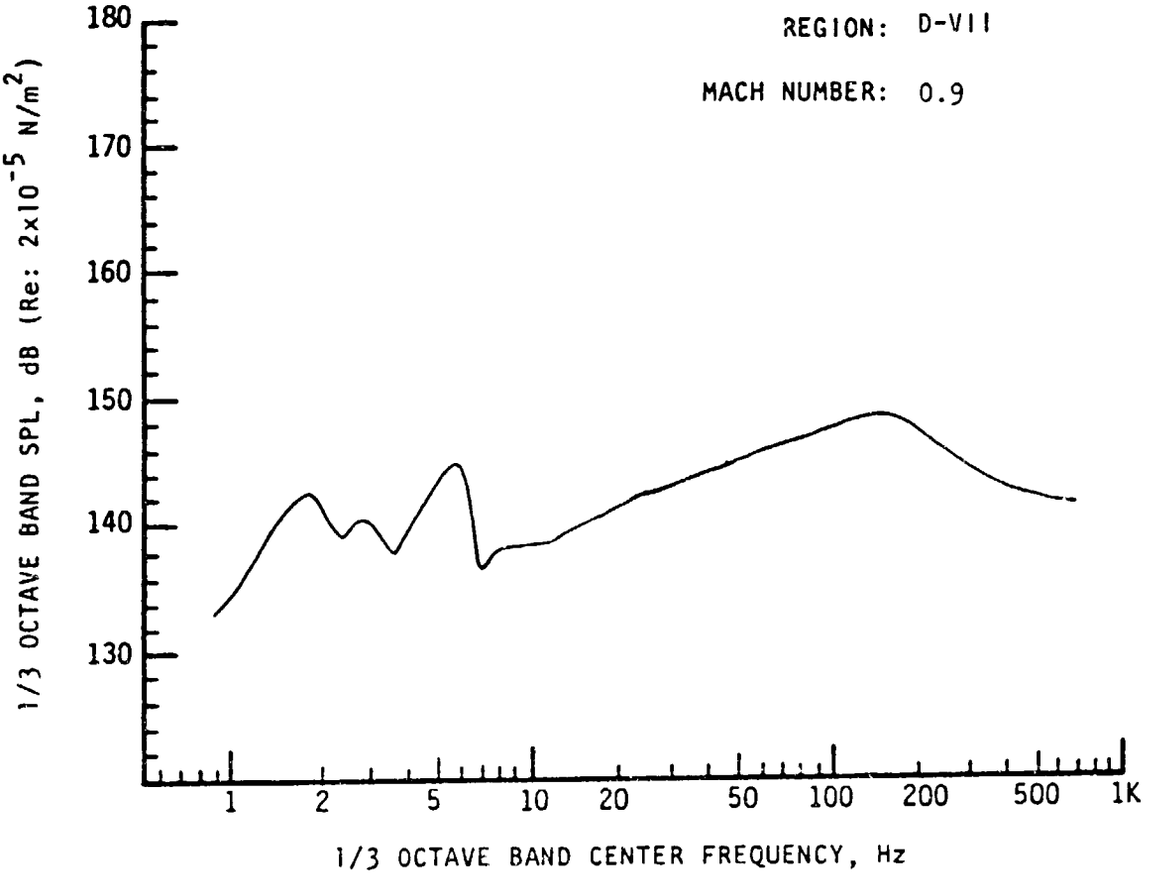

Note: Results based on 95 percentile OAFPL from Monte Carlo trajectory simulation.

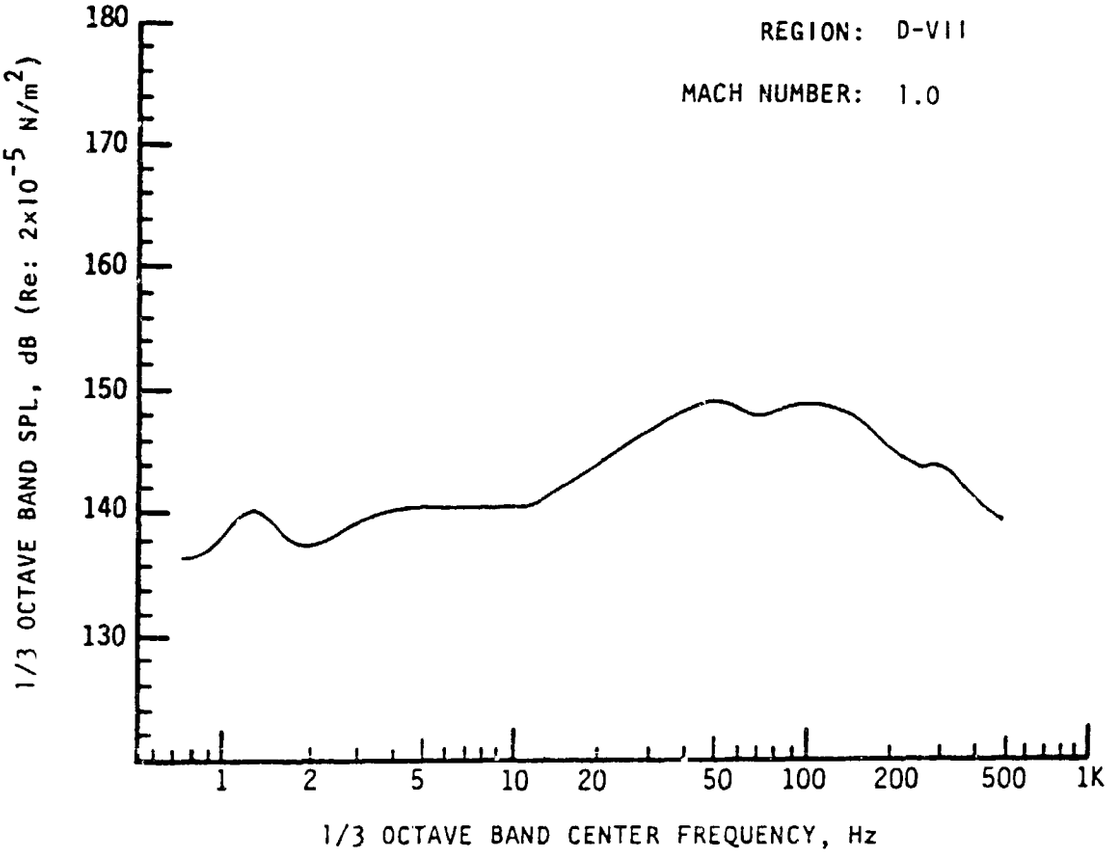

Note: Results based on 95 percentile OAFPL from Monte Carlo trajectory simulation.

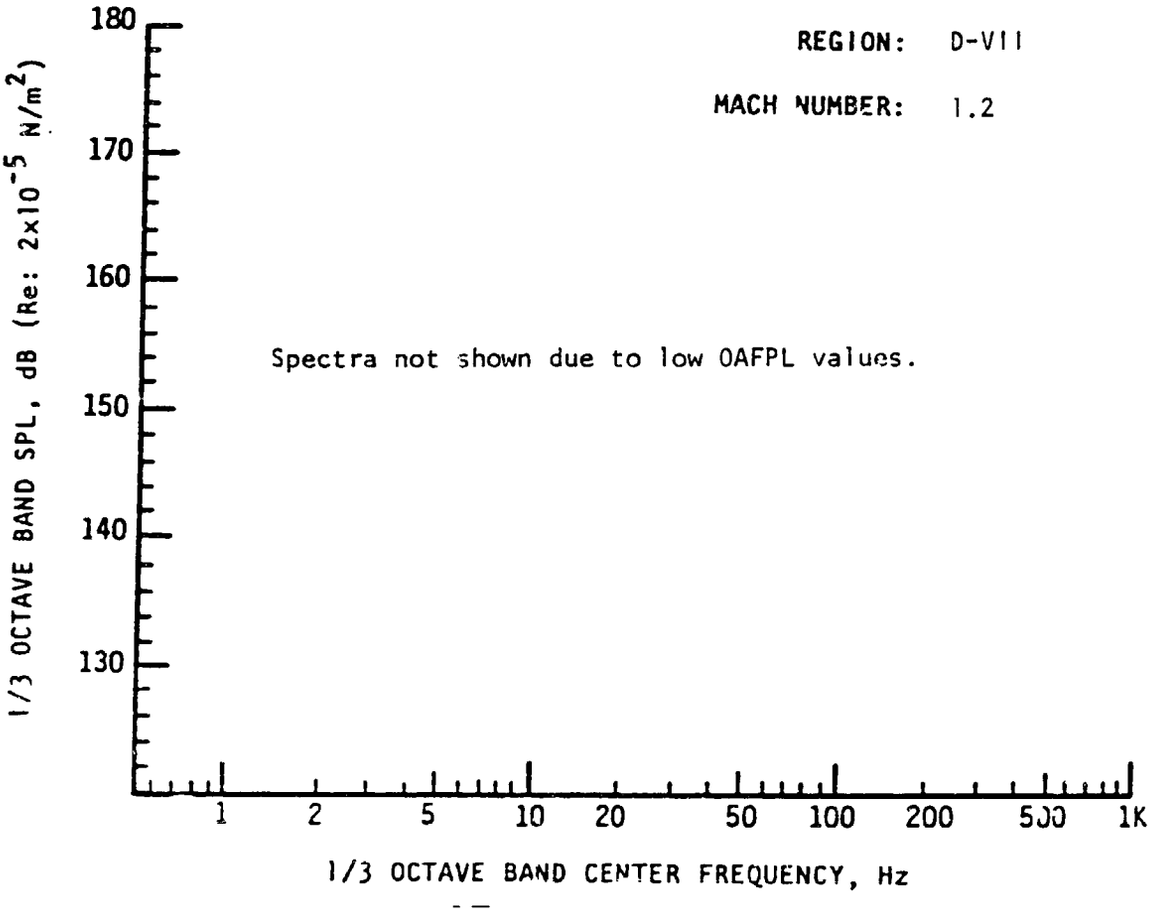

Note: Results based on 95 percentile OAFPL from Monte Carlo trajectory simulation.

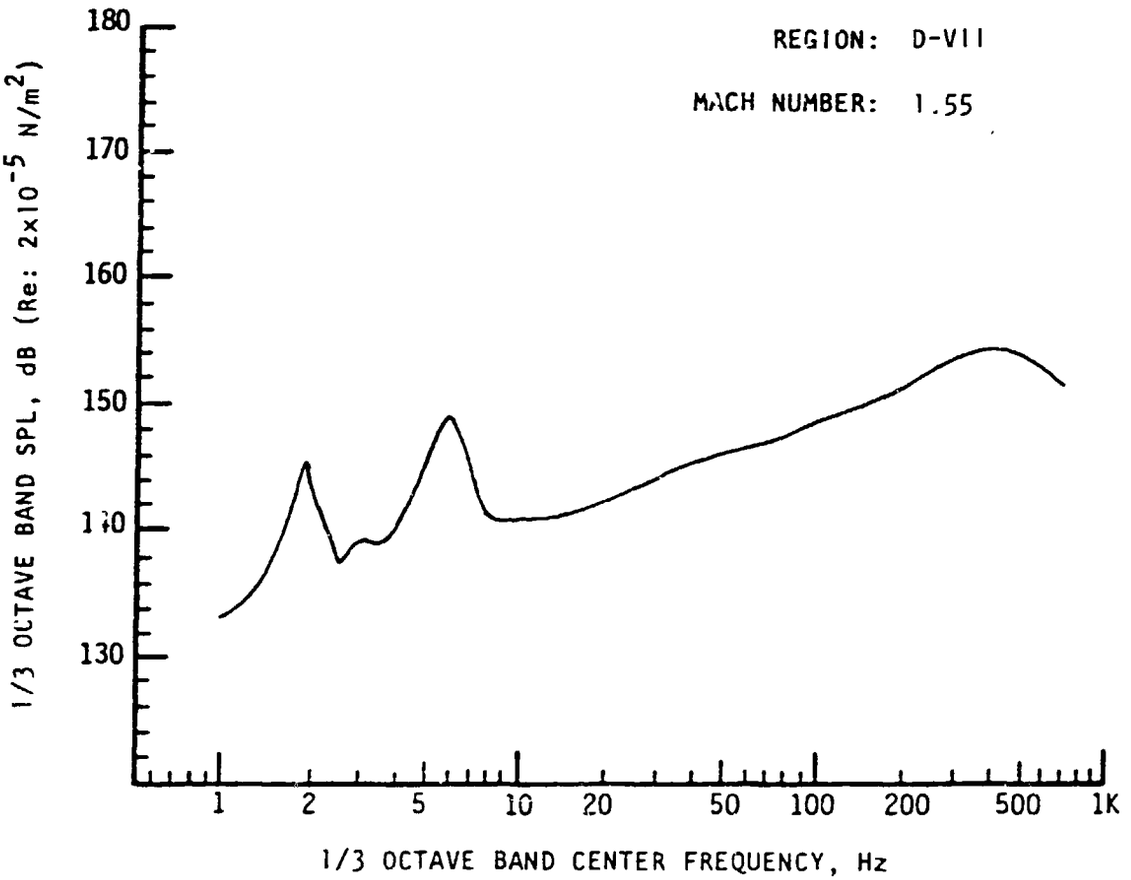

Note: Results based on 95 percentile OAFPL from Monte Carlo trajectory simulation.

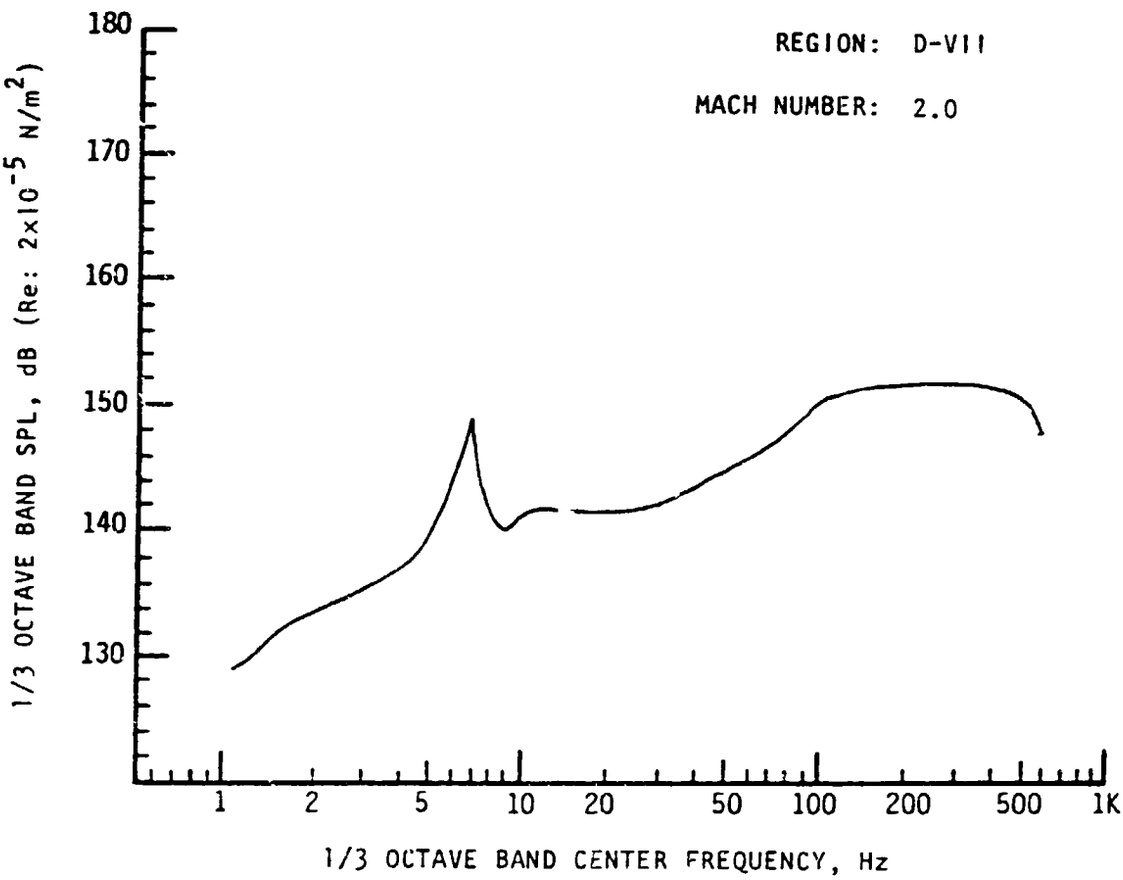

Note: Results based on 95 percentile OAFPL from Monte Carlo trajectory simulation.

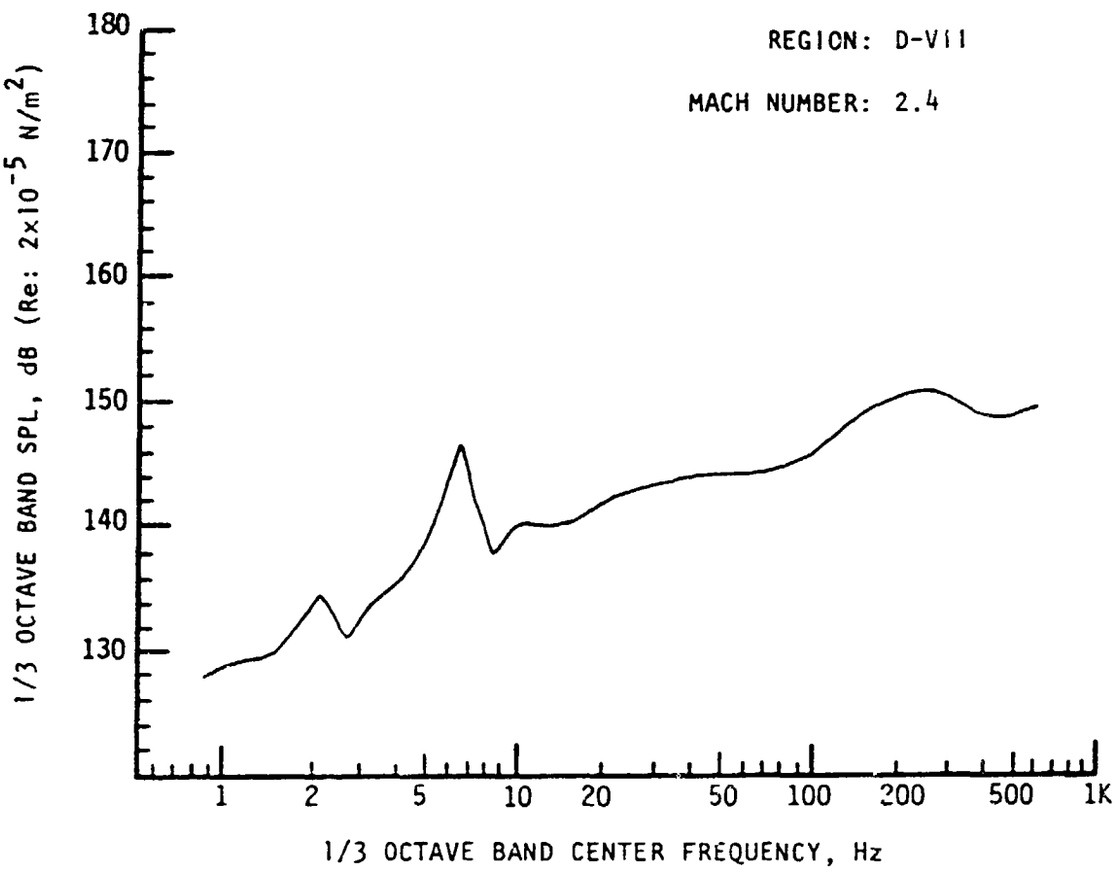

Note: Results based on 95 percentile OAFPL from Monte Carlo trajectory simulation.

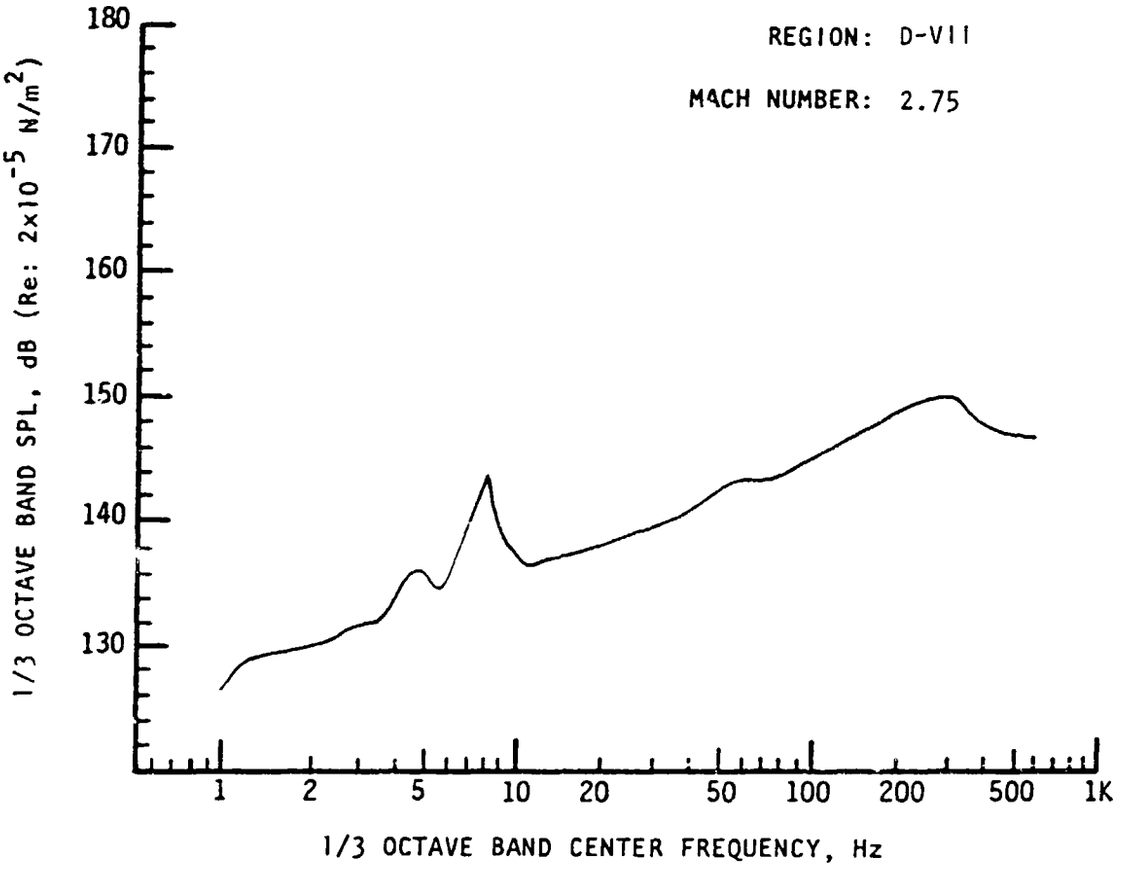

Note: Results based on 95 percentile OAFPL from Monte Carlo trajectory simulation.

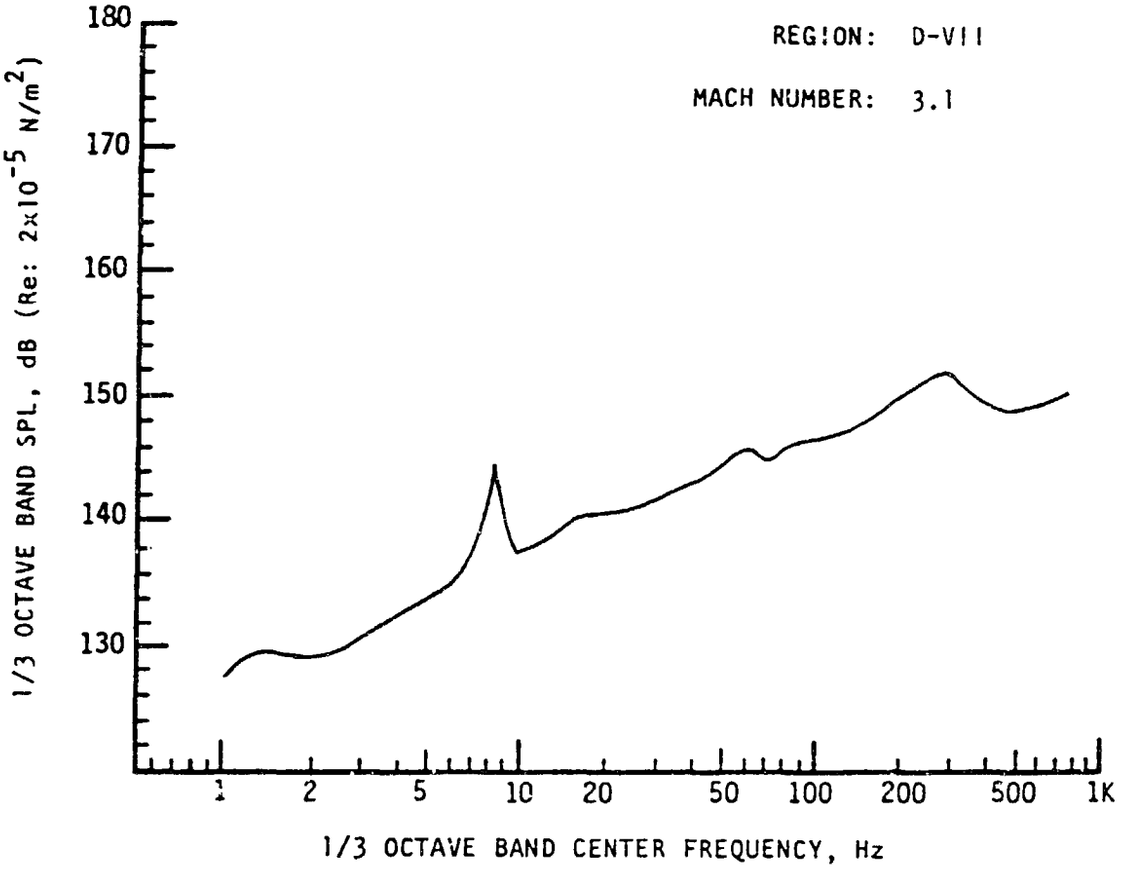

Note: Results based on 95 percentile OAFPL from Monte Carlo trajectory simulation.

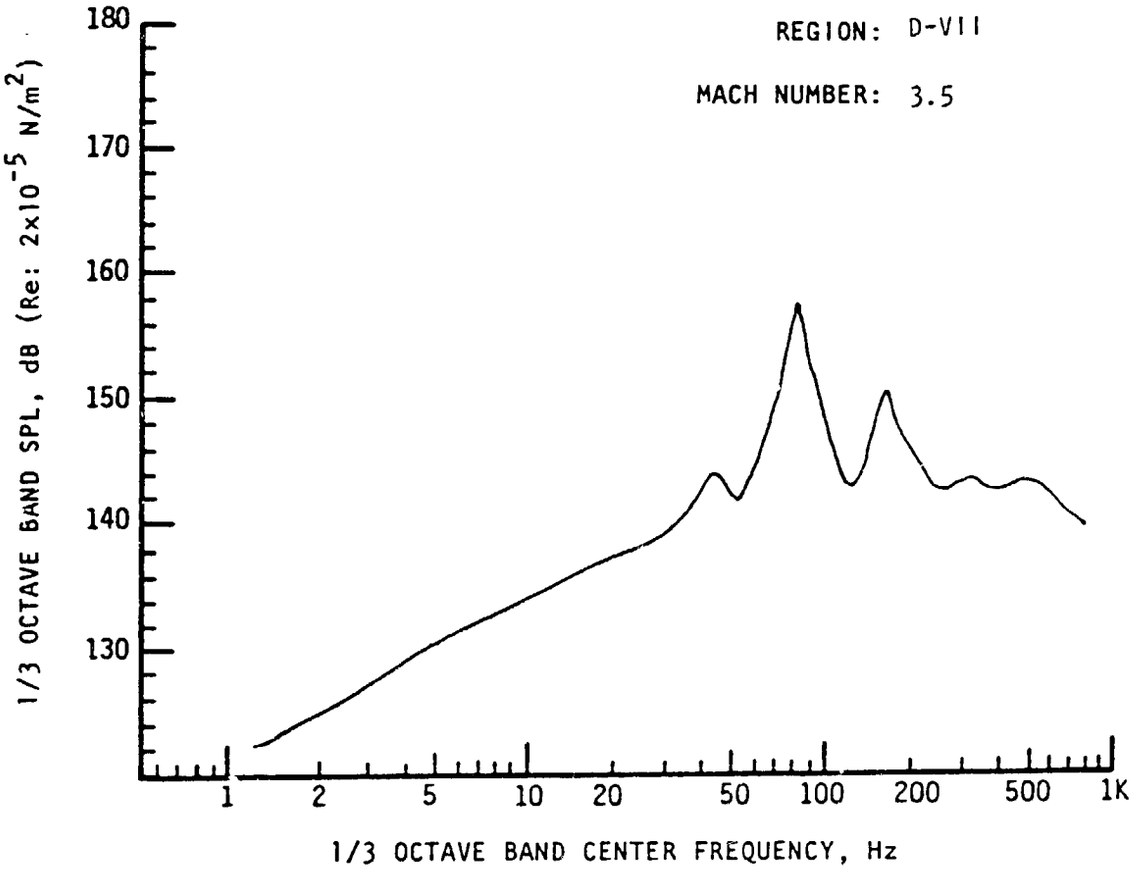

Note: Results based on 95 percentile OAFPL from Monte Carlo trajectory mulation.

APPENDIX D-VIII

SRB FLEXIBLE HEAT SHIELD CONFIGURATION
ONE-THIRD OCTAVE-BAND AEROACOUSTIC SPECTRA FOR REGION D-VIII
SEPARATION MOTOR SUBREGION
(TRANSDUCER 106)

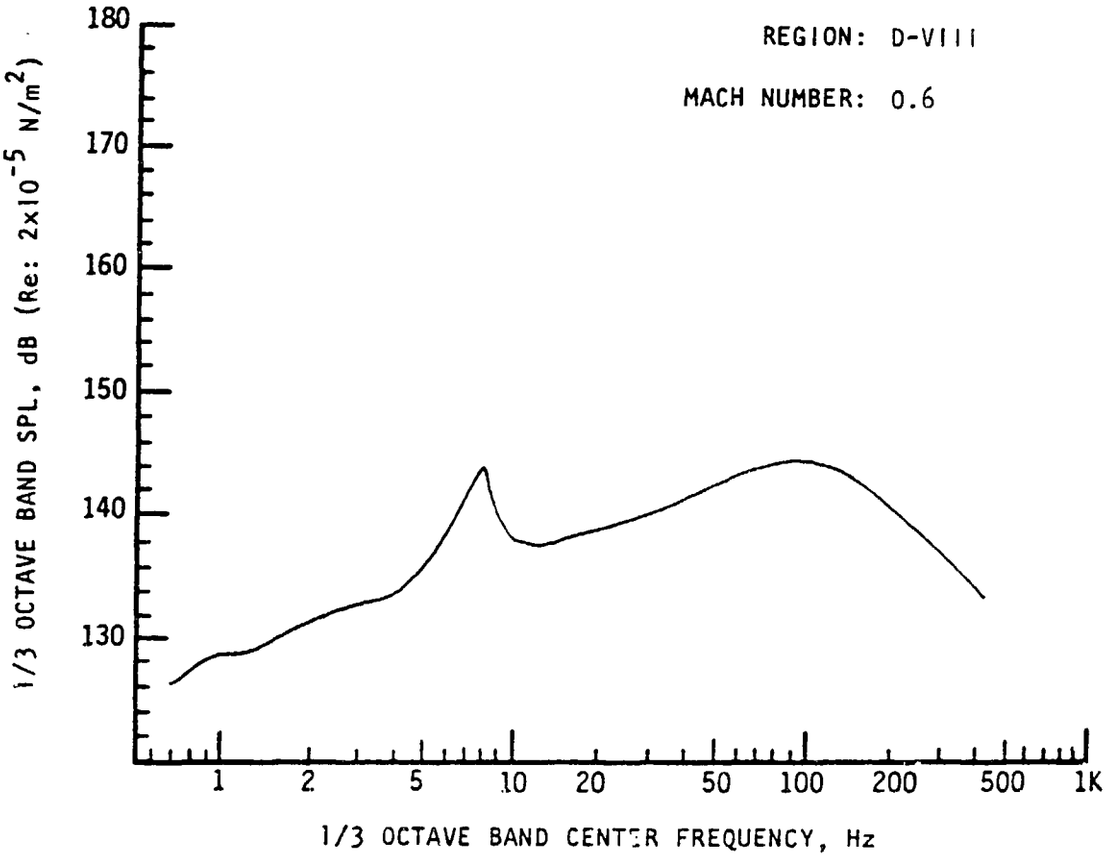

Note: Results based on 95 percentile OAFPL from Monte Carlo trajectory simulation.

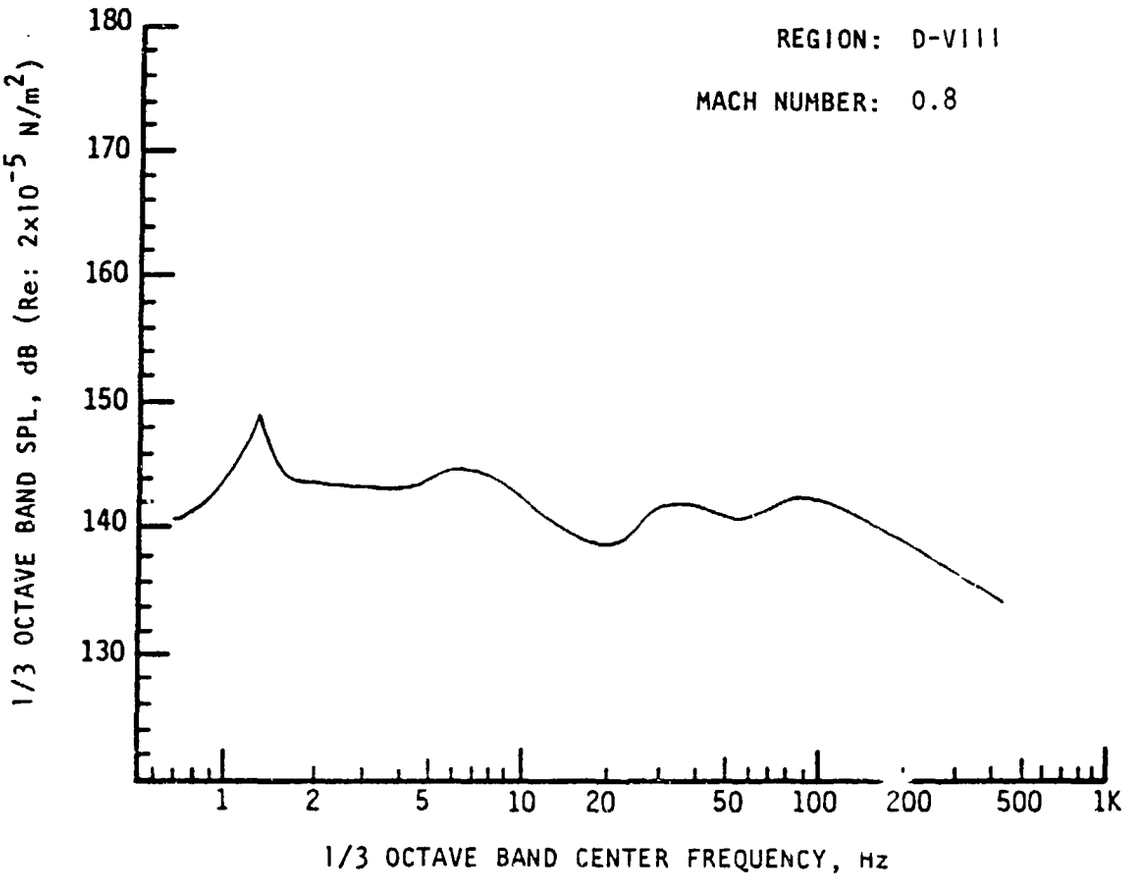

Note: Results based on 95 percentile OAFPL from Monte Carlo trajectory simulation.

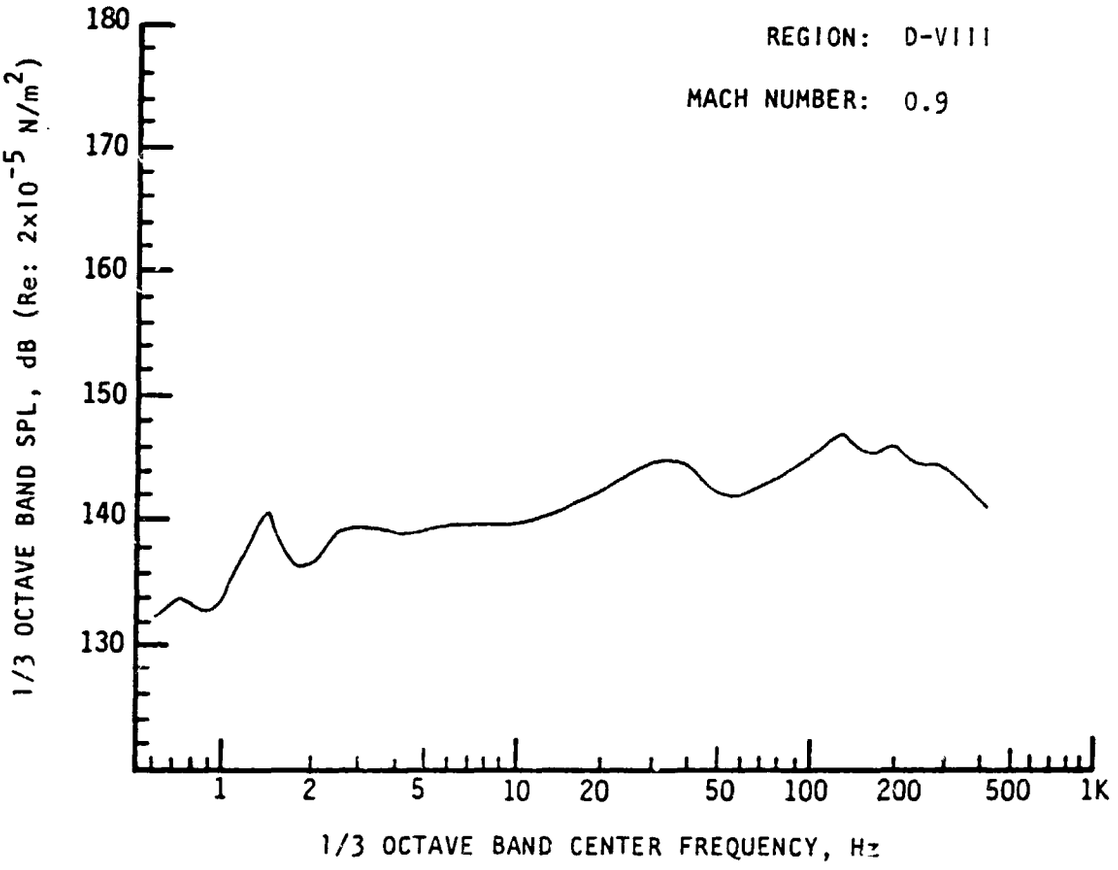

Note: Results based on 95 percentile OAFPL from Monte Carlo trajectory simulation.

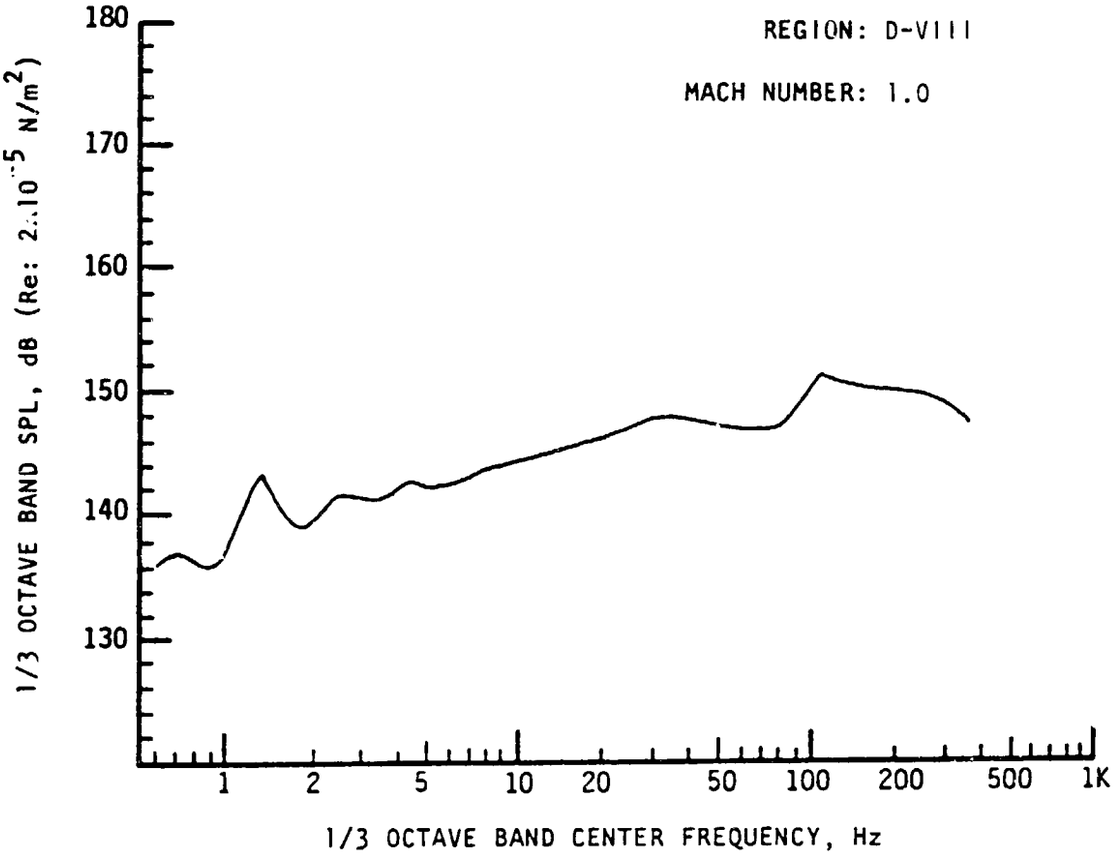

Note: Results based on 95 percentile OAFPL from Monte Carlo trajectory simulation.

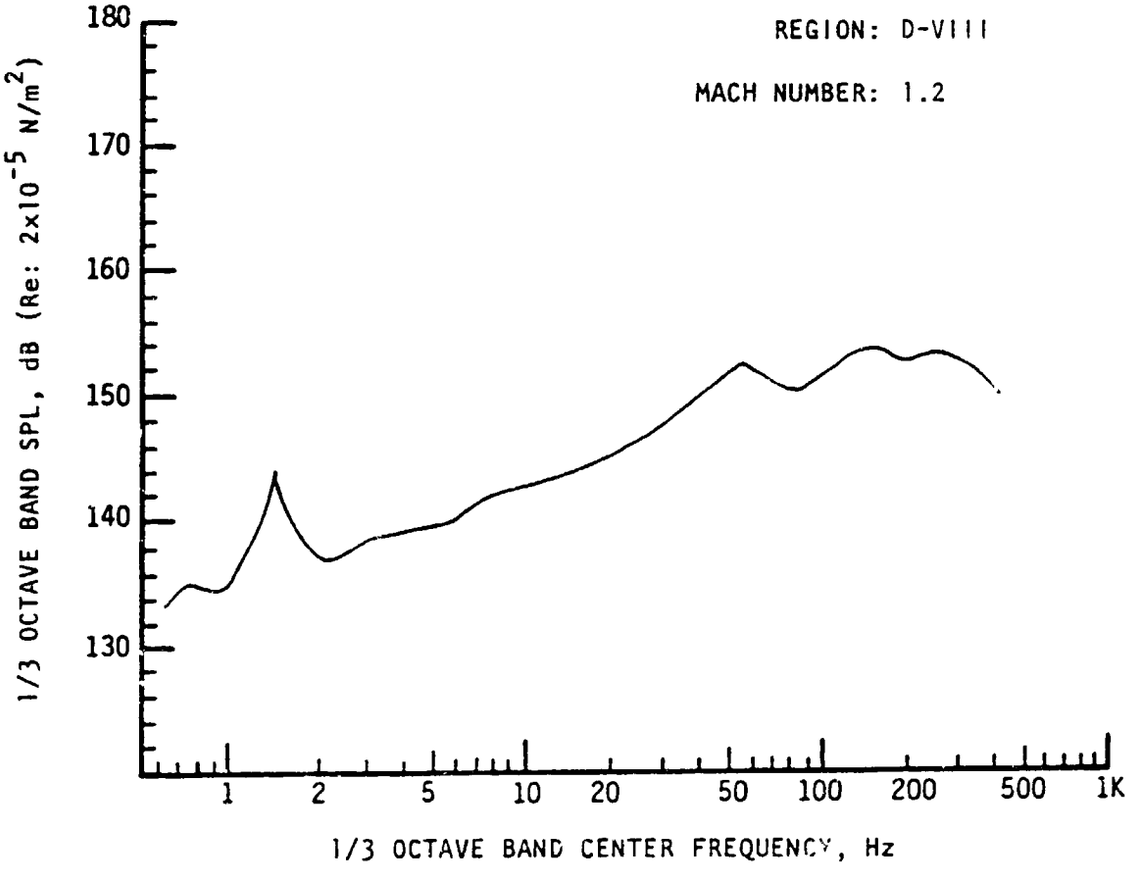

Note: Results based on 95 percentile OAFPL from Monte Carlo trajectory simulation.

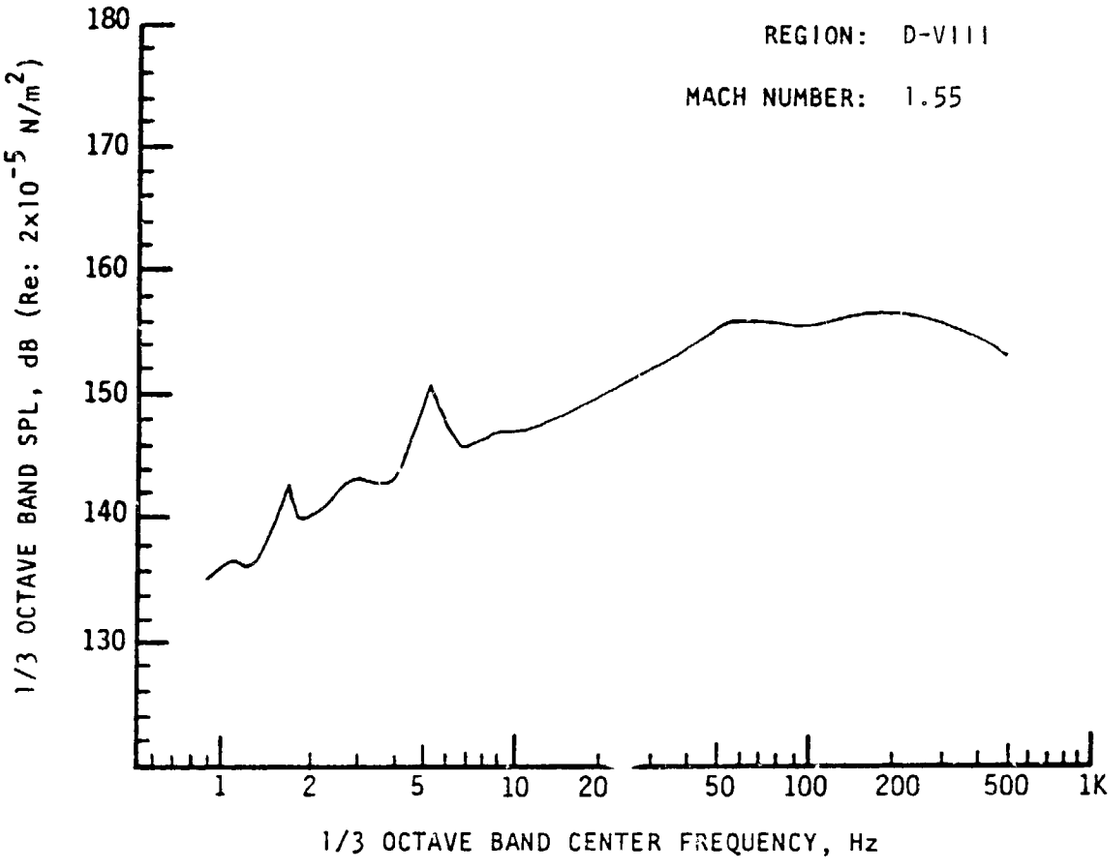

Note: Results based on 95 percentile OAFPL from Monte Carlo trajectory simulation.

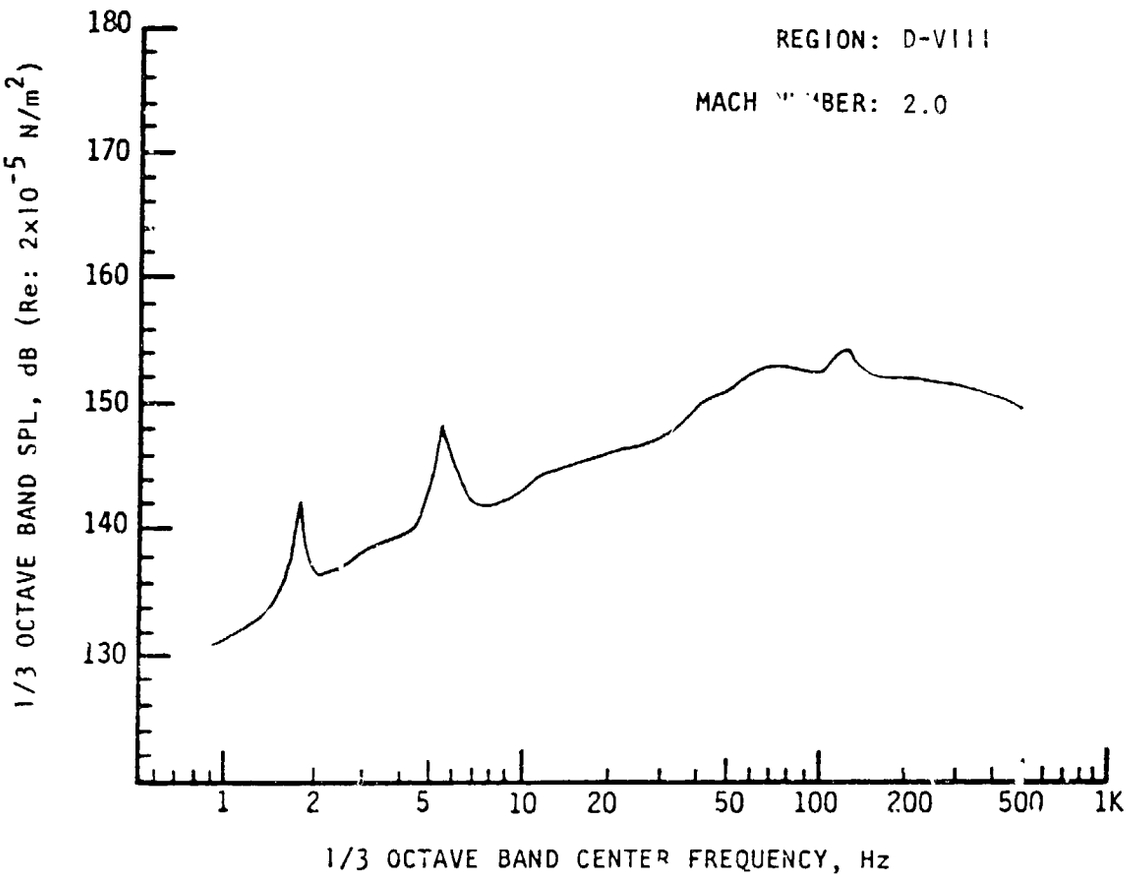

Note: Results based on 95 percentile OAFPL from Monte Carlo trajectory simulation.

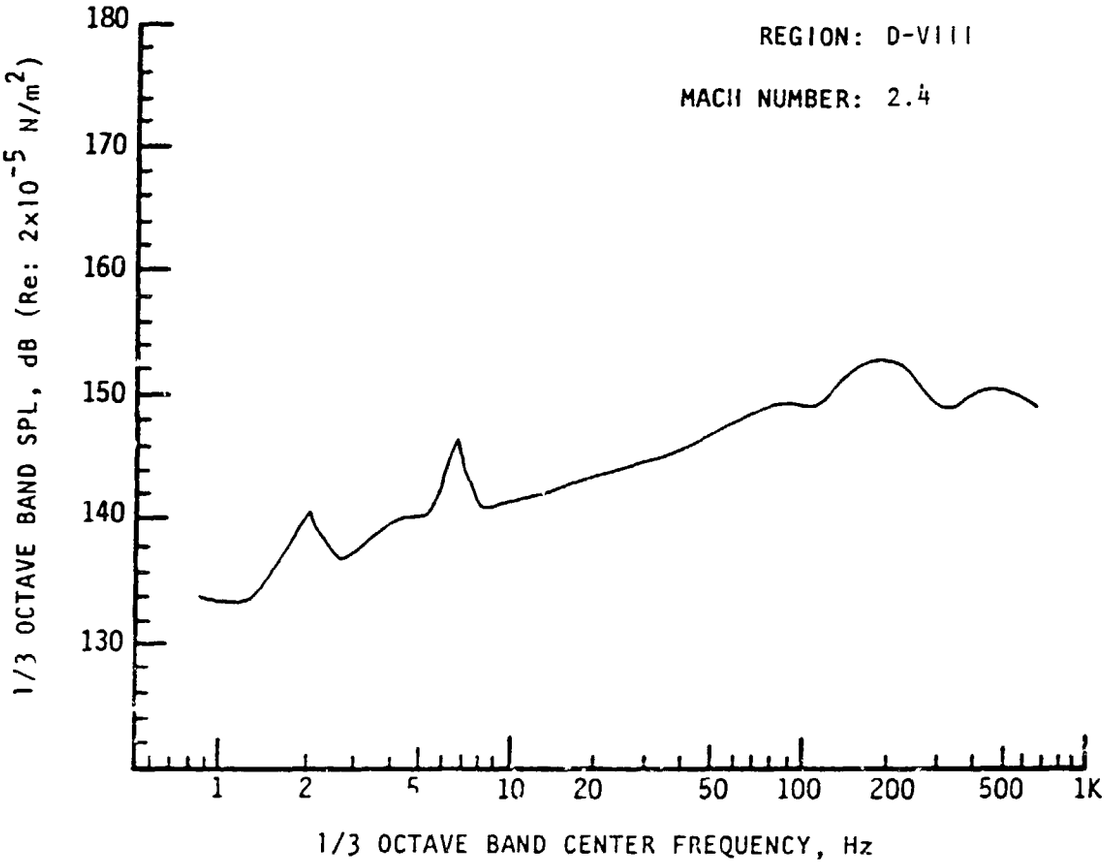

Note: Results based on 95 percentile OAPPL from Monte Carlo trajectory simulation.

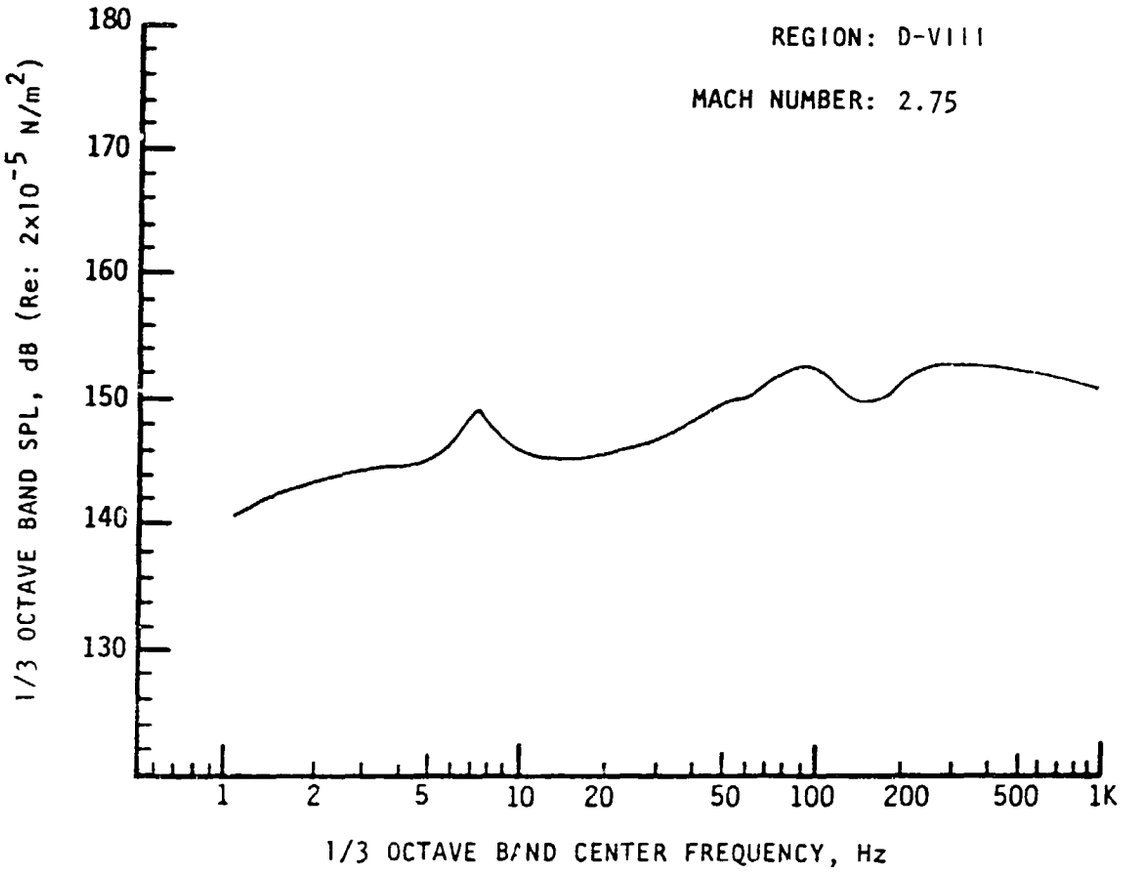

Note: Results based on 95 percentile OAFPL from Monte Carlo trajectory simulation.

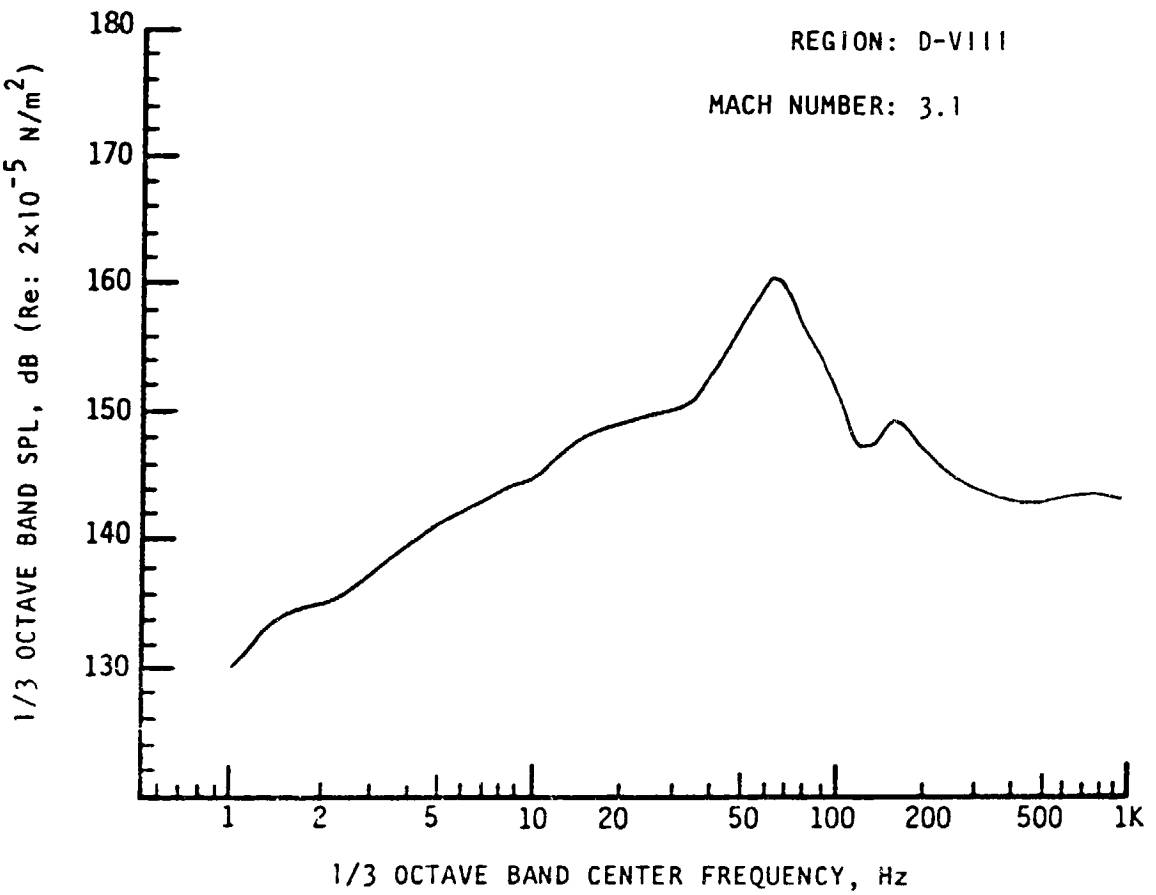

Note: Results based on 95 percentile OAFPL from Monte Carlo trajectory simulation.

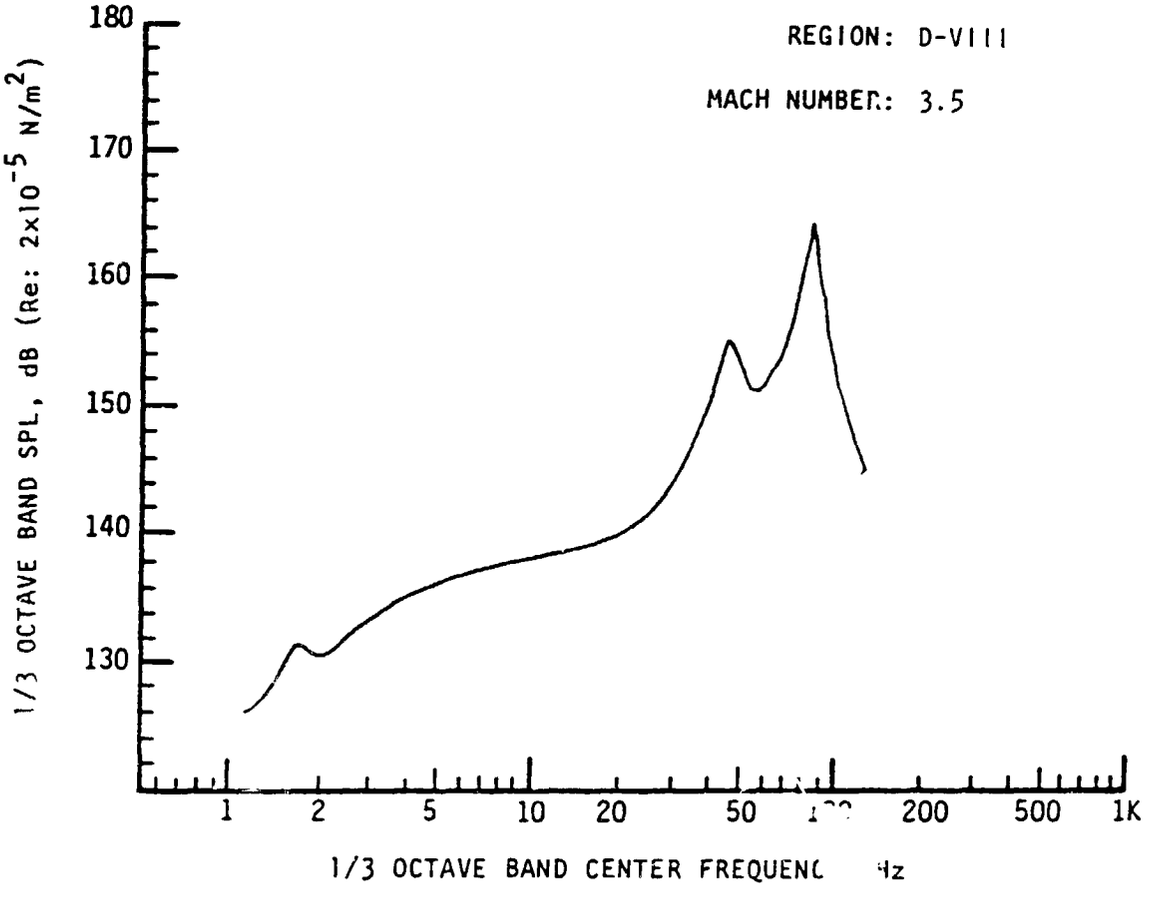

Note: Results based on 95 percentile OAFPL from Monte Carlo trajectory simulation.

APPENDIX E

SRB FLEXIBLE HEAT SHIELD CONFIGURATION
ONE-THIRD OCTAVE-BAND AEROACOUSTIC SPECTRA FOR REGION E
INTERNAL MOTOR VOLUME
(TRANSDUCER 121)

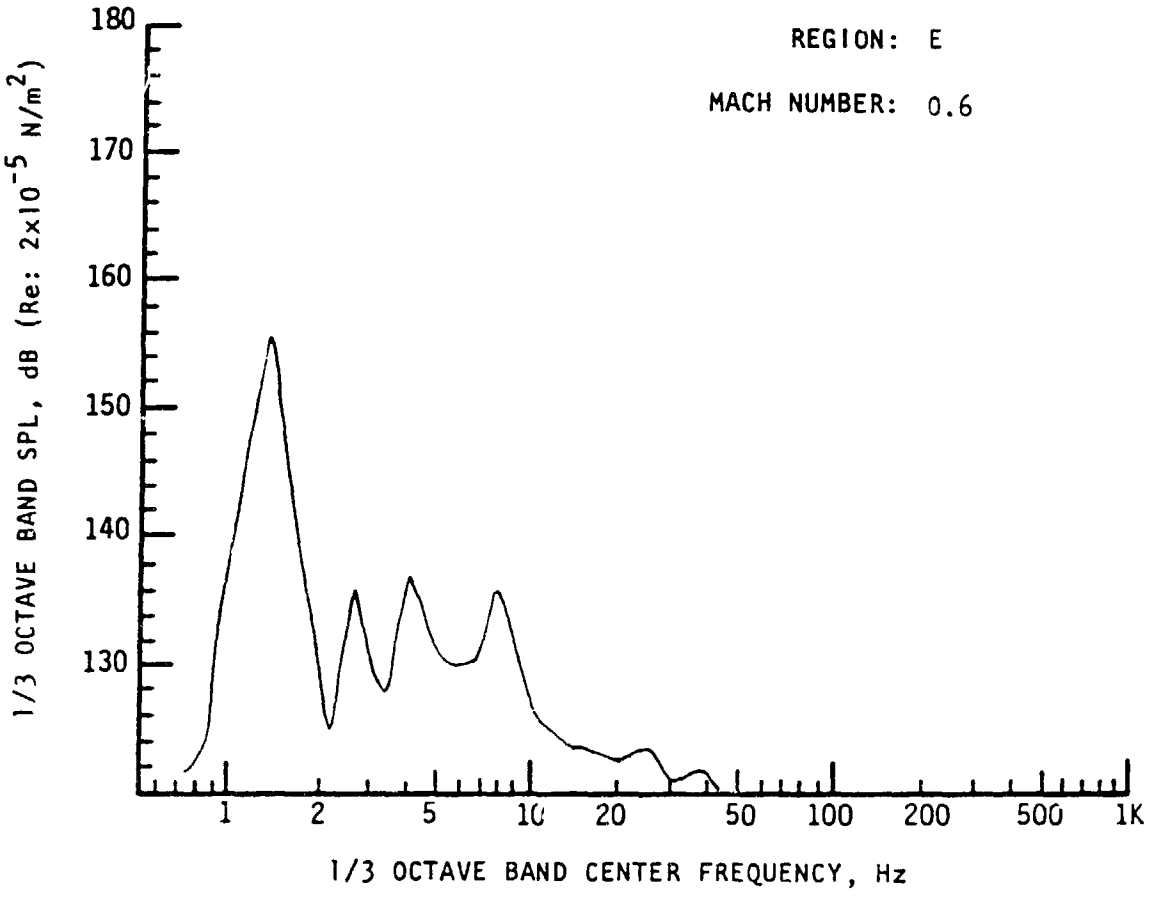

Note: Results based on 95 percentile OAFPL from Monte Carlo trajectory simulation.

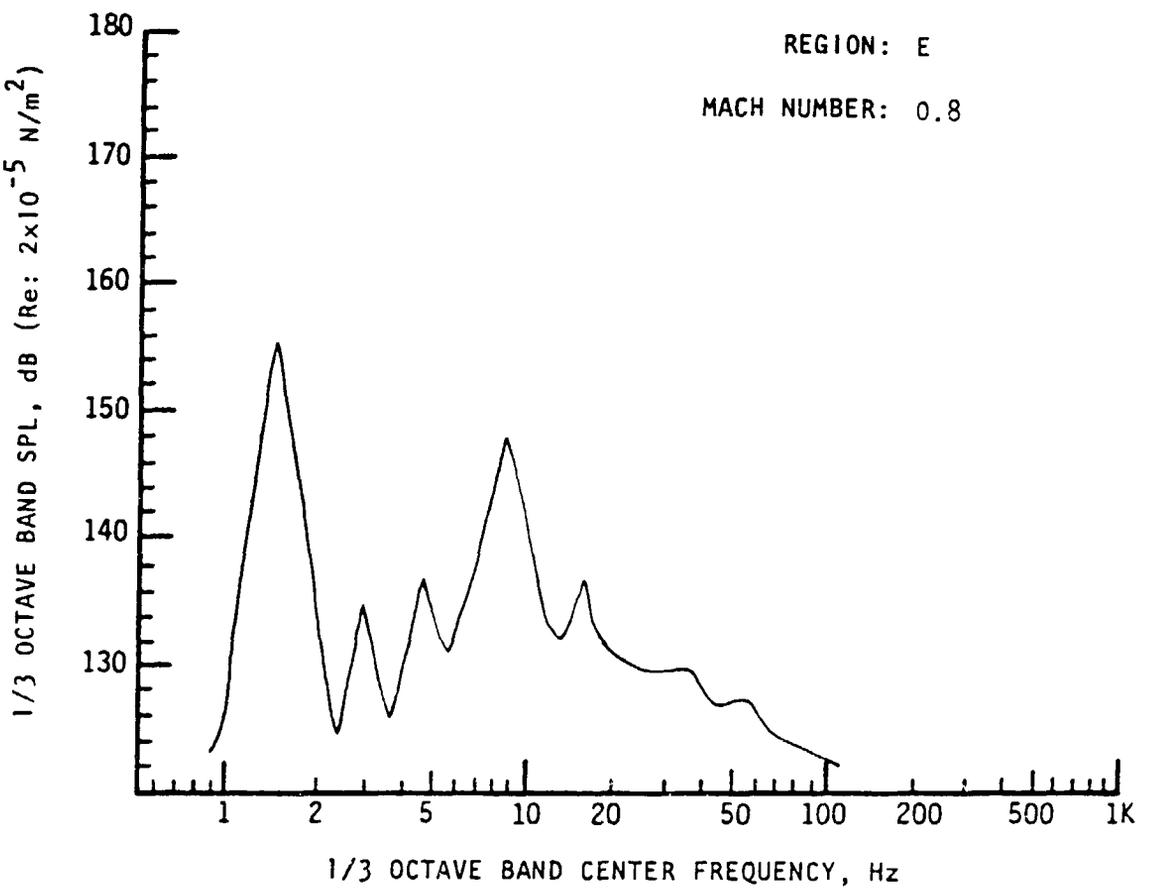

Note: Results based on 95 percentile OAFPL from Monte Carlo trajectory simulation.

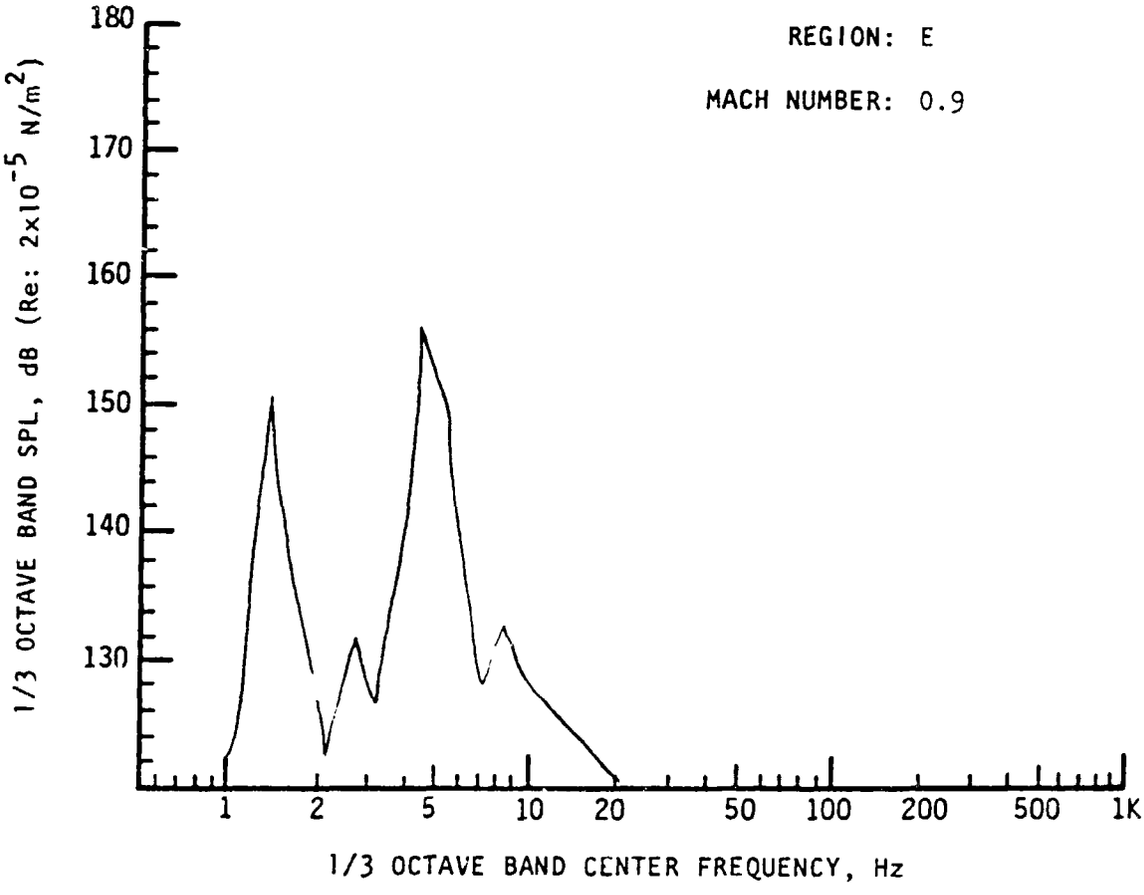

Note: Results based on 95 percentile OAFPL from Monte Carlo trajectory simulation.

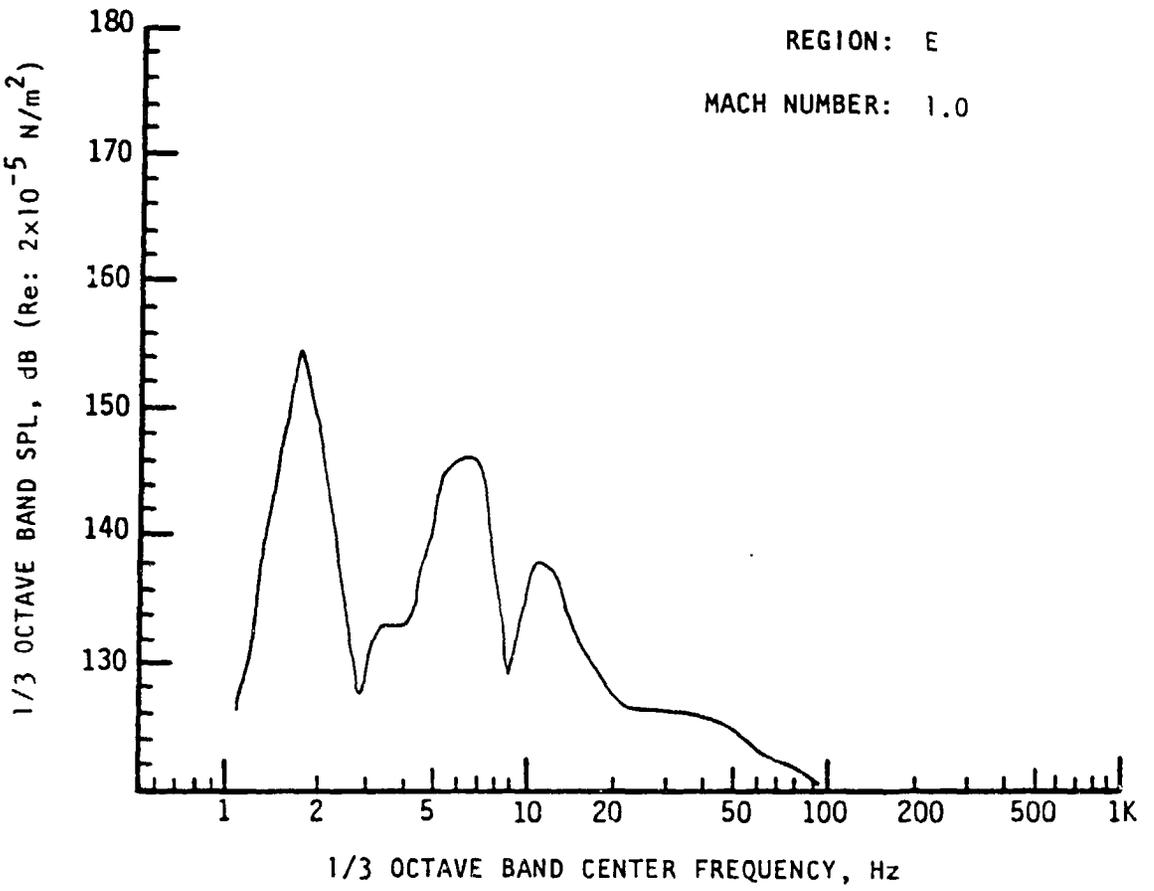

Note: Results based on 95 percentile OAFPL from Monte Carlo trajectory simulation.

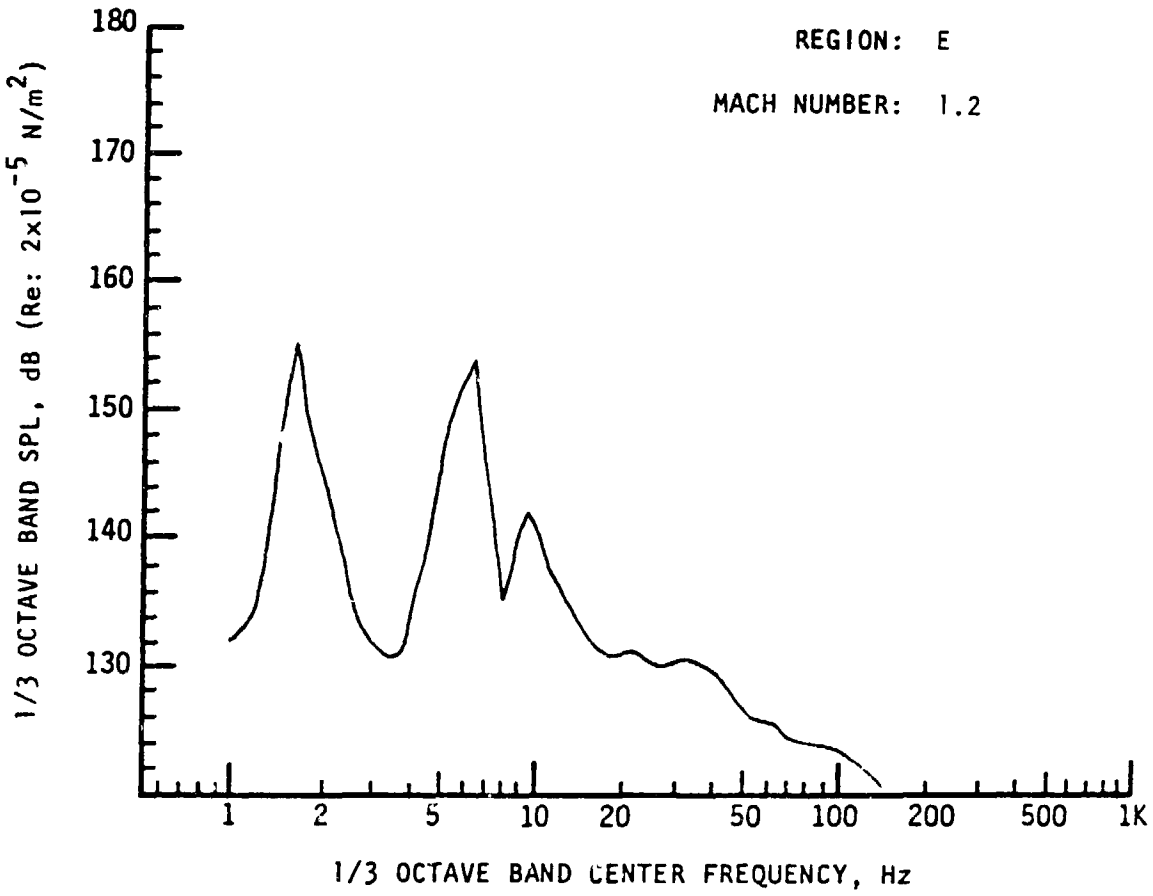

Note: Results based on 95 percentile OAFPL from Monte Carlo trajectory simulation.

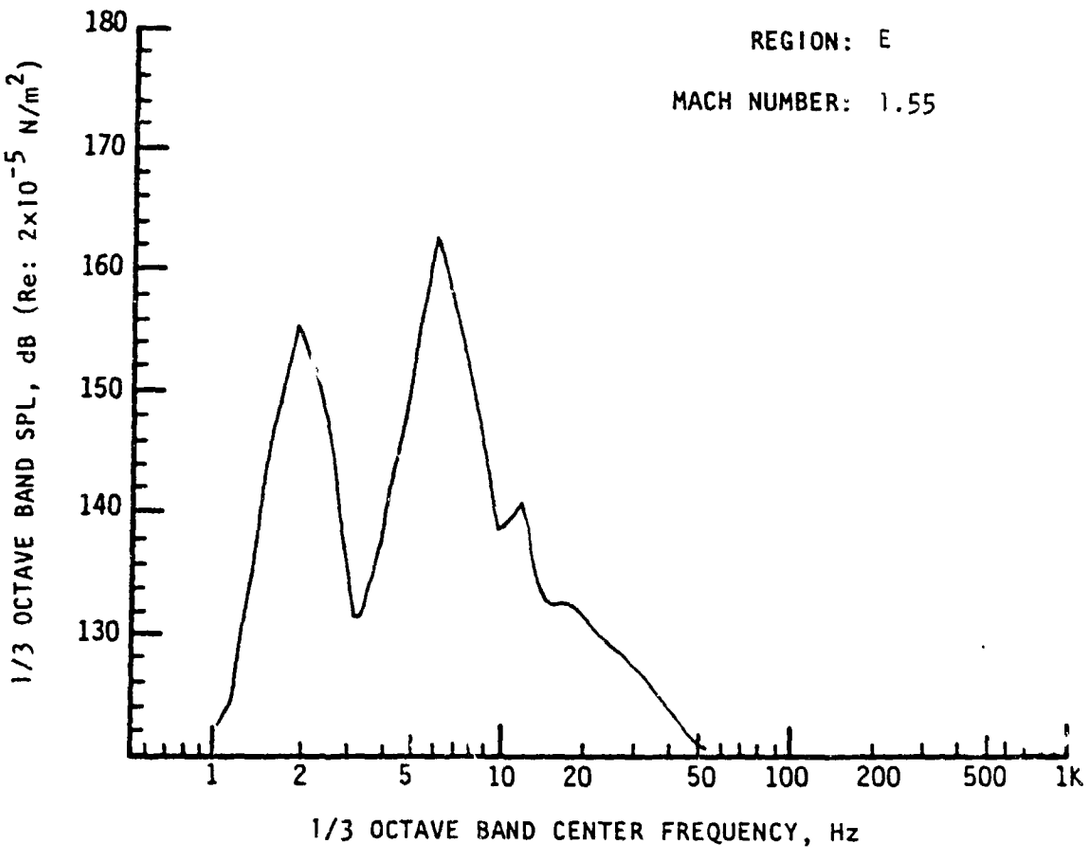

Note: Results based on 95 percentile OAFPL from Monte Carlo trajectory simulation.

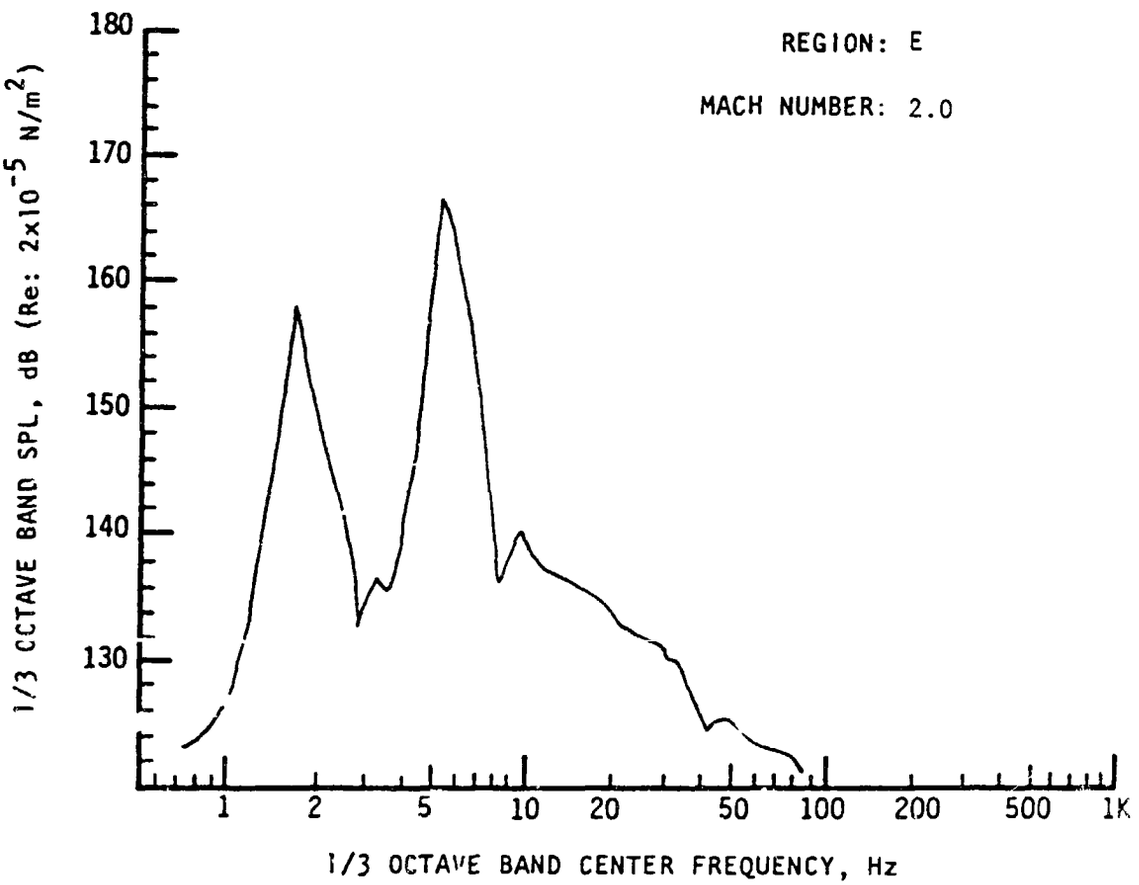

Note: Results based on 95 percentile OAFPL from Monte Carlo trajectory simulation.

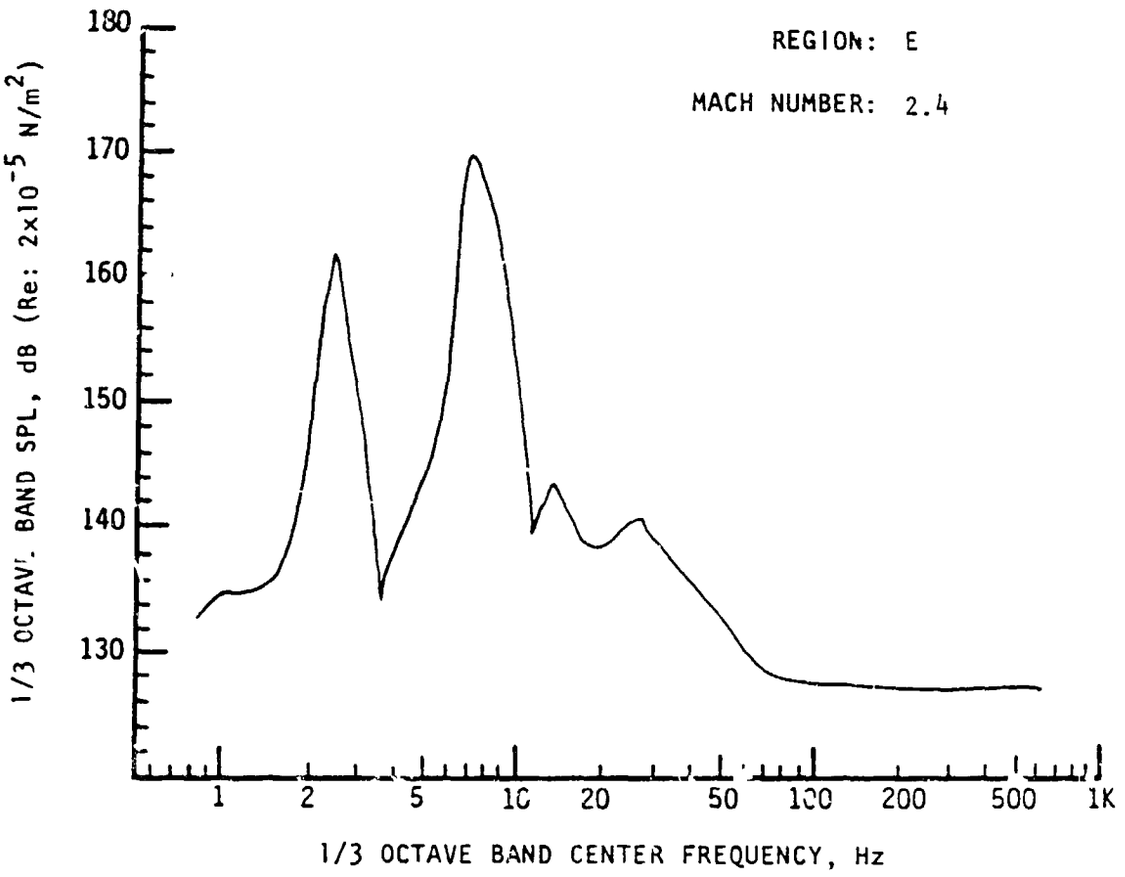

Note: Results based on 95 percentile OAFPL from Monte Carlo trajectory simulation.

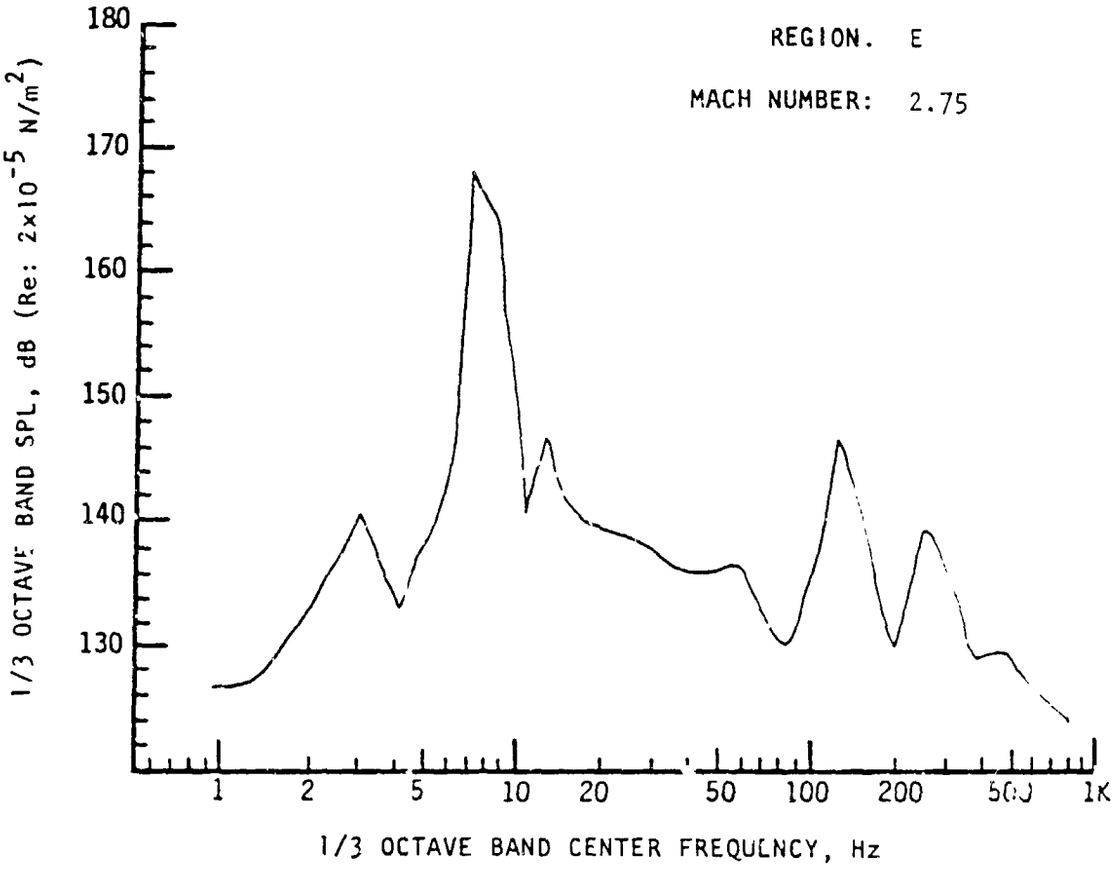

Note: Results based on 95 percentile OAFPL from Monte Carlo trajectory simulation.

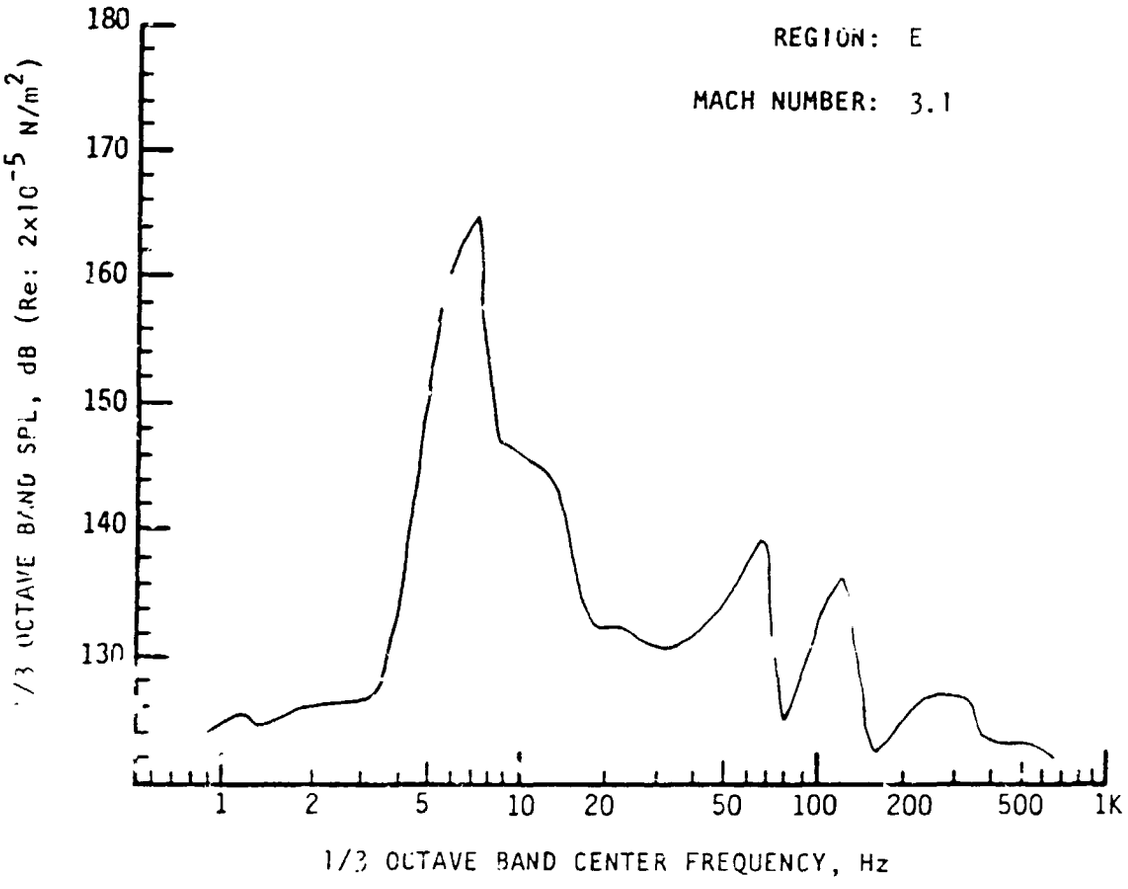

Note: Results based on 95 percentile OAFPL from Monte Carlo trajectory simulation.

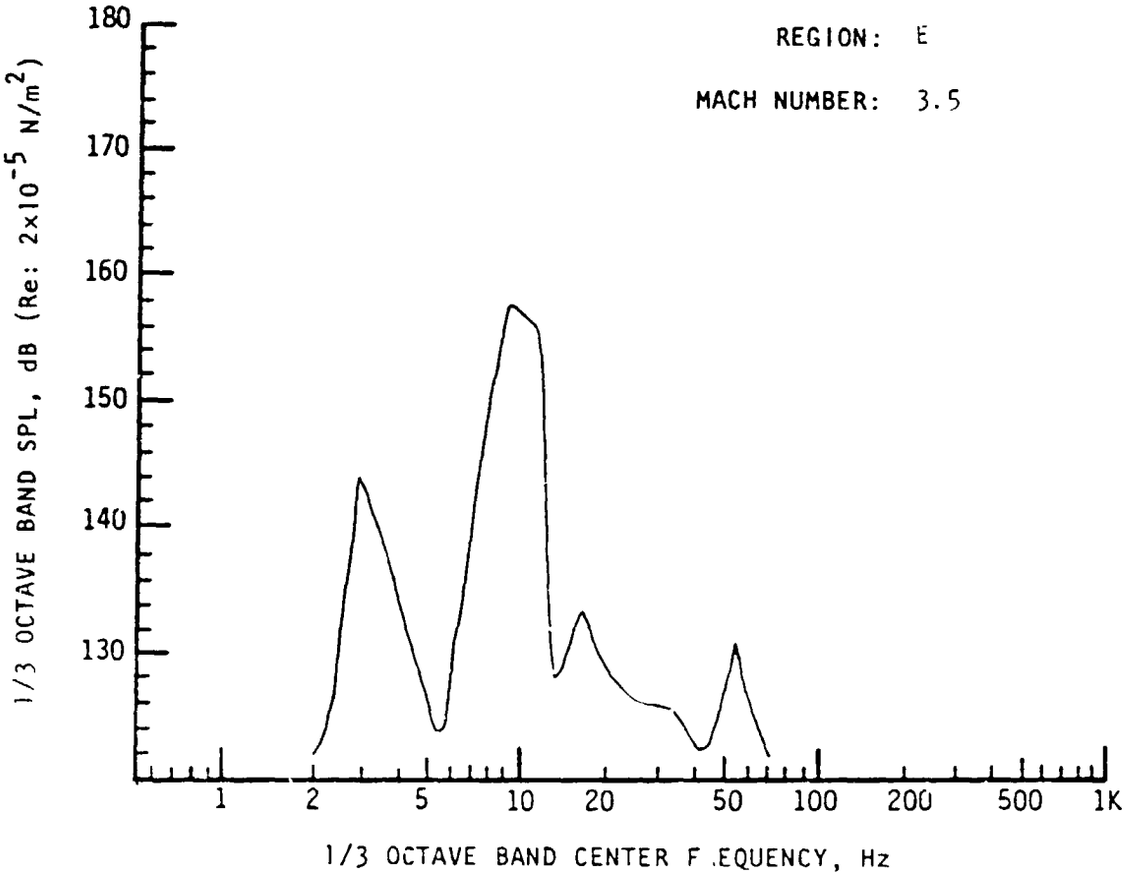

Note: Results based on 95 percentile OAFPL from Monte Carlo trajectory simulation.